Investigating the role of truncated receptors in plant immunity

Anastasia Kanali

Thesis submitted to the University of Warwick, Department of Life Sciences for the degree of Doctor of Philosophy in Life Sciences

October 2021

THE UNIVERSITY OF WARWICK

Table of Contents

List of Tables

List of Figures

Acknowledgements

I would like to thank everyone that helped me with their support throughout this PhD. Regardless of the contribution being big or small, or them been near or far.

- To my parents and family, for doing everything in their power to get me where I am.
- To my dear friends from Greece for never losing faith in me. Especially Eirini, Foteini B, Margarita, and Myrto, for always being understanding and supporting and some of the best friends one can have. For being here, no matter how far away.
- To my best friend Foteini M., for always being there, throughout the good and the bad times. 18 years and counting.
- To my friends Eva and Georgia, because that day you came to talk to me in high school was lifechanging.
- To my lifelong friend Mara, for it is rare for two people to understand each other that deeply.
- To my friend Achilleas and all the Funko Pops that accompanied my journey over the last 5 years.
- To Stelios and Alexandros, for being my UK family. For being the best thing MIBTP had to offer.
- To my dear friend Despoina, for being the best and brightest colleague one can have and a pillar during these trying times.
- To Estelle, for always being a ray of sunshine. For being positive and supportive even during the darkest times.
- To Chantal, for never forgetting to check on me and encourage me.
- To Claudia, for all the help and all the times we were there for each other.
- To Dan, for embracing my cynicism and offering me some of the best conversations one can have.

- To my Bubble: “Believe in the me that believes in you”. For believing in me when I don’t believe in myself.
- To Eduardo, for being my own Samwise. For carrying me to the very end of this. For being much more than just a friend. For being remarkable. I wouldn’t have made it here without you.
- To Lauren, for being incredible, understanding and kind. For enduring all my rants. For a great friendship.

- To my supervisor, Prof. Vardis Ntoukakis, for the opportunity to be part of this project and gain experience in a complex lab environment.
- To all my lab mates and members of C030 and C046. Special thanks to my post-docs, Daniela, Ana, and Vesi for all their help and support. Also, to my colleagues Anna and Cantug, for guiding me and helping me with my lab work.
- To all the people in my D&D groups, for embracing my geekiness and helping me escape reality.
- To all the friends that I made during the PhD journey.

Declaration

I declare that this thesis is submitted to the University of Warwick in support of my application for the degree of Doctor of Philosophy. It has been composed by me and has not been submitted in any previous application for any degree.

The work presented (including data generated and data analysis) was carried out by me except in the cases outlined below:

Preliminary transcriptomics data on *TN* gene expression (Figures 1.10 and 3.1) that initiated this PhD project were previously generated by Lewis et al. (2015).

Constructs *promAT1G72940::LUC* as well as the initial vectors containing the *TN* genes and used as a template to generate the new *promoterTN* and *TN* gene constructs were generated and kindly donated by Prof. Murray Grant and his research group (University of Warwick, UK).

Transgenic *Arabidopsis thaliana* lines promDEX::AT1G72940, promDEX::AT1G72940:HA:FLAG and CRISPR-Cas9 TN knockout lines used in Chapter 4 of this thesis for immunity assays, were generated and kindly donated by Prof. Murray Grant and his research group (University of Warwick, UK).

Preliminary data on effector screening assays of *promAT1G72940::LUC* and *promAT1G72940::LUC m1, m2, m3,* and *m1-2* (Figure 3. 4. A and B, Figure 3. 10) were generated and kindly donated by Dr WeiJei Huang (John Innes Centre, UK).

The library containing 1,956 of the known *A. thaliana* transcription factors (Pruneda-Paz et al., 2014) acting as prey for the Y1H was already prepared and transferred into the *S. cerevisiae* strain Y8800 by Dr. Ana Dominguez-Ferreras (University of Warwick, UK).

Abstract

Overpopulation of the planet, climate change and the limitations in the available arable land are undoubtedly among the major problems of modern era that threaten global food security. Crop losses due to diseases in the field caused by plant pathogens account as one of the most daunting obstacles for food security in the 21st century. Engineering plants with durable resistance against pathogenic microbes is arising as a key strategy for sustainable food production. We aimed to unravel novel pathways for robust plant production and minimise crop losses to pathogenic infections by elucidating the role of uncharacterised "truncated" receptors in plant immunity. "Truncated" TIR-NB (TN) proteins are structurally similar to NLR immune receptors, without the LRR domain. Increasing evidence show that TN proteins may be important players in plant immune responses, possibly due to the role of the TIR domain. A transcriptomics study (Lewis et al., 2015) on *Arabidopsis thaliana* when challenged with the pathogenic bacteria *Pseudomonas syringae* pv. *tomato* (*Pst* DC3000) showed rapid upregulation of 4 *TN* genes from the same genetic locus: *AT1G72920, AT1G72930, AT1G72940,* and *AT1G72950*.

RT-q-PCR confirmed that *A. thaliana TN* genes *AT1G72920* and *AT1G72940* are upregulated specifically in response to *Pst* DC3000, but not to the mutant strain *Pst* DC3000 *hrpA* that cannot deliver effectors, or in response to any of the other biotic and abiotic stresses tested. Analysis of *TN* promoter regulation showed that *Pst* DC3000 effectors HopQ1-1, HopAI1, HopB1, AvrPto, HopF2 and HopAB2 correlate with *TN* promoter induction when co-expressed in protoplasts. A study by (Mine et al., 2018) using chromatin immunoprecipitation (ChIP) showed that ERF6 transcription factor (TF) binds on *AT1G72920* and *AT1G72940* promoters, and suggests that more ERFs may regulate *TN* expression. Yeast expression vectors were generated with promoter *AT1G72940* and versions of it with mutations on three motifs for TF recognition, to facilitate large scale yeast-one-hybrid screenings of a transcription factor library, to identify candidates that mediate *TN* promoter regulation.

Pst DC3000 assays on knockout plants missing the *TN* locus did not reveal significant differences to wild type plants, possibly due to functional redundancy. A range of *A. thaliana* lines were generated, selected and characterised for constitutive and inducible overexpression of *AT1G72940* to facilitate immunity assays and high-throughput experiments that can elucidate the role of *AT1G72940* in plant immunity. Characterisation of overexpressing *AT1G72940* lines showed that protein AT1G72940 is not detected beyond the early plant developmental stages, suggesting epigenetic silencing of transgene expression and/or protein degradation in adult plants. Preliminary results of *Pst* DC3000 bacterial growth indicate susceptibility to infection of the same plants when compared to wild type, which is inconsistent with the lack of protein detection. Nevertheless, the generation and selection of *A. thaliana* transgenic plants for *AT1G72940* with many combinations of different promoters and tags offers many possibilities for future work in the field.

List of abbreviations

A	Absorbance
A. thaliana	*Arabidopsis thaliana*
A. tumefaciens	*Agrobacterium tumefaciens (Rhizobium radiobacter)*
AAA-ATPase	ATPases Associated with diverse cellular Activities
ABA	Abscisic Acid
ABRE	ABA Response Element
ADP	Adenosine Diphosphate
ADPR	ADP-ribose
ADR1	Activated Disease Resistance 1
AGI	the *Arabidopsis* Genome Initiative
AGO	Argonaute
Agroecosystem(s)	Agricultural ecosystem(s)
Amp	Ampicillin
AP2/ERF	Apetala2/ethylene-responsive factors
ATP	Adenosine Triphosphate
Avr	Avirulent
B. cinerea	*Botrytis cinerea*
BAK1	BRI1-Associated Receptor Kinase 1
BIK1	*Botrytis*-Induced Kinase 1
Bp	Base pairs
BSK1	BR-Signalling Kinase1
BSRs	Bacterial Suppressors of RNA silencing
cADPR	cyclic ADPR
CC	Coiled Coil
CCR	RPW8-like CC
CDKs	Calcium-Dependent Kinases
cDNA	complementary DNA
CERK1	Chitin Elicitor Receptor Kinase 1

CFU	Colony Forming Unit
ChIP	Chromatin Immuno-Precipitation
CHS1	Chilling Sensitive 1
CNGCs	Cyclic Nucleotide-Gated Channels
CNL	CC-NB-LRR
Col-0	Columbia-0
DAMPs	Damage-Associated Molecular Patterns
DCL	Dicer-like
dcl4	*dicer-like 4*
dde2	*delayed dehiscence2* mutant
DEPC	Diethyl Pyrocarbonate
DEX	Dexamethasone
DNA	Deoxyribonucleic Acid
DPI	Days Post Inoculation
dsRNA	double-stranded RNA
E. coli	*Escherichia coli*
EAR	Transcriptional repressor motif
EBS	EIN3 Binding Site
EDS1	Enhanced Diseased Susceptibility 1
EFR	Elongation Factor Tu Receptor
ein2	*ethylene insensitive2 mutant*
EIN3	Ethylene Insensitive 3
EMS	Ethyl methanesulfonate
ER	Endoplasmic Reticulum
ERF6	Ethylene Response Factor 6
ETI	Effector-Triggered Immunity
ETS	Effector-Triggered Susceptibility
EXO70B1	Exocyst Subunit EXO70 Family Protein B1
FAO	Food and Agriculture Organisation (of the United Nations)
FAOSTAT	Statistics Division of FAO
FLS2	Flagellin-Sensitive 2
GFP	Green Fluorescent Protein

GG	Golden Gate
GG PPK	Golden Gate Plant Parts Kit
GR	Glucocorticoid Receptor
GTPases	Guanosine Triphosphate Hydrolases
GUS	β-glucuronidase
HBD	Hormone Binding Domain
hc-siRNAs	Heterochromatic siRNAs
HDGS	Homology-Dependent Gene Silencing
HPLC	High-Performance Liquid Chromatography
HR	Hypersensitive Response
Hrs	Hours
HSE	Heat Shock Element
HSP90	Heat Shock Protein 90
ID (NLR)	Integrated Domain
incRNAs	lncRNAs produced from introns
IP(s)	Immunogenic Pattern(s)
IPCC	Intergovernmental Panel on Climate Change
IPR(s)	Invasion Pattern Receptor(s)
IPTG	Isopropyl β- d-1-thiogalactopyranoside
IPTRs	IP-Triggered Responses
JA	Jasmonic Acid
KB	King's B medium
L0	Level-0 vector
L1	Level-1 vector
L1P1	Level-1 Position-1 plasmid vector
L1P2	Level-1 Position-2 plasmid vector
L1P3	Level-1 Position-3 plasmid vector
L2	Level-2 vector
LB	Lysogeny (or Luria) Broth medium
lincRNAs	Long Intergenic ncRNAs
lncRNAs	Long Non-Coding RNAs
LRR	Leucine-rich Repeat Receptors
LRT	Low Temperature Responsive Element

lsiRNAs	long siRNAs
LUC	Luciferase
MAMPs	Microbial-Associated Molecular Patterns
MAPK	Mitogen-Activated Protein Kinase
MAPKKK	MAPK Kinase Kinase
miRNAs	microRNAs
MLA10	Barley CNL Mildew A 10
MOS6	Importin-a3/Modifier Of SNC1 6
MS	Murashige and Skoog
MTI	MAMP-Triggered Immunity
MUG	4-Methylumbelliferyl Glucuronide
n	Number of transgenic line/mother plant
N. benthamiana	*Nicotiana benthamiana*
NAD	Nicotinamide Adenine Dinucleotide
NADP	Nicotinamide Adenine Dinucleotide Phosphate
NAM	Nicotinamide
NATs	Antisense RNAs and Natural Antisense Transcripts
nat-siRNAs	Natural antisense transcripts-derived siRNAs
NB or NBD	Nucleotide-Binding Domain
NB-ARC	Nucleotide-Binding Adaptor shared by APAF-1, certain R gene products and CED-4
NLRs	NB-LRRs
npr1-1	Non expressor of Pathogenesis1-1
NRCs	NLR-Required for Cell death
NRG1	N Requirement Gene 1
O/N	Overnight
OD	Optical Density
P. infestans	*Phytophthora infestans*
P. syringae	*Pseudomonas syringae*
pad4	*phytoalexin4 mutant*
PAMPs	Pathogen-Associated Molecular Patterns
PCD	Programmed Cell Death

PCR	Polymerase Chain Reaction
pDEX	Dexamethasone-induced promoter
PEG	Polyethylene Glycol
pESTR	Estradiol-induced promoter
phasiRNAs	Secondary phased siRNAs
Pik-1/Pik-2	Rice blast resistance genes 1 and 2
PR	Pathogenesis-Related
prom	Promoter
prom35S/p35S	Promoter 35S of the Cauliflower Mosaic Virus
PRRs	Pattern Recognition Receptors
PSII	Photosystem II
***Pst/Pto* DC3000**	*Pseudomonas syringae* pv. *tomato* DC3000
PTGS	Post-Transcriptional Gene Silencing
Pv.	Pathovar(s)
R genes/proteins	Resistance genes/proteins
R. solanacearum	*Ralstonia solanacearum*
RBA1	Response to the bacterial type III effector protein HopBA1
RBOHs	Respiratory Burst Oxidase Homologues
Rcf	Relative Rentrifugal Force
RdDM	siRNA-dependent DNA Methylation
RDRs	RNA-dependent RNA polymerases
RdRP	RNA-directed RNA Polymerase
RFP	Red Fluorescent Protein
RGA4/RGA5	Rice disease resistance proteins RG4 and RG5
RIN4	RMP1-Interacting protein 4
RKs	Receptor Kinases
RLCKs	Receptor-Like Cytoplasmic Kinases
RLPs	Receptor-Like Proteins
RNA	Ribonucleic Acid
RNAi	RNA interference
RNL	NB-ARC-LRR
ROS	Reactive Oxygen Species

Rpm	Revolutions per minute
RPM1	Resistance to *Pseudomonas Syringae* pv. *Maculicola* 1
RPP4	Recognition of *Peronospora Parasitica* 4
RPS2	Resistance to *Pseudomonas Syringae* 2
RPS4	Resistance to *Pseudomonas Syringae* 4
RPS4B	Resistance to *Pseudomonas Syringae* 4B
RPW8	Resistance to Powdery Mildew 8 - like
RRS1	Resistance to *Ralstonia Solanacearum* 1
RRS1B	Resistance to *Ralstonia Solanacearum* 1B
RT	Room Temperature
SA	Salicylic Acid
SAR	Systemic Aquired Resistance
SARM1	Sterile Alpha and TIR Motif-containing 1
SAUL1	Senescence-Associated E3 Ubiquitin Ligase 1
SDG	Sustainable Development Goals
sid2	*salicylic acid induction deficient 2*
siRNAs	small-interfering RNAs
smRNAs/sRNAs	Small RNAs
SNC1	Suppressor of npr1-1 constitutive 1
SOC3	Suppressors of *chs1-2*,3
STAND	Signal Transduction ATPases with Numerous Domains
STB	Septoria tritici blotch
T-DNA	Transfer DNA
T3SS	Type III Secretion System
TAIR	The *Arabidopsis* Information Resource
ta-siRNAs	Trans-acting siRNAs
TFBSs	Transcription Factor Binding Sites
TFs	Transcription Factors
TGS	Transcriptional Gene Silencing
TIR	Toll Interleukin-1 Receptor
TN	TIR-NBD

TNL	TIR-NBS-LRR
TX	TIR-X
UAS	Upstream Sctivating Sequence of GAL4
UN	United Nations
UPS	Ubiquitin Proteasome System
UTR	Untranslated Region
UV	Ultraviolet
v-cADPR	Variant cADPR
VP16	Viral Protein 16
WRKY	transcription factors with the WRKY amino acid signature
WT	Wild Type
X-gal	5-bromo-4-chloro-3-indolyl-β-D-galactopyranoside
Y1H	Yeast-One-Hybrid
Y2H	Yeast-Two-Hybrid
ZAR1	HopZ-Activated Resistance 1

1. Introduction

1.1 Overpopulation, climate change and the need for increased crop food sustainability

One major issue of the modern era is the rapid increase of human population over the last three centuries, as it raises concerns regarding the capacity of the available natural resources to sustain both the present and future increasing population (Ime Edet et al., 2014). More specifically, global population has more than doubled over the last 50 years, increasing from 3 billion in 1959, to 6.7 billion in 2009 and hitting the milestone of 7 billion in 2011 (UN, 2022). Given the rate of increase, it is currently expected to increase up to 9.7 billion persons in 2050, while it could peak around 2100 at approximately 11 billion. Rapid rise of human population leads to considerable challenges, including increased demand for food and fresh water, malnutrition resulting from lack of nutritious food and overexploitation of other natural resources (Obaisi, 2017).

Overpopulation describes the number of people in a region exceeding the region's capacity to sustain them, thus posing one of the major challenges to food security for the coming years. "*Food security*", as defined by the United Nations' (UN) Committee on World Food Security, "*means that all people, at all times, have physical, social and economic access to sufficient, safe and nutritious food that meets their food preferences and dietary needs for an active and healthy life*" (World Food Summit, 1996). So far, and despite the joint efforts, the number of malnourished and hungry people is not sufficiently decreasing. The Food and Agriculture Organisation of the United Nations (FAO) estimates that about 11% of the global population is malnourished, focusing especially on a number of food insecure countries in Sub-Saharan Africa, Southeast Asia and West Asia (Prosekov and Ivanova, 2018).

The UN's 2030 Agenda for Sustainable Development Goals (SDG) aims to minimise environmental degradation worldwide and end poverty at all forms, thus making food security one of their primary targets (UN, 2020). Taking into

consideration the current figures and pandemics and assuming a stable population growth, the target of achieving global food security and eradication of hunger by 2050 becomes increasingly challenging (WHO, 2021; FAO, 2009). . In fact, according to the 2022 Food Security update of the World Bank, many countries are facing growing levels of food insecurity, due to the fact that factors such as conflict, socio-economic conditions, natural hazards, climate change, and pests give rise to chronic and acute hunger. Furthermore, the COVID-19 pandemic further reduced incomes and disrupted supply chains, while the war in Ukraine is expected to add risk to global food security by keeping food prices high and pushing many more people to hunger (The World Bank, 2022).

Arguably, there is amble food in the world to feed the entire population and it is widely admitted that hunger does not primarily occur due to globally depleted food stocks (Udmale et al., 2020). It is rather due to the uneven food distribution between developed, developing and least developed economies, which is facilitated by financial inaccessibility of food for a large number of people (Prosekov and Ivanova, 2018). The inequality deriving by different economies suggests that any attempt to fight poverty and move towards food security should primarily aim to decrease the cost of food production, especially in developing countries. An estimated 75% of the world's poor are depended on agriculture for their main income since they live in rural areas of developing countries. An additional 2.4 billion people are expected to be living in those areas by 2050 (Lipper et al., 2014), making it of great importance to increase current crop production in a sustainable manner.

Nations occasionally face food shortages caused by circumstances critical to food production, supply chain disruptions, economic shocks and pandemics (FSIN and Global Network Against Food Crises, 2021). On top of the recent environmental changes causing food crises, such as droughts, wildfires, floods etc, the ongoing COVID-19 pandemic is an unprecedented factor threatening global food security (Mardones et al., 2020). The COVID-19 pandemic arose as an additional challenge to global food security during late 2019 (Béné et al., 2021). At the time of this writing, it has already been almost 2.5 years since

the identification of the first COVID-19 case (China, late 2019), and more than 2 years of the world experiencing the most threatening pandemic since the 1918 Spanish flu. SARS-CoV-2 is a respiratory coronavirus responsible for the COVID-19 epidemic, which was declared a global public health emergency by the World Health Organisation (WHO) on March 11, 2020 (Zhu et al., 2020). Since then, more than 500 million confirmed cases of COVID-19 have been detected globally, while more than 6 million people have died with the disease (WHO COVID-19 Dashboard, 2022).

COVID-19 triggered global economic and social impacts, as most countries implemented strict measures to keep transmission of the virus at bay (Mardones et al., 2020). Those measures included restrictions in international travel, quarantining of millions of people, and national or regional lockdowns, which, together with the consequences of the disease itself, resulted to the disruption of supply chains for food, medicines, and manufactured products. The pandemic so far has had a substantial impact on the food system, affecting directly or indirectly not only the lives of people, but also plants and animals. The main consequences include changes in public policies, restrictions in agriculture, food availability and food safety, plant and animal health, as well as human nutrition and health (Mardones et al., 2020).

FAO states that COVID-19 affects the supply and demand for food, thus affecting agriculture and putting food security at risk in the short-, medium- and long-term (FAO, 2020). The lockdowns and trade and transportation restrictions disrupted the fresh food supply chain at a time when global food security was already compromised (Béné et al., 2021). The need for more sustainable and resilient food systems, together with a change in food policies to ensure food security in challenging times for resource-poor economies, became dire during the pandemic (Swinnen and McDermott, 2020). According to the 2020 UN report, approximately 30% of the global population didn't have access to adequate food due to COVID-19. Up to 811 million people in low-income countries went hungry due to increased food insecurity resulting from the rapid raise in food prices during 2020 (The World Bank, 2021). Furthermore, the pandemic together with climate change has compounded the

impacts of both existing and emerging animal and plant diseases, due to the fact that people were restricted by public health guidelines and were therefore unable to control them (Mardones et al., 2020). One example has been the desert locust plague, with locusts decimating food crops and forage in East Africa, India, and Pakistan. Therefore, the need arose to plan and prepare for pest and disease control when resources are deployed due to unprecedented events, to prevent food insecurity resulting from crop loses, especially given the fact that the land available for crop production has natural limitations.

The availability of arable land has always been an important factor for consideration, as 78% of the Earth's land has natural limitations that deem it unsuitable for agriculture (Prosekov and Ivanova, 2018). According to FAO experts, only 11% of the total land area is arable land, while an extra 24% is occupied by livestock. UN data for more than a decade suggest that agricultural production may need to be increased by 75% by 2050 to meet the dietary needs of the population (Godfray *et al.*, 2010; Alexandratos and Bruinsma, 2012). However, climate change has already been negatively affecting the global crop production, as reported by the Intergovernmental Panel on Climate Change (IPCC, 2014), with developing countries exhibiting higher vulnerability. Natural events with high impact in agriculture are amplified and accelerated as a direct result of climate change, such as drought, excessive rain, flooding and constantly increasing maximum temperatures (Lipper et al., 2014). Climate change reduces agricultural production and incomes, thus posing a threat to food security (Lipper et al., 2014).

The main strategy so far to meet increased food demands has been "extensification" of agriculture, essentially converting natural ecosystems into agriculturally exploited ecosystems or agroecosystems (Tilman et al., 2001). However, this process is now considered unsustainable, given that an extra billion of hectares will be needed to meet the crop production demands by 2050. To prevent further exploitation of natural ecosystems and the ecological disasters it entails, a new course of action has been suggested towards ensuring future sufficient food supply known as "sustainable intensification". Intensification describes the global effort of increasing food production while

using the same arable land and without necessarily further degrading natural ecosystems (Godfray, 2015). Sustainable intensification can be achieved by a combination of approaches focusing on the optimisation of numerous factors, such as soil fertility, water-use efficiency and sustainable increase in productivity (Grafton et al., 2015). Many of these factors can be tackled with modern technologies, such as utilizing renewable sources of energy, ocean water as well as advances in plant genomics to improve crops (Prosekov and Ivanova, 2018). Nevertheless, investment in research and biosecurity is of vital importance and should not be disregarded (Hertel, 2015) due to the considerable impact of plant and livestock diseases on food production (Grafton et al., 2015).

Plant diseases are considered to be one of the most daunting obstacles for food security in the 21st century, as human population is rapidly rising and the demand for sustainable food production is increasing (Velásquez et al., 2018). Loss of major agricultural crops to biotic stress is well documented through the years and it is estimated to be between 20% to 40% of the total crop production (Oerke, 2006; Savary et al., 2012), which can lead to catastrophic consequences worldwide on an economic, social and ecological level. Many plant diseases are quite resilient through time, but the change in environmental conditions as well as the pest/pathogen-host coevolution continues to give rise to new ones globally. It is unknown how plant pests and pathogens will adapt to climate change; however, most simulation studies predict that the survival of most pathogens will be favoured due to global warming and changes in precipitation patterns (Juroszek and Von Tiedemann, 2015). Nevertheless, there is a range of adaptation strategies which could potentially reduce the negative impact on crop production and/or even create a positive one (Olesen et al., 2011).

Ten basic crops account for 58% of the total global cultivated area, but not all of them are equally important in human nutrition. According to 2013 estimates, only five crops account for 50% of the global human calorie intake: wheat (18.3%), rice (18.9%), maize (5.4%), potato (2.2%) and soybean (3.3%) (Statistics Division of FAO, FAOSTAT, 2018). Nowadays it is estimated that

the global crop losses caused by pathogens and/or pests in the field for each one of those 5 crops is 21.5%, 30.0%, 22.6%, 17.2% and 21.4%, respectively (Savary et al., 2019). Despite the fact that these numbers reflect the impact of pathogens and pests only on crops with high global demand, it is important to remember that all cultivated crops suffer substantial losses to plant diseases (Velásquez et al., 2018). Therefore, it is expected that minimizing agricultural losses from pathogens will substantially increase crop yield and decrease the cost of food production.

Improving global agriculture and ensuring reliable food systems is considerably based on managing the spread of crop pests and pathogens (Esker et al., 2012). Plant scientists are facing the pressuring challenge of deciphering plant diseases on a molecular, epidemiological and ecological level in order to be able to provide with effective and long-lasting solutions to mitigate their impact on global crop losses. The catastrophic impact of some plant diseases is widely known to have caused excessive human deaths and migration, as well as having environmental impact. The potato late blight in Ireland in the 1840s (Fry et al., 2015) and chestnut blight in the United States in the early 1900s (Anagnostakis, 1987) are two very characteristic examples.

1.2 Plant pathogens and diseases in the field

Pathogens and plants form a dynamic relationship between them and their environment, known as the ‘disease triangle’, which highlights the importance of their interaction. For successful development of disease, all three factors must be met: a susceptible plant host, a virulent pathogen, and the optimal environmental conditions (Stevens, 1960). Those optimal environmental conditions will define the disease outbreaks, as they favour growth and propagation of both plants and pathogens (Juroszek and Von Tiedemann, 2015). Therefore, it is understandable that the ongoing climate change will likely affect the environmental variables shaping optimal conditions, thus causing both parts of the equation to either adapt or become extinct. It is also expected to affect the severity of the already established diseases, although whether positively or negatively will probably depend on many factors

(Juroszek and Von Tiedemann, 2015).

The very selective and homogeneous environment of the agricultural ecosystems (agroecosystems) has already become quite divergent from natural ecosystems. This outcome is often favouring the development of new 'domesticated' crop pathogens that are host-specific, as well as more virulent compared to the 'wild' strains they rapidly evolved from (McDonald and Stukenbrock, 2016). Pathogen transmission is favoured by the increased planting density of crops in agroecosystems, thus enhancing virulence and pathogen population (Read, 1994). This leads to accumulation of mutations and increase in genetic diversity of pathogens in agroecosystems (Stukenbrock et al., 2011). Multi-infections are also favoured by increased host density in the field, which also increases the possibility of simultaneous infections by different pathogen species (Alizon et al., 2013), potentially leading to horizontal gene transfer (Gardiner et al., 2012) of genes affecting virulence among different pathogens of the same host. Taking these into account along with the spread of highly dangerous crop pathogens worldwide, like *Phytophthora infestans* (*P. infestans*) responsible for potato late blight (Goss et al., 2011), and wheat blast pathogen *Pyricularia graminis-tritici* reaching Asia (Callaway, 2016) being accelerated by global trade, becomes increasingly worrying in respect to global food security.

More examples of crop infecting pathogens causing severe plant diseases can be found in both fungi and prokaryotes. The bacterium *Xanthomonas axonopodis* pv. *citri* is a biotroph particularly devastating for the citrus industry. It causes citrus canker by colonizing the apoplast of citrus plants, aiming to maintain a healthy host by regulating its homeostasis via the secretion of a natriuretic peptide-like protein (Gottig et al., 2010). One of the most destructive plant pathogens is the bacteria *Ralstonia solanacearum* (*R. solanacearum*), which has caused yield losses greater than 14% in potato crops in Bangladesh and other places (Elphinstone *et al.*, 2005) and can be identified by the fast development of bacterial wilt symptoms (Yuliar *et al*., 2015). *R. solanacearum* blocks the plant vasculature by secreting vast amounts of extracellular polysaccharides and has a broad range of hosts beyond potato (e.g., banana)

(Prior *et al*., 1997). The saprotroph fungal pathogen *Mycosphaerella graminicola* survives on decaying organic matter and is responsible for the most widespread wheat disease (Suffert *et al*., 2011) accounting for 5-10% of the crop's losses, costing the UK alone up to 140 million Euros (Fones and Gurr, 2015), known as Septoria tritici blotch (STB).

Nevertheless, advances in biotechnology allow plant scientists to combat plant pathogens by shifting the balance of the plant-pathogen interaction to favour the host plant (Dangl et al., 2013). *Agrobacterium tumefaciens* (*A. tumefaciens*) mediated transformation was achieved in strawberry plants, of the gene *CH5B* encoding for a chitinase with the power to prevent degradation of the plant's cell wall, thus conferring high levels of resistance to the powdery mildew caused by the fungus *Botrytis cinerea* (Vellicce *et al.*, 2006; Olivier *et al.*,2018). Overexpression of the transcription factor WRKY45 in rice regulates the signalling of the pathogenic defence phytohormone Salicylic Acid (SA) resulting in enhanced resistance against the pathogen *Xanthomonas oryzae* (Takatsuji, 2014). These are just a couple of quite a few examples of ongoing field and/or large-scale trials of biotechnology-induced resistance to pathogens, which show encouraging results. However, as crop plants usually have a long life cycle and in many cases, their genomes are either not fully sequenced or not easily manipulated, scientists worldwide are using model plants as their primary research, aiming to apply the relevant findings in the field. It is therefore clear that deciphering the mechanisms facilitating plant disease resistance and underlying plant-pathogen interactions using model pathosystems, is crucial for the development of disease-resistant crops that will contribute to sustainable agriculture and subsequently, to global food security.

1.2.1 The model pathosystem Arabidopsis thaliana - Pseudomonas syringae

Arabidopsis thaliana (*A. thaliana*) is a small dicotyledonous flowering plant (**Figure 1.1**), that is not economically significant, but is very important to biotechnology and research. Nevertheless, it belongs to the Brassicaceae

family, which makes it a wild relative of many important crop plants like cabbage, broccoli, and turnip. It is undeniably the most well-studied species in plant biology since the 1980s, when it started as model system for genetic, biochemical, and physiological study and evolved as the main model plant system used by the scientific community (The *Arabidopsis* Information Resource, TAIR). The accession Col-0 is the first fully sequenced plant genome (the *Arabidopsis* Genome Initiative, AGI 2000) which enabled research in all aspects of plant biology. As all model organisms, *A. thaliana* is characterised by a collection of traits that make it ideal for lab-based research, like easy cultivation in restricted space due to its small size, a relatively fast life cycle of approximately 2 months between generations, the advantage of producing numerous self-progenies and a small fully mapped genome (5 chromosomes) that makes it suitable for genetic engineering (Koornneef and Meinke, 2010).

Furthermore, advances in *A. tumefaciens* mediated transformation of plants via T-DNA (transfer DNA) genome insertions as well as EMS (Ethyl methanesulfonate) mutagenesis can be performed with great efficiency in *A. thaliana*. Those tools lead to an abundance of mutant lines and genomic resources to become available, providing researchers worldwide with the opportunity to study gene function through reverse genetics (Koornneef and Meinke, 2010). Meanwhile, extensive research on *A. thaliana* led to the development of a variety of tools and well-established experimental protocols on the molecular, biochemical, and phenotypical level, setting the basis for applied research in economically important crops. When *A. thaliana* emerged as a model system for plant research in the mid 1980s, the general belief was that it is not susceptible to pathogens. Nowadays, it is still a fact that *A. thaliana* is not a host to many important crop pathogens, however we know that it is susceptible to a wide variety of viruses, fungi and bacteria, like *Pseudomonas syringae,* making it suitable for a pathosystem (Katagiri et al., 2002).

Figure 1.1 **The model plant Arabidopsis thaliana Col-0 accession.**

Pseudomonas syringae (P. syringae) is a hemibiotrophic gram-negative pathogenic bacteria that has a wide variety of economically important plant hosts. Environmental conditions such as high humidity and mild temperature favour a very aggressive *P. syringae* multiplication in a susceptible host plant (Agrios, 1997). Since the early 1980s, various *P. syringae* strains have served as models to elucidate the mechanisms underlying host-pathogen interactions. *P. syringae* enters the plant through natural openings (stomata) or wounds and it rapidly multiplies in the apoplast of (mainly) susceptible hosts (Hirano and Upper, 2000). *P. syringae* strains are grouped into pathovars (pv.) due to the high degree of host specificity they exhibit between species and cultivars (Gardan *et al.*, 1999). In 1991, *A. thaliana* was identified as a host of *P. syringae* pathovar *tomato* (*Pst* or *Pto*) strain, DC3000, besides tomato (*Solanum lycopersicum*), its natural host (Gizjen, 2008). *Pst* DC3000 is responsible for the bacterial speck disease of tomato (**Figure. 1.2**), which causes severe loss in fruit yield (up to 75% in plants infected at an early stage) and quality (up to 52% loss of fruit weight) globally (Ortigosa et al., 2019), as happened in 2010 in Florida and California (Cai et al., 2011).

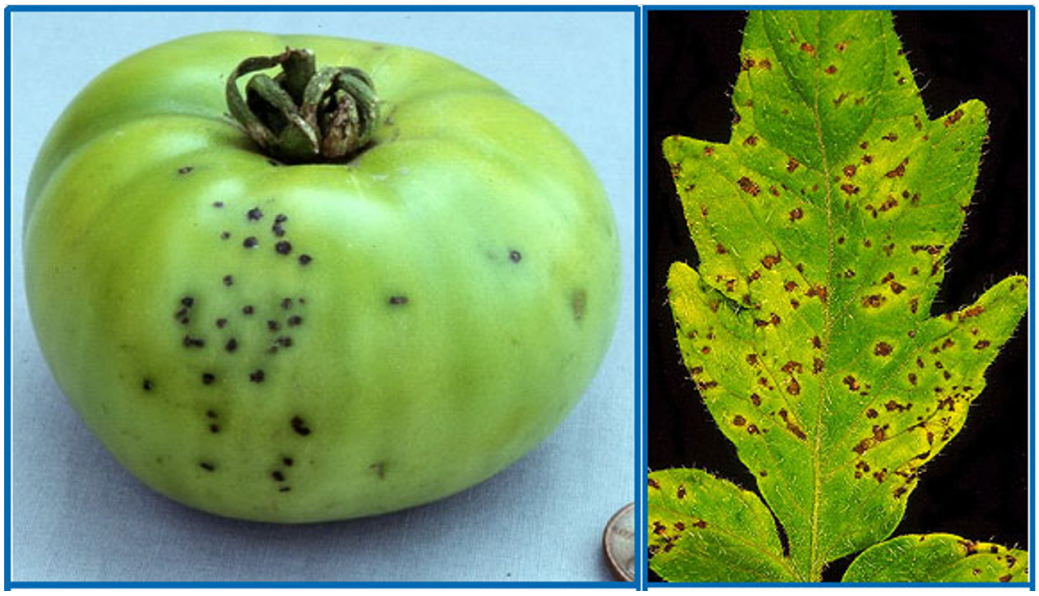

***Figure 1.2* Symptoms of bacterial speck on tomato (*Solanum lycopersicum*) fruit (left) and leaf (right) caused by *P. syringae* pv. *tomato* DC3000.**

Source: Bacterial Speck of Tomato, Alexandra Kravik, University of Wisconsin Garden Facts. Photo credits: S.T. Koike (left) and Allan Collmer (right).

The susceptibility of *A. thaliana* to *Pst* DC3000 (**Figure 1.3**) subsequently fuelled the efforts to characterize the molecular mechanisms underlying the development of disease in plants. *Pst* DC3000 is equipped with a broad repertoire of virulence proteins called effectors, which are delivered to the plant cells through the type III secretion system (T3SS), as well as a phytotoxin that structurally resembles the plant hormone jasmonic acid (JA), known as coronatine (Zhao et al., 2003). Molecular biology research on the *Pst* DC3000 pathogenesis has mainly focused on elucidating how a bacterial pathogen promotes disease susceptibility by employing type III effectors which are able to suppress plant immune responses. Moreover, it unveiled function of stomata in plant immunity and key components of JA signalling in plants. The knowledge resulted from studying the pathosystem of *A. thaliana* and *Pst* DC3000 are hoped to shed light towards understanding pathogenesis on other plant pathogens, plant immunity and infer what might be happening in the primary host (Xin and He, 2013).

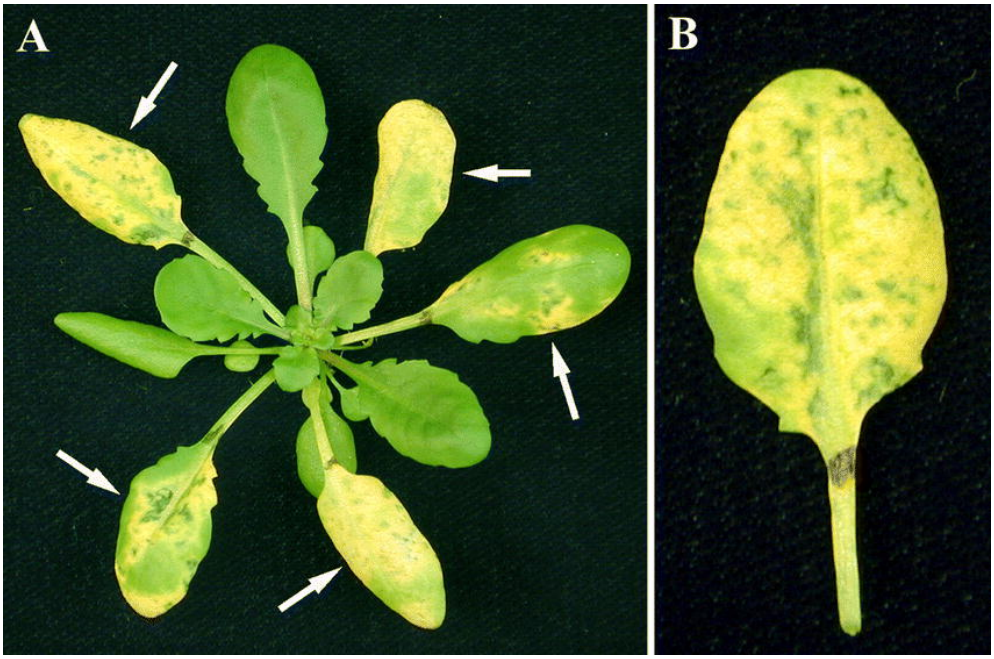

Figure 1.3 **Disease symptoms in *A. thaliana* rosette leaves post infection with *Pst* DC3000 (Katagiri, Thilmony and He, 2002).**

1.3 The Arabidopsis thaliana immune system

Plant pathologists worldwide count almost thirty years of extensive research that aims to decipher the inner workings of plant immune mechanisms, hoping to shed some light on the ways plants deal with pathogens and gain insight as of how to engineer robust plants with enhanced resistance to diseases in the field (Zhang *et al.*, 2020a). Despite the aforementioned effort, the specifics behind molecular plant-microbe interactions still remain largely unknown, leaving the plant pathology scientific community with more questions than answers (Zhang et al., 2020a).

Unlike animals, plants are sessile organisms, meaning that their natural obstacle of immobility prevents them from escaping extreme environmental conditions and/or biotic stresses, including pathogen invasion. More specifically, vertebrates use a combination of innate and adaptive immune responses to combat pathogens (Vance et al., 2009). The adaptive immune system confers immunological memory to the host, providing specific protection against specific pathogens by the acquisition of receptors (e.g., immunoglobulins) that recognise pathogen-derived molecules (antigens). On the contrary, plants are not equipped with a circulatory blood system and the

ability to produce specialized immune cells. Therefore, plants have evolved to defend themselves against the numerous microbial pathogens that they get exposed to, relying mainly on their innate immunity, which comprises of several components and systemic signals triggered on the site of infections (Jones and Dangl, 2006). Lacking adaptive immunity, each single plant cell must be able to perceive microbial pathogens and activate efficient defence responses (Keller et al., 2016).

1.3.1 Extracellular defence responses and MAMP-triggered immunity (MTI)

The plant's immune system employs extracellular and intracellular molecules moderating defence responses to pathogenic microbes (Zhang et al., 2020a). Upon perception of pathogens the plant triggers a basal resistance response by recognising evolutionary conserved pathogen- (or microbial-) associated molecular patterns (PAMPs or MAMPs), using the extracellular surface pattern recognition receptors (PRRs), that include mainly receptor kinases (RKs) and receptor-like proteins (RLPs) (Tang et al., 2017; Zipfel and Oldroyd, 2017). An additional role of PRRs is to perceive Damage- Associated Molecular Patterns (DAMPs) coming from the host, such as parts released from plant cell walls, extracellular adenosine triphosphate (ATP), and nicotinamide adenine nucleotide (NAD) (Bacete et al., 2018; Choi et al., 2014; Wang et al., 2017), which indicate a pathological state characteristic pathogen invasion (Cook et al., 2015). Plants also produce phytocytokines, which are analogous to animal cytokines immunogenic peptides and are perceived by PRRs to modulate immune responses (Gust et al., 2017).

Plants are equipped with natural barriers to prevent invasion; however, pathogens have evolved to bypass them. Stomata are normally found in leaf surface, and they have a vital role in plant development, consisting natural openings who control the plant's gas exchange and water loss. Unfortunately, in many cases they can also be the gate used by bacterial pathogens, leading to the apoplastic space (Zeng et al., 2011). MAMPs are recognized by PRRs upon contact with the pathogens, thus inducing stomatal closure and

restricting further entry of bacterial microbes (Thor et al., 2020) while also triggering hormonal signalling pathways, like abscisic acid (ABA) which induces stomatal closure (Joshi-Saha et al., 2011). Another physical barrier preventing the pathogen from accessing the cells is the plant cell wall, which the pathogens counteract by secreting cell-wall-degrading enzymes to cause modifications in the cell-wall integrity (De Lorenzo et al., 2019) thus activating immune signalling via the production of pattern signals. Once pathogens have successfully colonised the apoplast, the plant secretes pathogenesis-related (PR) proteins, antimicrobial secondary metabolites, and lytic enzymes. Those enzymes initially aimed to degrade pathogen-derived components as an offensive strategy, but through evolution plants acquired the ability to detect the products of this degradation (MAMPs) within complicated pathogen surface structures, such as the bacterial flagellin epitope flg22 and peptidyglycan, to trigger pathogen perception (Liu et al., 2014).

This first response to pathogen detection is called MAMP-triggered immunity (MTI) and it consists the first barrier of plant's defence (Dangl et al., 2013). The activation of these cell-surface immune receptors, which are analogous to animals' Toll-like receptors, restricts the colonization of pathogens by triggering intracellular signalling, transcriptional reprogramming and biosynthesis of a complex downstream responsive pathway. Following activation by PRRs, there are receptor-like cytoplasmic kinases (RLCKs) that trigger immune signalling events such as reactive oxygen species (ROS) production, rapid influx of calcium ions, and activation of mitogen-activated protein kinase (MAPK) cascades, through the phosphorylation of downstream partners. This early signalling event activation is underlined by molecular mechanisms that have been unveiled after extensive analysis of many *A. thaliana* PRRs, such as FLAGELLIN-SENSITIVE 2 (FLS2) and ELONGATION FACTOR TU RECEPTOR (EFR). Furthermore, some RLCKs directly connect PRRs to downstream components, including BOTRYTIS-INDUCED KINASE1 (BIK1) and BR-SIGNALING KINASE1 (BSK1) (Lu et al., 2010; Majhi et al., 2019).

BIK1 is an interesting example, as it can positively regulate calcium influx by phosphorylating cyclic nucleotide-gated channels (CNGCs), an important step in immune responses as calcium regulates key regulatory proteins of immunity, such as calcium-dependent kinases (CDKs), respiratory burst oxidase homologues (RBOHs), transcription factors (TFs) and calcium-dependent metacaspases (Tian et al., 2019; Jiachang Wang et al., 2019). The phosphorylation of the N terminus of RBOHD by BIK1 initiates rapid ROS production, another immune activation signal (Kadota et al., 2014; L. Li et al., 2014). Moreover, BIK1 and BSK1 phosphorylate MAPK kinase kinase (MAPKKK) kinases to activate MAPK cascades, leading to defence activation (Bi et al., 2018). Nevertheless, it is still not completely clear how these early signalling events lead to downstream defence.

1.3.2 Intracellular defence responses and effector-triggered immunity (ETI)

Further to extracellular immunity, plants have also evolved intracellular immunity mechanisms relying on nucleotide-binding (NB) leucine-rich repeat (LRR) receptors encoded by the plant's resistance (R) genes (NB-LRRs or NLRs; (Jones et al., 2016). Successful bacterial pathogens use their T3SS to overcome MTI by delivering a broad spectrum of effector molecules into the plant, which modulate plant physiology and modify host proteins to increase pathogen virulence, resulting in effector-triggered susceptibility (ETS) (Galan and Collmer, 1999). When avirulence (Avr) effector molecules interact and get recognised by NLR proteins, they induce a strong resistance response called effector-triggered immunity (ETI) (Dangl and Jones, 2001). ETI comprises the second barrier of defence, which acts mainly inside the cell.

Plants have a great number of R genes, mainly encoding NLR proteins with characteristic NB and LRR domains, which are activated directly or indirectly by effectors (Chisholm et al., 2006). Direct recognition occurs via a physical interaction between an NLR and an effector, whereas indirect recognition takes place when an NLR interacts instead with an effector–target protein inside the host cell. The recognition of one effector by one NLR protein

activates an amplified defence response that triggers ETI, that often leads to the induction of hypersensitive response (HR), which is localised programmed cell death at the infection site to restrict pathogen growth in plant cells (Lee and Yeom, 2015). Despite the many years of research on plant-pathogen interactions, the exact molecular mechanisms highlighting the action of most NLRs remain to be deciphered. However, our understanding of how NLRs are activated to initiate defence signalling has progressed due to new findings, which are more extensively discussed in **Section 1.4**.

1.3.3 Current perspective on plant immune responses

Throughout the years, many conceptual models have been proposed as an attempt to understand and describe the plant immune system. One of the first models for plant immunity was the "Guard Model", proposed originally in 1998 by Van der Biezen and Jones to describe the recognition of *Pst* DC3000 effector AvrPto by the Pto/Prf proteins in tomato and was later generalized to other proteins (Dangl and Jones, 2001). The Guard Model describes indirect recognition of effectors by NLRs, predicting that NLRs act as guards to the effector target (guardee), and are activated by perceiving any modifications caused by the effector on that target, thus triggering immune defences. This indirect perception mechanism explained the need of only a small NLR repertoire employed by the plant to recognise multiple effectors from a broad range of pathogens (Dangl and Jones, 2001). However, it became quickly evident that the guardee is subjected to two conflicting natural selection forces due to NLR population polymorphism, making an unstable evolutionary choice. Instead, some host targets of indirectly recognised effectors act as decoys mimicking effector targets to trigger NLR recognition (Zhou and Chai, 2008), leading to the introduction of the Decoy Model (Van Der Hoorn and Kamoun, 2008).

1.3.3.1 The "zigzag" model

For years, the most famous and widely accepted hypothesis was described by Jones and Dangl, (2006), and it is known as the four phased "zigzag" model (**Figure 1.4**), which integrates both the original gene-for-gene hypothesis and

the recognition of general elicitors in one model. According to them, in phase 1, MTI is triggered by PRRs recognising MAMPs and restricting further colonization of the pathogen. Successful pathogens proceed to phase 2, where they use effectors virulence to promote virulence and suppress MTI, resulting in ETS. When a specific effector gets recognized by a specific NLR protein directly or indirectly, ETI is triggered in phase 3, resulting in disease resistance and HR at the infection site. Finally, in phase 4 pathogens are driven by natural selection to evolve and supress ETI, by either alter the specific effector that got recognised or the acquisition of new effectors. In parallel, the plant is also driven by natural selection to acquire new specific NLRs to counteract pathogen evolution by triggering ETI again.

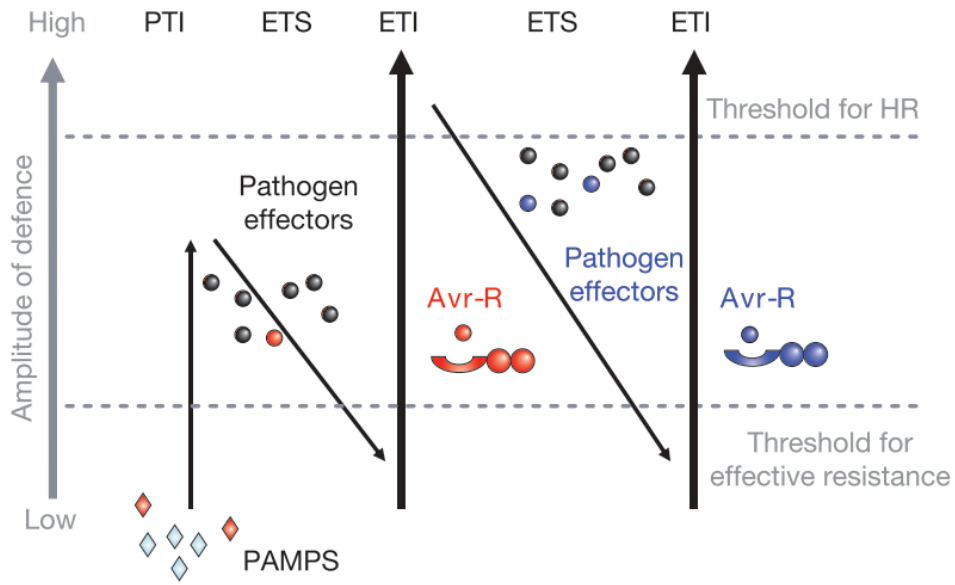

Figure 1.4 **The "zigzag" model of plant immune responses.**

As described by Jones and Dangl in 2006 (*Nature Reviews*), plants trigger PAMP/MAMP-triggered immunity (PTI/MTI) via the detection of microbial/pathogen-associated molecular patterns (MAMPs/ PAMPs, red diamonds) using PRRs. Successful pathogens overcome PTI by delivering virulence effectors, triggering effector-triggered susceptibility (ETS). When one effector (red) gets recognised by an NLR resistance protein, effector-triggered immunity (ETI) is activated, often leading to the induction of hypersensitive response-induced cell death (HR). Finally, pathogens evolve to lose the recognised red effector and perhaps acquire new ones (blue), trying to overcome, which ultimately favours new plant NLRs with new effector specificities, resulting again in ETI.

Despite the fact that the “zigzag” model has provided a convenient framework for explaining the molecular plant–microbe interactions for more than 10 years (Jones and Dangl, 2006), it is now widely accepted that the MTI-ETI dichotomy bears several misconceptions. This is focusing mainly on the assumption that MTI and ETI mechanisms are strictly separated and do not overlap, implying that plant immunity is not perceived as a continuous system that evolves to detect pathogenic invasion. Furthermore, the “zigzag” does not take into account endogenous DAMPs as inducers of immunity (Thomma et al., 2011) or the combined action of multiple receptor ligands. Another limitation is that according to the “zigzag” model, disease susceptibility derives from the suppression of the plant’s defence mechanisms during the evolutionary arms race between host and pathogens. This makes the “zigzag” model suitable for biotrophic plant pathogens, but fails to describe interactions with necrotrophs, insects, and mutualists (Cook et al., 2015). However, the “zigzag” model is potentially a versatile tool applying to most host–pathogen interactions, when suppressed immune responses are not taken as the only cause for disease susceptibility.

1.3.3.2 The Invasion Model

Alternatively, the Invasion Model is being proposed to discuss plant-invader interactions, as plants deploy a range of receptors that detect invasion patterns (IP), meaning immunogenic ligands produced by the invader and characterise invasion (Cook et al., 2015). Immunogenic ligands can derive by either the host or the invader and it is clear that the molecules responsible for these ligands can have diverse physiological functions. The host’s invasion pattern receptors (IPRs) detect the IP(s), which are either modified-self ligands that indicate invasion or externally encoded. The Invasion Model proposes the concept that any molecule can serve as a ligand, but the probability of creating an IPR-IP complex increases based on the molecular function of the ligand and its ability to facilitate symbiosis and accessibility. The concept of ligand-host receptor interactions can incorporate molecules ranging from flagellin-FLS2 to specific effector-R protein interactions, as well as DAMPs and modified guardees (Cook et al., 2015).

One important aspect of the Invasion Model is that it separates IPs from the molecules or processes that produce them (Cook et al., 2015). This allows researchers to describe the function of these molecules in a more accurate way, e.g., being important for host defence suppression or signalling, instead of labelling them as either MAMPs or effectors. Furthermore, the Model suggests that IP-triggered responses (IPTRs) do not necessarily result in immunity, rather, perception of an IP can result in either the end of symbiosis or the continuation of it. The outcome is depended on mechanisms defined by the perspective of the invader. Cook *et al*. (2015) support that the Invasion Model can describe host-invader interactions over a diverse set of systems, and aid in breeding for durable resistance via focusing on key receptor-ligand interactions.

1.3.3.3 A holistic view of the plant immune system

Recent reviews for advances in the field are pointing out the importance of a holistic view of the different immunogenic signals and the particular circumstances modulating plant immunity (**Figure 1.5**). For example, it has been recently shown that both PRRs and NLRs are needed to stimulate a strong immune response and fully induced disease resistance, whereas sole activation of NLRs only results in a mild immune response (Ngou et al., 2020). Other parameters that should be taken into account are the heterogeneity of immune responses within tissues and cells, the translational regulation during infection, and the hormonal crosstalk.

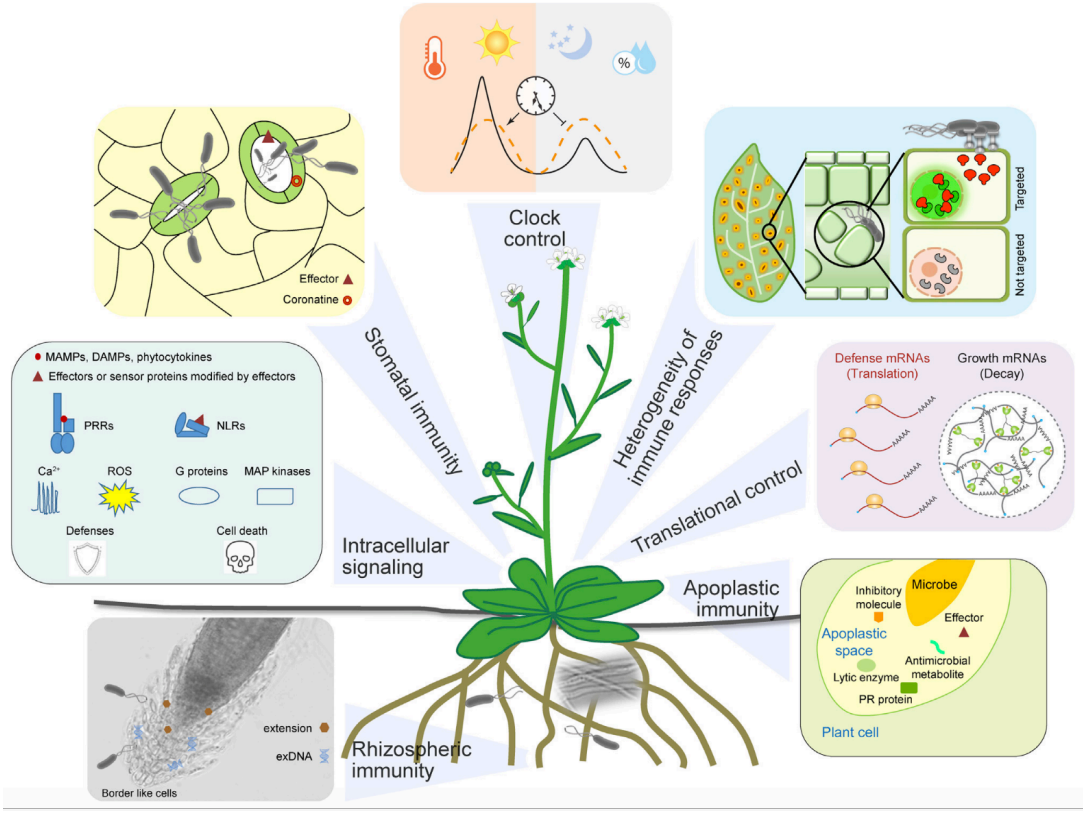

***Figure 1.5* Holistic point of view of the plant immune mechanisms.**

The front line of plant defence occurs in the stomata, rhizosphere, and apoplast. The recognition of MAMPs by the plant triggers stomatal closure to restrict the entry of microbes. To counteract this, microbes produce effectors and coronatine to promote stomatal opening. In roots, extensins, border and border-like cells, and extracellular DNAs (exDNAs) contribute to rhizospheric immunity that functions in attracting beneficial microbes while repelling pathogens. In the apoplastic space, plants produce lytic enzymes to release MAMPs and PR proteins and metabolites to restrict the proliferation of invading pathogens. Microbes can use effectors and inhibitory molecules to counteract plants' apoplastic immunity. The recognition of MAMPs and pathogen effectors activate PRRs on the cell surface and NLRs inside the cell to trigger PTI and ETI, respectively. These immune receptors signal through Ca2+, ROS, G proteins, and MAP kinase cascades to confer resistance, in which ETI is often associated with cell death. The induction of both PTI and ETI involves reprogramming of the plant proteome through the decay of housekeeping mRNAs (perhaps inside stress granules; circle) and the activation of translation of defence proteins. Heterogeneity exists in plant responses to infection due to differential pathogen distribution and host immune sensitivity. Plant immune responses are also regulated by the circadian clock, which not only helps plants anticipate infection but also gates immune responses when infection occurs to minimize effects on plant physiology and fitness. Figure and description belongs to (Zhang et al., 2020b).

The role of the circadian clock in controlling plant immunity is less obvious than in other plant functions, such as growth and reproduction, because defence against pathogens should occur regardless of the time of the day. However, the fact that both plants and some of the pathogens infecting them are dictated by the diurnal cycle of the Earth suggests that the function of the circadian clock can help the host anticipate infection when that can be predicted. The influence of the circadian clock has recently been proven to be a key mechanism regulating and/or being regulated by the disease triangle: a virulent pathogen, a susceptible host and a favourable environment (Zhang et al., 2020b).

Briefly, the discovery of circadian oscillations in basal levels of the plant defence hormones SA and JA, suggests that the circadian clock may have a role in plant defence (Goodspeed et al., 2012). Moreover, the circadian clock of plants has the ability to sense humidity, which may be of importance when it comes to battling pathogenic infection as high environmental humidity favours plant diseases (Xin et al., 2016). It has also been shown that SA treatment and daily humidity oscillation can increase the amplitude of the circadian clock, affecting plant defence via regulating water transport (Zhou et al., 2015). Thus, the circadian clock also regulates immune responses upon infection to minimize conflict with other physiological functions (Zhang et al., 2020b).

Another factor to be taken into account when describing a holistic view of plant defence responses is the function of small RNAs. Upon microbial infection, the host's immune responses rely on comprehensive and precise transcriptional reprogramming and communication between hosts and microbes (Huang et al., 2019). Eukaryotic small RNAs (sRNAs) are short non-coding regulatory molecules that induce RNA interference (RNAi). sRNAs and the RNAi machinery have emerged as key regulators of the reprogramming of gene expression during plant-microbe interactions, namely in plant immune responses and pathogen virulence. The majority of eukaryotes generate sRNAs via the ribonuclease III-like enzyme Dicer or Dicer-like (DCL) proteins. sRNAs are incorporated into Argonaute (AGO) proteins to induce gene

silencing using sequence specificity, mostly through mRNA cleavage and degradation, translational inhibition, or transcriptional gene silencing (Baulcombe, 2004).

Plant sRNAs can be classified as microRNAs (miRNAs) or small-interfering RNAs (siRNAs). miRNAs are generally derived from single-stranded RNA precursors with stem-loop structures, whereas siRNAs are processed from long double-stranded RNAs (dsRNAs) deriving from invert repeats, sense-antisense transcript pairs or products of RNA-dependent RNA polymerases (RDRs). Plant siRNAs can be further divided into trans-acting siRNAs (ta-siRNAs) or secondary phased siRNAs (phasiRNAs), natural antisense transcripts-derived siRNAs (nat-siRNAs), heterochromatic siRNAs (hc-siRNAs), and long siRNAs (lsiRNAs) based on their distinct biogenesis pathways (Katiyar-Agarwal and Jin, 2010).

Host RNAi machinery is highly regulated during microbial infection and contributes to reprogramming gene expression and balancing plant immunity and growth. Different classes of plant endogenous sRNAs are involved in regulating immune responses. *Arabidopsis* miR393 is the first miRNA found to participate in plant immunity by activating PTI, as it is induced by flg22 and silences auxin receptors to turn down the auxin signalling pathway (Navarro et al., 2006). nat-siRNAATGB2 is the first siRNA reported to regulate plant immunity by silencing a negative regulator of plant defence and promoting ETI upon infection. It derives from the overlap region of an antisense transcript pair and is highly and specifically induced by the bacterial pathogen *Pst* DC3000 carrying the effector AvrRpt2 (Katiyar-Agarwal et al., 2006).

Endogenous sRNAs have a key role in limiting the fitness cost associated with immune responses, like in the case of *Arabidopsis* miR8633p which can fine-tune the timing and amplitude of immune responses during infection, as well as sequentially silence both negative and positive regulators of plant immunity (Niu et al., 2016). Moreover, expression of some NLR and PRR genes is tightly suppressed by miRNAs and secondary phasiRNAs when pathogens are not present, in order to avoid autoimmune responses and to save energy for plant

growth. When pathogens are present, the 22 nt miRNA and the phasiRNAs are downregulated, leading to the upregulation of NLRs and subsequent activation of immune responses (Fei et al., 2013). In addition, many NLR are controlled by hc-siRNA-mediated epigenetic regulation (RNA- directed DNA methylation, RdDM) due to the fact that the specific NLR loci or clusters are associated with transposable elements or repeats (Cambiagno et al., 2018).

Some pathogens have evolved effector proteins to inhibit the host RNAi pathways as a response to the importance of the plant RNAi machinery and sRNAs in pathogen defence (Huang et al., 2019). *Pst* DC3000 produces several effector proteins that act as bacterial suppressors of RNA silencing (BSRs) to inhibit host RNAi and overcome PTI (Navarro et al., 2008). For example, effector AvrPto possibly interferes with the processing of miRNA precursors of some host miRNAs, thus suppressing their accumulation. Additionally, microbe-derived sRNAs are important in regulating pathogen virulence, especially in fungi and oomycetes. While most sRNAs function endogenously, some can travel between hosts and microbes, using a mechanism called ‘‘cross-kingdom RNAi’’ to silence genes *in trans* in interacting organisms. During the co-evolutionary arms race between fungi and plants, some fungi developed the ability to send sRNAs as effector molecules into plant cells to silence plant immunity genes as a novel virulence mechanism (Huang et al., 2019). Finally, plants also transport sRNAs, mainly using extracellular vesicles, into the pathogens to suppress virulence-related genes. These discoveries have provided new tools for crop protection, as the development of effective disease management in economically important crops is more critical than ever due to climate change that favours diseases in the field.

1.4 NB-LRR resistance proteins in plant defence response

The most commonly known R proteins in plants belong to the NLR superfamily. NLRs are ATPases belonging to the STAND (Signal Transduction ATPases with Numerous Domains) subclade of the AAA-ATPase superfamily. STAND proteins are regulated by nucleotide binding, nucleotide hydrolysis

and intramolecular domain interactions (Eitas and Dangl, 2010). NLRs first appeared in green algae and although both plant and animal NLRs share common structural features, our current perception is that they evolved independently (Jones et al., 2016). The main structure of NLRs is characterized by a centrally located NBD, a variable number of highly polymorphic C-terminal LRRs and diverse N-termini.

The N-terminal domain classifies *A. thaliana* NLRs into three major groups (**Figure 1.6**): TIR-NB-LRR (TNL) proteins with a Toll Interleukin-1 Receptor (TIR) domain, CC-NB-LRR (CNL) proteins carrying a coiled coil (CC) domain, and RPW8-NB-ARC-LRR (RNL) proteins, carrying a CCR domain (RPW8-like CC, resistance to powdery mildew 8) (Shao et al., 2016). RNLs are a small class of NLRs highly conserved across different plant species, as opposed to fast evolving TNLs and CNLs, classified into the *N. benthamiana* N REQUIREMENT GENE1 (NRG1) and ACTIVATED DISEASE RESISTANCE1 (ADR1) subclasses (Jubic et al., 2019). The LRR domain is usually responsible for direct effector recognition, although exceptions have been reported (Cui et al., 2015). The NBD defines the active/inactive state of the NLR upon pathogen recognition. A conformational change allows the bound ADP to be exchanged for ATP, switching from the NLR “off” face to the active “on” state which initiates downstream signalling (Bonardi et al., 2012). ATP hydrolysis regulates this switch and ensures return to the inactive state. The TIR and CC domains function in signalling (Jubic et al., 2019), whereas the TIR domain has been shown to play an important antimicrobial role in plants (Eitas and Dangl, 2010) and animals (Jenkins and Mansell, 2010) and to be involved in the formation of homodimers required to activate defence signalling (Burch-Smith and Dinesh-Kumar, 2007). NLR-triggered immunity is known to cause induction of HR leading to programmed cell death.

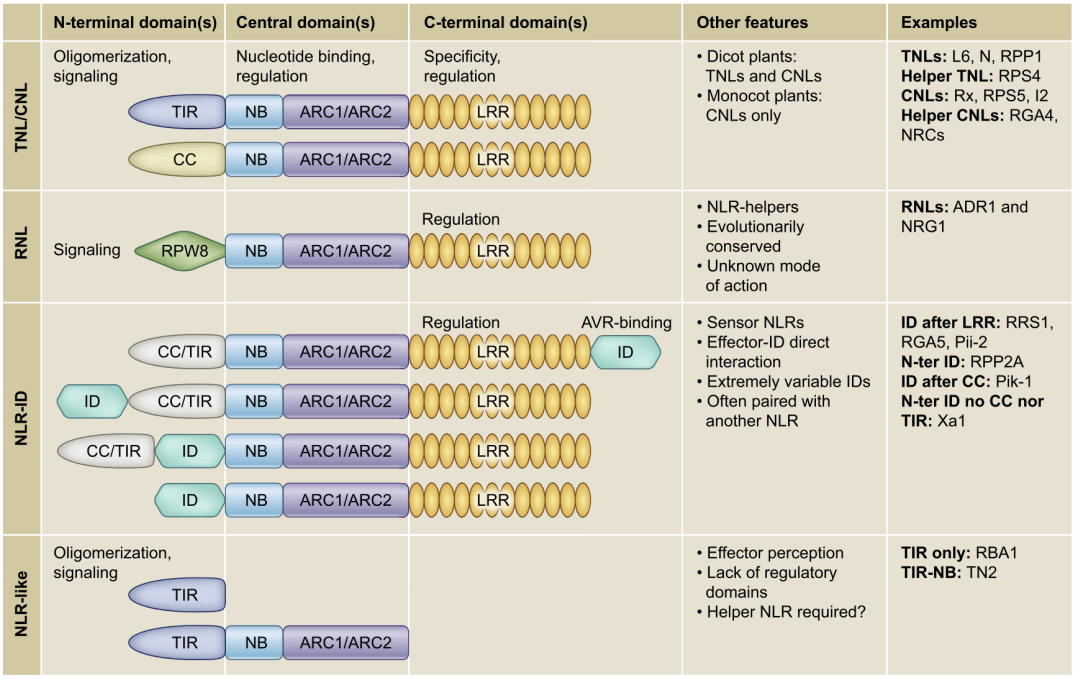

***Figure 1.6* Flexibility and diversity of the architecture of plant NLRs.**

Predicted and experimentally documented functions or properties of individual domains are indicated, as well as particular features and examples. Domains are not drawn to scale. CC, coiled-coil; TIR, toll/interleukin-1 receptor; NB, nucleotide binding; ARC1/2, Apaf-1, R-gene products, and CED4; LRR, leucine-rich repeat; ID, integrated domain; RPW8, resistance to powdery mildew 8; NLR, nucleotide- binding and leucine-rich repeat-containing protein; TNL, TIR-NLR; CNL, CC-NLR; RNL, RPW8-NLR. Figure and legend belong to (Cesari, 2018).

Recent findings indicate that NLRs play diverse roles in the perception of effectors and immune signalling. Many TNLs and CNLs work in pairs, one of them mainly being a sensor for effector presence while the other one acts as a helper to trigger signalling (Adachi et al., 2019a). However, some of them can act as singletons in effector perception and signalling. RNLs are known to function as facilitators of SA production or HR, acting downstream of some CNLs and all known TNLs to date (Zhou and Zhang, 2020). In addition to these NLR classes, plants from the *Solanaceae* family have an extra, slow-evolving class of CNLs called NLR-REQUIRED FOR CELL DEATH (NRCs), required for the function of different sensor NLRs (Wu et al., 2017).

NLR interacting proteins can be divided into seven major categories based on their function, which is defined by the different domains (Sun et al., 2020).

Those interactors can be transcriptional regulators as signalling components in NLR-mediated immunity, which is probably the most commonly observed class. It includes examples of WRKY1 and MYB6 which interact with the barley CNL mildew A 10 (MLA10) (Chang et al., 2013), which confers resistance to powdery mildew, as well as transcriptional regulators interacting with the *A. thaliana* TNL, suppressor of *npr1-1* (non expressor of pathogenesis1-1) constitutive 1 (SNC1) (Xu et al., 2014). Another class of NLR-interacting proteins are kinases and pseudokinases acting as guardees or decoys, as the case of the *A. thaliana* ZAR1 (HOPZ-ACTIVATED RESISTANCE 1) NLR protein, the interactors of which have been extensively described (Wang et al., 2015). Molecular chaperones and co-chaperones regulate the stability of NLRs, like the heat shock protein 90 (HSP90) family members regulating different NLR-mediated defence responses (Huang et al., 2014; Hubert et al., 2003). Several small GTPase-related (guanosine triphosphate hydrolase) proteins act as downstream signalling components of NLR-mediated immunity. Additionally, there are other types of NLR interactors that are vital for immune responses, such as the lipase-like protein EDS1 (ENHANCED DISEASE SUSCEPTIBILITY 1) that acts downstream of many TNLs and CLNs (Aarts et al., 1998; Xiao et al., 2005).

It is often the case that different NLRs work together to mediate plant immunity, either by functioning as paired NLRs or as sensor/helper NLRs. Paired NLRs genes are located at the same genomic locus adjacently arranged in a head-to-head orientation under the regulation of the same promoter (Baggs et al., 2017). The most commonly known cases of paired NLRs include the *A. thaliana* RRS1/RPS4 pair (RESISTANCE TO RALSTONIA SOLANACEARUM 1/ RESISTANCE TO PSEUDOMONAS SYRINGAE 4) (Williams *et al.*, 2014; Le Roux *et al.*, 2015; Sarris *et al.*, 2015), the RRS1B/RPS4B (Saucet et al., 2015), as well as the rice pairs RGA5/RGA4 (Cesari et al., 2013; Césari et al., 2014) and Pik-1/Pik-2 (Maqbool et al., 2015). Usually, the sensor NLR has an ID (Integrated Domain), which likely interacts with one pathogen effector, whereas the canonical NLR acts as a signal transducer to activate defence mechanisms (Zhang et al., 2017). Sensor NLR IDs are mainly WRKY domains and protein kinases, but rare types of IDs are

also quite frequent, and it is hypothesized that they sense targets of many as yet uncharacterized effectors (Sarris et al., 2016).

In other cases, instead of a canonical NLR there is a helper NLR, which can act downstream of the sensor NLR, as in the case of ADR1 during RPS2-(RESISTANCE TO PSEUDOMONAS SYRINGAE 2) and RPP4-(RECOGNITION OF PERONOSPORA PARASITICA 4) mediated immunity (Bonardi et al., 2017), as well as the NRG1 and NRC families (Sun et al., 2020). Interestingly enough, all helper NLRs identified to date are CNLs, they are not necessarily located in the same genomic locus, and the mechanisms by which sensor NLRs transduce the signal to them are unknown. A hypothesis is that helper NLRs are believed to be key components to complex NLR network conferring immunity to different pathogens (Adachi et al., 2019a; Wu et al., 2017).

Furthermore, many studies have indicated that E3 ubiquitin ligases regulate the stability of NLRs, facilitating immune responses (Duplan and Rivas, 2014). The ubiquitin-mediated protein degradation pathway keeps NLRs under tight regulation to ensure NLR homeostasis, as overaccumulation of NLR proteins in the plant cell can often lead to unnecessary activation and cause significant growth and yield issues (Li et al., 2015). E3 ligases interact with NLRs to prevent accumulation when there's no pathogen invasion, but pathogen effectors have the ability to disrupt this interaction to release NLRs and induce a defence response (Wang et al., 2016). It is of great importance to future prospects of NLR engineering in crop plants to take into account the sophisticated and fine-tuned activity by which they are naturally regulated by the plants, to maintain the equilibrium between disease resistance and fitness cost associated with their activation (Sun et al., 2020).

The most recent breakthroughs reported on the function of NLRs include findings indicating that dimerization of the TIR domain confers NADase activity on TNLs, and this reaction is producing an unidentified metabolite(s) that may act as a signal triggering EDS1-mediated immunity, potentially activating NRGs and ADRs through mechanisms that cannot yet be defined (Horsefield

et al., 2019; Wan et al., 2019). Moreover, ZAR1 (a singleton NLR with a canonical CC domain), has been shown to form a resistosome: a pentameric complex occurring through oligomerization, when it senses effector activity (Jizong Wang et al., 2019a, 2019b). The N-terminal a1 helix of ZAR1 in this complex forms a funnel-shaped structure, creating a pore-like structure on the plasma membrane which is essential for cell death and antibacterial immunity. Nevertheless, the specifics of how this pore facilitates immune responses and cell death remain largely unknown.

In mammals, it is a common immunological strategy of activated NLR receptors to form specific macromolecular structures in order to protect organisms against pathogen invasion (Chai and Shi, 2014). However, such structures have not been observed in plants until 2019, when the first plant 'resistosome' structure was reported (Jizong Wang et al., 2019a, 2019b), showing insightful structural similarities to mammalian apoptosome and inflammasome structures (Mermigka et al., 2020). The evidence of plants being able to form a resistosome is quite exciting and the signalling mechanism described appears to fit functionally a group of CNLs, such as the NRC proteins of *N. benthamiana* as well as some canonical CNLs (Adachi et al., 2019b). It is now speculated that the confirmation of the first plant NLR complex has the potential to provide plant immunologists with more information regarding the specific mechanisms underlying the role of NLRs in signal transduction upon pathogen perception, and in the long run, assist the generation of crops with durable resistance to pathogens.

1.4.1 TIR-NB truncated receptors and the role of TIR domain in plant immunity

As it was previously discussed, almost half of *A. thaliana* genes coding for NLR proteins are naturally organised in unevenly distributed clusters across the genome (Meyers et al., 2003; Van de Weyer et al., 2019). Duplication of genes in *NLR* clusters offers a great source of genetic variation and most importantly, it allows functional variation (Barragan, 2021). Furthermore, when an *NLR* gene moves to an unlinked genomic locus, away from its cluster, it

has the potential to develop a new function instead of preserving its original function (Baumgarten et al., 2003; Leister, 2004). Therefore, the plant has the potential to expand the repertoire of pathogen effectors it can recognise through neofunctionalization of duplicated/translocated *NLR* genes (Botella et al., 1998; Kim et al., 2017).

It is now well evidenced that apart from the full length NLR immune receptors in plants, there is an additional group of atypical or "truncated" NLRs that lack LRR domain. Two families of proteins containing the TIR domain were identified in the *A. thaliana* Col-0 accession by Meyers et al. in 2002, the TIR-X (TX) family, which also lacks the NBD domain, and the TIR-NBD (TN) family only lacking the LRR domain. According to them, both families together encode for approximately 50 Col-0 genes, 20 of which belong to the *TN* family and 4 of which appear to be pseudogenes. At the same time, phylogenetic analysis suggests that the increased number of those truncated receptors are likely the result of multiple duplication events in the *Arabidopsis* genome. The fact that basal level of expression has been detected for most of the *TN* family genes and about half of the *TX*, indicated that they produce functional proteins, likely analogous to the TIR proteins in animal innate immunity. Furthermore, truncated *NLRs* are abundant in coniferous plants, they can be found in mosses and have also been identified in *Medicago* and soybean (Cannon et al., 2002).

TN genes have been found to cluster with *TNL* genes in the *Arabidopsis* Col-0 genome (**Figure 1.7**). It is generally suggested that linked genes are required to initiate a defence response in plants (Eitas and Dangl, 2010). Previous studies indicate that despite lacking the LRR domain, TN proteins could potentially act in guard complexes monitoring pathogen effectors (Nandety et al., 2013). Although they are implicated in plant immunity, their specific function is yet to be understood. The TIR domain, besides playing an antimicrobial role in both plants and animals (Eitas and Dangl, 2010; Jenkins and Mansell, 2010), it is also involved in the oligomerization of proteins, leading to defence signalling (Burch-Smith et al., 2007). The oligomerization of two different interfaces, equally important for self-association and defence

signalling has been observed in many plant TIR domains following their structural characterization, suggesting that *TN* or *TNL* genes may follow a common TIR-dependent mechanism to initiate defence signalling (Nishimura et al., 2017; Zhang et al., 2017). Moreover, it has been shown that overexpression of TX and TN proteins can trigger EDS1-dependent cell death (Nandety et al., 2013).

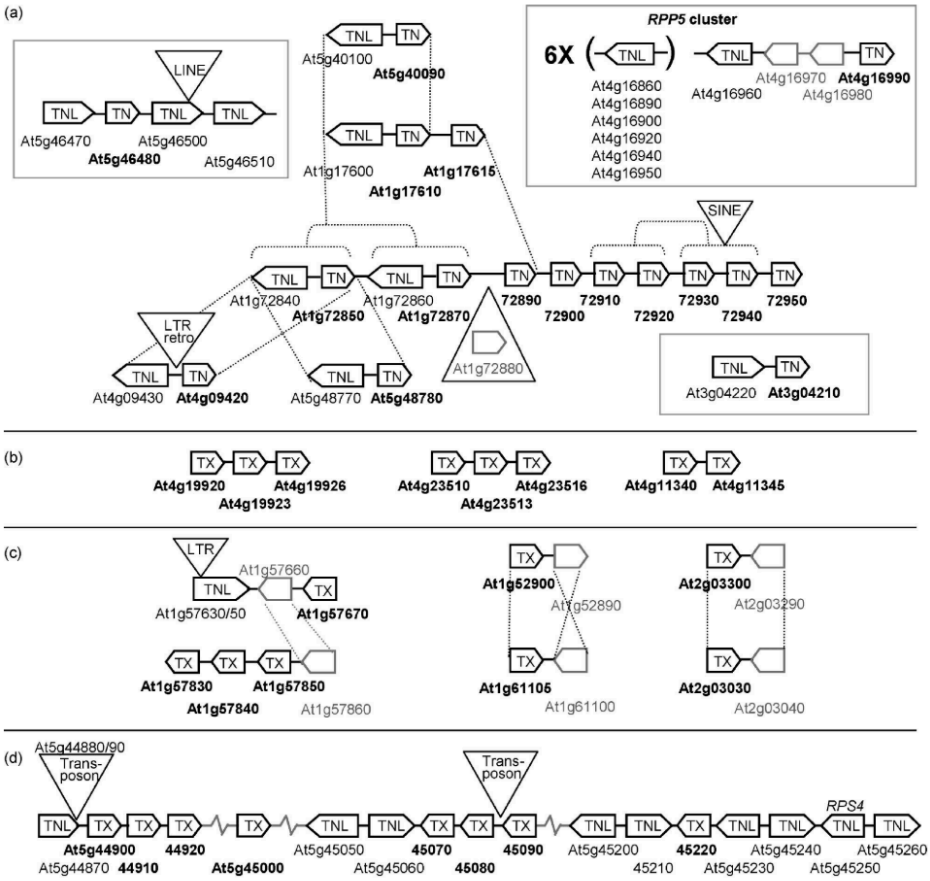

***Figure 1.7 TN* and *TNL* genes form gene clusters in the *A. thaliana* Col-0 accession.**

Arrangements of physically clustered genes are shown with orientations of the genes indicated by the direction of each box. Unrelated genes are indicated in grey. *TX* and *TN* genes shown in bold. 'LTR' is a long-terminal repeat retrotransposon. 'SINE' is a short, interspersed element and 'LINE' is a long, interspersed repetitive element. Dotted lines indicate blocks of homologous sequences that have been duplicated to local or more distant physical positions. Chromosome identifiers in some names have been removed to accommodate the labels in the diagram. (a) *TN* genes found adjacent to *TNL* genes. (b) Clusters of genes may result from localized duplications. (c) Duplications within the genome including adjacent, unrelated genes. (d) A complex cluster of *TX* and *TNL* genes. Figure and legend belong to (Meyers et al., 2002).

Although plant *TN* and *TX f*amilies have not been extensively researched and characterized to date, there are a few examples of such truncated receptors that provide plant immunologists with a better understanding of their role in plant immunity. Nishimura et al. (2017) isolated the gene Response to the Bacterial type III effector protein HopBA1 (RBA1), which appears to be a *TX* pseudogene in the Col-0 genome, but in other *A. thaliana* accessions it encodes for a protein missing all other NLR domains but the TIR domain. They showed that the self-interaction and association of RBA1 with HopBA1 is sufficient to trigger cell death, supporting that TIR dimerization activates signalling. The RBA1 findings suggest that distinct structural interfaces lead to a more complex model of TIR oligomerization. In parallel, Roth et al. (2017) demonstrated the ability of the truncated NLR protein TN13 to selectively bind to *Arabidopsis* IMPORTIN-a3/MODIFIER OF SNC1 6 (MOS6) *in planta*, thus being implicated in plant immune responses regulated by IMPORTIN-a3/MOS6. They hypothesize that upon pathogen perception, TN13 is released from the ER membrane and translocated to the nucleus as to facilitate defence signalling.

Another example is the TN2 protein which guards a potential target of unidentified fungal effectors, the plant EXO70B1 protein (Liu et al., 2017). TN2 requires a calcium-dependent protein kinase to function and, which may be targeted by unknown fungal effectors. This is analogous to the RPS2/ RIN4 (RPM1-interacting protein 4) NLR/guardee model, except that in the TN2 case, the canonical LRR domain is missing (Cesari, 2018). TN proteins have also shown to be responsible for the regulation of full-length TNLs. It has been recently shown that the TNL Suppressors of *chs1-2*,3 (SOC3) pairs with the TN proteins Chilling Sensitive 1 (CHS1) or TN2 to ensure the homeostasis of the Senescence-associated E3 ubiquitin ligase 1 (SAUL1) (Liang et al., 2019). More specifically, the pair SOC3-TN2 monitors the overaccumulation of SAUL1, whereas SOC3-CHS1 prevents SAUL1 from depletion. Interestingly enough, SOC3, CHS1 and TN2 are located head-to-tail on the genome, a fact that could imply transcriptional co-regulation.

Recently, it was discovered that the animal TIR protein SARM1 (sterile alpha and TIR motif-containing 1) has enzymatic activity (**Figure 1.8**), functioning as NAD+-hydrolase, which is dependent on oligomerization and TIR-TIR associations (Essuman et al., 2017). It was also shown that a conserved glutamic acid (E642) required for NAD+-hydrolysis was present in the active site of the SARM TIR- domain (Horsefield et al., 2019) . When NAD+ is hydrolysed by SARM1, the products generated by the enzymatic reaction are ADPR (ADP-ribose), cyclic ADPR (c-ADPR) and NAM (nicotinamide) (**Figure 1.8**) (Essuman et al., 2017). cADPR and ADPR are known to mobilize Ca2+, therefore they may affect Ca2+ signalling (Zhao et al., 2019). Furthermore, the crystal structure generated by Horsefield et al. in 2019 of the SARM1 TIR domain showed that it is conserved across plant and prokaryotic TIR-domains. When SARM1 was transiently expressed in the leaves of *N. benthamiana*, it triggered cell death, which is thought to require NADase function but at the same time, it occurs independently of the plant TIR-signalling proteins EDS1 and NRG1 (Horsefield et al., 2019; Wan et al., 2019).

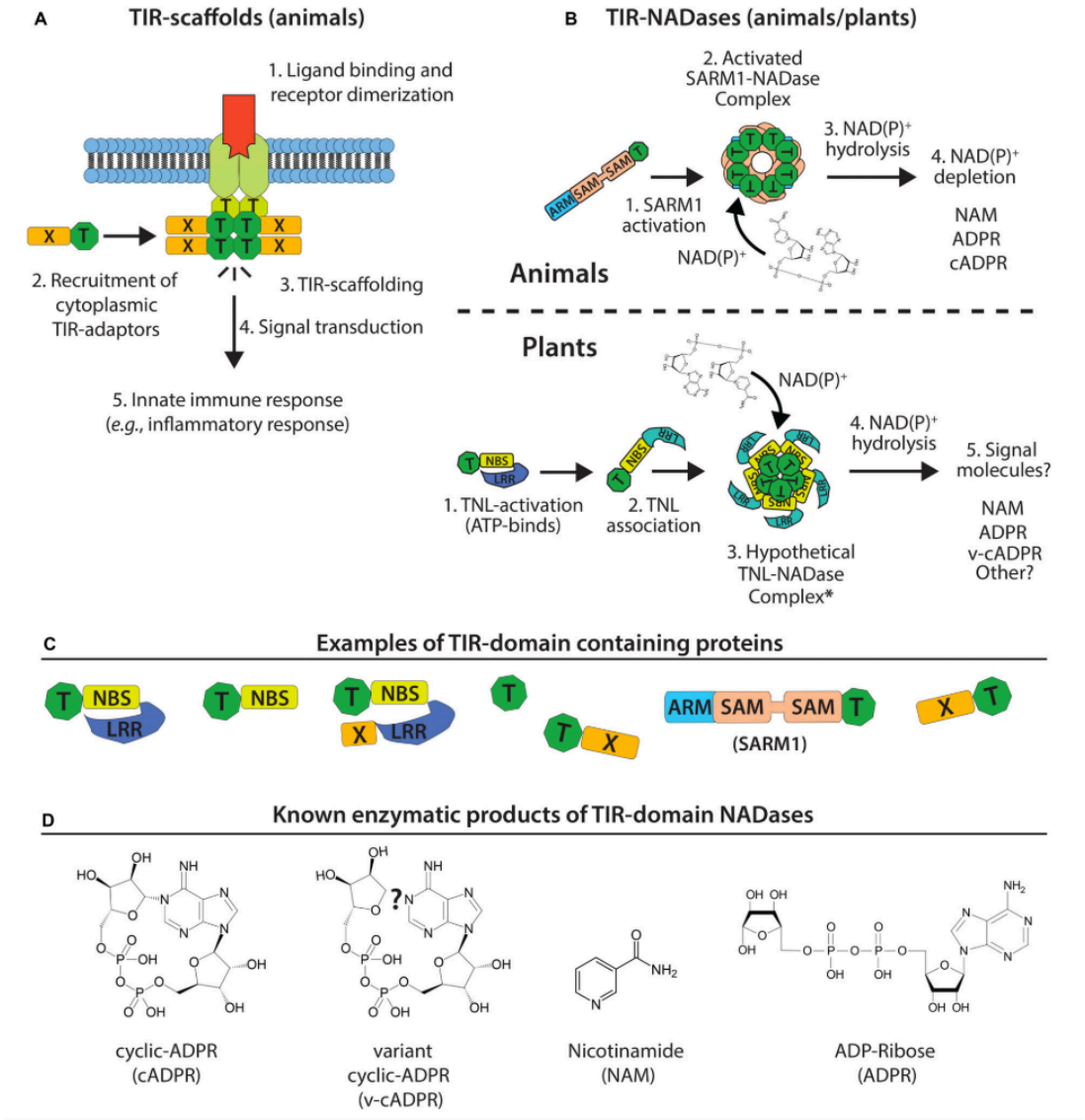

Figure 1.8 **Model of TIR-domain activity in animals and plants.**

(A) TIR-scaffold function in animals: TIR-TIR interactions promote signal complex formation and innate immune signal transduction. (B) Top: animal TIR NADases (e.g., SARM1) assemble into high order complexes, and hydrolyze NAD(P)+ substrate and alter NAD(P)+ pools. Bottom: assembly of plant TIR-domains into hypothetical NADase complex (resistosome-like?) and generation of immunomodulatory signals. (C) Numerous TIR-domain configurations are present in animal, plant, and bacterial proteins. Plant TIR-domains are often found in modular NBS-LRRs, TIR-NBS, TIR-X or TIR-only proteins. -X corresponds to atypical or undefined domains. The animal SARM1 TIR is located at the C-terminus; the SARM1 SAM-domains promote oligomerization. (D) Known products of TIR NADases; plant TIRs produce variant cyclic-ADPR (v-cADPR), whose structure is currently unknown. Figure and legend belong to (Bayless and Nishimura, 2020)

It was recently indicated that plant TIRs may also demonstrate NAD+ hydrolase activity required for immune signal transduction (**Figure 1.8**) (Horsefield et al., 2019; Wan et al., 2019). The putative catalytic glutamate characterising NADase activity was shown to be highly conserved (~90%) across the TIR domains of all available plant genomes (Wan et al., 2019), whereas the remaining 10% seem to be 'sensor- type' TNLs that lack the ability to trigger cell death in the absence of their paired TNL (Wan et al., 2019). TIR-domains originating from full length TNLs and TX proteins demonstrated NADase cleavage activity *in vitro*, using NAD+ and NADP+ as a substrate (Horsefield et al., 2019; Wan et al., 2019). However, the products deriving from plant TIR NADse activity where slightly different than the ones from animal SARM1, as they included NAM, ADPR, and v-cADPR (variant cADPR). Production of cyclic-ADPR was not detected in the case of plant TIRs, while v-cADPR is a different compound with unknown chemical structure (**Fig. 1.8**), that has a near identical high-performance liquid chromatography (HPLC) retention time and molecular mass to the product of an archaeal TIR, TcpO (Essuman et al., 2018; Wan et al., 2019).

Two interfaces are known to facilitate TIR-TIR self-association in plants, the AE and DE, formed by pairs of alpha helices (α) that are necessary to activate HR (Williams et al., 2016). The strength of TIR-TIR self-associations in plant TIR domains varies while sometimes it is indicative of the downstream function (Zhang et al., 2017). Both AE and DE interfaces are required in the case of RBA1 self-association and HR induction (Nishimura et al., 2017). Similar to HR induction and activation of defence mechanisms, successful enzymatic activity of the plant TIR NADase function requires both AE and DE interfaces, as it seems a higher-order oligomer formation is a prerequisite (Horsefield et al., 2019; Wan et al., 2019). As there is no available structure of a full length TNL to date, it remains unknown how the NBS facilitating TNL oligomerization affects TIR–TIR associations.

Although in the case of animal SARM1 the depletion of NAD+ seems to be initiating cell death, it is evident that plant TIRs do not cause considerable NAD+ depletion in planta (Wan et al., 2019). It is speculated that the

compounds generated by plant TIR NAD+ consumption may be signalling downstream immune components. Furthermore, plant TIRs produced v-cADPR and not c-ADPR, which was also detected after activation of RBA1 upon recognition of the *Pst* DC3000 effector HopBA1 (Wan et al., 2019). Additionally, activated TIRs in planta did not require EDS1 or NRG1, which are known signalling components downstream of TIR containing proteins (Wan et al., 2019), which indicates that v-cADPR accumulation occurs upstream of both known signalling mechanisms initiated by TIR proteins and HR. Interestingly enough, generation of v-cADPR by TIR-domains originating from full length TNLs was significantly lower (approximately 100-fold) than when using TIR-only proteins in planta (Wan et al., 2019).

Similar to other NAD+-deriving compounds, like cADPR, ADPR, and NAAD which are believed to be Ca2+ channel activators, thus facilitating important immune response signalling and HR, v-cADPR could also exhibit signalling properties (Grant et al., 2000; Marcec et al., 2019). Since the production of v-cADPR is so far correlated to TIR enzymatic function, it can serve as a biomarker for plant TIR activity. Nevertheless, there is still not enough evidence to support if it is sufficient to trigger cell death and defence, since it is still to be detected *in planta* (Horsefield et al., 2019). It is speculated that EDS1- being a downstream component of TIR-proteins signalling – would make a reasonable target of v-cADPR signal transduction, but it is yet to be understood how this compound is implicated in plant immune responses.

1.5 Working towards generating plants with durable resistance against plant pathogens

Scientific research and the availability of model pathosystems have made significant progress in describing the plant immune system, but there is admittedly a long way to cover to connect all the dots. The host-pathogen arms race coevolution can be described as a futile cycle where the pathogen is constantly trying to overcome the defence mechanisms of its host plant to prevail, and the plan as a response is evolving its surveillance mechanisms to keep the pathogen at bay. As discussed so far, NLRs are the most

sophisticated and fine-tuned weapon the plant has employed to combat pathogen invasion. Unfortunately, the deployment of most NLRs in monoculture means their function often becomes redundant, due to the fact that it favours pathogen variants that have already lost or mutated the targeted effectors (Dangl et al., 2013). Since effectors are not the only cause of the pathogen's virulence, the pathogen can often lose effector genes with a lesser cost to its virulence, especially in cases where the same host signalling pathways are targeted by many different effectors. However, as the pathogen deploys new effectors or acquires mutations to the already existing ones, the chances of new outbreaks in the field increasing loss of crops due to disease, are rising (Dangl et al., 2013).

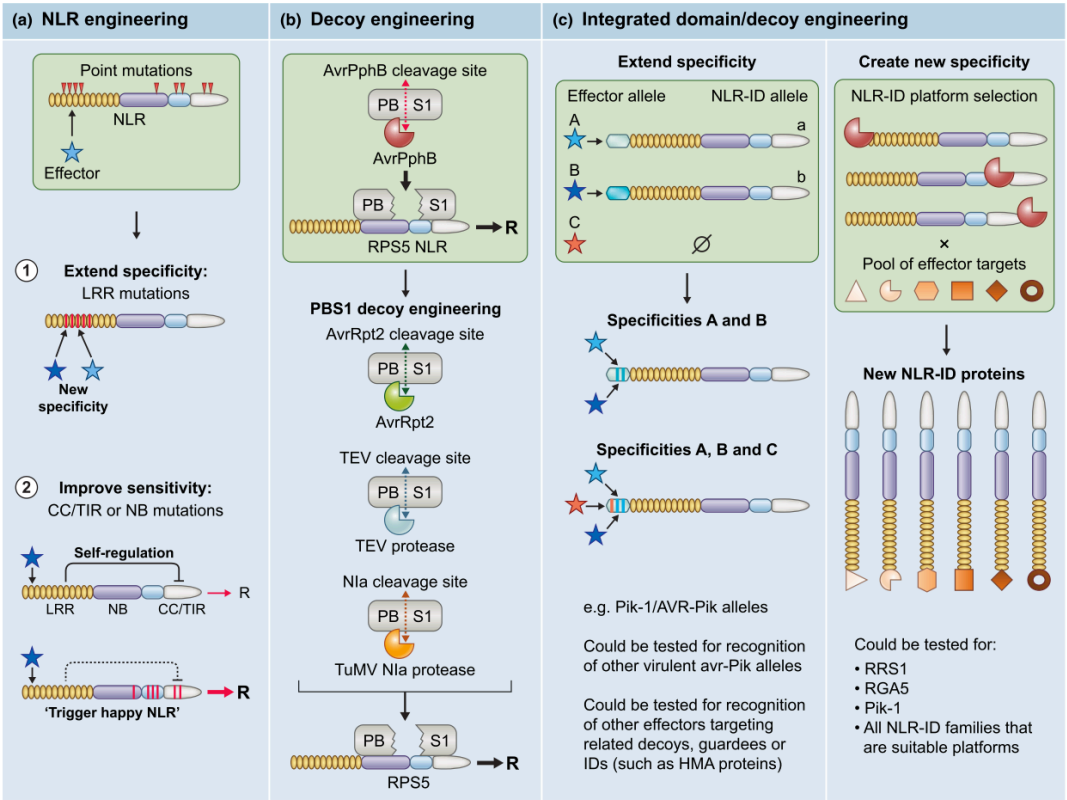

Figure 1.9 **NLR-engineered strategies for disease resistance, summarised by Stella Cesari (2017, *New Phytologist*).**

(a) Targeted point mutations or mutational screens of NLRs can extend their recognition specificities/ activation properties. (b) Decoy proteins can be engineered to fit other post-translational modifications, indicating effector activity. (c) Engineering NLR IDs can either extend recognition specificity or create new specificities.

To date, there are only a few examples reported of engineering NLRs (**Figure 1.9**) into plants to enhance immunity against disease (Cesari, 2018). However, advances in biotechnology and gene engineering have introduces a variety of possible approaches. One of them is to genetically modify the NLR protein, mainly via the changing amino acids of the LRR domain, to alter its specificity in recognising effectors, like in the case of potato R3a protein which was screened for mutations that would enable it to recognise *Phytophthora infestans* strains that secrete the effector AVR3aEM isoform besides the AVR3aKI ones that it naturally recognises (Segretin et al., 2014). Another strategy is to enhance the strength of immune response by modifying NLR activation sensitivity, as it was demonstrated via altering two amino acids in the NB domain of the Pm3 protein of the wheat powdery mildew (Stirnweis et al., 2014). Both strategies can be simultaneously employed, as Harris et al. showed in 2013 with the Rx protein of the potato virus X.

Decoy engineering is also a considerable approach, as decoy proteins can be modified to sense types of post-translational modifications caused by effectors, thus broadening the spectrum of recognisable effectors. One example is engineering the protease cleavage site of PBS1 decoy protein of *A. thaliana* to be recognised by more effector proteases than AvrPphB, a modification that is later detected by the NLR RPS5 (Kim et al., 2016; Shao et al., 2003). At the same time, IDs in NLRs seem a promising but challenging choice for NLR modification, as mutations in the ID has the potential to produce new specificities but it can also affect their structure and function (Ortiz et al., 2017).

Despite the considerable effort, engineering novel NLR recognition specificities remains challenging. However, full length NLRs are not the only plant proteins implicated in immune responses. As described in **Section 1.4.1**, truncated NLR receptors are arising as important defence players that can potentially provide more options regarding the engineering of crop plants with enhanced disease resistance.

1.6 Project background, aims and objectives

When describing the evolution of models describing the plant immune system over the years, one of the keys points that became more and more clear to researchers by emerging evidence was that the assumption of the MTI-ETI dichotomy does not accurately fit the plant defence responses (Cook et al., 2015). The perception of plant immunity as a continuous system that evolves to detect pathogenic invasion takes into account the overlapping of mechanisms and different responses that formulate plant immunity. A key mechanism that takes place upon detecting pathogenic invasion is transcriptional reprogramming of the host. Pathogen-derived effector molecules are secreted into the plant host by the pathogen to suppress defence responses, acting both on the transcriptional and posttranscriptional level.

The attempt to discriminate between MTI- and ETS-associated transcriptional reprogramming can be challenging, but it is considered essential in understanding disease and defence responses. The *A. thaliana* - *Pst* DC3000 pathosystem is ideally suited to pinpoint the different transcriptional processes associated with MTI and ETS. *Pst* DC3000 is highly virulent on *Arabidopsis* in the lab and uses the T3SS to directly deliver 28 effector proteins in the host. The non-pathogenic mutant strain DC3000*hrpA*- (hereafter *hrpA*) mutants activate MTI but cannot form a T3SS to deliver effectors to suppress it. A transcriptomics (microarrays) study contacted by Lewis *et al.*, (2015) in *A. thaliana* Col-0 plants following challenge with *Pst* DC3000 and *hrpA* investigated genome-wide expression changes over a high-resolution time course. Detailed comparisons between mock, *hrpA,* and DC3000 treatments helped the authors of the study to capture gene expression differences and establish, among other things, causal links between the activities of effectors and the suppression of MTI, and identify processes specifically targeted by effector molecules. Furthermore, they showed that most genes implicated in disease or defence are induced within 6h post-infection (Lewis et al., 2015).

Further computational analysis of this data set provided with new insight into early transcriptional events triggered by effector delivery. The Murray Grant group (University of Warwick), who were part of the production of this information-rich dataset, focused on some of the preliminary data regarding the *A. thaliana TN* family. The data (**Figures 1.10 and 1.11b**) suggests that the expression levels of three *TN* genes (*AT1G72920, AT1G72940, AT1G72950*) are upregulated following infections with *Pst* DC3000, but not when plants were infected with *hrpA,* which is unable to deliver effectors due to the lack of a type III secretion system (Lewis et al., 2015)**.** Based on this, they initially hypothesized that bacterial-delivered effectors upregulate the three *TN* genes as a virulent mechanism aiming to dampen NLR- mediated resistance.

We further hypothesized that specific bacterial effectors upregulate the expression of these *TN* genes, directly or indirectly. TN proteins may share domain homology with full length TNLs, which could potentially allow them to form heterodimers. TNLs use either their LRR (direct recognition) or TIR domain (indirect recognition) to recognise effector molecules, thus triggering ETI and leading to defence activation. By forming heterodimers, TNs could act as negative regulators of immunity, preventing the TNLs from recognising the effectors, thus disrupting ETI. However, as new information arose regarding the function of TIR domain and its enzymatic activity as NAD+ hydrolase, the *TN* genes being activated upon effector delivery to facilitate defence signal transduction also became a possibility. Therefore, the focus of this project shifted in identifying the role of these truncated *A. thaliana* NLR genes in plant immunity and unravelling the molecular mechanism underlying the direct or indirect induction of their expression when effector molecules are delivered by the plant pathogen *Pst* DC3000.

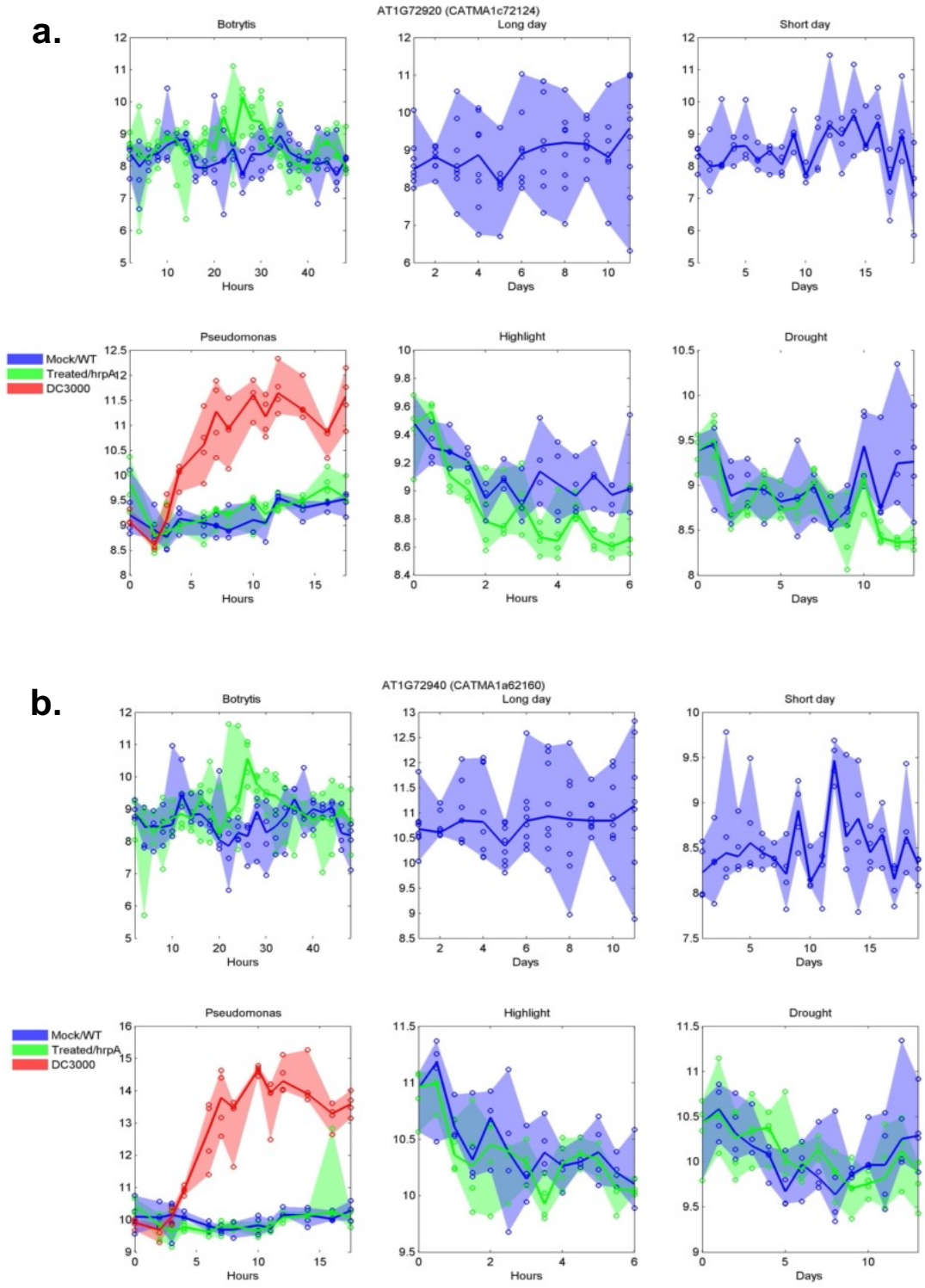

Figure 1.10 **Transcriptional profiling of *AT1G72920* and *AT1G72940* in Col-0 under biotic and abiotic stresses.**

A. thaliana Col-0 adult plants were subjected to a variety of biotic (*B. cinerea*, *Pst* DC3000, *Pst* DC3000 *hrpA*) and abiotic (long day, short day, highlight, drought) treatments and/or conditions to identify pathogenesis-related gene expression. The expression levels of genes *AT1G72920* **(a.)** and *AT1G72940* **(b.)** increase only in response to *Pst* DC3000 infection (red line) and the peak of

the expression is observed between 5 and 9 hrs post infection, approximately. Those preliminary results were kindly donated for the purposes of this thesis by Prof. Murray Grant (University of Warwick) *B. cinerea* data were kindly provided by Dr. Emily Breeze (University of Warwick).

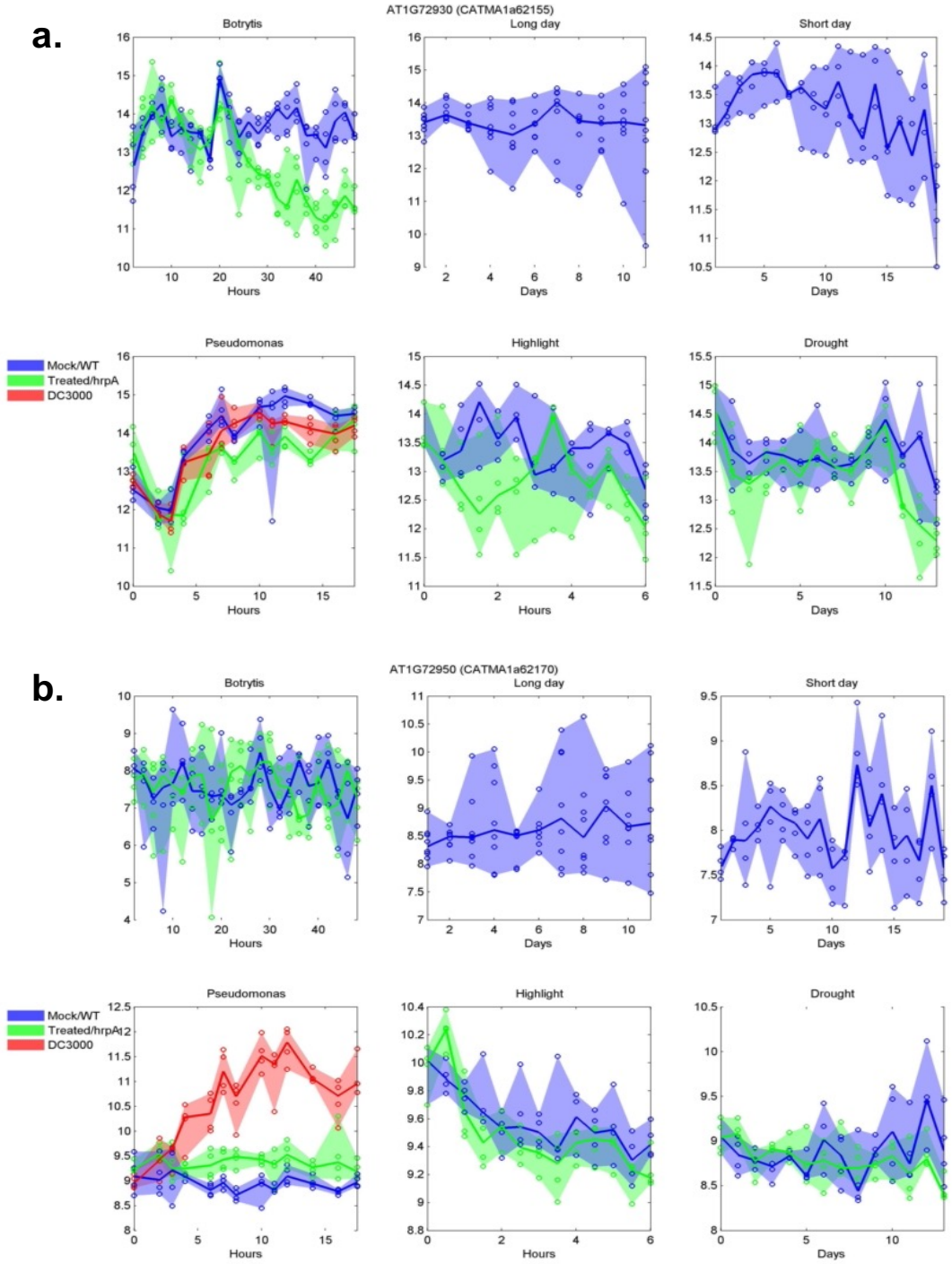

Figure 1.11 **Transcriptional profiling of *AT1G72930* and *AT1G72950* in Col-0 under biotic and abiotic stresses.**

A. thaliana Col-0 adult plants were subjected to a variety of biotic (*B. cinerea*, *Pst* DC3000, *Pst* DC3000 *hrpA*) and abiotic (long day, short day, highlight, drought) treatments and/or conditions to identify pathogenesis-related gene expression. Expression of gene *AT1G72930* **(a.)** seems to not be specific to *Pst* DC3000, as it is also positively regulated in response to *Pst* DC3000 *hrpA* and mock (10mM MgCl2) treatment. The expression levels of *AT1G72950* **(b.)** increase only in response to *Pst* DC3000 infection (red line) and the peak of the expression is observed between 5 and 9 hrs post infection, approximately. Those preliminary results were kindly donated for the purposes of this thesis by Prof. Murray Grant (University of Warwick) *B. cinerea* data were kindly provided by Dr. Emily Breeze (University of Warwick).

The function and the molecular mechanisms underlying most TN receptors and their role in plant defence against pathogens remain widely unknown. The aim of this project was to understand the mechanisms responsible for the upregulation of *A. thaliana TN* expression in the presence of the bacterial pathogen *Pst* DC3000, working towards utilizing this knowledge in future applications to engineer plants with durable resistance to pathogenic infection and minimise crop losses. Pathogen assays and a range of engineered *A. thaliana* lines (knockout and overexpressing TN proteins), as well as protoplast screening and a yeast-one-hybrid system were used throughout this PhD research to achieve said aim. More specifically, the objectives of the project are outlined here in the order they are addresed in the experimental chapters:

- Show *TN* gene expression is upregulated post *Pst* DC3000 infection, but not after *hrpA* or mock treatments, using the RT-q-PCR method as an alternative to microarrays.
- Identify the specific *Pst DC3000* effectors correlated with the *TN* promoter upregulation, via transiently co-express them in leaf protoplasts and use luciferase bioluminescence to measure changes in promoter regulation in the presence of effectors.
- Set up a yeast-one-hybrid screening system for DNA-protein interactions to identify potential *A. thaliana* transcription factors implicated in the regulation of expression of *TN* genes.

- Investigate the susceptibility of dexamethasone-inducible *A. thaliana* overexpressing lines of *TN* gene *AT1G72940* against *Pst* DC3000, using bacterial growth and chlorophyl fluorescence imaging assays.
- Measure the relative expression levels of *AT1G72940* in the same lines in response to dexamethasone, to test the efficacy of these plants for future experiments.
- Investigate the susceptibility of CRIPR/Cas9 knockout *A. thaliana* lines lacking the *TN* locus against various strains of Pst, using bacterial growth and chlorophyl fluorescence imaging assays.

- Design and generate the molecular tools to create new *A. thaliana* stable transgenic lines with constitutive and inducible overexpression of *TN* genes *AT1G72940* and *AT1G72950*.
- Generate *A. thaliana* stable transgenic lines overexpressing *AT1G72940,* select them for homozygocity, genotype them and check their transcript and protein levels to determine if they are suitable for immunity assays.
- Perform *Pst* DC3000 bacterial growth assays on the same lines and evaluate the preliminary results.

2. Materials and Methods

2.1 Plant materials and growth conditions

The plant material required for the purposes of this project comprises of two individual plant species: *Arabidopsis thaliana* and *Nicotiana benthamiana*. Unless stated otherwise, the *A. thaliana* and *N. benthamiana* plants were grown in Aralab growth chambers (by ARALAB) with 12-hour photoperiod at 22^{o}C, 60% relative humidity and light irradiance of 100μmol $m^{-2}s^{-1}$. The reproducibility of previous experiments and need of comparable results required the *A. thaliana* lines used for bacterial growth and protoplast generation to be grown in a different Aralab growth chamber, with same growth conditions but set on a photoperiod of 10-hour day/14-hour night.

For the great majority of experiments, seeds were sown on soil suitable to the needs of each plant. For *N. benthamiana* two different types of soil were used: seeds were sown on Levington Advanced Seed & Modular F2 compost (ICL, UK) and then seedlings were transferred and fully grown on Levington Advanced Pot & Bedding M2 compost (ICL, UK). *A. thaliana* plants were sown and grown on *Arabidopsis* mix (F2 compost, silver sand, fine vermiculite, intercept). Pots were placed into trays and covered with appropriate lids to maintain humidity, further covered with aluminium foil to prevent exposure to light sources and allowed to stratify for a minimum of 48 hours in the dark at 4^{o}C. Post-stratification, seeds were transferred into the Aralab to germinate. Two weeks following germination, seedlings were transferred with forceps into individual pots and the trays were covered with plastic translucent lids allowing ventilation for 3 to 5 days, to allow adaptation to the new soil environment.

For experiments requiring consistency maintaining the same developmental stage between biological replicates, the leaves where numbered (Farmer et al., 2013) when plants reached 4-5 weeks of age post germination. Numbering of leaves was performed manually on each individual plant, and the desirable leaves were marked with a permanent marker. The number refers to the developmental order by which the leaves sprout in the rosette. The order can

be defined starting from the newest (smaller) leaf in the centre of the rosette and counting round in a triangle towards the direction of the next-in-size leaf, until the first pair of true leaves and the cotyledons are reached. Once there, and having defined the direction by which the leaves have sprouted, the numbering starts from the 1st pair of true leaves (excluding the cotyledons) until leaves number 7 to 9 are determined and marked.

For the purposes of bacterial growth in seedlings, seeds were sown on solid ½ Murashige and Skoog (MS) plant growth media [2.15g/L MS salts (Murashige and Skoog, 1962), 10g/L sucrose, 5g/L phytagel, pH 5.8], and grown for 2 weeks in preparation for each experiment. For the selection of homozygous transgenic lines where the selection marker used is a gene coding for resistance in the antibiotic Hygromycin, the antibiotic was added to the media in a working concentration of 20µg/ml.

The *N. benthamiana* plants used were *dcl4 (dicer-like 4)* mutant lines. All *A. thaliana* transgenic and knock-out lines used in this work were produced using as a background the wild type (WT) *A. thaliana* ecotype Columbia (Col-0) genotype. The *A. thaliana* homozygous CRISPR/Cas9 TIR-NB (TN) genetic locus deletion lines (#2 and #11), as well as the *promDEX::AT1G72940* and *promDEX::AT1G72940:HA:FLAG* were kindly donated by Prof. Murray Grant (University of Warwick, UK).

2.2 Bacterial strains and media

All bacterial strains were kept in 20% glycerol stocks and stored in deep freezers (-80ºC). Immunity related assays were performed using bacterial cultures of *Pseudomonas syringae* pv. *tomato* (*Pst*) DC3000, grown overnight in King's B (KB) medium (20g/L proteose peptone, 8.6mM K_2HPO_4, 163mM glycerol, pH adjusted to 7.0 with HCl before autoclaving; liquid, or solid, with the addition of 1.5% agar) (KING et al., 1954), at 28ºC. *Escherichia coli* TOP10 bacterial cells (strain DH10B™) were used throughout all the molecular cloning required for this work. *E. coli* bacteria were grown on Lysogeny (or Luria) Broth (LB) medium (1% tryptone, 0.5% yeast extract, 1% NaCl liquid, or solid, with the addition of 1.5% agar) (BERTANI, 1951), at 37ºC overnight.

Agrobacterium tumefaciens (*Rhizobium radiobacter*) strain GV3101 bacteria was used for the purpose of transient gene expression in *N. benthamiana* plants and stable transformation of *A. thaliana* Col-0. *A. tumefaciens* bacteria were grown on LB medium for up to 48 hours at 28°C. All growth media contain the appropriate antibiotics (**Table 2.1**) allowing for the selection of the specific bacterial strains and/or the desirable plasmid vectors bearing the antibiotic resistance gene for selection. The antibiotics were added to the media post-autoclaving and in aseptic conditions when the media temperature was between 55-60°C.

For single colony isolation, bacteria were retrieved from the glycerol stock by streaking on a solid medium plate containing the appropriate antibiotic(s), in aseptic conditions. A single colony was then picked and inoculated into the respective liquid growth medium, containing the appropriate antibiotic(s) and incubated in a shaker incubator set at the respective temperature and at 220 revolutions-per-minute (rpm).

Table 2.1 **Bacterial strains and antibiotic resistance used in this study.**

Species	Strain	Expressing	Vector	Selection	Citation
E. coli	TOP10 (DH10B™)	-	-	-	Thermo Fisher, C404010
A. tumefaciens	GV3101	-	-	Rifampicin 100 µg/mL Gentamycin 20 µg/mL Construct-dependent antibiotic	(Holsters et al., 1980)
P. syringae	Pv *tomato* DC3000	-	-	Rifampicin 100 µg/mL	(Cuppels, 1986)
P. syringae	Pv *tomato* DC3000	-	pVSP61	Rifampicin 100 µg/mL Kanamycin 25 µg/ml	(Cuppels, 1986)
P. syringae	Pv *tomato* DC3000*hrpA*-	-		Rifampicin 100 µg/mL Kanamycin 25 µg/ml	
P. syringae	Pv *tomato* DC3000*hrcC*-	-		Rifampicin 100 µg/mL Kanamycin 25 µg/ml	
P. syringae	Pv *tomato* DC3000	AvrRPS4	pVSP61	Rifampicin 100 µg/mL Kanamycin 25 µg/ml	
P. syringae	Pv *tomato* DC3000	AvrRPM1	pVSP61	Rifampicin 100 µg/mL Kanamycin 25 µg/ml	
P. syringae	Pv *tomato* DC3000	AvrRPT2	pVSP61	Rifampicin 100 µg/mL Kanamycin 25 µg/ml	
P. syringae	Pv *tomato* DC3000	?	pVSP61	Rifampicin 100 µg/mL Kanamycin 25 µg/ml	

2.3 Protoplast assays

The analysis of the promoter regulation of the *A. thaliana TN* gene family in the presence of *Pst* DC3000 effector molecules was performed in *A. thaliana* Col-0 protoplasts.

2.3.1 Generation of protoplasts

Protoplasts were generated following a modified version of the "tape-*Arabidopsis* sandwich" method, as previously described by Wu et al. (2009), where further details regarding the methods and buffers can be found. Leaves number 7, 8 and 9 were collected from the rosettes of *A. thaliana* Col-0 adult plants (5 to 6 weeks old) and two kinds of tape were used to isolate leaf mesophyll protoplasts: Time Tape® (PDC Healthcare) adhered to the upper epidermis and Scotch® Magic™ invisible tape (Scotch® Brand, 3M) to the lower epidermis. Removing of the Magic tape allows for complete removal of the lower epidermis, thus exposing the mesophyll cells to an enzyme solution, containing cell wall digesting enzymes. Mesophyll protoplasts were retrieved from the enzyme solution and resuspended to a final concentration of 4 x 10^5 protoplasts/ml in MMG buffer.

2.3.2 Protoplast transfection

The plasmid vectors containing the promoters of *TN* genes fused with the luciferase reporter gene (*promAT1G72920::LUC*, *promAT1G72940::LUC*, *promAT1G72930::LUC* or *promAT1G72950::LUC*) were prepared and kindly donated for the purposes of this thesis by Prof. Murray Grant and his group (University of Warwick, UK).

To study the role of candidate effector regulators, protoplasts were triple-transfected with a combination of the following plasmid vectors: a specific reporter comprising of one of the *TN* gene promoters (*prom*) fused with the luciferase (LUC) reporter gene (*promAT1G72920::LUC*, *promAT1G72940::LUC*, *promAT1G72930::LUC* or *promAT1G72950::LUC*), either the pEG201 plasmid encoding one of a collection of 23 *Pst* DC3000 effectors (**Table 2.2**) or the empty vector pEG201, and a transfection control

reporter (*promUbiquitin::GUS*), used at a ratio of 5:4:1. Protoplasts and plasmid vectors were incubated for 20-30 min in a PEG (polyethylene glycol) solution for the transfection. Then, they were collected using low speed centrifugation (2 min, 100 x g), resuspended into W5 solution and aliquoted into 4 replicate wells in a 96-well plate. The plate was sealed with a translucent lid and paper towel and kept incubating overnight (~16 hours) in a Sanyo growth cabinet with a photoperiod of 10-hour day/14-hour night.

***Table 2.2 Pst* DC3000 effector library in *E. coli*, used for the transfection of *A. thaliana* Col-0 protoplasts.**

Construct	*Pst* DC3000 ID	Vector	Selection
prom35S::HopO1-1:GFP	HopPtoS1	p2GWF7	Ampicillin 100µg/mL
prom35S::HopN1:GFP	HopPtoN	p2GWF7	Ampicillin 100µg/mL
prom35S::HopAD1:GFP	HopPtoI	p2GWF7	Ampicillin 100µg/mL
prom35S::HopY1:GFP	AvrPpiB12	p2GWF7	Ampicillin 100µg/mL
prom35S::HopT1-1:GFP	HopPtoT1	p2GWF7	Ampicillin 100µg/mL
prom35S::HopAB2:GFP	VirPphA	p2GWF7	Ampicillin 100µg/mL
prom35S::HopP1:GFP	HopPtoF	p2GWF7	Ampicillin 100µg/mL
prom35S::HopC1:GFP	AvrPphC	p2GWF7	Ampicillin 100µg/mL
prom35S::HopF2:GFP	AvrPphF	p2GWF7	Ampicillin 100µg/mL
prom35S::HopAF1:GFP	AvrXv3	p2GWF7	Ampicillin 100µg/mL
prom35S::HopA1:GFP	HopPsyA	p2GWF7	Ampicillin 100µg/mL
prom35S::HopB1:GFP	HopPtoB	p2GWF7	Ampicillin 100µg/mL
prom35S::HopH1:GFP	HopPtoH	p2GWF7	Ampicillin 100µg/mL
prom35S::HopG1:GFP	HopPtoG	p2GWF7	Ampicillin 100µg/mL
prom35S::HopAO1:GFP	AvrPphD2	p2GWF7	Ampicillin 100µg/mL
prom35S::HopAI1:GFP		p2GWF7	Ampicillin 100µg/mL
prom35S::HopK1:GFP	AvrRps4	p2GWF7	Ampicillin 100µg/mL
prom35S::AvrPto:GFP	AvrPto	p2GWF7	Ampicillin 100µg/mL
prom35S::HopQ1-1:GFP	HopPtoQ	p2GWF7	Ampicillin 100µg/mL
prom35S::HopV1:GFP	HopPtoV	p2GWF7	Ampicillin 100µg/mL
prom35S::HopD1:GFP	AvrPphD1	p2GWF7	Ampicillin 100µg/mL
prom35S::AvrRPT2:GFP	AvrRPT2	p2GWF7	Ampicillin 100µg/mL

2.3.3 Bioluminescence image analysis of protoplasts

Luciferin, the substrate for luciferase (LUC) is added to the protoplasts 16hrs after protoplast transfection (10-11 am on the following morning), to incubate for 15-30 min prior to analysis. The plate was placed under a photodetector camera (by Photek Ltd) to measure the bioluminescence via photon counting.

Image 32 software (by Photek Ltd) is an image processing and data acquisition software designe to analyse data from Photek camera systems. Signal integration length was 2hrs on average, but time periods varied depending on the experiment and/or signal intensity.

Following the end of signal integration, a lysis buffer was added to the protoplasts, the cell debris were centrifuged, and the lysate was added into a new plate with 4-Methylumbelliferyl glucuronide (MUG) substrate for β-glucuronidase (GUS) detection. The plate was incubated at 37^{o}C for 1-1.5 hours and then transferred to a plate reader. The Magellan3 software (Tecan Trading AG, Switzerland) was used to measure the fluorescence (excitation filter at 360nm; emission filter at 465nm; 40μs integration time).

The GUS measurement data are representative of the efficiency of the protoplast transfection; therefore, they were used to normalise the LUC measurements and produce comparable results for each individual effector.

2.4 Biotic stress assays

To assess the susceptibility of *A. thaliana* to the pathogen *Pseudomonas syringae*, two different biotic stress assays were followed. The first approach was monitoring the pathogenicity from the perception of the pathogen, focusing on the measurement of the levels of the bacterial growth in each plant genotype in comparison to the wild type plants. The second approach was plant-focused, monitoring the efficiency of the plant cell photosystems post bacterial infection using a CF Imager machine (by Technologica Ltd, Colchester, UK).

2.4.1 Bacterial growth in A. thaliana rosette leaves

Bacterial growth assays were performed via leaf infiltration of *A. thaliana* plants with *Pst* DC3000 bacterial suspension. To generate the bacterial suspension, isolation of a single colony of the desirable strain of *Pst* DC3000 was generated from a glycerol stock, inoculated, and grown into a 10mL bacterial liquid culture as described in **Section 2.2** with the appropriate

selection antibiotics. The *Pst* DC3000 bacterial culture was centrifuged on a benchtop centrifuge at 23°C and 3200 rcf for 10 minutes. The supernatant was discarded, the bacterial pellet was washed and resuspended in 10ml of $MgCl_2$ 10mM buffer and the centrifugation step was repeated once more. The bacterial pellet was resuspended in 3mL of $MgCl_2$ 10mM and a dilution of 1:10 was generated to measure the optical density (OD) of the suspension. The OD was determined by measuring the light absorbance of the dilution at 600nm using a spectrophotometer and calculating the OD_{600} of the concentrated suspension. Due to differences between the bacterial growth protocols between the Grant and Ntoukakis groups, the desirable OD_{600} for the bacterial growth assay was determined by the needs of each experiment. The OD_{600} was set to either 0.0002 (Grant lab protocol) when working with the dexamethasone-inducible lines of *AT1G72940* over the first year of experiments, or 0.001 (Ntoukakis lab protocol) for every other *A. thaliana* transgenic line tested in this thesis. In either case, the concentration is far lower than the measuring capacity of a spectrophotometer, so instead an OD_{600}= 0.1 was calculated and then the desirable working concentration was generated by serial dilutions in a final volume of 50mL.

A. thaliana plants that were to be subjected in a bacterial growth assay were grown for 5 to 6 weeks post-germination. For each strain of *Pst* DC3000 used in the assay, six plants per genotype were selected and their rosette leaves numbers 7-8-9 were marked prior to infiltration. Said leaves were pressure-infiltrated in the abaxial side of the leaf using a needleless syringe (1ml) with the bacterial suspension(s) and the plants were placed back to the same growth cabinet. The days when samples were harvested to determine the bacterial growth are indicated as days post inoculation (dpi).

2 leaf disks per plant were harvested via alternative sampling from the infiltrated leaves using a cork borer of size 4 (8.75mm diameter), at 3dpi unless stated otherwise. Leaf disks were placed in pairs into sterile Eppendorf tubes (2ml) with 200µl $MgCl_2$ 10mM and 2 sterile metal beads and tissue was lysed using a Mixer Mill TissueLyser (Qiagen) for 30 seconds at 25 Hz twice. Each pair of leaf disks represents one biological sample, resulting in a total of 6

biological replicates per genotype and treatment. Post lysing $MgCl_2$ 10mM was added to the lysed tissue to a total volume of 1ml, mixed and then a dilution of 1:2 was generated to a total of 200µl. After that, several serial ten-fold dilutions followed to ensure that colony counting will be feasible. All dilutions were performed in 96-well-plates for tissue culture, each plate corresponding to one genotype and treatment. Each well was pipetted 10-20 times between dilutions and prior to plating. Dilutions were surface plated (10µl each) on square petri dishes containing solid KB media with appropriate antibiotics. Both dilutions and plating were performed with a multichannel Gilson pipette, in sterile conditions.

Plates were incubated at 28^{o}C for 24-48 hrs to allow colony formation and growth of *Pst* DC3000 isolated from the lysed tissue. Colony counting was carried out over the course of 2 days for each dilution. Numbers were used to calculate the colony forming unit (CFU) per ml, which corresponds to a leaf surface area of 1cm^2.

Transgenic plant lines with chemically-inducible promoters for conditional protein expression were induced with the chemical approximately 16 hrs prior to infection. In the case of dexamethasone (DEX) induced lines, the selected leaves were surface-painted with the induction solution consisting of 10µM DEX and 0.02% of the surfactant Silwet L-77, unless stated otherwise. In all cases, the times of induction (~5pm) and infection (~10am) of the plants were kept relatively stable, taking into consideration the circadian clock of the plants.

2.4.2 Bacterial growth in A. thaliana seedlings

Bacterial growth was further tested on seedlings (6 days old) of selected transgenic *A. thaliana* lines (*prom35S::AT1G72940:GFP/FLAG)* constitutively expressing the *AT1G72940* gene regulated by the promoter *35S* of the Cauliflower Mosaic Virus (*prom35SCaMV*, hereafter referred to as *prom35S* or *p35S*). The same principals apply as with adult plants, with a few minor adjustments due to technical issues. 40 seedlings (pool of 10/biological

replicate) of each genotype per condition were transferred in a petri dish (or 6-well tissue culture plate) full of sterile water. The bacterial inoculum was prepared as described in **Section 2.4.1**, estimating a higher volume of bacteria and a final OD_{600} equal to 0.01. Due to the size and developmental stage of the plants, the infection with the desirable *Pst* DC3000 strain was performed by removing the water and submerging the seedlings in the bacterial inoculum. The seedlings were then incubated with the bacteria on a shaker, for 1hr at RT (~22^{o}C).

After the hour has passed, the seedlings were transferred to a laminar flow hood and the inoculum was removed. Seedlings are cleaned from excessive bacteria by washing, shaking, and removing sterile water, repeated three times. Following the washes, 10 seedlings per genotype per condition were separated and transferred into 24-well tissue culture plates, that have been previously prepared with 500μl of sterile water per well. Plates were sealed with micropore tape and incubated for 48hrs in the Sanyo growth chamber (10-hour day/14-hour night photoperiod).

After 48hrs, the seedlings were moved back to laminar flow hood, to get surface-sterilised from the remnants of the bacterial inoculum. Initially, the water was removed and 500μl of 70% ethanol solution was added in each well, shaking for 1 min. Ethanol was removed and sterile water was added to wash, shake, and remove; washes were repeated three times. Seedlings corresponding to each biological replicate per genotype and treatment were gently lifted using sterile forceps, the excess water was removed on clean tissue paper, and they were transferred into previously prepared sterile Eppendorf tubes containing 200μl of 10mM $MgCl_2$ and 3-4 glass beads. From that step onwards the protocol was performed as described in **Section 2.4.1**. When calculating the total number of bacteria, the counts were expressed per 10 seedlings.

2.4.3 Quantum efficiency of the photosystem post bacterial infection – Chlorophyll Fluorescence Imaging System

A different way to measure the effect of the biotic stress imposed on the different plant lines by the *Pst* DC3000 infection is to determine how the maximum quantum efficiency of the photosystem II (PSII) photochemistry is affected post infection. PSII chlorophyll fluorescence imaging of *A. thaliana* rosette leaves was performed with a CF Imager (Technologica Ltd, Colchester, UK). Bacterial suspensions were prepared as described in **Section 2.4.1**, and the OD_{600} of the inoculum was adjusted to 0.15 before pressure infiltrating the abaxial side of the chosen rosette leaves. For the control treatment, leaves were infiltrated with a mock solution of the infiltration buffer $MgCl_2$ (10mM). Excess solution was removed from the leaf surface gently with tissue paper. In the event of testing transgenic lines where the gene expression is driven by inducible promoters, the induction with the respective chemical was performed as described in **Section 2.4.1**.

The protocol of chlorophyll fluorescence imaging used for these experiments was based on the methods described by (Zabala et al., 2015). Specifically, infected plants were then placed in the CF Imager chamber for 40 minutes post infiltration and allowed to dark adapt for 20 minutes. This was followed by a saturating light pulse (6,349 µmol $m^{-2}s^{-1}$ for 0.8 seconds) to maximum obtain dark-adapted fluorescence (F_m). Actinic light (120 µmol $m^{-2}s^{-1}$ – the same as plant growth light intensity) was then applied for 15 minutes, followed by a saturating pulse to obtain maximum light adapted fluorescence (F_m'). Following that, the plants were left for 24 more minutes in actinic light and then dark for 20 more minutes. This full cycle of measurements of 59 minutes duration in total was repeated 23 times. The values F_m, F_m' and F_o (minimal fluorescence with fully oxidized PSII centres) were used to calculate chlorophyll fluorescence parameters related to photosystem II, such as F_v/F_m, which represents the maximum dark-adapted quantum efficiency, and F_v'/F_m', which represents the maximum light adapted quantum efficiency. The values were calculated as described previously by (Baker, 2008). The rate F_v/F_m calculated from the values calculated over the 24hrs timeframe, was then plotted against time, to represent the maximum quantum efficiency of the PSII.

2.5 Molecular Biology methods

2.5.1 Plant DNA extraction for genotyping

The *A. thaliana* lines used in this study required genotyping PCR (Polymerase Chain Reaction) to verify the presence or absence of specific genetic loci, such as transfer DNA (T-DNA) insertions. To obtain the DNA (deoxyribonucleic acid) template for the PCR (polymerase chain reaction), plant material (usually young leaves, ~ 0.5 cm^2 surface) was collected in PCR tubes with 100µL of 5% Chelex® 100 Resin (Biorad) suspension. Samples were ground manually with a pestle in room temperature, further mixed by vortexing and incubated at 99^oC in a thermocycler for 5 minutes. To separate the lysate from the remaining tissue debris, the samples were centrifuged using a benchtop centrifuge for PCR tube strips, at maximum speed for 10 minutes. 30µL of the supernatant were collected with a pipette, transferred to a new tube, and stored temporarily at 4^oC until the genotyping was completed.

To set up the genotyping PCR, 1µL of the lysate was used initially as a template. In cases where the crude extract inhibited the reaction, the lysate was further diluted prior to the PCR reaction.

2.5.2 Polymerase Chain Reaction (PCR)

DNA fragments from either recombinant plasmid vectors or plant material were amplified through the method of PCR. The reaction was set up in PCR tubes, strips, or plates according to the needs of each experiment and the standard reaction mixture consisted of the following components: DNA template, 1x DNA Polymerase Buffer, 100µM dNTPs, 500nM Forward Primer, 500nM Reverse Primer, DNA Polymerase enzyme (units used according to the company manual) and autoclaved double distilled water to a final volume of 20 or 50µL. The high-fidelity DNA Polymerase used for PCR reactions intended for cloning in this thesis was Q5® High Fidelity DNA Polymerase (M0491S, NEB) or KAPA HiFi PCR Kit (KK2103 - 07958854001, Kapabiosystems). Unless stated otherwise, PCR reactions were performed using the KAPA-Taq PCR Kit (KK1014 – 07958579001, Kapabiosystems). All

reactions were carried out following a standard thermocycling protocol adjusted to the specifications of each polymerase and the melting temperature of the primers (Tm).

2.5.3 Molecular Cloning

For the purposes of the Yeast-One-Hybrid (Y1H) screening, the generation of stable *A. thaliana* transgenic lines and transient protein expression in *N. benthamiana*, a series of constructs were assembled and subcloned in plasmid vectors using a variety of molecular cloning techniques. Unless stated otherwise, all constructs were generated using sequences amplified from templates of pre-existing recombinant plasmid vectors containing the Golden Gate (GG) domesticated truncated *TN* promoters and/or genes of interest, which were kindly donated by Prof. Murray Grant (University of Warwick, UK) (**Table 2.3)**.

Table 2.3 **List of the pre-existing glycerol stocks containing the recombinant plasmid vectors used as template for the amplification and subcloning of the truncated *TN* promoters and/or genes of interest.**

Constructs were donated by Prof. Murray Grant (University of Warwick, UK).

	Construct	Bacterial strain	Vector	Antibiotic Resistance
1.	*L2P1/p2940::Yell.Luc P2-Basta*	*E. coli*	unknown	unknown
2.	*ProAT1G72930::LucP7*	*E. coli*	pCambia	unknown
3.	*FL1P1/Promoter AT1G72950*	*E. coli*	unknown	Ampicillin 100µg/mL
4.	*FL1P1/pAT1G72940::YellowLuc:Act2*	*E. coli*	unknown	Ampicillin 100µg/mL
5.	*FL1P1/proAT1G72940::YellowLuc:Act2 motif 1 mutated*	*E. coli*	unknown	Ampicillin 100µg/mL
6.	*FL1P1/proAT1G72940::YellowLuc:Act2 motif 2 mutated*	*E. coli*	unknown	Ampicillin 100µg/mL
7.	*FL1P1/proAT1G72940::YellowLuc:Act2 motif 3 mutated*	*E. coli*	unknown	Ampicillin 100µg/mL
8.	*FL1P1/proAT1G72940::YellowLuc:Act2 motifs 1&2 mutated*	*E. coli*	unknown	Ampicillin 100µg/mL
9.	*L2P1/p2940::YellowLuc P2-Basta*	*A. tumefaciens*	unknown	unknown

10.	*FL1P1/promoter AT1G72920*	*E. coli*	unknown	Ampicillin 100µg/mL
11.	*pEX-A2/promoter AT1G72950*	*E. coli*	pEX-A2	Ampicillin 100µg/mL
12.	*pEX-A2/promoter AT1G72920*	*E. coli*	pEX-A2	Ampicillin 100µg/mL
13.	*FL1P1/promoter AT1G72920*	*A. tumefaciens*	unknown	unknown
14.	*pTA70002-BZ/AT1G72940:3HA:FLAG*	*E. coli*	pTA70002	Kanamycin 25 µg/mL
15.	*pTA70002/AT1G72920 L2*	*E. coli*	pTA70002	Kanamycin 25 µg/mL
16.	*pTA70002/AT1G72930 L1*	*E. coli*	pTA70002	Kanamycin 25 µg/mL
17.	*pTA70002-GG/promDEX::AT1G72950*	*E. coli*	pTA70002	Kanamycin 25 µg/mL
18.	*pTA70002-GG/promDEX::AT1G72940*	*E. coli*	pTA70002	Kanamycin 25 µg/mL
19.	*pTA70002/3HA:FLAG:AT1G72930*	*A. tumefaciens*	pTA70002	Rifampicin 100 µg/mL and Gentamycin 20 µg/mL and Kanamycin 25 µg/mL

2.5.3.1 Type II Restriction enzymes (classical) cloning

The Y1H screening required to further subclone the wild type (WT) and mutated versions of the DNA sequence corresponding to the putative promoter region locating upstream of the gene *AT1G72940* in the *A. thaliana* Col-0 genome. Initially, the vector available in the lab for yeast expression vector was *pHIS3LEU2* (see map as described by Davies, S., 2013 in **Section 7.1**), which requires a cloning strategy based on type II restriction enzymes.

Table 2.4 **Primers designed to sequence the original constructs containing the *TN* promoters** (see no. 1-13, Table 2.3**).**

Stock name	Primer name	Sequence (5' to 3')	Tm
VN997	prom20seqR1	CATTTTGATTTTTGATTCTCTCTATTGAGA	52.8°C
VN998	prom20seqR2	CTGTAGTAGTGTATTACTATTATTGGAGG	52.5°C

VN999	prom30seqR1	CATTTTGATTTTTGATTCTCAATGAGTGAT	53.7°C
VN1000	prom30seqR2	GTGGTGTCAATAGATGATTTTGTAGTATGG	55.7°C
VN1001	prom40seqR1	CATTTTGATTTTTGATTCTCTCTATTGAGAACT	54.8°C
VN1002	prom40seqR2	GCATAAATCAGTGGCTTTGAACTGT	56.2°C
VN1003	prom40seqR3	TTCTCAACTTCGTAGACTTCTTTTA	51.9°C
VN1004	prom40seqR4	TCCCTCTTCAAAACCAAAGAGAATTCT	56.5°C
VN1005	prom50seqR1	CATTTCATTGATTCTAAAGAGAAATGG	51.3°C
VN1006	prom50seqR2	TAGATTCCAACTTTGAGCTATGAAC	52.9°C

The pre-existing recombinant plasmid vectors containing these promoter versions (stocks no. 4-8, **Table 2.3**) were sequenced using primers VN1001, VN1002, VN1003 and VN1004 (**Table 2.4**) to confirm the length, as well as the start and end point of the region upstream of *AT1G72940* that has been assumed to contain the promoter of the gene and thus, has been synthesized and subcloned. The sequencing results identified a sequence of 1,400 base pairs (bp) as well as the exact point mutations that produced the different mutated motif versions of *proAT1G72940* (for sequences see **Section 7.2**). The recognition sites for the restriction enzymes SacI and MluI were considered suitable for the cloning, as they are located prior to the HISTIDINE sequence on the *pHIS3LEU2* vector, and they do not exist in the *promAT1G72940* sequence. A pair of primers was designed to amplify all the *promAT1G72940* versions out of the corresponding vectors and introduce the recognition sites for SacI (forward primer) and MluI (reverse primer), flanking the amplified fragments. Both primers were also designed to introduce a nested NcoI recognition site, to allow the *promAT1G72940* to be easily restricted out of the plasmid with NcoI for future applications.

The *promAT1G72940* fragments were amplified with Q5 DNA polymerase, primer annealing temperature of 60°C, 45 seconds extension time and a total of 20 cycles. The resulted PCR fragments were adenylated using Kapa-Taq DNA polymerase and 200μM dATP at 72°C, to add -A overhangs. The adenylated fragments were then ligated into the pGEM®-T Easy (A1360, Promega) cloning vector using the T4 DNA ligase (M0202S, NEB) at room temperature (RT) for 1 hour. 5μl of the ligation mixture were transformed into *E. coli* TOP10 chemical competent cells, as described in **Section 2.5.4**. The

transformed cells were plated on LB plates with ampicillin (Amp) containing 5-bromo-4-chloro-3-indolyl-β-D-galactopyranoside (X-gal, Corning B.V Life Sciences) and Isopropyl β- d-1-thiogalactopyranoside (IPTG, Invitrogen™). The following day the white-coloured colonies were inoculated into liquid LB/Amp, grown and the recombinant plasmid vectors containing *promAT1G72940* were extracted as described in **Section 2.5.7**.

Both *promAT1G72940/pGEM-T-easy* (WT and mutated versions) and *pHIS3LEU2* were double-digested with SacI-HF® (R3156S, NEB) and MluI-HF® (R3198S, NEB) for 1 hour at 37°C, using the CutSmart® Buffer (NEB), in a final reaction volume of 50μl. The digested bands were loaded and analysed in 1% agarose gel, as described in **Section 2.5.8**. The desirable SacI/MluI digested DNA bands from each vector (1.4Kb *promAT1G72940,* 8Kb linearised *pHIS3LEU2*) were cut out and purified from the gel, as described in **Section 2.5.9**.

2.5.3.2 Cloning with Gateway® Technology

As previously mentioned, the Y1H cloning strategy had to be adapted to a new yeast expression vector that would be suitable for Y1H interactions and compatible with the *S. cerevisiae* strain used in the lab. Vector *pMW#3* (see map in **Section 7.1**) was selected due to its previous use in Y1H experiments (Deplancke et al., 2006) as well as the fact that it is said to be Gateway® compatible and for offering a different selection marker to test for interactions. *pMW#3* was donated to Addgene by Marian Walhout (Addgene plasmid # 13350 ; http://n2t.net/addgene:13350 ; RRID:Addgene_13350), where it was purchased from for the needs of this project.

Initially, a pair of primers (VN1045/VN1046, **Table 2.5**) was designed to amplify all the *promAT1G72940* versions out of the corresponding vectors and introduce the Gateway® sites for BP recombination reactions: *att*B1 site (forward primer, VN1045) and *att*B2 site (reverse primer, VN1046) flanking the amplified fragments. The *promAT1G72940* fragments were amplified with Q5

DNA polymerase, primer annealing temperature of 60ºC, 45 seconds extension time and a total of 19 cycles. The PCR products were run on 1% agarose gel next to the molecular weight standards of a Quick-Load® 2-Log DNA Ladder (N0469S, NEB) to verify their molecular weight and band specificity.

Table 2.5 **Primers designed to amplify the WT and mutated motif versions of promoter *AT1G72940,* introducing the *att*B1 and *att*B2 recombination sites for Gateway® cloning.**

Stock name	Primer name	Sequence (5' to 3')	Tm (Tm with overhang)
VN1045	**pAT1G72940_Y1H_GW_F**	GGGGACAAGTTTGTACAAAAAAGCAGG CTAGGTTCTGCTTGTGGCAGACGACG	63.4ºC (70ºC)
VN1046	**pAT1G72940_Y1H_GW_R**	GGGGACCACTTTGTACAAGAAAGCTGG GTCTTTGATTTTTGATTCTCTCTATTG	48 ºC (66.1 ºC)

Each different *promAT1G72940* version was then used to set up individual BP recombination reactions with the Gateway® donor vector pDONR™/Zeo (ThermoFisher Scientific), using a reaction setup of 1µl of vector (~300ng/µl), 1µl of the respective PCR product (50-100ng) and 0.5µl of 5x Gateway® BP Clonase™ II Enzyme Mix (Cat. No. 11789-020, Invitrogen™). The reactions were set in PCR tubes and incubated in a thermocycler machine at 25ºC for 3-4 hrs, or alternatively overnight (O/N) to increase the efficiency. Following the end of the recombination, the entire reaction volume (2.5µl) was transformed into *E. coli* TOP10 chemical competent cells, as described in **Section 2.5.4**. The transformed cells were plated on LB plates with Zeocin (Zeo).

The following day, the successfully grown colonies were tested with colony PCR (described in **Section 2.5.6**) using primers VN1045/VN1046 for the presence of the insert (*promAT1G72940)*, in addition to their double selection via Zeocin resistance and the absence of *ccd*B "suicide" gene. From the PCR positive colonies, two were selected per construct to inoculate into liquid LB/Zeo, grow at 37ºC O/N and extract the recombinant plasmid vectors containing *promAT1G72940,* as described in **Section 2.5.7**. Entry clones

promAT1G72940/ pDONR™-Zeo (WT, m1, m2, m3, m1-2) were prepared for sequencing analysis, using universal primers M13 Forward and M13 Reverse, flanking the recombination sites on the vector.

Fully sequenced entry clones of *promAT1G72940/* pDONR™-Zeo (WT, m1, m2, m3, m1-2) were then set up for LR recombination reactions with the destination/yeast expression vector *pMW#3*. The reaction setup consisted of 1µl of destination vector *pMW#3* (~300ng/µl), 1µl of the respective entry clone (~300ng/µl) and 0.5µl of 5x Gateway® LR Clonase™ II Enzyme Mix (Cat. No. 11791-020, Invitrogen™). The reactions were set in PCR tubes and incubated in a thermocycler machine at 25°C for 3-4 hrs or O/N (alternatively, to increase the efficiency). Following the end of the recombination, the entire reaction volume (2.5µl) was transformed into *E. coli* TOP10 chemical competent cells, as described in **section 2.5.4**. The transformed cells were plated on LB/Amp plates and incubated O/N at 37°C.

Two type II restriction enzymes were deemed suitable for the subcloning of *promAT1G72940* sequence into *pMW#3* (see map in **Section 7.1**): SpeI and XbaI recognition sites are flanking the *ccd*B/CmR cassette on the vector, allowing for the cassette to be removed and replaced by the insertion of the *promAT1G72940* sequence upstream of the LacZ reporter gene. Furthermore, neither SpeI nor XbaI seem to have a recognition site in the sequence of *promAT1G72940,* allowing for those sites to be introduced in the 5' and 3' of the *promAT1G72940* sequence. A new pair of primers (see **Table 2.6**) was designed to PCR amplify the *promAT1G72940* versions out of the entry clones: VN1059 (For) introducing SpeI recognition site on the 5' end and VN1060 (Rev) introducing XbaI recognition site on the 3' end of *promAT1G72940.*

Table 2.6 **Primers designed to amplify the WT and mutated motif versions of promoter *AT1G72940,* introducing recognition sites for SpeI (For) and XbaI (Rev) for cloning into pMW#3 vector.**

Stock name	Primer name	Sequence (5' to 3')	Tm (Tm with overhang)
VN1059	pAT1G72940_Y1H_For	ATTAACTAGTAGGTTCTGCTTGTG GCAGACGACG	63.4°C (63.5°C)
VN1060	pAT1G72940_Y1H_Rev	TATTATCTAGATTTGATTTTTGATT CTCTCTATTG	47.6°C (52.7°C)

The previously sequenced entry clones *promAT1G72940/ pDONR™-Zeo* (WT, m1, m2, m3, m1-2) were used as templates for the amplification of *promAT1G72940* fragments with Q5 DNA polymerase, primer annealing temperature of 60°C, 45 seconds extension time and a total of 19 cycles. The PCR products as well as the plasmid *pMW#3* were double digested for 1.5hrs at 37°C, with SpeI (R0133S, NEB) and XbaI (R0145S, NEB) using the CutSmart® Buffer (NEB), in a final reaction volume of 50µl. The SpeI/XbaI digested products were run on 1% agarose gel and the desirable bands of each construct (1.4Kb insert, 8.3Kb vector) were cut out of the gel and the DNA was extracted as described in **Section 2.5.7**. The inserts were ligated into the *pMW#3* vector in a ratio 5:1 of insert:vector, using the T4 DNA Ligase (M0202S, NEB) and the T4 DNA Ligase Buffer (NEB) at a final volume of 20µl. The reaction was incubated O/N in the thermocycler at 16°C. The ratios for the ligation were calculated using the NEBioCalculator® (http://nebiocalculator.neb.com/#!/ligation), after measuring the concentrations using a Nanodrop.

10µl of the ligation mixture was transformed into *E. coli* TOP10 chemical competent cells, as described in **Section 2.5.4**. The transformed cells were plated on LB plates with ampicillin (Amp). The following day, the successfully grown colonies were tested with colony PCR (see **Section 2.5.6**) using primers VN1059/VN1060 (**Table 2.6**) for the presence of the insert (*promAT1G72940).* From the PCR positive colonies, two were selected per construct to inoculate into liquid LB/Amp and grow O/N at 37°C. The next day,

recombinant plasmids were extracted and prepared for sequencing, using primers VN1053/VN1054 (See **Table 2.7**).

***Table 2.7* Primers suggested by Addgene for sequencing inserts subcloned into *pMW#3* yeast expression vector.**

Stock name	Primer name	Sequence (5' to 3')
VN1053	1HIFW	GTTCGGAGATTACCGAATCAA
VN1054	LacZ592RV	ATGCGCTCAGGTCAAATTCAGA

The correct clones were selected with colony PCR designed to show the orientation of the insert (VN1059/VN1054, see **Tables 2.6** and **2.7**).

2.5.3.3 Golden Gate assembly

The constructs intended for *A. thaliana* stable transformation were generated using the Golden Gate (GG) assembly technique, offering standardised enzymatic reactions, primer design principles and a broad collection of standard module parts described in the MoClo Plant Parts Kit (Engler et al., 2014).

In order to subclone the *TN* genes *AT1G72920, AT1G72930, AT1G72940 and AT1G72950* into the GG Level-0 (L0) acceptor plasmid *pAGM1287* (F2, MoClo Plant Tool Kit, SD2, Engler et al., 2014), a set of primers (VN989/VN990, VN991/VN992, VN993/VN994, VN995/VN996; **Table 2.8**) were designed according to the GG specifications, to amplify each gene and introduce the recognition site of the type IIs restriction enzyme BpiI (BbsI). The *TN* genes were amplified using as a template previously made constructs (see plasmids No. 15-18, **Table 2.3**) containing GG domesticated sequences of each *TN* gene.

Table 2.8 **Primers designed to amplify the *TN* genes and introduce the Golden Gate sites for cloning into Level-0 acceptor plasmids.**

Stock name	Primer name	Sequence (5' to 3')	Tm
VN989	AT1G72920-FOR	TTGAAGACAAAATGTCTTCTCCTACTGCGACTAAGTACG	62.4ºC
VN990	AT1G72920-REV	TTGAAGACAACGAACCCTCAGTTTTAAAAGAGTGATGTGA	62.9 ºC
VN991	AT1G72930-FOR	TTGAAGACAAAATGTCTTCTCATACTGCAACTAAGTATG	59.7 ºC
VN992	AT1G72930-REV	TTGAAGACAACGAACCTATTGTTGCATAAATCGTCTTCTT	62 ºC
VN993	AT1G72940-FOR	TTGAAGACAAAATGACTTCTCCTACTGCGACTAAGTATG	61.4 ºC
VN994	AT1G72940-REV	TTGAAGACAACGAACCACCAGATCTACCACTTAGACAACC	64.6 ºC
VN995	AT1G72950-FOR	TTGAAGACAAAATGTCAGATTCTTCAAACACCCTCCCAA	63.3 ºC
VN996	AT1G72950-REV	TTGAAGACAACGAACCACCTGATCTACCACATATACAACC	63.6 ºC

TN genes were amplified using 1 Unit of Q5® High Fidelity DNA Polymerase (M0491S, NEB), ~50ng of pDNA template, 1x Q5 reaction buffer, 100µM dNTPs, 500nM Forward Primer, 500nM Reverse Primer and sterile Milli-q® water up to 50µl. The thermocycler protocol was defined according to the manufacturer's instruction, using an annealing temperature of 60ºC and 19 amplification cycles. The PCR products were analysed with agarose gel electrophoresis to check the molecular weight and the integrity of the bands. The assembly of the L0 module for each *TN* gene was performed according to the manufacturer's instructions, using 5 Units BpiI (ER1011, Thermo Scientific™), 200 cohesive end units (ceu) of T4 DNA Ligase (M0202S, NEB) and approximately 100ng of L0 acceptor plasmid and PCR insert. 2µl of the GG L0 mixture was transformed into *E. coli* TOP10 competent cells as described before (**Section 2.5.4**) and plated on LBA/Spectinomycin (Spec) plates with Xgal/IPTG to grow O/N at 37ºC. White colonies were checked with colony PCR (see **Section 2.5.6**) using the same primer pairs, and the positive colonies of each *TN* gene were sent for sequencing (see **Section 2.6**).

The mutation detected in *AT1G72940/pAGM1287* clones was inverted with site-directed mutagenesis PCR using primers designed with the NEBaseChanger (NEB) tool (VN1066/VN1067, VN1068/VN1069, see **Table 2.9**) and the enzyme DpnI (NEB) to digest the original mutated plasmid.

Table 2.9 **Primers designed for site-directed mutagenesis of *AT1G72940* in *pAGM1278*, to invert the single point mutation causing the amino acid change.**

Stock name	Primer name	Sequence (5' to 3')	Tm
VN1066	AT1G72940_mut_FW3	AGTTTTCTCTACAAAGAATTCGTTCGAAGG	57.2°C
VN1067	AT1G72940_mut_RV3	TGTAGAGAAAACTGATGAAGTTGCGACGAG	60 °C
VN1068	AT1G72940_mut_FW4	CTTCATCAGTTTTCTCTACAAAGAATTCG	54.5 °C
VN1069	AT1G72940_mut_RV4	CGAATTCTTTGTAGAGAAAACTGATGAAG	54.5 °C

The GG L0 modules *AT1G72940/pAGM1287* and *AT1G72950/pAGM1287* were used to assemble complete transcriptional units in the Level-1 Position 1 (L1P1) acceptor plasmid *pICH47732*. The Golden Gate Plant Parts Kit (GG PPK) and custom made L0 modules used to create these transcriptional units included *p35SCaMV/pICH51266* (GG PPH2), *pDEX/L0* (dexamethasone-induced promoter), *pESTR/L0 (*estradiol-induced promoter*)*, *CT-GFP/pICSL50008* (GG PPG8), *CT-3xFLAG/pICSL50007* (GG PPA8), *CT-6xHA/pICSL50009* (GG PPB8) and *3U+Ter-AtACT2/pICH44300* (GG PPA12). Each transcriptional unit was created based on the following pattern:

Promoter+5UTR/L0 + TNgene/L0 + CT-tag/L0 + 3UTR+Ter/L0 + L1P1

The GG Level-1 assembly reaction was performed similarly to the one described for L0 modules, with the difference of using more parts and the restriction enzyme type IIs BsaI (Eco31I, ER0291, Thermo Scientific™) instead of BpiI. The same protocol was followed, and the transformed cells are plated on LBA/Amp plates with Xgal/IPTG. The white-coloured colonies were sequenced using external and internal primers for both *AT1G72940* and *AT1G72950* (see **Table 2.10**). A list of the resulted L1P1 modules can be found in **Table 2.11**.

Table 2.10 **Primers designed for sequencing Golden Gate clones.**

Stock name	Primer name	Sequence (5' to 3')	Tm
VN1070	p35S_3'_FW	ATGACGCACAATCCCACTATC	59.8ºC
VN1071	p35S_FW	TCTGAGCTTAACAGCACAGTTGC	57.7 ºC
VN1072	p35S_RV	TGTAAATGTAATTGTAATGTTG	44.9 ºC
VN1073	3FLAG_int_RV	TCGAGGTCATGGTCCTTATAGTC	55.4 ºC
VN1074	6HA_int_RV	AACGTCATATGGATACAATCCTG	52.4 ºC
VN1075	GFP_5'_RV	TCGCCGTCCAGCTCGACCAG	64.3 ºC
VN1076	3'UTR-ACT2_RV	TGTGAATGGAACACATGTAACG	53.4 ºC
VN1077	pDEX_FW	GGAGAGCTTGCATGCCGGTC	61.3 ºC
VN1078	pESTR_FW	GGAGCTTGGGCTGCAGGTCG	63.6 ºC
VN1079	AT1G72940_int_RV	AGCTAAAGCTGATCTACCATTG	52.4 ºC
VN1080	AT1G72940_int_FW	TGACTGTTACAACAATAAGCAATGG	53.9 ºC
VN1081	AT1G72950_int_RV	AGCTGATCTACCATTGCCTC	54.4 ºC
VN1082	AT1G72950_int_FW	ATGACTCGAAGATGGTCGAAG	54.2 ºC
VN1085	Level_0 F	CGTTATCCCCTGATTCTGTGGATAAC	57 ºC
VN1086	Level_0 R	GTCTCATGAGCGGATACATATTTGAATG	55.8 ºC
VN1087	Level_1 F	GAACCCTGTGGTTGGCATGCACATAC	62.1 ºC
VN1088	Level_1 R	CTGGTGGCAGGATATATTGTGGTG	57.5 ºC
VN1089	Level_2 F	GTGGTGTAAACAAATTGACGC	52.8 ºC
VN1090	Level_2 R	GGATAAACCTTTTCACGCCC	54.1 ºC
VN1091	Level-0_UA Fwd	TTACGGTTCCTGCACTCTGTG	57.7 ºC
VN1092	Level-0_UA_Rev	GCTTATGTCCACTGGGTTCGT	57.2 ºC
VN1093	L0-F2-seq	GTGAGCGAGGAAGCGGAAG	58.4 ºC
VN1094	L0-R2-seq	TGCCACCTGACGTCTAAG	54.2 ºC

The sequencing of L1P1 clones of *AT1G72950* showed that all constructs were carrying an extra triplet exactly at the 3' end of the gene. The L1P1 assembly was repeated using a different *AT1G72950/pAGM1287* clone, but the result was the same. The mutation probably pre-existed on the original clone but was not covered by the initial sequencing. The sequencing of L1P1 clones (see **Table 2. 10**) of *AT1G72940* revealed that all clones were correct.

Table 2.11 **List of Golden Gate constructs of *TN* genes in Level-1 Position-1 (L1P1) acceptor plasmids.**

GG L1P1 recombinant plasmids	Cells	Antibiotic resistance
p35S::AT1G72940:GFP/pICH47732 (L1P1)	*E. coli* TOP10	Ampicillin [100μg/μl]
p35S::AT1G72940:FLAG/pICH47732 (L1P1)	*E. coli* TOP10	Ampicillin [100μg/μl]
p35S::AT1G72940:HA/pICH47732 (L1P1)	*E. coli* TOP10	Ampicillin [100μg/μl]
pDEX::AT1G72940:GFP/pICH47732 (L1P1)	*E. coli* TOP10	Ampicillin [100μg/μl]
pDEX::AT1G72940:FLAG/pICH47732 (L1P1)	*E. coli* TOP10	Ampicillin [100μg/μl]
pDEX::AT1G72940:HA/pICH47732 (L1P1)	*E. coli* TOP10	Ampicillin [100μg/μl]
pESTR::AT1G72940:GFP/pICH47732 (L1P1)	*E. coli* TOP10	Ampicillin [100μg/μl]
pESTR::AT1G72940:HA/pICH47732 (L1P1)	*E. coli* TOP10	Ampicillin [100μg/μl]
pESTR::AT1G72940:FLAG/pICH47732 (L1P1)	*E. coli* TOP10	Ampicillin [100μg/μl]
p35S::AT1G72950:GFP/pICH47732 (L1P1)	*E. coli* TOP10	Ampicillin [100μg/μl]
p35S::AT1G72950:FLAG/pICH47732 (L1P1)	*E. coli* TOP10	Ampicillin [100μg/μl]
p35S::AT1G72950:HA/pICH47732 (L1P1)	*E. coli* TOP10	Ampicillin [100μg/μl]
pDEX::AT1G72950:GFP/pICH47732 (L1P1)	*E. coli* TOP10	Ampicillin [100μg/μl]
pDEX::AT1G72950:FLAG/pICH47732 (L1P1)	*E. coli* TOP10	Ampicillin [100μg/μl]
pDEX::AT1G72950:HA/pICH47732 (L1P1)	*E. coli* TOP10	Ampicillin [100μg/μl]
pESTR::AT1G72950:GFP/pICH47732 (L1P1)	*E. coli* TOP10	Ampicillin [100μg/μl]
pESTR::AT1G72950:HA/pICH47732 (L1P1)	*E. coli* TOP10	Ampicillin [100μg/μl]
pESTR::AT1G72950:FLAG/pICH47732 (L1P1)	*E. coli* TOP10	Ampicillin [100μg/μl]

For the assembly of the Level-2 modules, three different L1 modules previously produced in the lab (kindly donated by Dr. Ana Dominguez-Ferreras, University of Warwick) were used along with the existing L1P1 constructs: the *p35S::XVEreceptor/L1P3* expressing the transactivator for estradiol inducible systems, the *p35S::GVGreceptor/L1P3* expressing the transactivator for dexamethasone inducible systems and the *pFAST-R/pICH47742* (L1P2) module containing the pFAST-R plant selection cassette, expressing the red fluorescent protein (RFP) at the seed stage allowing for fast selection of transgenic plant lines. Additionally, the Level-2 end linkers, *End-link-2/pICH41744* (MoClo PTC5) and *End-link-3/pICH41766* (MoClo PTD5) were used for assembling L1 parts into L2 acceptors. The assembly in the L2 acceptor *pICSL4723* was performed with the same reaction as L0 (BpiI), using different parts and linkers according to the following pattern:

L1P1(p35SCaMV) + L1P2(pFAST-R) + End-link-2 + L2 acceptor

L1P1(pDEX) + L1P2(pFAST-R) + L1P3(GVG) + End-link-3 + L2 acceptor

L1P1(pESTR) + L1P2(pFAST-R) + L1P3(XVE) + End-link-3 + L2 acceptor

L2 reactions were transformed into *E. coli* TOP10 and plated on LBA/Kan. Successful white colonies were selected with 3 positive colony PCRs (one per L1 module included) and sequenced with external and internal primers (see **Table 2.10**). A list of the resulted L2 modules can be found in **Table 2.12.**

Table 2.12 **List of GG constructs of *TN* genes in Level-2 (L2) acceptors.**

GG L2 recombinant plasmids	Cells	Antibiotic resistance	Plant selection
p35S::AT1G72940:GFP/pICSL4723	TOP10	Kanamycin [25µg/µl]	pFAST-R
p35S::AT1G72940:FLAG/pICSL4723	TOP10	Kanamycin [25µg/µl]	pFAST-R
p35S::AT1G72940:HA/pICSL4723	TOP10	Kanamycin [25µg/µl]	pFAST-R
pDEX::AT1G72940:GFP/pICSL4723 [GVG]	TOP10	Kanamycin [25µg/µl]	pFAST-R
pDEX::AT1G72940:FLAG/pICSL4723 [GVG]	TOP10	Kanamycin [25µg/µl]	pFAST-R
pDEX::AT1G72940:HA/pICSL4723 [GVG]	TOP10	Kanamycin [25µg/µl]	pFAST-R
pESTR::AT1G72940:GFP/pICSL4723 [XVE]	TOP10	Kanamycin [25µg/µl]	pFAST-R
pESTR::AT1G72940:FLAG/pICSL4723 [XVE]	TOP10	Kanamycin [25µg/µl]	pFAST-R
pESTR::AT1G72940:HA/pICSL4723 [XVE]	TOP10	Kanamycin [25µg/µl]	pFAST-R
p35S::AT1G72950:GFP/pICSL4723	TOP10	Kanamycin [25µg/µl]	pFAST-R
p35S::AT1G72950:FLAG/pICSL4723	TOP10	Kanamycin [25µg/µl]	pFAST-R
p35S::AT1G72950:HA/pICSL4723	TOP10	Kanamycin [25µg/µl]	pFAST-R
pDEX::AT1G72950:GFP/pICSL4723 [GVG]	TOP10	Kanamycin [25µg/µl]	pFAST-R
pDEX::AT1G72950:FLAG/pICSL4723 [GVG]	TOP10	Kanamycin [25µg/µl]	pFAST-R
pDEX::AT1G72950:HA/pICSL4723 [GVG]	TOP10	Kanamycin [25µg/µl]	pFAST-R
pESTR::AT1G72950:GFP/pICSL4723 [XVE]	TOP10	Kanamycin [25µg/µl]	pFAST-R
pESTR::AT1G72950:FLAG/pICSL4723 [XVE]	TOP10	Kanamycin [25µg/µl]	pFAST-R
pESTR::AT1G72950:HA/pICSL4723 [XVE]	TOP10	Kanamycin [25µg/µl]	pFAST-R

The estradiol inducible promoter system was kindly donated by Dr. Nicola Patron (The Sainsbury Laboratory, UK) including the estradiol inducible promoter (*LexA* operator) paired with a 5' UTR within the pICSL120005 vector, as well as the dexamethasone inducible promoter system, including the

dexamethasone inducible promoter (*6GAL4UAS*) paired with a 5' UTR within the *pUAP12013* vector. The sequence for the XVE receptor protein which binds the estradiol inducible promoter in the presence of b-estradiol (Zuo et al., 2000) contained within the *pICSL80003* vector was assembled along with the standard MoClo level 0 modules encoding a 35S promoter and 5'UTR (*pICSL13001*) and a 3'UTR and terminator (*pICH44300*) into the level 1 position 3 (L1P3) vector *pICH47751*. The sequence for the GVG receptor protein which binds the dexamethasone inducible promoter in the presence of dexamethasone contained within the *pICSL80020* vector was assembled into L1P3 similarly to XVE. The FAST-R seed selection cassette (Shimada et al., 2010, standard MoClo level 0 module *pICSL70008*) was assembled into the level 1 position 2 (L1P2) vector *pICH47742* with the same promoter and terminator modules as the *XVE* L1P3 construct.

Constructs in L2 acceptor plasmids were transformed into *A. tumefaciens* GV3101 cells following the procedure described in **Section 2.5.5,** in order to facilitate plant transformation. *A. tumefaciens* successful clones were selected with colony PCR only for the presence of the respective *TN* gene. A full list of the *A. tumefaciens TN* containing clones is included in the **Section 7.4**.

2.5.4 Transformation of E. coli chemical competent cells

Initially, an aliquot of *E. coli* TOP10 competent cells was left to thaw on ice. Once thawed, the appropriate amount or recombinant plasmid defined by each cloning method (see **Section 2.5.3**) was pipetted into the aliquot of competent cells, and the mixture was left on ice for at least 30min. The cell mixture was then transferred to a heat block or water bath set at 42^{o}C, where heat shock was applied for 30 sec. After the heat shock, 200µl of sterile LB medium was added to the mixture and the cells were allowed to recover and propagate in an incubator at 37^{o}C for at least 1hr, shaking regularly. Following the recovery, the transformed cells were split into aliquots of 50µl and 150µl and spread on LBA plates containing appropriate selection antibiotics. The plates were incubated at 37^{o}C O/N.

2.5.5 Transformation of *A. tumefaciens* electro-competent cells

Transformation of *A. tumefaciens* cells was performed with electroporation, using a MicroPulser Electroporator (Bio-Rad Laboratories). An aliquot of *A. tumefaciens* GV3101 electro-competent cells (50μl) was thawed on ice before mixing with 1.5μl of the recombinant plasmid vector. The mixture was transferred inside a prechilled electroporation cuvette and then to the electroporator, where the pulse was applied according to the manufacturer's instruction. The transformed cells were recovered using 250μl of LB medium, incubating at 28^{o}C for 3 to 5hrs. After the recovery, the transformed cells were plated on LBA plates containing the appropriate selection antibiotics and incubated at 28^{o}C for 2-3 days.

2.5.6 Colony PCR

Depending on the efficiency of the cloning method used as well as the selection methods applied, a number of colonies is selected for PCR per construct (minimum 10). Each colony is individually numbered and diluted in 15μl of sterile water or plain LB. An aliquot of 3μl is used as template for the PCR reaction, with 0.5U of KapaTaq DNA polymerase, 1x KapaTaq Buffer, 100μM dNTPs, 500nM Forward Primer, 500nM Reverse Primer and sterile water up to 20μl final volume. The thermocycler program was set according to the KapaTaq DNA polymerase manual, using 15-18 cycles and annealing temperature suitable to the pair of primers used. Choice of primers depends on the desirable amplicon and whether orientation of the insert is of importance. Analysis of the PCR product via agarose gel electrophoresis was used to reveal the presence of a DNA band and assess the molecular weight, allowing for the selection of the positive recombinant plasmid vectors. The colonies corresponding to the positive PCR products were then inoculated in LB liquid cultures with appropriate antibiotics and incubated O/N at 37^{o}C.

2.5.7 Plasmid preparation

Plasmid preparation from both *E. coli* and *A. tumefaciens* liquid cultures was performed using the NucleoSpin® Plasmid Kit (Macherey-Nagel), following the manufacturer's protocol. Plasmids were eluted in 30μl of sterile Milli-Q® water.

In the case of *A. tumefaciens,* the time of cell lysis was increased to 10 min to meet the needs of the bacteria. When a higher concentration of plasmid was required (protoplast transformation experiments), the preparation was performed using the ZymoPURE II midiprep kit (Zymo Research) following the manufacturer's protocol.

2.5.8 Agarose gel electrophoresis

The integrity and molecular weight of DNA and RNA (ribonucleic acid) molecules for the purposes of this thesis was analysed and visualised via agarose gel electrophoresis. Unless stated otherwise, a solution of 1% w/v agarose electrophoresis grade was prepared in 1x Tris-Acetate-EDTA (TAE, 40mM Tris Base, 1mM EDTA, 20mM acetic acid, pH=8.0) buffer and heated until completely homogenised. GelRed® Nucleic Acid Gel Stain (Biotium) was added to the gel solution in a concentration of 3µl/100ml. The agarose gel solution was then poured into a gel tray with the appropriate combs and allowed to set for 30-40 min. The gel was transferred into an electrophoresis apparatus, completely submerged into 1xTAE buffer. The combs were removed and the DNA or RNA molecules to be analysed are loaded into the wells, using Orange G dye (Sigma-Aldrich) and a DNA ladder for reference. When an electric field is applied, the negatively-charged nucleic acids move towards the positive electrode and get separated based on their molecular weight. After running the gel, it was transferred into a gel imaging apparatus equipped with a UV (ultraviolet) lamp for visualisation. GelRed® binds DNA or RNA and in the presence of UV excitation, it allows the visualisation of the nucleic acids. The gel was imaged using a UV transilluminator (Gel Doc 1000, Bio-Rad).

2.5.9 DNA purification from agarose gel

DNA purification from agarose gel was performed using the Monarch® DNA Gel Extraction Kit (T1020S, NEB) following the manufacturer's protocol. DNA bands were then eluted in 30µl of sterile Milli-Q® water.

2.6 Sequencing of plasmids

Recombinant plasmid vectors were quantified using a Nanodrop ND 1000 spectrophotometer (ThermoFisher Scientific). The sequencing reaction was set up in a total volume of 10µl, according to the specifications of Eurofins-GATC: plasmid at a final concentration of 100ng/µl and the chosen primer at a final concentration of 10µM. Samples were barcoded with stickers and sent for next-day sequencing (Eurofins-GATC). A full list of the primers used for sequencing in this thesis is included in the **Section 7.3**.

2.7 Generation of competent cells

Two different types of competent cells were generated and used: *E. coli* TOP10 chemical competent cells and *A. tumefaciens* GV3101 electro-competent cells.

2.7.1 E. coli chemical competent cells

For the preparation of E. coli TOP10 chemical competent cells, the glycerol stock of the WT TOP10 cells was streaked on LBA plate without antibiotics and incubated O/N at 37°C, to produce single colonies. A single colony was inoculated into LB liquid culture without antibiotics and incubated O/N at 37°C shaker. A stock solution of 1M $CaCl_2$ was prepared and filter-sterilised. The stock solution was used to prepare 100mM $CaCl_2$ solution (can be autoclaved or filter-sterilised) and 100mM $CaCl_2$ solution containing 15% glycerol (autoclaved), both cooled at 4°C prior to use.

On the day of the cell preparation, 1mL of the TOP10 pre-culture was inoculated into 100mL of LB using a 500mL sterile flask to subculture at 37°C shaker, checking periodically until the OD_{600} reaches ~ 0.25-0.3 (approximately 2hrs post-inoculation). The culture then was chilled on ice for 15min before separated into 50mL Falcon tubes and centrifuged at 4°C at 4000rpm for 10min, using a precooled benchtop centrifuge. The supernatant was discarded, and the pellets resuspended in 40mL ice-cold 100mM $CaCl_2$ solution. The resuspended cells remained in ice for 30 min, before centrifuging again at 4°C at 4000rpm for 10min. The supernatant was discarded, and the

pellets resuspended in 5mL ice-cold 100mM $CaCl_2$ solution containing 15% glycerol. Finally, the cells were split in precooled Eppendorf tubes in 50µl aliquots.

The chemical competent *E. coli* TOP10 aliquots were immediately snap-frozen in liquid nitrogen and stored at -80°C deep freezer. A couple of aliquots were used to transform with supercoiled plasmids of known concentration, to assess the transformation efficiency of the cells by calculating the cell forming units per µg of DNA (cfu/µg). The transformation efficiency (TE) was calculated according to the following equation:

TE= Colonies/ µg/ Dilution
Where:
Colonies = the number of colonies counted on the plate
µg = the amount of DNA transformed expressed in µg
Dilution = the total dilution of the DNA before plating

2.7.2 A. tumefaciens electro-competent cells

Following the preparation of chemical competent cells, a final culture of 500mL of *A. tumefaciens* GV3101 was grown at 28°C to an OD_{600} equal to 0.5. The culture was chilled on ice for 30 min and centrifuged at 4000G for 15 min at 4°C. The supernatant was discarded, and the pellet resuspended in ice-cold sterile water and spun down again twice in volumes of 500mL and 250mL respectively, then resuspended and spun again in the same conditions in ice cold 10% glycerol in 10mL and 3mL respectively. The transformation efficiency of the electro-competent *A. tumefaciens* GV3101 was assessed as described in **Section 2.7.1**.

2.8 RNA methods

2.8.1 RNA extraction with Trizol

Unless stated otherwise, RNA extractions for the purposes of this project were performed using the Trizol™ (Invitrogen™ 15596018) extraction method. *A. thaliana* ecotype Col-0 plants were grown to 6 weeks of age (post sowing) and

leaf #8 of the adult rosette was identified and collected for RNA extraction from either treated or untreated plants. Leaves from 2 individual plants of the same genotype where pooled for each biological sample. The leaves were collected in 2mL Eppendorf tubes and immediately frozen in liquid nitrogen. Each leaf sample was ground to a fine powder in the tube using a precooled drill and the tube was kept in a tank of liquid nitrogen to keep the powder from thawing.

Initially 500μl of Trizol were added to the ground powder and the mixture was further ground with the drill, before adding another 500μl of Trizol and vortexing briefly to completely homogenise. The mixture was incubated in RT for 5min before adding 200μl of chloroform. The samples were shaken by hand as intensely as possible for up to 1 min and immediately set to centrifuge at 11,400 rpm for 20 min at 4^{o}C. After centrifugation, the samples were very carefully moved out of the centrifuge to not disturb the 3 separated phases: the aqueous phase where the RNA is extracted (upper phase), the genomic DNA phase (intermediate) and the organic phase (lower phase). 400-600μl of the aqueous upper phase was very carefully transferred to a new sterile tube, avoiding the disruption or aspiration of the other phases. An equal volume of ice-cold isopropanol was added to the retrieved supernatant and the tube was inverted by hand several times before transferred to -20^{o}C freezer, where the RNA was left to precipitate O/N (or for 2hrs minimum).

The next day, samples were moved from -20^{o}C to a precooled centrifuge (4^{o}C) and spun down at 13,300 rpm for 40 min. The supernatant was discarded, and tubes were assessed for the presence of a white pellet, before adding 1mL 70% ethanol in Diethyl Pyrocarbonate -treated water (DEPC, Sigma-Aldrich), vortexed briefly and centrifuged at 13,400 rpm for 5 min, repeating twice. The pellets were allowed to dry completely from any remaining ethanol residues that could not be removed with a pipette, before adding 50μl of sterile DEPC-treated water and left for the pellet to resuspend by incubating at 53^{o}C. Resuspended RNA samples were stored at -80^{o}C.

2.8.2 RNA extraction using the RNeasy Plant Mini Kit

The final experiments (**Chapter 5**) requiring RNA extractions for the purposes of this thesis were performed using the RNeasy Plant Mini Kit (74904, Qiagen). Unless stated otherwise, each sample of seedlings was composed of 10 *A. thaliana* seedings, and each sample of leaves composed of 3 *A. thaliana* rosette leaves #8 pooled from individual plants of the same genotype. Samples were ground as previously described (**Section 2.8.1**) to a fine powder and the extraction was performed according to the manufacturer's instructions. Extracted RNA was eluted in 50µl RNAse-free water (supplied in the kit).

2.8.3 DNAse treatment and RNA quality assessment

Extracted RNA was treated with Invitrogen™ TURBO DNA-free ™ Kit (Invitrogen™ AM1907, Fisher Scientific) to remove any contamination of DNA molecules that would interfere with enzymatic reactions. The reaction was set up using the entirety of extracted RNA per sample, 0.1 of volume TURBO DNase™ Buffer and 2 Units of TURBO DNase™ Enzyme. The reaction was incubated at 37°C for 30 min, followed by inactivation of the enzyme by adding 0.1 of volume DNase inactivation reagent. The samples were centrifuged according to the manufacturer's instructions. 40µl of the supernatant was very carefully aspirated from the mixture, avoiding disturbing the pelleted inactivation buffer that would compromise the quality of RNA. The quantity and quality of the DNA-free RNA samples were assessed as below.

Initially, using the RNA mode of a Nanodrop ND 1000 spectrophotometer (ThermoFisher Scientific) the DNA-free RNA samples were quantified as ng/µl and the quality assessment absorbance (A) ratios were calculated for each sample: A_{260}/A_{280} of ~2.0 and A_{260}/A_{230} of 2.0-2.2, where A_{260} measures the absorbance of nucleic acids, A_{280} primarily the absorbance of proteins and residual phenol, and A_{230} the absorbance of other organic contaminants such as residual phenol, guanidine, chloroform, alcohols and carbohydrate carryover in particular for plants. Low ratios indicate either contamination from

residual substances that can compromise the following enzymatic reactions or low RNA concentration.

In parallel, the quality of the samples was also assessed via agarose gel electrophoresis, as described in **Section 2.5.8**. The mRNA is less than 1% of the total RNA extraction so it cannot be visualised in a gel, but the integrity of the rRNA bands of the eucaryotic ribosomal subunits (18S, 5.8S and 25S) which most of the extracted RNA consist of, can be very informative.

2.8.4 Complementary DNA (cDNA) synthesis

Initially, the DNA-free RNA samples were all diluted to a concentration of 500ng/µl, verified with the Nanodrop. The cDNA synthesis reaction was set up in sterile PCR strips kept on ice at all times. For most reactions, a total of 2µg DNA-free RNA was mixed with 2.5nM oligodT19 primer (VN40, 5' – TTTTTTTTTTTTTTTTTTTVN - 3'), 0.5mM dNTPs in DEPC-treated water and DEPC-treated water up to 14µl. The mixture was denatured at 65^{o}C for 5 min in a thermocycler, immediately chilled on ice and added 0.2 of volume 5X first-strand buffer and 20mM DTT, before incubating at 42^{o}C for 2 min. Finally, 100 Units of SuperScript^{TM} II Reverse Transcriptase (18064022, ThermoFisher Scientific) was added to the reaction and it was left to incubate in the thermocycler for 50 min at 42^{o}C and a further 15min at 70^{o}C. The resulted cDNA was then diluted up to 60µl with DEPC-treated water and stored at -20^{o}C.

2.8.5 Real-time quantitative Polymerase Chain Reaction (RT-qPCR)

The Real-Time quantitative PCR (RT-qPCR) method was employed to quantify the level of representation of the genes of interest in the cDNA we synthesized from the extracted RNA pool. The quantification was performed using the CFX384 Touch Real-Time PCR machine (Bio-Rad).

All RT-qPCR reactions were prepared using the same reaction setup comprising of a master-mix of 3µl cDNA template, 450nM of each primer, nuclease-free water up to 40µl and 20µl of SYBR® Green JumpStart^{TM} Taq

ReadyMix™ (Sigma-Aldrich). Each master-mix was split into 3 technical replicates, using a 384 RT-qPCR plate. The thermocycler program was set according to the manufacturer's instructions. Expression levels were calculated relative to the expression of the housekeeping gene *α-TUBULIN* (*α-TUB, AT1G04820*), although *ACTIN* (*ACT8, AT1G49240*) was also used in several cases (see **Table 2.13**). C_T values (theoretical cycle to overcome a threshold) deriving from each RT-qPCR were imported into an excel file and analysed with the $\Delta\Delta C_T$ method (Livak and Schmittgen, 2001).

***Table 2.13* RT-qPCR primers for housekeeping genes *a-TUB* and *ACT8*.**

Stock name	Primer name	Sequence (5' to 3')
VN707	qaTUB_F	TACACCAACCTCAACCGCCT
VN708	qaTUB_R	TGGGGCATAGGAGGAAAGCA
VN500	ACT8-F	CCAGTGGTCGTACAACCGGTA
VN501	ACT8-R	TAGTTCTTTTCGATGGAGGAGCTG

All primers used for RT-qPCR experiments were designed at the 3' end of the genes, using the primer3 software (https://primer3.ut.ee/) and their specificity for each gene of interest was tested using Primer-BLAST (https://www.ncbi.nlm.nih.gov/tools/primer-blast/index.cgi). The default values in primer3 were changed to specific parameters used for the selection of RT-qPCR primers, which are described as follows: 21 mers for primer size (optimal), 62 degrees for Tm (optimal), a range of 110-240 bp for product size (optimal is 180 bp, the range can be extended from 100bp to 300bp). All primer pairs were selected to have a value of less than 3 for the 3' end complementation and less than 10 for any complementation, as well as %GC between 40 and 60.

The primers used to confirm the microarray data regarding the upregulation of TN genes post effector delivery by the bacteria *P. syringae* pv *tomato* DC3000 using RT-qPCR analysis in this thesis are listed in **Table 2.14.**

Table 2.14 **RT-qPCR primers designed to amplify *TN* genes to assess expression levels.**

Stock name	Primer name	Sequence (5' to 3')
VN899	TN8_Q_F1	AGAGTTTTGCCACGGAATGTT
VN900	TN8_Q_R1	TTTTCTACACCCCAAGAGCAA
VN901	TN9_Q_F1	TCGTTGGTTGAAGGTTGCACA
VN902	TN9_Q_R1	TGGGTTATTGGTTTGGTTGGCT
VN903	TN9_Q_F2	TGAAGGTTGGTTGGTTGAAGGT
VN904	TN9_Q_R2	CGGGTTATTGATTGGCTGGCT
VN905	TN10.1_Q_F1	CGAAGCTGGTGGACAAAATTGC
VN906	TN10.1_Q_R1	ATACTTTGGATTGGGCATGCG
VN907	TN10.1_Q_F2	GGTGATGATGACTCGAAGCTGG
VN908	TN10.1_Q_R2	TGGGCCTTCTCCTTTCTTCTTCT
VN909	TN11_Q_F1	CTGCTGCGGTCAAGTTGGTTT
VN910	TN11_Q_R1	CGGAAGGTTATTTGGAGAGGCT
VN911	TN12_Q_F1	ATTTCTGCTGCGTTCGAGGTG
VN912	TN12_Q_R1	ACACCAGCAACACACTCCAAA
VN913	TN12_Q_F2	AGACATTTCTGCTGCGTTCGA
VN914	TN12_Q_R2	CCTACTTCTAAGCCACAATCACA

Primers used to assess the expression levels of *AT1G72940* gene in the stably transformed *A. thaliana* lines, as well as the presence of the appropriate tags in the mRNA, are listed in **Table 2.15**.

Table 2.15 **RT-qPCR primers used to check the expression levels of *AT1G72940,* as well as the presence of GFP and FLAG tags in the corresponding *A. thaliana* transgenic lines.**

Stock name	Primer name	Sequence (5' to 3')
VN1145	AT1G72940-GFP-q-F1	ATCTGGTGGTTCGGTGAGCAA
VN1146	AT1G72940-GFP-q-R1	CCGGTGGTGCAGATGAACTTC
VN1147	AT1G72940-GFP-q-F2	GTGGTAGATCTGGTGGTTCGGT
VN1148	AT1G72940-GFP-q-R2	TGGTGCAGATGAACTTCAGGGT
VN1149	AT1G72940-FLAG-q-F1	CTGCTGCGGTCAAGTTGGTTT
VN1150	AT1G72940-FLAG-q-R1	CATGGTCCTTATAGTCTCCGTCA
VN1151	AT1G72940-HA-q-F1	GCTGCGGTCAAGTTGGTTTACT
VN1152	AT1G72940-HA-q-R1	GCTCTAGTGGCGTAATCTGG
VN1153	AT1G72940_q_FOR	CACATGAAGGCTCTTAACAAA
VN1154	AT1G72940_q_REV	GACGACCCTGAGAAATCCTT

2.9 *Agrobacterium* mediated stable transformation of *A. thaliana* using Golden Gate constructs

A. tumefaciens GV3101 carrying the respective constructs mentioned in **Chapter 5** were used to stably transform *A. thaliana* ecotype Col-0 plants using the floral painting method. The selected glycerol stock of each construct was streaked on LBA/Rif-Gen-Kan plates to produce singles colonies, one of which was then inoculated into 10mL liquid LB/ Rif-Gen-Kan cultures, grown for 48hrs at 28^{o}C. The bacterial inoculum was prepared for each construct and used with a brush to paint the floral buds and central bolt of *A. thaliana* ecotype Col-0 plants (10 plants per construct). The transformed plants remained covered in cling film for 3 days to maintain humidity. They were then uncovered and plants were bagged in appropriate-sized bags allowing ventilation and left to flower and produce seeds (approximately 2 months).

From a pool of seeds collected by the T0 plants (plants transformed with *A. tumefaciens*), the transgenic seeds were selected from the WT by identifying the red fluorescence (RFP) deriving from the expression of the pFAST-R cassette at the seed developmental stage, using a fluorescence stereoscope. A full list of the transgenic lines selected in each *A. thaliana* generation can be found in the **Section 7.5**.

2.10 Working with Yeast

2.10.1 Yeast strains, media, and growth condition

For the purposes of this thesis, two strains of haploid *Saccharomyces cerevisiae* yeast were used to carry the bait and the target sequences of the prospective Yeast-One-Hybrid screening (Y1H): Y8930 (baits) and Y8800 (prey). Both yeasts in their WT state survive only in rich Yeast Extract Peptide Dextrose (YEPD) medium (Dreze et al., 2010). When transformed with the bait's yeast expression vector (pMW#3), y8930 strain can survive in Synthetic Complete (SC) media lacking the amino acid Uracil (SC-Ura). The SC medium for the bait sequence was prepared using 3.8g Yeast Nitrogen Base (YNB),

10g ammonium sulfate (NH_4SO_4), 40g glucose, 2.8g of drop-out amino acid mix prepared by Sigma-Aldrich (Y2001-20G, lacking histidine, leucine, tryptophane and uracil), sterile water up to 1L and the pH adjusted to 5.9 with NaOH. When transformed with the prey's yeast expression vector (pDEST22), Y8800 strain can survive in SC media lacking the amino acid Tryptophane (SC-Trp). The SC medium for the prey sequences was prepared similarly to the one for the bait, only using an in-house made drop-out amino acid mix containing uracil and lacking histidine, leucine, tryptophane and adenine. The diploid yeast resulting of the bait x prey mating can survive in SC-Ura-Trp. All strains were grown in 28^{o}C for 48hrs.

2.10.2 Yeast transformation

The library containing 1,956 (approximately 80%) of the known *A. thaliana* transcription factors (TF) (Pruneda-Paz et al., 2014) acting as prey for the Y1H was already prepared and transferred into the *S. cerevisiae* strain Y8800 by Dr. Ana Dominguez-Ferreras (University of Warwick, UK). Therefore, the only yeast transformations performed for this thesis were the ones concerning the preparation of the baits.

For bait transformation, the strain *S. cerevisiae* Y8930 was inoculated in 4mL YEPD (rich media) and grown at 28^{o}C for 48hrs. Cultures were transferred in 1.5mL Eppendorf tubes to centrifuge at 2500rpm and the resulted pellet was resuspended in 300µl of sterile 0.1M LiAc. The mixture was further centrifuged at 2500rpm for 5 min at RT and then resuspended in 20µl 0.1M LiAc, to which were then added 30µl 1M LiAc, 40µl 2mg/ml ssDNA (salmon sperm DNA), 10µl sterile Milli-Q® water and ~300ng of the desirable yeast expression vector carrying the bait sequence. The tube contents were mixed gently before adding 200µl of 50% PEG 4000 solution and inverting the tube several times.

The transformation mixture was incubated for 1hr at 42^{o}C in a water bath. After the transformation, the yeast cells were isolated from the mixture by spinning down at 2500rpm for 5 min at RT, followed by removing the supernatant and resuspending the pellet using SC-Ura medium. The resuspended pellet was

inoculated into a 4mL culture of SC-Ura medium and incubated at 28°C shaking for 48hrs, to select for the transformed Y8930 cells.

2.10.3 Yeast One-Hybrid and identification of potential TF targets using beta-galactosidase assay

The yeast one-hybrid (Y1H) assay was performed using as prey an established collection of *A. thaliana* transcription factors, subcloned in the +Tryptophane (Trp) *pDEST-22* yeast expression vector (also known as pDEST-AD) and transformed into haploid Y8800 *S. cerevisiae* (TF Y8800 library, prepared by Dr. Ana Dominguez-Ferreras, University of Warwick, UK). The subcloning of the baits into the +Uracil (Ura) vector *pMW#3* for Y1H is described in detail in **Section 2.5.3.2**. The *proAT1G72940/pMW#3* (WT and mutated motifs) bait constructs were transformed into haploid Y8930 *S. cerevisiae.* The *pDEST22* vector confers the yeast the ability to synthesise tryptophane constitutively and pMW#3 vector confers the yeast the ability to synthesise uracil constitutively, as well as the β-galactosidase enzyme (LacZ), in the event that the binding and activation domains of the two appropriate yeast vectors are able to interact with one another.

Haploid Y8930 yeast transformed with the *pMW#3*(EV), *proAT1G72940-WT, proAT1G72940-m1, proAT1G72940-m2, proAT1G72940-m3* and *proAT1G72940-m1-2* bait constructs were mated with the haploid Y8800 containing either the *pDEST22*(EV) or the prey *ERF6* transcription factor (*AT4G17490*), to generate diploid yeast expressing both vectors and create the negative control (*pMW#3-EV*/Y8930 x *pDEST22-EV*/Y8800) and the designated positive control (*proAT1G72940-WT/Y*8930 x *ERF6*/Y8800) for the interactions. This was performed prior to the mating of the bait *proAT1G72940-WT/Y*8930 with the entire TF Y8800 library, to assess the effectiveness of the β-galactosidase assay.

Cell cultures of mated yeast were grown in SC media lacking uracil and tryptophane (-UT) at 28°C shaking for 48hrs. The selection process was repeated 2 or 3 times through subculture in fresh SC-UT to verify that the

constructs of interest were successfully integrated in the diploid yeast. All haploid and diploid yeasts were tested by growing on various SC media (-T, -U, -UT) to verify their specificity in growing only on the selective SC lacking the appropriate amino acids.

The β-galactosidase assay used to identify interactions was adapted for the purposes of this thesis by the colony-lift filter assay described in the Yeast Protocols Handbook (Protocol No. PT3024-1, Clontech Laboratories, Inc.). For the first screening the assay was performed exactly how the protocol describes, and then it was altered to fit the needs of liquid yeast cultures in 96-well-plates: the diploid yeasts resulted from the previously mentioned mating combinations were grown in SC-UT medium in 96-well-plates at 28^{o}C for 48hrs and then it was diluted 0, 1:10 and 1:100. 5μl of each yeast dilution was transferred on sterile Whatman No. 5 paper filters, which were completely submerged in a pool of liquid nitrogen for 10 seconds and then allowed to thaw in RT, to permeabilise the cells. The filters were carefully placed on the surface of a second Whatman No. 5, which was previously soaked in Z-Buffer/X-gal solution prepared according to protocol's instructions. The yeast cells were incubated in the Z-Buffer/X-gal solution at 28^{o}C O/N and checked every 30min for the first 4hrs for the appearance of blue colour.

2.11 Induction of Hypersensitive Response (HR) in *N. benthamiana*

Leaves of *N. benthamiana* plants used for Hypersensitive Response (HR) induction were 5 to 6 weeks old and the leaves used for the analysis were the first fully expanded one and the two immediately younger leaves. Leaves were infiltrated with *A. tumefaciens* bacterial suspensions made to an OD_{600} of 0.4, 0.8 or 1.0. More specifically, Golden Gate Level-2 constructs *p35S::AT1G72940:GFP*, *p35S::AT1G72940:FLAG* and *p35S::AT1G72940:HA* in *A. tumefaciens* GV3101 were used to generate bacterial suspensions, along with *a p35S::GFP* construct (kindly donated by Dr. Ana Dominguez-Ferreras, University of Warwick) as a negative control and *p35S::HOPQ1-1:GFP* (in pGWB5) as a positive control for HR induction.

Each leaf was sequentially infiltrated with 2 different construct combinations with a 30 min drying gap between them, creating two overlapping circles, one of which being an *AT1G72940* construct and the other expressing either *HOPQ1-1* or *GFP,* as well as a control expressing *HOPQ1-1* and *GFP*. In parallel, different plants were chosen to have whole leaves infiltrated with each of the above-mentioned constructs to check the effect on the whole leaf and collect samples for protein extraction. Leaves were assessed and imaged with a digital camera at 2 and 3dpi (days post infiltration).

2.12 Biochemistry methods

The majority of stably transformed *A. thaliana* lines and transiently transformed *N. benthamiana* leaves were meant to constitutively express truncated TIR-NB (TNs) proteins tagged with a variety of epitopes. Therefore, the presence of the protein in these lines was assessed via crude protein extraction and western blot protein detection.

2.12.1 Protein extraction

To extract the constitutively expressed AT1G72940 protein from the plants of interest, a crude extraction protocol was followed. Initially, treated or untreated plant tissue was collected and flash-frozen in liquid nitrogen. Samples were pulverised into fine powder and approximately 150-200mg of powder was used per sample. Crude extraction was performed by preparing 6X SDS loading buffer (4.8gr SDS electrophoresis grade, 4.8ml of Tris-HCl 1M pH=6.8, 24mg bromophenol blue, 18.8mL glycerol and sterile Milli-Q® water up to 32mL), diluting it 6 times and adding 1M DTT (50µl per 1mL 6X SDS loading buffer) prior to use to produce the 1XSDS+DTT extraction buffer. As a general practise, a 1:1 (or 2:1) ratio of tissue powder to extraction buffer was used, by adding the extraction buffer to the pulverised tissue in a 2mL Eppendorf tube, vortex until completely homogenised, then boiled at 95^{o}C for 10 min. The mixture was then centrifuged at 13,300rpm for 15 min at RT. Depending on the original volumes used for the extraction, approximately 60-100µl of supernatant were retrieved and transferred to a new tube. Extracted proteins were stored at -80^{o}C.

2.12.2 SDS PAGE Electrophoresis

Extracted proteins were analysed using the method of SDS PAGE electrophoresis. Protein extracts were loaded in 10% SDS PAGE gels (29:1 ratio of acrylamide:bis-acrylamide), prepared by following the pre-established protocol in the lab. 5µl of PageRuler^{TM} Prestained Protein Ladder (26616, ThermoFisher Scientific) were loaded to each gel as reference for the protein molecular weights. 1L of SDS Running Buffer was prepared (25mM Tris Base, 192mM Glycine, 0.1% SDS electrophoresis grade, pH adjusted to 8.3 with HCl) and added to the tank containing the SDS PAGE gels. Proteins have been denatured by boiling (95^{o}C) prior to loading the gel. An electric field of 100V was applied to move proteins through the stacking part, increased to 160V through the resolving part of the gel. The SDS PAGE electrophoresis ran until proteins were fully separated through the gel.

2.12.3 Coomassie Brilliant Blue gel staining

After the end of the electrophoresis, gels were carefully removed from in between the glasses and the ones meant for protein staining were transferred to appropriate boxes, where they were completely submerged in a staining solution of Coomassie Brilliant Blue R-250 (ThermoFisher Scientific). Gels were incubated on a shaker in RT for 1hr or O/N. The staining solution was then replaced by a de-staining solution (20% methanol, 10% glacial acetic acid and ddH_2O up to 1L) to remove excess dye. The de-staining solution was renewed regularly until only the protein bands remained visible on the gel.

2.12.4 *Immuno-blot protein detection (western blot)*

Following the end of the SDS PAGE electrophoresis, the gels intended for immuno-blot protein detection (Western blot) were prepared for wet transfer. The transfer buffer was prepared in advance (SDS Running buffer with 20% methanol and Milli-Q® water up to 1L) and was kept cold at 4^{o}C. All sponges and Whatman papers were fully soaked in transfer buffer prior to assembling the transfer cassette and the PVDF membrane was activated in methanol, before added on top of the gel. The cassette was fully submerged in transfer

buffer inside the transfer apparatus, along with an ice block and a magnet, to maintain the buffer in low temperature. The transfer apparatus was taken to the cold room (4^{o}C), placed on top of a magnetic stirrer and an electric field of 30V was applied O/N. Alternatively, the transfer was performed for 1.5hrs at 100V.

After the end of the transfer, the cassette was disassembled and the membrane was transferred in a tray, with the protein side facing up. The membrane was completely submerged into the blocking solution, consisting of 5% non-fat dried milk in Tris-Buffered Saline (TBS, 24.2g Tris base, 80g NaCl, pH=7.6 and adjusted to IL with ddH20) with 0.1% Tween-20 (TBS-T) and incubated on a belly-dancer shaker for 1hr at RT. The blocking solution was removed and replaced by the appropriate primary antibody solution (in 5% milk/ TBS-Tween buffer), where it was incubated for 1-4hrs at RT. The primary antibodies used for the purposes of this study were the α-GFP-HRP (monoclonal, Santa Cruz Biotechnology) used in a concentration 1:10000, the monoclonal α-FLAG® M2 produced in mouse (F3165, Merck) used in a concentration 1:2000, and the polyclonal α-FLAG® produced in rabbit (F7425, Merck) used in a concentration 1:5000.

Since only the α-GFP is HRP-conjugated, the membranes bearing FLAG-tagged proteins needed to further incubate into secondary, HRP-conjugated antibodies: the α-mouse-HRP (Merck) produced in goat and used in a concentration of 1:10000, and the α-rabbit-HRP (A0545, Merck) produced in goat and used in a concentration of 1:10000, respectively. Between the different antibodies, the membranes were washed in 1X TBS-T Buffer, 3 times for 10 min each in RT. The membranes were incubated in the secondary antibodies for 1hr in RT. After that, the washes were repeated, followed by one further wash in TBS Buffer.

A film exposure cassette was prepared with the membranes and the ICL™ Kit (Thomas Scientific) was used as a chemiluminescent substrate to facilitate the exposure of the HRP signal on clear blue X-ray film (CL-Xposure™ Film, Thermo Scientific), thus allowing the visualisation of the tagged proteins on

the membrane. The exposed film was developed and imaged using an X-ray developer.

2.12.5 Coomassie Brilliant Blue and Ponceau S staining of PVDF membranes

Following film exposure, the membranes were removed from the cassette and stained, to assess the efficiency of the transfer. In the cases when the membranes were intended to be used again, Ponceau S (Merck) dye was used to temporarily reveal the presence of proteins before it was washed off the membranes. In every other case, the membranes were stained with Coomassie Brilliant Blue staining solution (0.5g Coomassie Brilliant Blue R-250, 250mL methanol and 250mL ddH_2O) for 5 min in RT. The membranes were then washed in de-staining solution until the protein bands were visible clearly.

3. Investigating the role of bacterial effectors and *Arabidopsis thaliana* transcription factors in regulating the expression of TN receptors using leaf protoplasts and *S. cerevisiae* Yeast One-Hybrid

3.1 Introduction

As previously discussed in **Chapter 1**, plants combat pathogenic infection through their innate immune system that mainly acts with two levels of response: PTI and ETI. During PTI and ETI, plants trigger different immune responses that collectively contribute to immunity both locally and systemically, such as generation of ROS, a burst of cellular Ca^{2+}, MAPK activation, production of phytohormones, and transcriptional reprogramming (Tsuda and Somssich, 2015). Plants need to coordinate stress responses with growth to reduce energy loss and maximise fitness (Denancé et al., 2013). Studies over the last decades have shown that both PTI and ETI responses following plant pathogenic infection are largely regulated at transcriptional level by transcriptional networks of many different plant transcription factors (Garner et al., 2016). *A. thaliana* and rice have found to have a large number of plant TFs, that are key players in modulating defence responses (Birkenbihl et al., 2017; Chen et al., 2017).

Transcription factors are proteins that act as on/off switch of gene expression and are responsible for the regulation of gene function through activation or suppression of gene transcription (Falak et al., 2021). TFs are transcribed in the nucleus, translated in the cytoplasm, and returned to the nucleus using their nuclear localization sites to find their DNA targets in the genome. They bind to TF binding sites (TFBSs), which are specific cis-regulatory elements located in the promoter region of a gene and have defined DNA-binding domains. TFBSs are usually highly conserved and are crucial for DNA binding.

They are also used for TF classification into families, such as MADS, WRKY, or APETALA2/ethylene-responsive factors (AP2/ERF). TFs bind on gene promoters in a spatiotemporal manner (Falak et al., 2021). They have a DNA-binding domain, that is highly conserved within members of the same TF family, and an effector domain, which regulates their interaction with other TFs or proteins necessary for transcription and is more rapidly evolving. TFs are involved in many biological functions, such as gene induction or repression, and response to signal transduction under various environmental conditions.

Transcriptional reprogramming has a major role in plant immunity and it is orchestrated by transcriptional complexes formed of TFs and co-regulatory proteins (Moore et al., 2011). Upon receptor activation, selected TFs within signalling pathways interpret the signal initiation in various ways that lead to a variety of transcriptional changes (Tsuda and Somssich, 2015).
A study in *A. thaliana* used high resolution temporal transcriptomic analyses to show that upon infection with the necrotrophic pathogen *Botrytis cinerea* at least one-third of the genome exhibited differential expression immediately post infection (Windram et al., 2012). It is also suggested that a metabolic shift between growth and immunity is required to reallocate resources for plant survival. Many TF families have been reported to play key roles in transcriptional reprogramming (Falak et al., 2021). WRKY, bHLH, AP2/ERF, NAM/ATAF/CUC (NAC), and MYB are among the major plant TF families that have been reported to play important roles in transcriptional reprogramming by regulating plant defence response upon infection (Seo and Choi, 2015).

WRKY TFs role in plant defence has been extensively studied in *A. thaliana*, and they can be both negatively and positively affecting the regulation of plant defence (Pandey and Somssich, 2009). Studies suggest that they regulate PAMP-signalling downstream of the MAPK signalling cascade (Asai et al., 2002), which plays a central role in defence responses via sensing PAMPs or ETI (Meng and Zhang, 2013). Many reports have shown that WRKY TFs also interact with plant resistant proteins and are therefore involved in ETI (Chen et al., 2010; Deslandes et al., 2002; Inoue et al., 2013; Narusaka et al., 2009). The MYB family of TFs is conserved among all eukaryotes as one of the most

functionally and structurally diverse families. They are classified based on the presence of a MYB domain. MYB TFs are reported to positively regulate the HR response, which is a form of programmed cell death (PCD) that host plants trigger against pathogenic infection (Daniel et al., 1999; Vailleau et al., 2002). Studies suggest that MYB TFs also contribute to another type of plant defence response known as systemic acquired resistance (SAR), where signalling transduction from the infection site systematically moves to other tissues to prepare them against the pathogen (Segarra et al., 2009). However, MYB family is less well studied for its role in plant defence compared to other families of transcription factors.

The AP2/ERF is a plant-specific TF family whose members are characterized by the presence of a conserved AP2 DNA binding domain, and has an important role in regulating plant stress responses (Nakano et al., 2006; Sakuma et al., 2002). They control the regulation of genes involved in growth and development, hormone signalling, and stress responses both transcriptionally and post-translationally (Gibbs et al., 2015; Licausi et al., 2013; Mizoi et al., 2012). Studies have shown that most of them have a low basal expression and their expression levels respond to external stress stimuli or hormonal imbalance (Feng et al., 2005; Li et al., 2017). Reports also indicate that the induction of AP2/ERFs depends on cis-regulatory elements of their promoters, such as HEAT SHOCK ELEMENT (HSE), ETHYLEN INSENSITIVE 3 (EIN3) BINDING SITE (EBS), LOW-TEMPERATURE RESPONSIVE ELEMENT (LRT), and ABA Response Element (ABRE) (Xie et al., 2019). The activity, expression levels and stability of AP2/ERFs are also controlled by post-translational changes, like phosphorylation. For example, in *A. thaliana*, TFs ERF6 and EFR104 are phosphorylated by mitogen-activated protein kinases (MAPKs) for positive regulation of pathogen responses (Bethke et al., 2009; Meng et al., 2013).

A. thaliana has approximately 145 members of the AP2/ERF family and about 65 of them are identified as ERFs (Feng et al., 2005). The ERF subfamily has been reported in studies for its role in plant defence responses. For example, when challenged with virulent *Pst* DC3000, tomato ERF proteins Pti4 and Pti5

are phosphorylated by Pto protein, which increases their binding to their target sequences in defence-related genes (Zhou et al., 1997). When tomato Pti4, Pti5, and Pti6 ERFs were overexpressed in *A. thaliana*, they contributed to resistance against *Pst* DC3000 by inducing defence responses (Gu et al., 2002). Similarly, constitutive expression of ERF1 in *A. thaliana* increases resistance against necrotrophic fungal pathogens (Berrocal-Lobo et al., 2002).

A study generated time-series RNA-sequencing data to compare temporal transcriptome dynamics of *A. thaliana* Col-0 and combinatorial mutants of *delayed dehiscence2* (*dde2*), *ethylene insensitive2* (*ein2*), *phytoalexin4* (*pad4*) and *salicylic acid induction deficient2* (*sid2*) during infection with *Pst* DC3000, *Pst* DC3000 AvrRpt2 or *Pst* DC3000 AvrRpm1 (Mine et al., 2018). They found that some genes were similarly induced between Col-0 and the mutants upon challenging with ETI-triggering strains *Pst* DC3000 AvrRpt2 and *Pst* DC3000 AvrRpm1, and these genes were enriched for immunity-related GO terms, suggesting they are actively contributing to immunity. 26 of these genes encode for TFs, including ERF5, ERF6, ERF104 and ERF105, which belong to the same subfamily and have reported to play redundant and ethylene-independent roles in stress responses and development (Dubois et al., 2013; Meng et al., 2013; Nakano et al., 2006; Xu et al., 2016).

When it comes to their role in plant immunity, expression of a dominant negative *ERF6* fused to the transcriptional repressor motif EAR (*ERF6-EAR*) was shown to compromise resistance against *Botrytis cinerea* (Meng et al., 2013) and that expression of *ERF5-EAR* increases susceptibility to virulent *Pst* DC3000 (Son et al., 2012). The authors of the study (Mine et al., 2018) found that the GCC-box (GCCGCC) which serves as the binding motif for ERFs, is overrepresented within the promoters of the genes induced independently of JA/ethylene/PAD4/SA signalling network during ETI. They selected *TN* genes *AT1G72920* and *AT1G72940* among other GCC box-containing genes, to test as potential targets of these ERF transcription factors. However, they focused particularly on ERF6, because it was previously reported to be activated through phosphorylation by MPK3 and MPK6 during ETI, and these MAP kinases are active upon ETI activation (Meng et al., 2013; Tsuda et al., 2013).

The authors of the study performed ChIP experiments using a transgenic line expressing constitutively active *ERF6* (*ERF6-4D*), which mimics the phosphorylated and active form of ERF6 (Meng et al., 2013), the results showed that ERF6 binds to the promoters of genes *WRKY33*, *MPK3*, *AT1G72920* and *AT1G72940*. Overexpression of *ERF6-EAR* reduced the expression levels of *AT1G72920* and *AT1G72940*, *WRKY33* and *MPK3*. Their results suggest that ERF6 and possibly its homologs ERF5, ERF104, and ERF105 contribute to the expression of genes in a manner independent of the JA/ethylene/PAD4/ SA network during ETI (Mine et al., 2018). They also suggest that ERF6 potentially plays an important role in the regulation of expression of TN genes *AT1G72920* and *AT1G72940.*

In this Chapter we present the results of *Pst* DC3000 infection on the expression levels of *TN* genes *AT1G72920, AT1G72930, AT1G72940* and *AT1G72950*, and we address the question of how the recorded transcriptional changes in the expression of those genes are connected to *Pst* DC3000 effector delivery. A set of 6 candidate *Pst* DC3000 effectors has been identified to play a role in *TN* gene upregulation upon infection. While the microarrays analysis showed that all 4 *TN* genes are upregulated in response to *Pst* DC3000 (**Figures 1.10** and **1.11**), gene *AT1G72940* showed the strongest response to infection (**Figure 1.10b**), which is also verified by the RT-q-PCR results in this Chapter. Additionally, among those 4 *TN* genes, *AT1G72940* is the one that has been experimentally studied the most (Nandety et al., 2013) and, together with *AT1G72920,* one known to be regulated by the transcription factor ERF6 (Mine et al., 2018). These, along with the fact that the cloning and production of transgenic lines was prioritised for *AT1G72940* prior to this PhD project, drew the focus mainly on *AT1G72940.* We attempted to identify more transcription factors that regulate the expression of *AT1G72940* via Yeast-One-Hybrid screening, in order to begin elucidating the mechanism which connects those bacterial effectors to the transcription of *TN* genes and their role in plant defence.

3.2 Results

3.2.1 Pst DC3000 WT infection of A. thaliana Col-0 plants resulted in the detection of elevated levels of TN transcripts, indicating a potential correlation between the regulation of TN gene expression and the bacterial infection

As discussed in **Section 1.6**, preliminary data of a microarray analysis conducted by (Lewis et al., 2015) indicated that the transcription levels of four gene members of the *A. thaliana TN* family (*AT1G72920, AT1G72930, AT1G72940, AT1G72950*) are upregulated in Col-0 upon infection with the bacterial pathogen *Pst* DC3000 (**Figures 1.10 & 1.11**). Data were collected after subjecting Col-0 rosette leaves to various biotic (*B. cinerea, Pst* DC3000 WT, *Pst* DC3000 *hrpA*) and abiotic (long day, short day, highlight, drought) treatments, aiming to characterize the plant's transcriptional response to stress. The transcriptional levels of genes *AT1G72920, AT1G72940* and *AT1G72950* of the *A. thaliana TN* family of interest appeared to not be affected by any other type of stress, including infection with *Pst* DC3000 *hrpA,* a mutant strain with a defective T3SS. Additionally, the transcription of gene *AT1G72930* seem to be positively regulated by a variety of treatments and it is not specifically triggered by *Pst* DC3000 WT. Collectively, the preliminary data suggested that there is a potential correlation between the infection with *Pst* DC3000 WT and the elevated transcriptional levels of *AT1G72920, AT1G72940* and *AT1G72950* genes.

Quantitative real-time PCR (RT-q-PCR) was used to measure the changes in the transcriptional levels of the *A. thaliana TN* family upon *Pst* DC3000 infection, as an alternative method to microarrays. RT-q-PCR-quality primers (listed in **Table 2.14)** were designed to amplify the mRNAs of each *TN* gene following the specifications described in **Section 2.8.5** and taking into account the high sequence homology between the *TN* genes of this locus. Alignment of the coding sequences (CDS) of *TN* genes *AT1G72920, AT1G72930,*

AT1G72940, and *AT1G72950* was performed with the Clustal Omega tool (EMBL-EBI, Hinxton) and is presented in **Figure 3.1**.

```
CLUSTAL O(1.2.4) multiple sequence alignment


AT1G72950.1      ATGTCAGATTCTTCAAACACCCTCCCAAAGTTTGATGTTTTTCTGAGCTTCAGAGGACTC   60
AT1G72930.1      ------ATGTCTTCTCATACTGCAACTAAGTATGATGTTTTCCTAAGTTTCAGAGGGCAT   54
AT1G72920.1      ------ATGTCTTCTCCTACTGCGACTAAGTACGACGTCTTTCTGAGTTTCAGAGGACTC   54
AT1G72940.1      ------ATGACTTCTCCTACTGCGACTAAGTATGATGTCTTTCTGAGTTTCAGAGGAGTC   54
                       ****    **     * ****  ** ** ** ** ** ********

AT1G72950.1      GACACTCGCCGCAGCTTCATCAGTTTCCTCTACAAAGAACTGATTCGAAGAAACATTCGA   120
AT1G72930.1      GACACTCGCCACAACTTCATCAGTTTTCTCTACAAAGAACTGGTTCGAAGGAGCATTCGA   114
AT1G72920.1      GACACTCGTCGCAACTTCATCAGTTTTCTCTACAAAGAACTCGTTCGAAGAAAAATTCGA   114
AT1G72940.1      GACACTCGTCGCAACTTCATCAGTTTTCTCTACAAAGAATTCGTTCGAAGGAAAATTCGA   114
                 ******** * ** ************ ************ *  ******* *  ******

AT1G72950.1      ACCTTTAAAGACGATAAGGAGTTGAAGAATGGCCGGAGGATTACGCCGGAGCTAATACGC   180
AT1G72930.1      ACCTTCAAAGACGACAAAGAGCTGGAGAATGGCCAGAGGTTTTCGCCGGAGCTCAAAAGC   174
AT1G72920.1      ACTTTCAAAGACGACAAGGAGCTCGAGAATGGCCGGAGGATTTCTCCGGAGCTCAAACGC   174
AT1G72940.1      ACTTTCAAAGACGACAAGGAGCTTGAGAATGGCCGGAGGATTTCTCCGGAGCTCAAACGC   174
                 ** ** ******** ** *** *  ********* **** ** * ******** * * **

AT1G72950.1      GCCATTGAAGGGTCGAGATTCGCAGTCGTTGTGGTCTCCGTGAATTACGCTGCGTCTCGT   240
AT1G72930.1      CCCATCGAGGTGTCAAGATTCGCCGTCGTTGTTGTCTCAGAGAACTATGCTGCGTCTTCT   234
AT1G72920.1      GCCATCGAGGAGTCGAAATTCGCCGTCGTTGTGGTCTCTGTGAACTACGCTGCGTCTCCT   234
AT1G72940.1      GCCATCGAGGAGTCGAAATTCGCCGTCGTTGTTGTCTCTGTAAACTACGCTGCGTCTCCT   234
                  **** ** * *** * ****** ******** ***** *  ** ** *********  *

AT1G72950.1      TGGTGTCTCGAAGAGCTCGTGAAGATTATGGATTTCGAAAACATGGGCTCGCTCAAGGTC   300
AT1G72930.1      TGGTGTCTCGATGAGCTCGTAACGATCATGGATTTCGAAAAAAAGGGTTCCATCACCGTG   294
AT1G72920.1      TGGTGTCTCGATGAGCTTGTGAAGATTATGGATTTCGAAAACAAGGGTTCCATCACCGTG   294
AT1G72940.1      TGGTGTCTCGATGAGCTTGTGAAGATTATGGATTTCGAAAACAAGGGTTCCATCACCGTG   294
                 *********** ***** ** * *** ************** * *** **  ***  **

AT1G72950.1      ATGCCTATCTTCTACGGCGTGGATCCGTGTCATGTGAGGAGACAGATCGGAGAAGTCGCT   360
AT1G72930.1      ATGCCCATCTTCTACGGCGTGGAACCGAATCATGTGAGGTGGCAGACCGGAGTACTCGCT   354
AT1G72920.1      ATGCCTATCTTCTACGGCGTGGATCCTTGTCATTTGAGGAGGCAGATCGGAGATGTCGCT   354
AT1G72940.1      ATGCCTATCTTCTACGGTGTGGATCCGTGTCATTTGAGGAGGCAGATCGGAGATGTCGCT   354
                 ***** *********** ***** **   **** ***** * **** *****   *****

AT1G72950.1      GAACAGTTTAAGAAGCATGAGGGTAGAGAA---GATCATGAGAAAGTGCTTTCATGGAGG   417
AT1G72930.1      GAACAGTTTAAGAAACATGCGAGTAGAGAA---GATCCTGAGAAAGTTCTTAAATGGAGG   411
AT1G72920.1      GAACAGTTTAAGAAGCACGAGGCTAGAGAAGAAGATCATGAGAAAGTAGCTTCGTGGAGA   414
AT1G72940.1      GAACAGTTTAAGAAGCACGAGGCTAGAGAAGAAGATCATGAGAAAGTTGCTTCGTGGAGA   414
                 ************** ** * *  *******   **** *********   *   *****

AT1G72950.1      CAAGCGTTGACTAATTTGGCGAGTATCTCCGGCGATTGTTCATGGAAATGGGAAGATGAC   477
AT1G72930.1      CAAGCATTGACCAATTTTGCGCAACTCTCCGGCGATTGTTCAGGT------GATGATGAC   465
AT1G72920.1      CGAGCATTGACCAGTTTAGCGAGTATCTCCGGCGAATGTTCATTGAAATGGGAAGATGAA   474
AT1G72940.1      CGAGCATTGACCAGTTTGGCTAGTATCTCCGGAGATTGTTCATCCAAATGTGAAGATGAA   474
                 * *** ***** * *** **     ******* ** ******         ** *****

AT1G72950.1      TCGAAGATGGTCGAAGAAATTACTGACAGGATATCAAAAGAGCTGATGATTGATACAACA   537
AT1G72930.1      TCGAAGCTGGTGGACAAAATTGCTAACGAGATATCAAACAAGAAGACGATTTATGCAACA   525
AT1G72920.1      GCGAATCTGGTGGACGAAATTGCTGACAAGATATCAAAAAATCTGATGACTGTTACAACA   534
AT1G72940.1      GCGAAGCTGGTGGACGAAATTGCTGACAAGATATCAAAAAATCTGATGACTGTTACAACA   534
                  ****  **** **  ***** ** **  *********  *   ** ** *  * *****

AT1G72950.1      AGAAGCAATGGGAGTGACCTTGAAGGGATTGATGCACACATGAAAGCTCTTCACCGTTTA   597
AT1G72930.1      ATATGA------------------------------------------------------   531
AT1G72920.1      ATAAGCAATGGGAGGGACCTAGTTGGGATTGATACACACATGAAGGCTCTTAACAAAAAA   594
AT1G72940.1      ATAAGCAATGGGAAGAACCTAGTTGGGATTGATACACACATGAAGGCTCTTAACAAAAAA   594
                 * * *

AT1G72950.1      TTGAATTTAAATTCTAAGAAAAGTGTGAGAGTGATTGGGATTTGGGCAAGAGGAGGCAAT   657
AT1G72930.1      ------------------------------------------------------------   531
AT1G72920.1      TTGGATTTGAATTCCAACAAAAGTTTGAGAGTGGTTGGGATTTGGGCAAGAGGATACAAT   654
AT1G72940.1      CTGGATTTGAATTCCAACAAAAGTTTGAGAGTGGTTGGGATTTGGGCAAGAGGATACAAT   654
```

```
AT1G72950.1     GGTAGATCAGCTTTAGCTAAATTTGTTTATCAGAACATCTGTCAACACTTCGAAAGCCAT   717
AT1G72930.1     ------------------------------------------------------------   531
AT1G72920.1     GGTAGATCAGCTTTAGCTAAATATGTTTATCAAGACATCTGTCATTGGTTGAAGGTTGGT   714
AT1G72940.1     GGTAGATCAGCTTTAGCTAAATATGTTTATCAAGACATCTGTCACCACTTTGACAGCCAT   714

AT1G72950.1     TGTTTCTTGGAAAGTGTGAAAAGGATTTCTCAGGATCGCCACCTGTCTCACTTACACGAA   777
AT1G72930.1     ------------------------------------------------------------   531
AT1G72920.1     TGGTTGAAGGTTTATCAAGATATCAAG--ACAGCTTCCAAACTTTATGTTTTAACTCGTT   772
AT1G72940.1     TGTTTCTTGGGAAGCGTGAAAAGGATTTCTCAGGGTCGTCACTTATCGCATCTACACGAA   774

AT1G72950.1     GAGTTTATGATACGGATTCAAGGAGAATGCTTGAGTAAATTAAGGCTCAAGAACCAAAAG   837
AT1G72930.1     ------------------------------------------------------------   531
AT1G72920.1     GGTTGAAGGTTGCACATTTGCTTCAT----AGATCACATCACTCTTTTAAAACTGAGTAG   828
AT1G72940.1     GAGTTTCTGATA-----AGGATTCAA----GGAAGTAAACATAATCTCAAGGACCAAAAG   825

AT1G72950.1     GTTCTGCTCGTGGCTGATGATGTGAATAAGCTTGAACAGTTAGATGCTCTTGCAGAGGAC   897
AT1G72930.1     ------------------------------------------------------------   531
AT1G72920.1     ------------------------------------------------------------   828
AT1G72940.1     GTTTTGCTTGTGGCTGATGATGTTTATAAGCTTGAACAGTTAGATGCTCTTGCTGAGGAT   885

AT1G72950.1     TTTAACTGCTTTGGTCCTGGGAGTATAGTTATTATCACTACACAAGACAGGCAGCTGCTT   957
AT1G72930.1     ------------------------------------------------------------   531
AT1G72920.1     ------------------------------------------------------------   828
AT1G72940.1     TTCAACGGGTTTGGTCCGGGAAGTGTTGTTATCATCACTACACAAGACAAGCATCTGTTT   945

AT1G72950.1     ATCTCTGCTGGCATAAAACTTGTTTATGAAGTAGAGCTTCTCAGATTCCAGAAAGTTCGT   1017
AT1G72930.1     ------------------------------------------------------------   531
AT1G72920.1     ------------------------------------------------------------   828
AT1G72940.1     GTTTCTGCTGGTATAAAGCTTGTCTACGAAGTTGAGCTTTTGAAATTCCAGAAAGTTTGT   1005

AT1G72950.1     GGACTCTTCAGACAATTAGCCTTCAAAGAGAAAGACATTTCTGCTGCGTTCGAGGTGTCT   1077
AT1G72930.1     ------------------------------------------------------------   531
AT1G72920.1     ------------------------------------------------------------   828
AT1G72940.1     GAACTCTTCCGACAATTCGCCTTTAAAAAGAGAGACATTTCTGCTGCGGTCAAGTTGGTT   1065

AT1G72950.1     TTGTATAGGGCAACGAATGTTGCCATGGAATGGTTAGGTTGTATATGTGGTAGATCAGGT   1137
AT1G72930.1     ------------------------------------------------------------   531
AT1G72920.1     ------------------------------------------------------------   828
AT1G72940.1     TACTATAGGGCAACAAATTGGT------------TAGGTTGTCTAAGTGGTAGATCTGGT   1113

AT1G72950.1     TAG    1140
AT1G72930.1     ---    531
AT1G72920.1     ---    828
AT1G72940.1     TAG    1116
```

***Figure 3.1* CDS sequence alignment among the 4 candidate genes of the *A. thaliana TN* family that are upregulated in response to *Pst* DC3000.**

The online bioinformatics tool Clustal Omega was used to create an alignment of the CDS of *Arabidopsis thaliana TN* genes *AT1G72920, AT1G72930, AT1G72940,* and *AT1G72950*. All 4 genes are shown to share high sequence homology, however gene *AT1G72930* is significantly shorter, thus compromising the output for the remaining genes at the 3' end of the sequence. The program's default parameters were used. Sequences appear in aligned order and not input order. Where the nucleotides are identical among all aligned sequences, the sequence is marked with an asterisk below these nucleotides.

RT-q-PCR primers are designed to target and amplify the 3' end of the mRNA, which is more stable and less likely to get degraded than the 5' end. Therefore, it was necessary to ensure that primers could be designed as close to the 3' end as possible but would also be able to differentiate between the different members of the family. *TN* genes differ in length in both genomic sequence and CDS, thus producing proteins of diverse molecular weights. The respective CDS lengths, according to TAIR: *AT1G72920* is 828bp, *AT1G72930* is 531bp, *AT1G72940* is 1116bp, and *AT1G72950* is 1140bp long.

As shown by the alignment (identical nucleotides are marked with an asterisk), all *TN* genes are highly homologous in the 5' end and middle of their CDS (**Figure 3.1).** Gene *AT1G72930* is much shorter than the rest, which restricts Clustal Omega from marking the homology between the remaining members of the family on the 3' end of the sequences. To counteract this issue, the sequence of *AT1G72930* was removed from the process and the alignment was performed again for the remaining *TN* genes. As shown in **Figure 3.2**, removing *AT1G72930* CDS produces a more clear picture of the homology among these genes, however *AT1G72920* is again shorter than *AT1G72940* and *AT1G72950,* resulting in the same problem for the 3' end. The process was repeated using only the sequences for genes *AT1G72940* and *AT1G72950*, and the alignment is presented in **Figure 3.3**. The results of the alignment made it clear that genes *AT1G72940* and *AT1G72950* share high homology at all regions of their CDS.

Collectively, the results of the alignments confirmed that the options for RT-q-PCR primers are limited due to high sequence homology among the members of the *TN* family. To overcome this problem, all primers were designed to amplify a small region between the 3' end of the CDS and the 3'UTR of each respective gene, which may not be translated but is transcribed as part of the mRNA. All primer pairs were checked with primer BLAST to ensure they don't amplify other *TN* members. Prior to RT-qPCR, all primer pairs for *TN* genes were tested both on Col-0 cDNA and genomic DNA, as an extra quality control step.

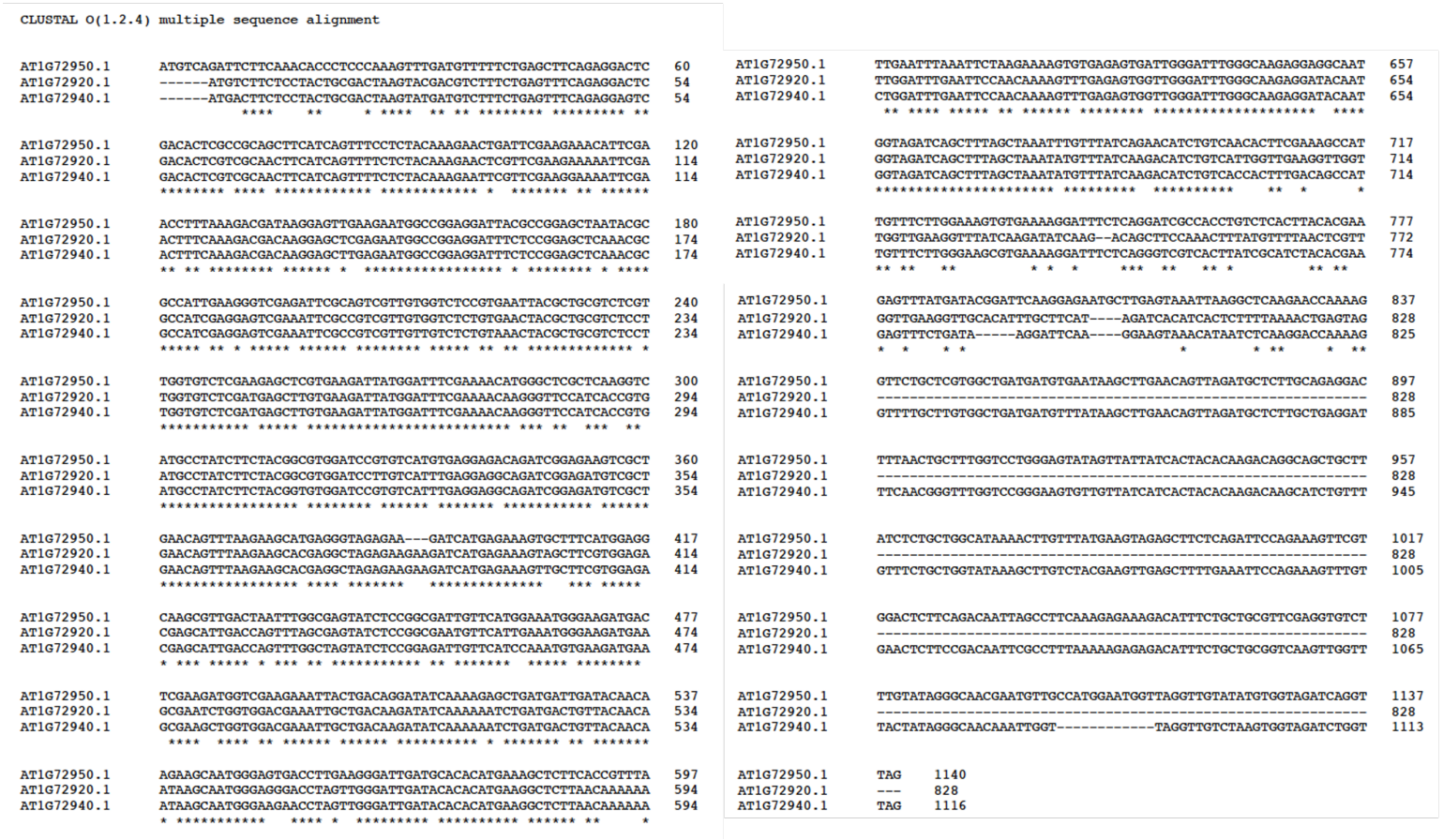

***Figure 3.2* Sequence alignment of *AT1G72920*, *AT1G72940*, and *AT1G72950* CDS.**

Clustal Omega was used to create an alignment of the CDS of *TN* genes *AT1G72920, AT1G72940,* and *AT1G72950*. All 3 genes share high sequence homology, but *AT1G72920* is shorter than the rest. The program's default parameters were used. Sequences appear in aligned order and not input order. Where the nucleotides are identical among all aligned sequences, the sequence is marked with an asterisk below these nucleotides.

***Figure 3.3* Sequence alignment of *AT1G72940* and *AT1G72950* CDS.**

Clustal Omega was used to create an alignment of the CDS of *TN* genes *AT1G72940,* and *AT1G72950*, which are highly homologous. The program's default parameters were used. Sequences appear in aligned order and not input order. Where the nucleotides are identical among all aligned sequences, the sequence is marked with an asterisk below these nucleotides**.**

Figure 3.4 presents the fold change expression of the *TN* genes post inoculation with *Pst* DC3000, *hrpA*, and mock over a time course of 12hrs, with samples taken at 0, 6, and 12hrs post inoculation. *TN* fold change expression was normalised against α-tubulin and is relative to the basal *TN* expression levels of the untreated sample. The results represent the average fold change out of three independent biological replicates.

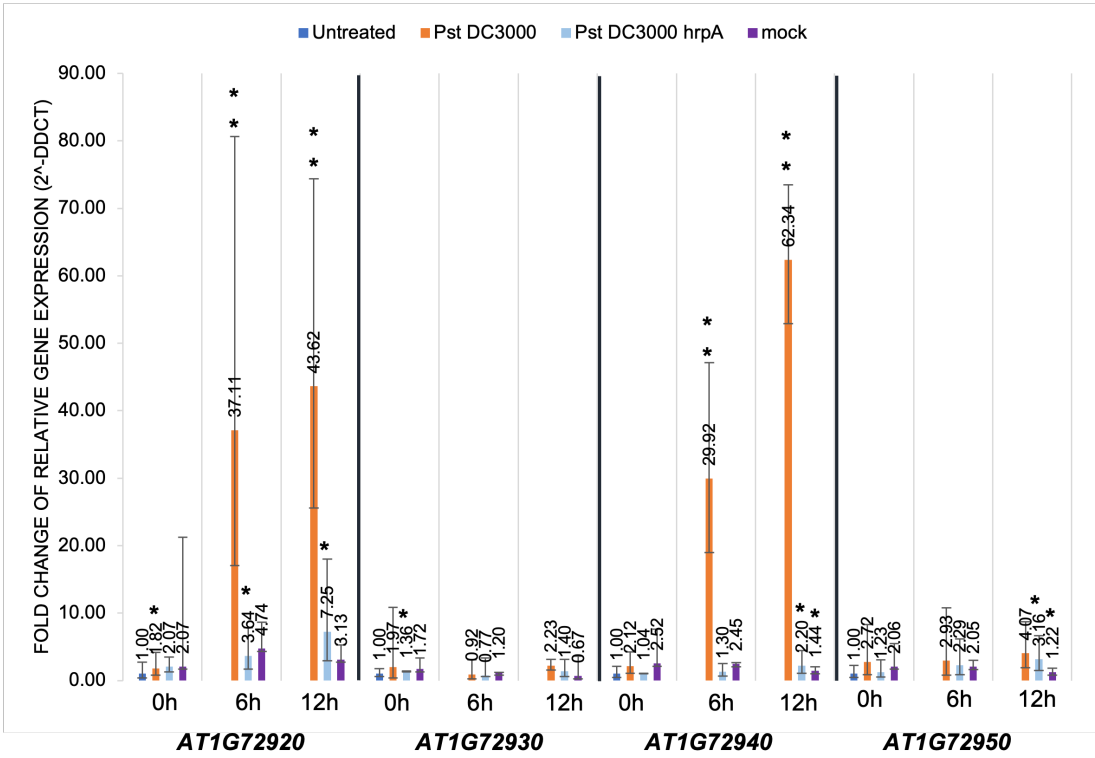

***Figure 3.4* Fold change of the expression of genes *AT1G72920, AT1G72930, AT1G72940*, and *AT1G72950* post inoculation with *Pst* DC3000, *hrpA*, and mock over a time course of 12hrs.**

RT-qPCR was performed to monitor the transcriptional changes of the *TN* genes in response to each treatment. For each biological replicate, leaf #8 of adult *A. thaliana* Col-0 rosettes was inoculated with either *Pst* DC3000 WT (orange) or *Pst* DC3000 *hrpA* (light blue) bacterial suspensions (O.D.= 0.15), or $MgCl_2$ (10mM) for mock treatment (purple). Untreated leaves (blue) were used as a control for basal gene expression. Leaves were harvested at 0, 6 and 12hrs post inoculation. Bar heights represent the average fold change in expression of each *TN* gene for each condition, calculated from 3 independent biological replicates. Error bars indicate the 95% confidence intervals for the fold change of relative Ct values. One asterisk (*) indicates statistically significant difference to 5%; two asterisks (**) indicate statistically significant difference to 1%. Due to small sample number, a two-tail t-test assuming unequal variances was selected for the statistical analysis.

As shown in **Figure 3.4,** increased transcript levels were observed for genes *AT1G72920* and *AT1G72940* in response to *Pst* DC3000 WT (orange bars), showing a 37- and 30-fold change relative to the untreated sample at 6hrs post-inoculation (P.I.), respectively. Both genes show further increase up to 44- and 63-fold increase at 12hrs P.I., compared to the untreated sample. In both cases, the fold change is statistically significant with a p-value smaller than 1%. Due to the small number of biological replicates (n=3), a two-tail t-test assuming unequal variances was used to determine the statistical significance of the observed difference in expression. Any differences in expression of *AT1G72920* and *AT1G72940* following *Pst* DC3000 *hrpA* and mock ($MgCl_2$) treatments are either not statistically significant, or the observed difference has a p-value of up to 5%.. Genes *AT1G72930* and *AT1G72950* did not show any significant response to any of the treatments.

Collectively, the RT-qPCR results provide substantial evidence that at least 2 members of the *TN* family (*AT1G72920* and *AT1G72940*) show a positive transcriptional response to *Pst* DC3000 WT infection recorded between 6 and 12hrs post treatment with the bacteria. The transcriptional levels of genes *AT1G72920* and *AT1G72940* appear to be consistently increased at 6 and 12hrs post inoculation across all 3 biological replicates.This tendency seems to be in line with the microarray pattern (**Figure 3. 1. a**. and **b.**), where the peak of gene expression is recorded between 5 and 9hrs post *Pst* DC3000 WT infection. On the contrary, the expression levels of genes *AT1G72930* and *AT1G72950* do not seem to follow the microarray profile.

The RT-qPCR analysis of the transcriptional response of the *TN* family members to bacterial infection is partially in line with the microarrays. Lack of response in the mock treatment indicates that the method of infiltration of the bacterial inoculum is not responsible for the change in gene expression. Additionally, the *hrpA* bacteria are unable to deliver effectors to the plant cells upon infection. Data showing a strong response of *AT1G72920* and *AT1G72940* to *Pst* DC3000 WT but not *hrpA* indicate that there may be a correlation between the delivery of bacterial effectors and the change in gene expression of some of the *TN* genes.

3.2.2 A protoplast-based Pst DC3000 effector screening identified 6 candidate effectors positively influencing the regulation of TIR-NB promoters

The results of the microarrays (**Figures 1.10 and 1.11**) and the RT-qPCR (**Figure 3.4**) as presented in **Section 3. 2. 1,** indicate a potential correlation between the regulation of gene expression of two members of the *A. thaliana TN* family and the bacterial infection caused by *Pst* DC3000 WT. Since the fundamental difference between *Pst* DC3000 WT and *Pst* DC3000 *hrpA* is that the latter is unable to deliver effectors in the plant, we hypothesized that the delivery of effectors by *Pst* DC3000 WT may be responsible for triggering the upregulation of the *TN* genes *AT1G72920* and *AT1G72940.*

To address this hypothesis, we investigated whether one or more of the known *Pst* DC3000 effectors is implicated in the regulation of expression of one or more members of the *TN* family. A screening of 22 known *Pst* DC3000 effectors was performed in *A. thaliana* Col-0 leaf protoplasts using the promoter regions of the *TN* genes fused with the luciferase (LUC) gene. In the presence of the substrate luciferin, the luciferase enzyme produces light which can be integrated with a camera and used to record the differences in gene expression by measuring the differences in light integration. The level of expression of the Luciferase gene is dependent on the regulation of the promoter fused to it, which allowed us to record and measure the response of each *TN* promoter to the presence of each individual *Pst* DC3000 effector. The protoplast-based effector screening method is schematically represented in **Figure 3. 3** and has been described in detail in **Section 2. 3** (**Materials and Methods**).

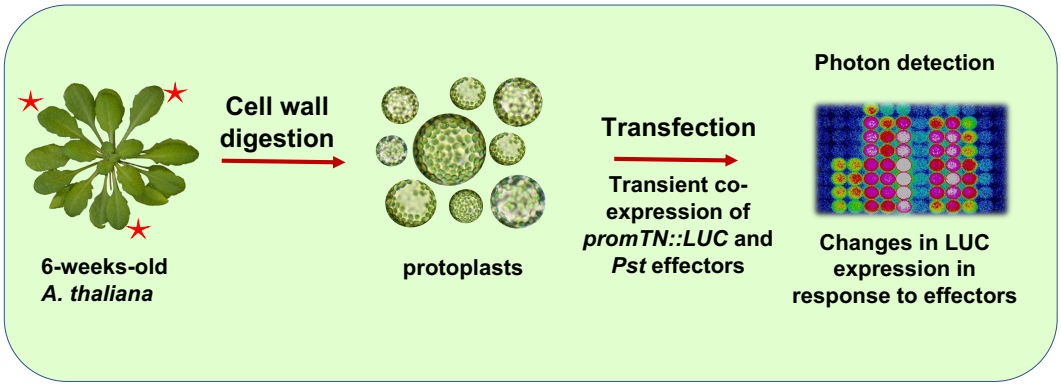

Figure 3.5 **Schematic representation of the *Pst* DC3000 effector screening method in *A. thaliana* leaf protoplasts.**

The protoplast-based assay utilizes the photon emmision resulting from the enzymatic activity of the transiently expressed Luciferase gene, to observe promoter activity. Luciferase expression is dependent on the transcriptional response of the *TN* promoters to the presence of *Pst* effectors, when they are transiently co-expressed in transfected protoplasts. Each individual assay includes the preparation of leaf mesophyll protoplast via the enzymatic digestion of the plant cell wall, followed by the transfection of the protoplasts with plasmid vectors containing the transcriptional unit of each effector and the transcriptional unit of each *TN* promoter fused with the luciferase gene. The protoplasts are then exposed to luciferin, which acts as a substrate for Luciferase. In the case that the expression of the effector protein is affecting the regulation of a *TN* promoter, the transcription of the Luciferase gene is affected, and substrate is catabolised accordingly, affecting the photon emission detected with a photon camera.

The protoplast transfection was performed using a *Pst* DC3000 effector library available in our lab (**Table 2.2, Materials and Methods**). Experiments preliminary to this project were conducted on promoter *AT1G72940* by Dr. WeiJei Huang (John Innes Centre, UK) and the data obtained were kindly provided for the purposes of this thesis (**Figure 3.6. a.** and **b.**). **Figure 3.6** shows the relative expression levels of the integrated luciferase signal after 3 biological repeats of the protoplast-based *Pst* DC3000 effector screening on promoter *AT1G72940.* The fold change of the *promAT1G72940::LUC* expression was calculated for each *Pst* DC3000 effector after the results were normalised against protoplasts transfected with an empty vector (EV) in place of the effector. Additionally, all effector screening assays conducted in the duration of this PhD included protoplasts transfected with a plasmid vector

expressing the GFP protein as an extra control reference, to ensure that the *TN* promoters were not affected by the expression of non-specific proteins.

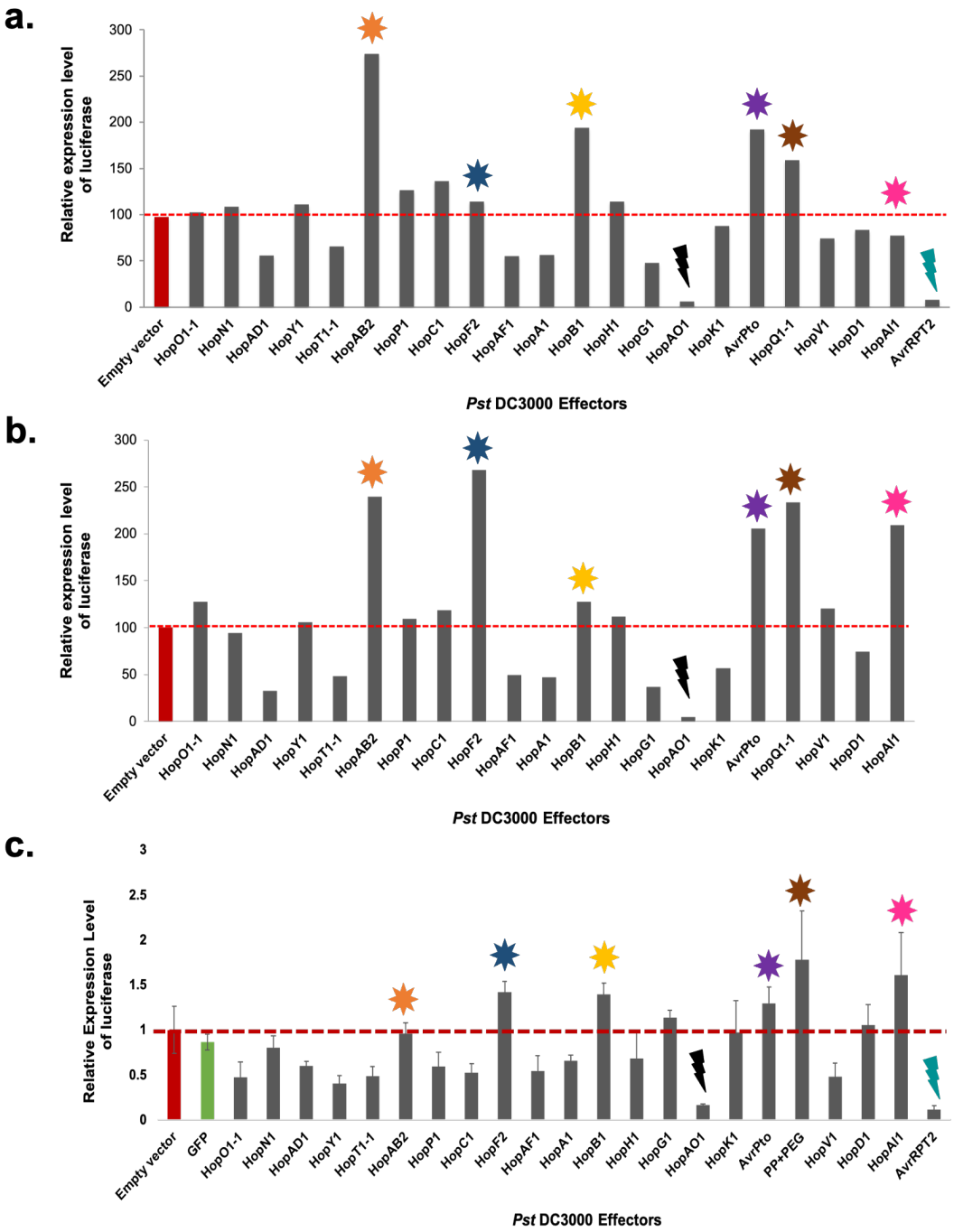

***Figure 3.6* Pst DC3000 effector screening on promAT1G72940::LUC using A. thaliana Col-0 mesophyll protoplasts.**

A. thaliana Col-0 protoplasts were transfected with *promAT1G72940::LUC* and a library of 22 *Pst* DC3000 effectors, to identify the potential effect of each effector on the regulation of promoter *AT1G72940*. Photon signal detection resulting from the expression of LUC was used as a measure to determine the

activity of the promoter in the presence of the effectors. The chart results presented in **a.** and **b.** were obtained and kindly provided for the purposes of this thesis by Dr. WeiJei Huang (John Innes Centre, UK). The third biological repeat presented in **c.** was produced with data obtained during this PhD project. Graphs present the fold change of relative expression levels of LUC in the presence of each effector, normalised against the results of the empty vector (EV). Bars marked with a star denote the effectors found to induce promoter *AT1G72940* in the preliminary experiments, while bars marked with a thunder denote the effectors associated with repression of *promAT1G72940,* to allow easy comparison with future biological replicates of the same and other *TN* promoters. The collective results of the three biological replicates indicate that promoter *AT1G72940* is induced in the presence of effectors HopAB2 (orange star), HopF2 (blue star), HopB1 (yellow star), AvrPto (purple star), HopQ1-1 (brown star), and HopAI1 (magenta star), whereas effectors HopAO1 (black thunder) and AvrRPT2 (teal thunder) appear to hinder the expression of LUC, indicating repression of promoter *AT1G72940.*

Due to the fact that the results on *promAT1G72940::LUC* were generated by different people, it was considered best to avoid combining them in one graph. To summarise the results of the three biological replicates of *promAT1G72940::LUC* effector screening, **Figure 3.6** shows that the presence of 6 out of the 22 effectors could induce *promAT1G72940::LUC,* whereas 2 of them seem to be associated with suppression of LUC expression. To allow for comparison between replicates of the same and other *TN* promoters, these effectors that were identified in the preliminary results of *promAT1G72940* are denoted with colour-coded star marks for induction and thunder marks for repression of the promoter, from **Figure 3.6** hereafter.

More specifically, HopAB2 (orange star), HopF2 (blue star), HopB1 (yellow star), AvrPto (purple star), HopQ1-1 (brown star), and HopAI1 (magenta star) induce *promAT1G72940::LUC.* Fold change differed for each effector between replicates, but in almost all cases the average change in LUC expression ranged between 1.5- and 3-fold relative to the EV. On the contrary, when effectors HopAO1 (black thunder) and AvrRPT2 (teal thunder) are expressed in the protoplasts, there is almost no LUC signal detected. The remaining effectors do not appear to cause any significant changes on *promAT1G72940::LUC* expression. The experiment was repeated several times in the duration of this PhD project, but the sensitivity of the protoplasts

during the preparation method and transfection often resulted to limited protoplast viability that hampered the outcome of the experiment.

Following the assay on *promAT1G72940::LUC*, the same *Pst* DC3000 effector library was used to screen for effectors potentially corelated to the regulation of the remaining *TN* promoters. **Figure 3.7** presents the results of two biological repeats (**A and C)** of the effector screening assay on *promAT1G72920::LUC*. The results show that the effectors found to induce *promAT1G72940::LUC* are also inducing *promAT1G72920::LUC,* when comparing between the two biological replicates. Similarly, effectors HopAO1 and AvrRPT2 seem to hinder the expression of LUC. **Figure 3.7.C** indicates that the presence of most effectors tested seem to induce *promAT1G72920::LUC*, however, so does the GFP-expressing vector, which should be at the same level as the EV. Collectively, effectors HopAB2 (orange star), HopF2 (blue star), HopB1 (yellow star), AvrPto (purple star), HopQ1-1 (brown star), and HopAI1 (magenta star) induce *promAT1G72920::LUC* in at least one of the two replicates. An additional effector, HopH1 (blue arrow) seems to be specific to *promAT1G72920::LUC* induction. Fold change differed for each effector between replicates, but in almost all cases the average change in LUC expression ranged between 1.5- and 3-fold, and some cases up to 10-fold relative to the EV.

Figure 3.8 presents the results of one biological repeat of the effector screening assay on *promAT1G72930::LUC*. The results show that the detected signal of LUC appears to be very low across the entire plate (**Figure 3.8.B**). Taking that into consideration, effectors HopQ1-1 and HopAI1 seem to be correlated with an induction of ~1.5-fold in LUC expression, while the presence of HopB1 and AvrPto results to an induction of 1.2- fold relative to the EV, and AvrRPT2 seem to repress *promAT1G72930::LUC*. This experiment was repeated multiple times, however the protoplast transfection was not always successful.

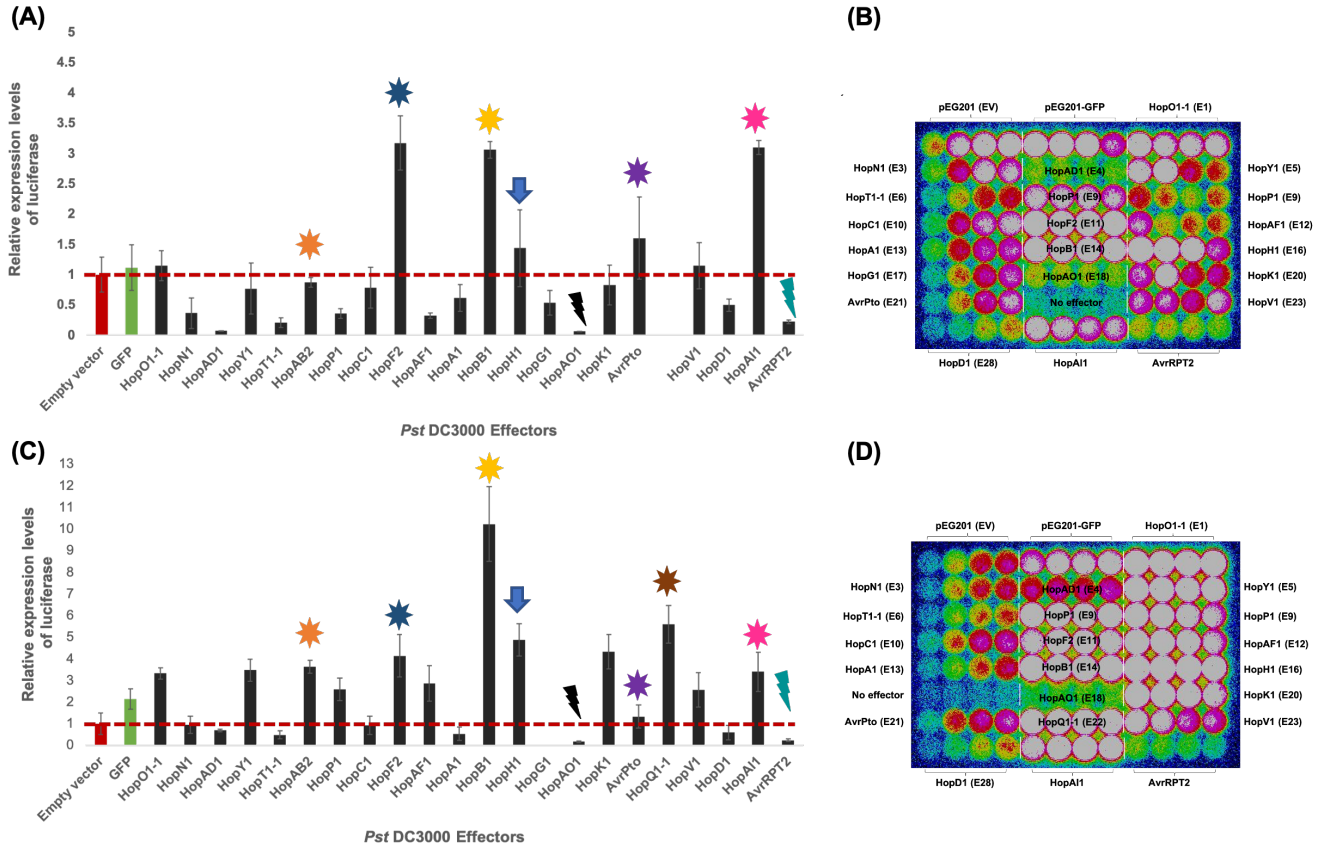

Figure 3.7 Pst **DC3000 effector screening on *promAT1G72920::LUC* using *A. thaliana* Col-0 mesophyll protoplasts.**

(A) and **(C)** depict the results of fold change of LUC relative expression of two biological repeats, and **(B)** and **(D)** the LUC photon signal detection . Star denote the effectors inducing *promAT1G72940* in the preliminary experiments, while thunders denote the ones associated with repression.. Collectively, promoter *AT1G72920* is also induced by HopAB2 (orange star), HopF2 (blue star), HopB1 (yellow star), AvrPto (purple star), HopQ1-1 (brown star), and HopAI1 (magenta star), and an additional effector HopH1 (blue arrow) specific to *promAT1G72920*. Effectors HopAO1 (black thunder) and AvrRPT2 (teal thunder) repress *promAT1G72920::LUC*.

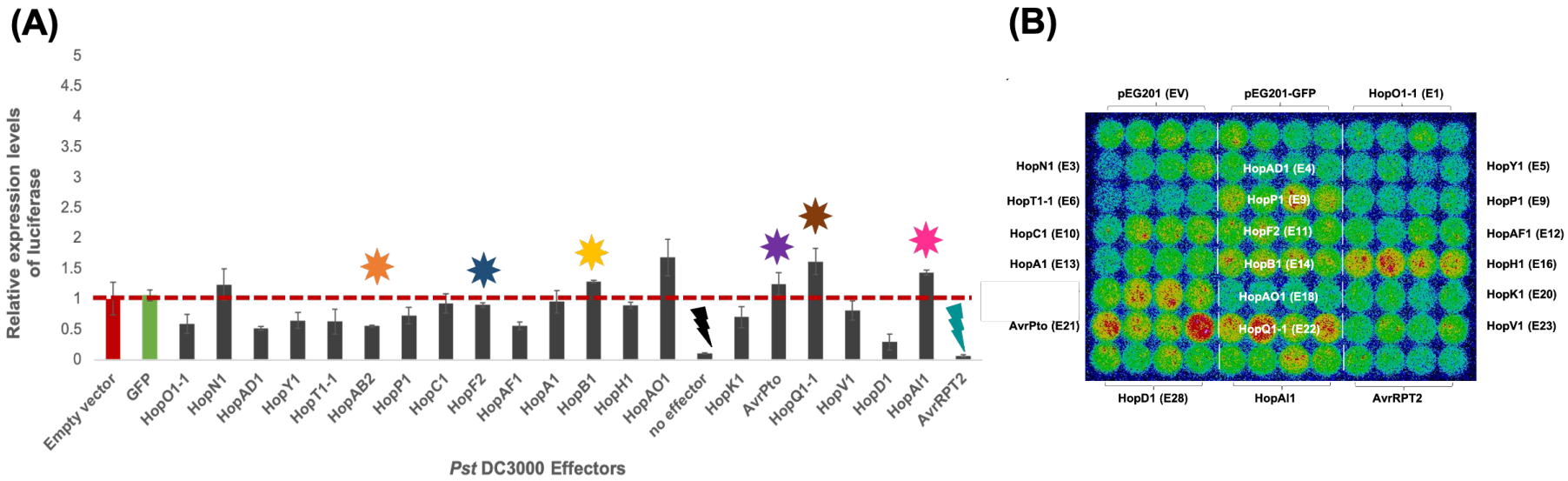

***Figure 3.8 Pst* DC3000 effector screening on *promAT1G72930::LUC* using *A. thaliana* Col-0 mesophyll protoplasts.**

Protoplasts were transfected with a library of 22 *Pst* DC3000 effectors and *promAT1G72930::LUC*. **(A)** depict the results of fold change of *LUC* relative expression of one biological repeat, and **(B)** the LUC photon signal detection. Star denote the effectors inducing *promAT1G72940* in the preliminary experiments, while thunders denote the ones associated with repression. Collectively, promoter *AT1G72930* is not induced by most effectors, except HopAO1, HopQ1-1 (brown star), and HopAI1 (magenta star). Effector AvrRPT2 (teal thunder) represses *promAT1G72930::LUC*.

Figure 3.9 presents the results of two biological repeats of the effector screening assay on *promAT1G72950::LUC*. The results show that most the effectors found to induce *promAT1G72940::LUC* are also inducing *promAT1G72950::LUC,* when comparing between the two biological replicates. Similarly, effectors HopAO1 and AvrRPT2 seem to hinder the expression of LUC. Collectively, effectors HopAB2 (orange star), HopF2 (blue star), HopB1 (yellow star), AvrPto (purple star), HopQ1-1 (brown star), and HopAI1 (magenta star) induce *promAT1G72950::LUC* in at least one of the two replicates. An additional effector, HopH1 (blue arrow) seems to be specific to *promAT1G72950::LUC* induction. Fold change differed for each effector between replicates, but in almost all cases the average change in LUC expression ranged between 1.5- and 2-fold, and some cases up to 5-fold relative to the EV.

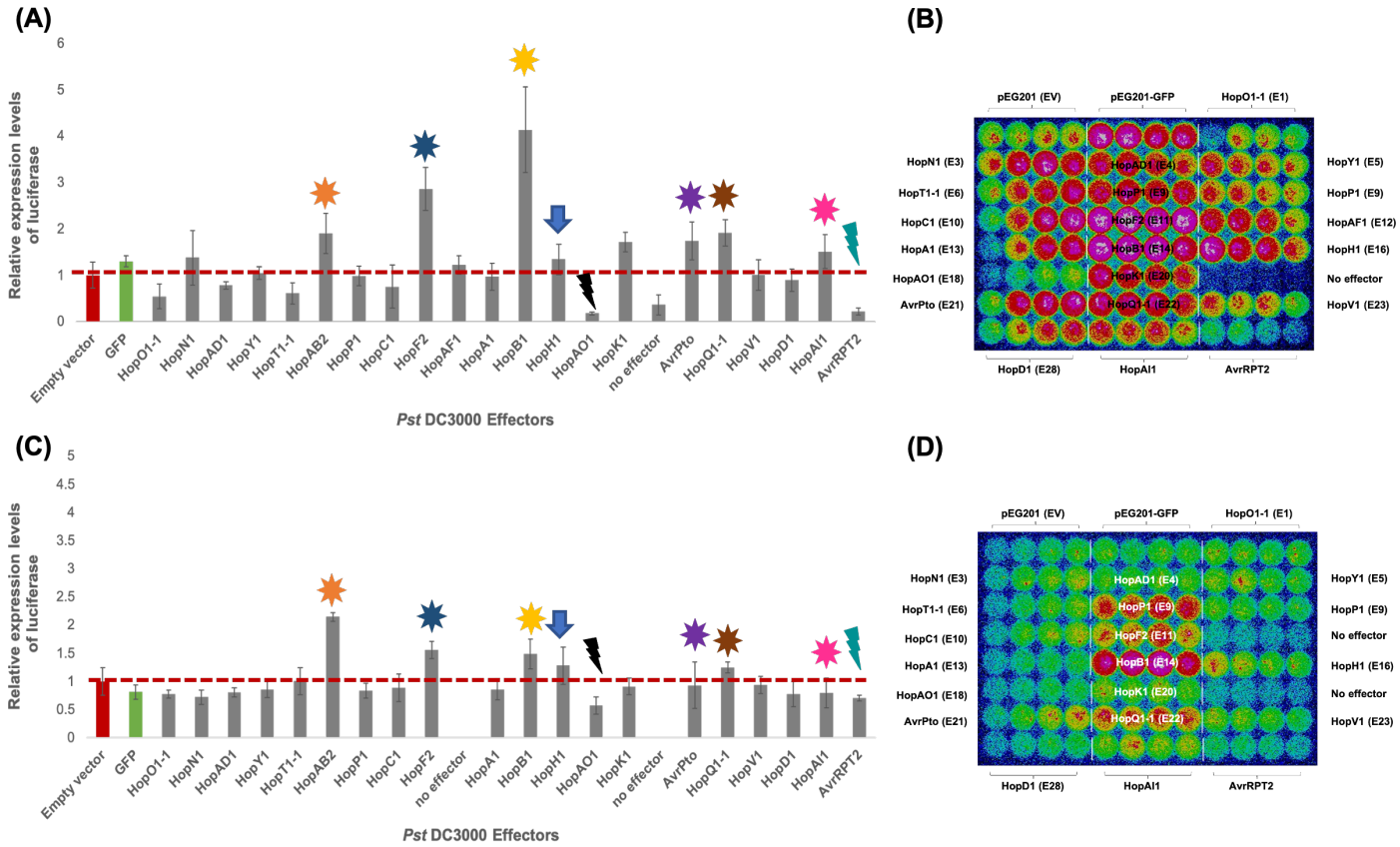

***Figure 3.9 Pst* DC3000 effector screening on *promAT1G72950::LUC* using *A. thaliana* Col-0 mesophyll protoplasts.**

(A) and **(C)** depict the results of fold change of *LUC* relative expression of two biological repeats, and **(B)** and **(D)** the LUC photon signal detection . Star denote the effectors inducing *promAT1G72940* in the preliminary experiments, while thunders denote the ones associated with repression.. Collectively, promoter *AT1G72950* is also induced by HopAB2 (orange star), HopF2 (blue star), HopB1 (yellow star), AvrPto (purple star), HopQ1-1 (brown star), and HopAI1 (magenta star), and an additional effector HopH1 (blue arrow) specific to *promAT1G72950*. Effectors HopAO1 (black thunder) and AvrRPT2 (teal thunder) repress *promAT1G72920::LUC*.

As previously mentioned, the *Pst* DC3000 effector screening assay was repeated more than 2 times for each *TN* promoter, however the sensitivity of protoplasts to preparation and transfection in many cases hampered their post-treatment viability. Each individual experiment indicated some differences to how different effectors affected the regulation of each *TN* promoter. Nevertheless, the collective results of LUC signal detection in transfected *A. thaliana* Col-0 protoplasts indicate a potential regulation pattern that *TN* promoters may have in common in the presence of specific *Pst* DC3000 effectors. **Table 3.1** presents the effect of each *Pst* DC3000 effector on the different *TN* promoters as resulted from each biological repeat. Results were colour-coded based on the relative level of induction or suppression associated to the presence of effectors, discussed previously in this Section. Effectors that showed a consistent correlation to the change of most *TN* promoters' regulation, were highlighted with yellow for upregulation and grey for downregulation.

Figure 3.10 is summarising the results of the *Pst* DC3000 effector library screening on *A. thaliana* Col-0 mesophyll protoplasts transfected with *promTN::LUC* constructs. When effectors HopQ1-1, HopAI1, HopB1, AvrPto, HopF2 and HopAB2 are co-expressed with most *promTN::LUC* constructs, higher levels of LUC activity are detected compared to the control, indicating that promoters *AT1G72920*, *AT1G72940* and *AT1G72950* are induced in their presence. On the contrary, the presence of effectors HopAO1 and AvrRPT2 appears to suppress *TN* promoters in almost all cases. Most importantly, these effectors that induce the expression of LUC are common between *promAT1G72920* and *promAT1G72940,* which are both regulated by ERF6 according to (Mine et al., 2018).

Table 3.1 **Colour-coded table of *Pst* DC3000 effectors and their effect on *TN* promoters' regulation as documented on *A. thaliana* Col-0 protoplasts.**

Results are colour-coded based on the level of induction (green spectrum) or repression (red spectrum) of LUC in response to the presence of effectors. In cases where the expression of LUC does not seem to be affected by an effector, the results are presented as neutral (beige). Overall, effectors that showed a consistent correlation to the change of most TN promoters' regulation, were highlighted with yellow for induction and grey for suppression.

Pst DC3000 Effectors	*promAT1G72920::LUC*		*promAT1G72930::LUC*		*promAT1G72940::LUC*			*promAT1G72950::LUC*	
	1st rep	2nd rep	1st rep	2nd rep	1st rep	2nd rep	3rd rep	1st rep	2nd rep
HopO1-1 (E1)									
HopN1 (E3)									
HopAD1 (E4)									
HopY1 (E5)									
HopT1-1 (E6)									
HopAB2 (E7)									
HopP1 (E9)									
HopC1 (E10)									
HopF2 (E11)									
HopAF1 (E12)									
HopA1 (E13)									
HopB1 (E14)									
HopH1 (E16)									
HopG1 (E17)									
HopAO1 (E18)									
HopK1 (E20)									
AvrPto (E21)									
HopQ1-1 (E22)									
HopV1 (E23)									
HopD1 (E28)									
HopAl1									
AvrRPT2									

neutral
mild upregulation
strong upregulation
mild downregulation
strong downregulation

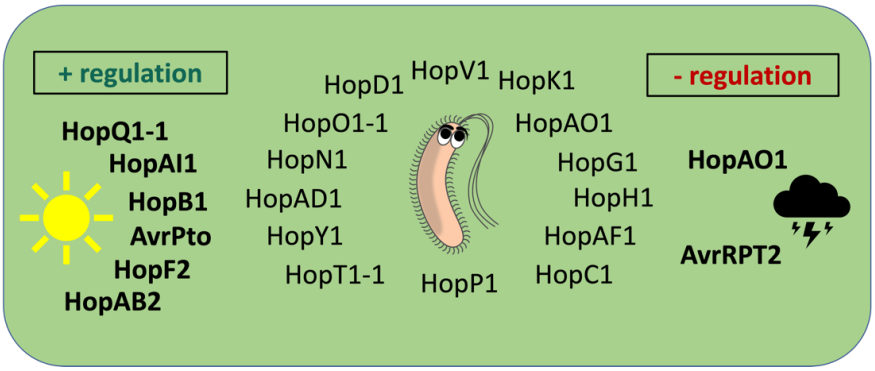

Figure 3.10 **Schematic categorisation of *Pst* DC3000 effectors based on their correlation to the positive or negative regulation of *TN* promoters.**

Effectors HopQ1-1, HopAl1, HopB1, AvrPto, HopF2 and HopAB2 are corelated to higher levels of LUC activity compared to the control, indicating that the *TN* promoters may be induced in their presence. On the contrary, the presence of effectors HopAO1 and AvrRPT2 appears to repress *TN* promoters in almost all cases.

3.2.3 Point mutagenesis of promAT1G72940 conserved TIR-NB family motifs changes the regulation of the promoter in the presence of Pst DC3000 effectors

The results of the *Pst* DC3000 effector screening in *A. thaliana* Col-0 mesophyll protoplasts presented in **Section 3.2.2** showed that the presence of some of those effectors may be corelated to the regulation of *TN* promoters. To further investigate the specifics of this mechanism of regulation, the putative promoter sequences upstream of the *TN* family genes were analysed using bioinformatics methods, to look for the presence of conserved motifs recognised by transcription factors. The results of the motif analysis were obtained and kindly provided for the purposes of this thesis by the group of Prof. Murray Grant (University of Warwick, UK). **Figure 3.11.A** shows the motifs identified on the *TN* promoters following the sequence analysis. The results show three different motifs conserved across the *TN* family promoters, each marked with a different colour.

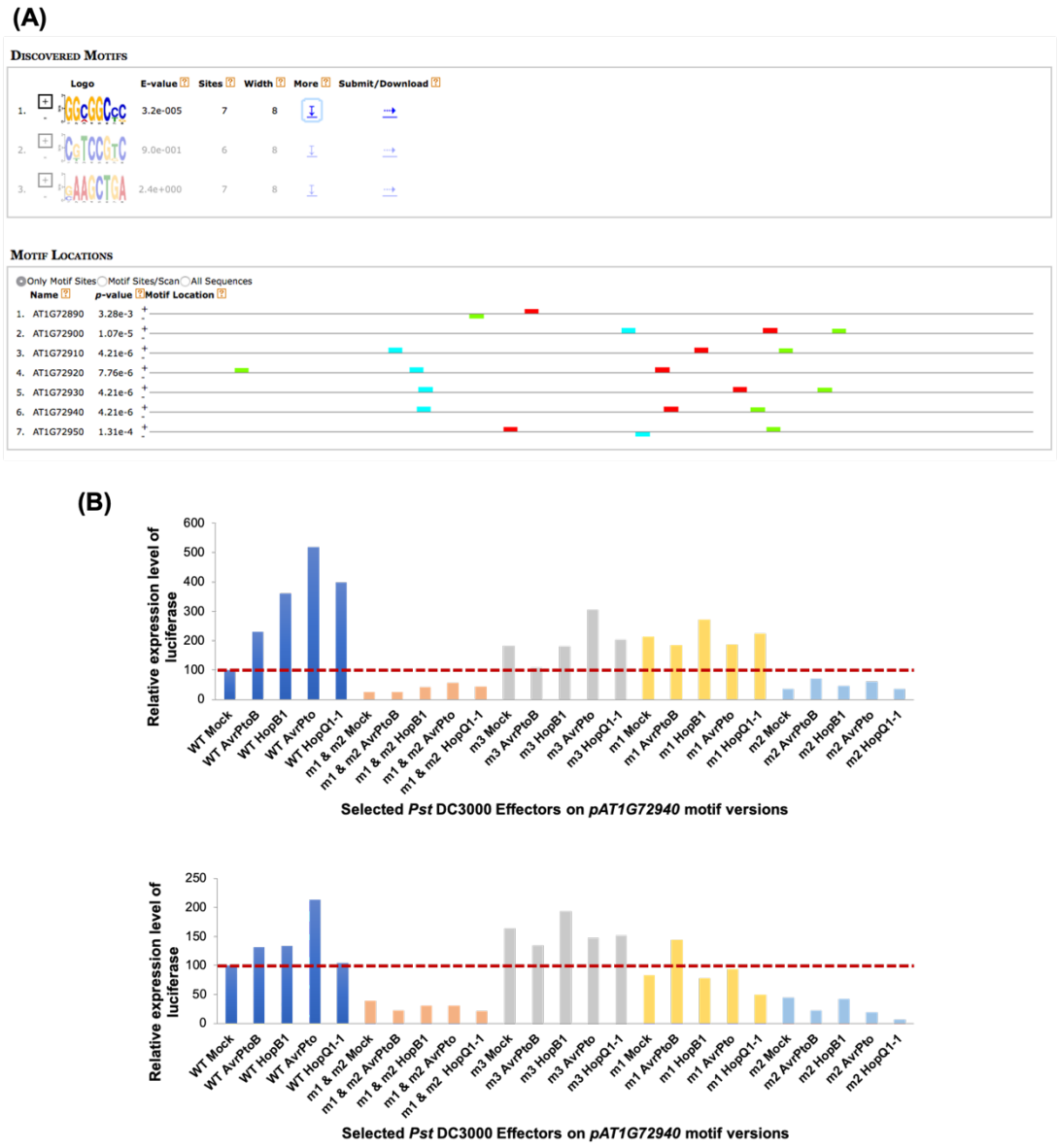

Figure 3.11 **Conserved motifs discovered on the putative promoter regions upstream of the *TN* genes are likely connected to the regulation of *TN* gene expression.**

(A) Bioinformatic analysis of the putative promoter regions locating upstream of the *A. thaliana TN* genes resulted in the discovery of three motifs (top picture) recognised by transcription factors, that are conserved among the different *TN* promoters. The position of those motifs on the different *TN* promoters varies (bottom picture), so each motif was numbered and marked with a different colour: turquoise for motif1 (m1), red for motif2 (m2), and neon green for motif3 (m3). **(B)** Point mutations were introduced to each motif to create recombinant vectors expressing mutated versions of *promAT1G72940::LUC,* including one bearing the mutations for both m1 and m2 motifs. Both the WT and the mutated versions were then transfected into *A. thaliana* Col-0 protoplasts, where they were tested in the presence of selected *Pst* DC3000 effectors. Effectors AvrPtoB (HopAB2), HopB1, AvrPto

and HopQ1-1 were previously shown to be corelated with the induction of the WT *promAT1G72940::LUC.* The results of the effector screening after 2 biological repeats of the assay showed that mutated motifs m1 and m3 do not seem to significantly affect the incuction of *promAT1G72940::LUC* in the presence of the selected effectors. However, the LUC expression is hardly detected when motif2 (m2) is mutated, indicating that the presence of motif2 is important for the regulation of promoter *AT1G72940.*

To identify the importance of each motif to the regulation of the respective promoters, Prof. Murray Grant's group proceeded with introducing point mutations where the motifs are localised, using promoter *AT1G72940* as a starting point. They created four different mutated versions of promoter *AT1G72940,* one for each of the motif1 (m1), motif2 (m2) and motif3 (m3) and one carrying the mutations for both motif1 and motif2 (m1-2). Both the wild type (WT) version of promoter *AT1G72940* and the four mutated versions were then fused with the *LUC* gene. The constructs were transfected into *A. thaliana* protoplasts along with the selected *Pst* DC3000 effectors to check how each mutated version of *promAT1G72940::LUC* reacts to the presence of effectors.

Figure 3.11.B presents the results of how each mutated motif affects the regulation of promoter *AT1G72940* in the presence of selected *Pst* DC3000 effectors, that have previously been corelated to upregulation of the promoter. These results were obtained and kindly provided by Dr. WeiJei Huang (John Innes Centre, UK) prior to the beginning of this PhD project. The figure presents the relative expression levels of *LUC* in response to effectors AvrPtoB (HopAB2), HopB1, AvrPto and HopQ1-1 after 2 biological repeats of the screening. In the case of *promAT1G72940::LUC (WT),* the majority of effectors seem to cause induction of *LUC* compared to the control. The mutations on m1 and m3 do not seem to affect the regulation of the promoter in the presence of any of the tested effectors. However, in the cases of m2 and m1-2, the expression levels of *LUC* have dropped compared to the WT, with more than 0.5 negative fold change, indicating that the mutation in motif2 (m2) may disrupt the proper regulation of promoter *AT1G72940.*

3.2.4 Generation of yeast "bait" vectors containing the wild type and mutated versions of promoter AT1G72940

The results presented on **Section 3.2.3** showed that mutated motif2 (m2) has proved disruptive of the proper regulation of promoter *AT1G72940* in the presence of *Pst* DC3000 effectors HopQ1-1, HopAI1, HopB1, AvrPto, HopF2 and HopAB2. Those findings indicate that this motif could be important for the regulation of *AT1G72940* upon pathogen perception. However, since the mechanism by which *TN* genes are regulated during the plant's transcriptional reprogramming upon infection is not yet known, we hypothesized that the presence of effectors directly or indirectly affects one or more transcription factors (TFs) that are responsible for said regulation.

To address this hypothesis, we decided to try and identify those transcription factors potentially implicated in *TN* gene regulation by performing a large-scale yeast-one-hybrid (Y1H) screening of a library containing 1,956 (approximately 80%) of the known *A. thaliana* TFs (Pruneda-Paz et al., 2014) expressed in *S. cerevisiae*. We proceeded with the construction of yeast expression vectors containing all the different versions of promoter *AT1G72940* (baits). However, since the *A. thaliana* TF library was already subcloned into pDEST22 and transferred in yeast strain Y8800 for the purposes of Y2H experiments in our lab, there were compatibility limitations regarding the yeast expression vector and the yeast strain to be used for the construction of the baits. To overcome the difficulties, three different strategies were followed to successfully subclone all versions of promoter *AT1G72940* into a suitable yeast expression vector, all of which have been described in detail in **Sections 2.5.3.1** and **2.5.3.2** of the **Materials and Methods** Chapter. Due to the future potentials of this project, the resulted recombinant cloning vectors and yeast expression vectors are presented and described as follows.

As explained in **Section 2.5.3.1**, versions WT, m1, m2, m3, and m1-2 of promoter *AT1G72940* already existed in cloning vectors created prior to the

start of this project for the purposes of the effector screening in protoplasts. The exact sequence region upstream of gene *AT1G72940* used as a putative promoter region, as well as the positions of the silent mutations introduced on the identified motifs, were deciphered through sequencing of the original plasmids. Initially, we amplified the promoters and created cloning vectors that would allow for the creation of constructs using the yeast expression vector *pHIS3LEU2,* which allows the yeast to grow on media lacking the amino-acid Histidine (His). This cloning strategy was interrupted, as the empty vector *pHIS3LEU2* proved repeatedly to be autoactive when transformed into the yeast *Saccharomyces cerevisiae* (*S. cerevisiae*), thus causing it to survive in the absence of the amino acid histidine, which is the growth marker indicating the presence of interactions. Nevertheless, as *pHIS3LEU2* was successfully used in the lab before for Y1H experiments, the constructs were kept in both glycerol and plasmid stocks for the possibility to resolve the autoactivation issue and utilise them in the future.

To achieve the creation of the Y1H baits, we acquired a new yeast expression vector (*pMW#3*) that has been previously used in Y1H screenings for protein-DNA interactions in *C. elegans* (Deplancke et al., 2006). *pMW#3* was also selected as a destination vector for conventional Gateway® LR reactions. However, the LR reaction of the entry clones with *pMW#3* did not produce any colonies for any of the constructs, despite the fact that it was repeated three times with various optimization adjustments. According to the depositor comments in Addgene, *pMW#3* is a Y1H Destination vector that can be used in conventional Gateway® LR cloning reactions as it contains a Gateway® cassette and a LacZ reporter gene. However, after more careful investigation and tracing back the creation of the vector in the published papers, it turned out that the recombination sites were *att*R4 and *att*L1 and the conventional LR reaction requires *att*R1 and *att*R2 sites for successful recombination. The *pMW#3* vector was designed to work with very specific entry clones that contain compatible sites for recombination, so it was not compatible with *promAT1G72940/* pDONR™-Zeo (WT, m1, m2, m3, m1-2) entry clones.

Vector *pMW#3* can be used for classical cloning with type II restriction enzymes, which allowed for the following cloning strategy to be applied. The *promAT1G72940/pDONR-Zeo* clones previously generated were used as a template to amplify all versions of promoter *AT1G72940,* which were then ligated into the selected SpeI and XbaI restriction sites of digested *pMW#3*, upstream of the *LacZ* reporter gene. **Figure 3.12** shows the confirmation of the successful amplification and purification of promoter *AT1G72940* WT, m1, m2, m3 and m1-2, as well as the double digestion of *pMW#3* with SpeI and XbaI, which also removes the *ccdB* "suicide" gene from the plasmid.

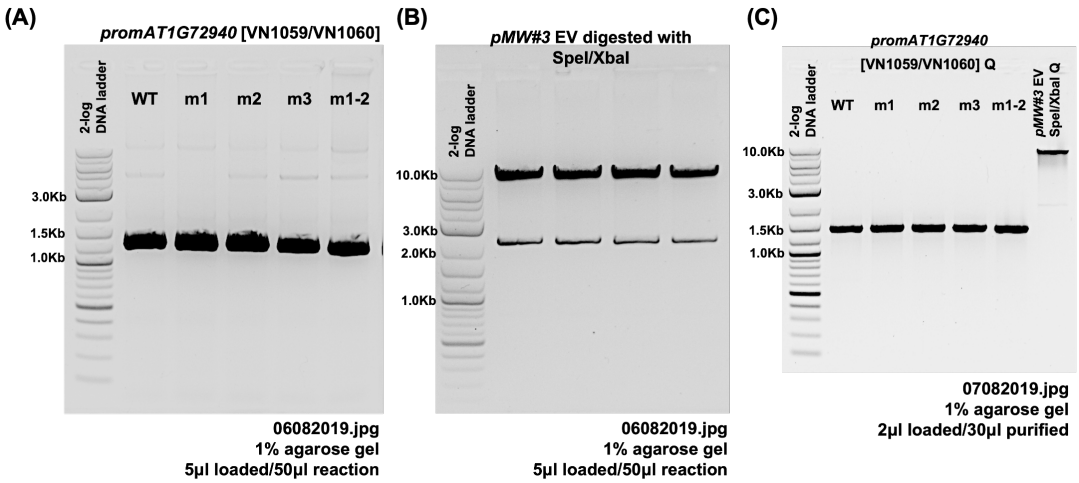

Figure 3.12 **Amplification and subcloning of *promAT1G72940* WT, m1, m2, m3 and m1-2 versions into the *pMW#3* yeast expression vector.**

(A) *promAT1G72940* (WT, m1, m2, m3 and m1-2) sequences were amplified from templates *promAT1G72940/pDONR-Zeo* (all versions) using primers pair VN1059/VN1060, which introduces the recognition sites for type II restriction enzymes SpeI (5' end) and XbaI (3' end). The expected PCR-amplified fragments were analysed using agarose gel electrophoresis and have a MW of ~1.4Kb. **(B)** yeast expression vector *pMW#3* was double digested with enzymes SpeI and XbaI, and the results were analysed with agarose gel electrophoresis. The digested DNA fragments are expected to be of MWs ~2.1Kb (*ccdB* & *CmR* genes) and ~8.3Kb (remaining vector). **(C)** PCR-amplified fragments of *promAT1G72940* (WT, m1, m2, m3 and m1-2) and SpeI/XbaI digested pMW#3 were cut off the gel, purified and analysed again with agarose gel electrophoresis to verify their purity, integrity and correct MWs prior to subcloning. *promAT1G72940* fragments were also double digested with SpeI/XbaI following purification and then proceeded to ligate into *pMW#3*[SpeI/XbaI], as explained in Materials and Methods. All displayed gels consist of 1% w/v agarose/TAE. 2log DNA Ladder (NEB) was used as a reference for molecular weights (MW).

Post amplification *promAT1G72940* fragments were also double digested with SpeI/XbaI and then ligated into *pMW#3*[SpeI/XbaI] and transformed into *E. coli* cells for propagation. **Figure 3.13** presents the results of colony PCR on the transformed *E. coli* to identify the recombinant *promAT1G72940/ pMW#3* [SpeI/XbaI] for each promoter version. Clones highlighted in red showed a positive result when amplified with primers VN1059/VN1060 and were therefore selected and analysed with sequencing. Analysis of the sequencing results showed that at least half of the clones were inserted with the opposite orientation, which is not expected in a site-directed ligation. Subsequently, the recombinant clones were digested with SpeI/XbaI looking for the presence of the insert, thus discovering that the clones with the opposite orientation would not get digested. Further research showed that SpeI and XbaI produce compatible cohesive ends, which makes them complementary to each other, causing the insert to be ligated in either orientation. Clones with sequencing results deemed unclear, mutated, or that showed opposite insert orientation (SpeI/XbaI produce compatible cohesive ends) were discarded.

The ligation and selection of clones was repeated until all constructs resulted with clones with the correct orientation, meaning the *promAT1G72940* facing the orientation of the *LacZ* reporter gene. Clones for m3 and m1-2 were selected in later ligation attempts, not shown here. All selected clones were also verified with SpeI/XbaI digestion. Collectively, the following clones were selected for each construct:

promAT1G72940/ pMW#3 [SpeI/XbaI] WT: clones #1 and #5
promAT1G72940/ pMW#3 [SpeI/XbaI] m1: clone #17
promAT1G72940/ pMW#3 [SpeI/XbaI] m2: clone #7 and #19
promAT1G72940/ pMW#3 [SpeI/XbaI] m3: clone #1, #14 and #26
promAT1G72940/ pMW#3 [SpeI/XbaI] m1-2: clone #20

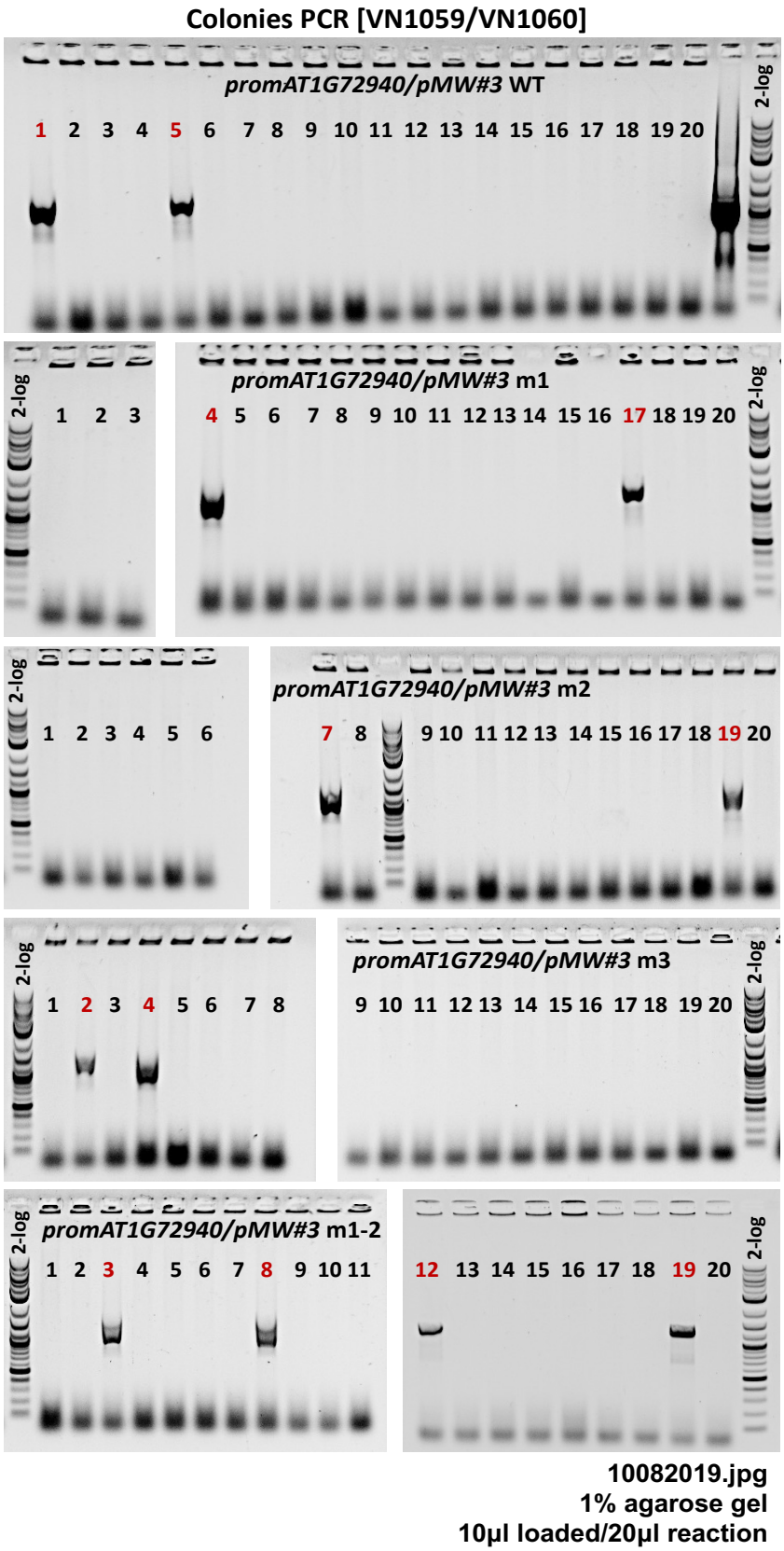

Figure 3.13 **Colony PCR for the selection of the successful recombinant clones of *promAT1G72940/ pMW#3* [SpeI/XbaI] (WT, m1, m2, m3, m1-2).**

Colony PCR was applied on the transformed *E. coli* to identify the recombinant *promAT1G72940/ pMW#3 [SpeI/XbaI]* for each promoter version. Primers VN1059/VN1060 were used to identify the insert of MW ~1.4Kb. Clones highlighted in red showed a positive result when amplified with primers VN1059/VN1060 and were therefore selected and analysed with sequencing. The process was repeated as the positive clones for m3 and m1-2 were found to have inserts either mutated or inserted in opposite orientation to the reporter gene (lacZ). All displayed gels consist of 1% w/v agarose/TAE. 2log DNA Ladder (NEB) was used as a reference for molecular weights (MW).

Figure 3.14 is a schematic representation of the final recombinant yeast expression vectors containing all the different promoter *AT1G72940* versions used for the creation of the bait yeast for Y1H. The main characteristics of *promAT1G72940/ pMW#3* is the Uracil (URA3) selective marker and the *promAT1G72940* located upstream of the reporter gene of *LacZ*.

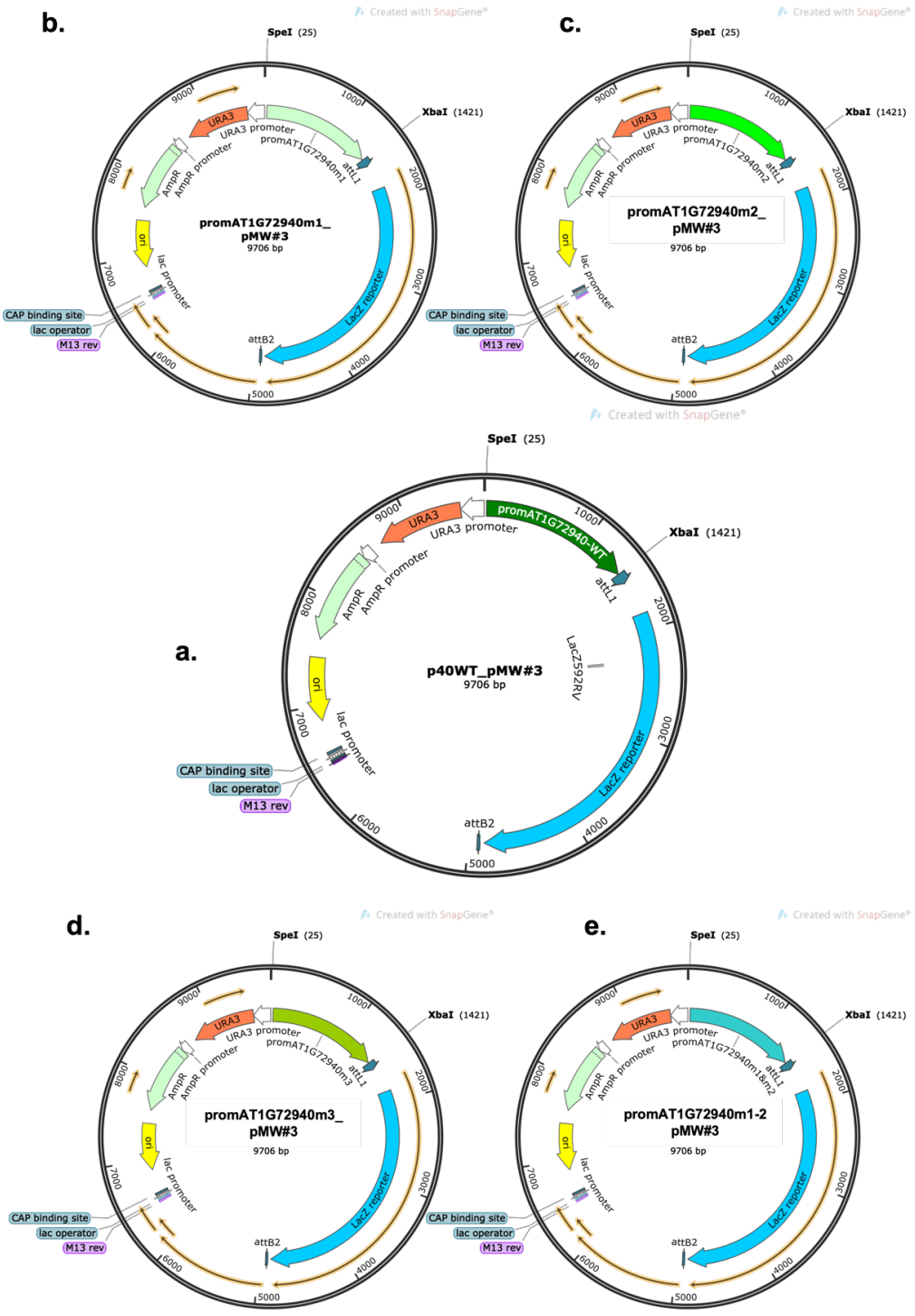

Figure 3.14 **Final form of yeast expression vectors containing the promAT1G72940 versions WT, m1, m2, m3 and m1-2 for Y8930 transformation.**

a. *promAT1G72940/ pMW#3 [SpeI/XbaI] WT*, b. *promAT1G72940/ pMW#3 [SpeI/XbaI] m1*, c. *promAT1G72940/ pMW#3 [SpeI/XbaI] m2*, d. *promAT1G72940/ pMW#3 [SpeI/XbaI] m3*, e. *promAT1G72940/ pMW#3 [SpeI/XbaI] m1-2*.

3.2.5 Yeast One-Hybrid screening of TF library

The construction of *promAT1G72940/pMW#3* yeast expression vectors containing versions WT, m1, m2, m3 and m1-2 (as described in the previous Section) facilitated the generation of bait yeast strains for the Y1H screening (**Section 2.11.2, Materials and Methods**). The baits underwent multiple selection steps in media lacking uracil. We planned for the screening of the yeast library containing 1,956 of the known *A. thaliana* TFs (Pruneda-Paz et al., 2014) to be initially performed only with *promAT1G72940*-WT(Y8930). Any identified TF interactors would then be confirmed via a smaller-scale Y1H experiment and proceed to be tested on the mutated *promAT1G72940* motifs (m1, m2, m3 and m1-2). The collective aim was to identify candidates to at least one or more TFs for *in planta* experiments.

As previously described in **Section 2.11.3** (**Materials and Methods)**, the haploid *promAT1G72940*-WT/Y8930 yeast bait was mated with the haploid *TF*/Y8800 yeasts of the library, and the resulting diploid yeasts were selected in the appropriate drop-out media. Following the instructions of the authors that created and provided the yeast expression vector *pMW#3* (Deplancke et al., 2006), we performed the beta galactosidase assay to reveal potential TF interactors. In the event that the binding domain (BD) of the TF candidate and the activation domain (AD) of *promAT1G72940*-WT are able to interact with one another, then the transcription of *LacZ* would be activated, producing the enzyme β-galactosidase. In the presence of the substrate (X-gal), the diploid yeasts that produce β-galactosidase show blue coloration. The strength of each interaction is determined when compared to the colour of the negative control (*pMW#3-EV*/Y8930 x *pDEST22-EV*/Y8800) and the interaction used as a positive control (*proAT1G72940-WT/*Y8930 x *ERF6*/Y8800).

The first attempt to screen for DNA-protein interactions between *promAT1G72940*-WT and the *A. thaliana* TF library was unsuccessful, thus not presented here**.** Following the β-galactosidase assay, the whole of the

mated yeast library was coloured blue, thus preventing the identification of specific interactions. The conclusion was that we have not been able to identify any DNA-protein interactions at this stage. The experiment was repeated, starting with the generation of fresh yeast baits. *promAT1G72940/pMW#3* WT, m1, m2, m3 and m1-2 were newly extracted and transformed into Y8930. The selection and mating process was performed as the first time. Before proceeding to the screening of the entire library, it was decided to carry out a smaller experiment, using the negative and positive controls as well as the haploid yeasts, in order to check for the efficiency of the β-galactosidase assay as well as the possibility of autoactivation of the *LacZ* reporter gene.

For the second attempt we decided to use liquid yeast cultures instead of colonies growing on solid media and perform the experiment both on the concentrated yeast culture as well as two different 10-fold dilutions (1/10 and 1/100). **Figure 3.15** presents the results of the β-galactosidase assay on the concentrated yeast cultures after O/N exposure to the substrate X-gal, along with the outline of the different constructs used. The plates were monitored every 30 mins for the first 3hrs of the experiment and then left O/N. This time, the negative controls did not react to the presence of X-gal but neither did the ERF6xWT mating we used as positive control (3B). Due to time limitations and lack of results that indicate the method and/or the available controls are functional, the experiment was not further repeated within the duration of this PhD project. Possible alternatives or future developments regarding the Y1H experiment are presented in the Discussion.

(A)

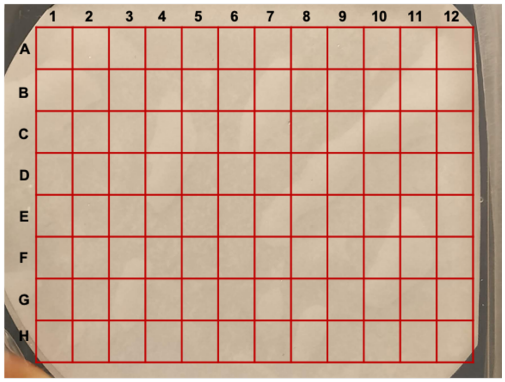

(B)

	1	2	3	4	5	6	7	8	9	10	11	12
A	EV x EV		ERF6 x EV		EV y8930				EV y8800			
B	EV x WT		ERF6 x WT		WT							
C	EV x m1		ERF6 x m1		m1				ERF6			
D	EV x m2		ERF6 x m2		m2							
E	EV x m3		ERF6 x m3		m3							
F	EV x m1-2		ERF6 x m1-2		m1-2							
G												
H												

Figure 3.15 **The β-galactosidase assay applied on both negative and positive controls for Y1H showed that the assay requires further modification and adjustment prior to screening the *A. thaliana* TF library with *promAT1G72940* to identify DNA-protein interactions.**

As shown in the outline of the plate **(A),** the following mated yeasts were prepared and grown for the purposes of the assay: (1A) *pMW#3*/Y8930 (EV in red) mated with *pDEST22*/Y8800 (EV in black) is the negative control used as reference for autoactivation of LacZ, (1B-F) pMW#3/Y8930 (EV in red) mated with *promAT1G72940*/Y8930 WT, m1, m2, m3 and m1-2, respectively, used as a reference for false positive activation of the promoters in the presence of *pDEST22*. (3A) *pMW#3*/Y8930 (EV in red) mated with *ERF6*/Y8800, (3B) *promAT1G72940-WT*/Y8930 mated with *ERF6*/Y8800 is the allegedly positive control of the interaction, based on published ChIP-qPCR data that prove the *in planta* interaction of ERF6 TF with *promAT1G72940* (Mine et al., 2018), (3C-F) *promAT1G72940*/Y8930 m1, m2, m3 and m1-2 mated with *ERF6*/Y8800 were intended to show whether the mutations on the respective motifs affect the binding of ERF6 on *promAT1G72940*. (5A-F) the haploid yeast Y8930 containing *pMW#3* (EV in red) and *promAT1G72940* WT, m1, m2, m3 and m1-2, used as a reference that LacZ does not get autoactivated in the haploid forms. (9A) haploid *pDEST22*/Y8800 (EV in black), and (9C) haploid *ERF6*/Y8800. **(B)** picture of the β-galactosidase assay following O/N exposure of the concentrated yeast cultures to the substrate X-gal. Liquid yeast cultures were used for this experiment, which was performed both on the concentrated yeast culture and two different 10-fold dilutions (1/10 and 1/100). The plates were monitored every 30 mins for the first 3hrs of the experiment and then left O/N. The negative controls (column 1) did not react to the presence of X-gal but neither did the allegedly positive control (3B).

3.3 Discussion

The RT-q-PCR quantification of *TN* gene expression in adult Col-0 plants showed that transcript levels of genes *AT1G72920* and *AT1G72940* are significantly higher between 6 and 12hrs following infection with virulent *Pst* DC3000 than in the untreated samples, while treatments with the mutant strain *Pst* DC3000 *hrpA* and mock solution ($MgCl_2$) do not affect the expression of either gene. Those findings are in line with the microarray results produced prior to the beginning of this PhD project and suggested that two members of the *TN* family of interest is positively regulated in *A. thaliana* upon bacterial infection. The results of *AT1G72950* expression are not equally consistent with the microarrays.

Pst DC3000 *hrpA* has a defective T3SS, which makes it unable to deliver effectors upon plant infection. We hypothesized that absence of *TN* gene induction of expression when infected with *Pst* DC3000 *hrpA* together with the upregulation recorded after virulent *Pst* DC3000, could indicate that induction of *TN* gene expression is correlated with bacterial effector delivery. When we transiently co-expressed the putative promoter regions of the *TN* genes of interest fused with the LUC reporter gene, with constitutively active constructs of 22 *Pst* DC3000 effectors in a protoplast-based screening, 6 candidate effectors were identified to lead to induction of *promAT1G72920, promAT1G72940*, and *promAT1G72950*: HopQ1-1, HopAI1, HopB1, AvrPto, HopF2 and HopAB2 (AvrPtoB). Effectors HopAO1 and AvrRPT2 lead to repression of *promAT1G72920, promAT1G72940*, and *promAT1G72950* in most cases.

Approximately 10% of the whole plant transcriptome reprograms its expression upon perception of pathogens (Moore et al., 2011; Navarro et al., 2004), to produce antimicrobial compounds and cell wall-reinforcing materials at the infection site amongst other processes. Type III effectors target host defence pathways to dampen plant immunity (Katagiri et al., 2002). Among other important processes, effectors affect phytohormone signalling,

proteasome-dependent protein degradation, cytoskeleton formation, manipulation of stomatal openings, establishment of intercellular apoplastic living spaces, and vesicle transport (Büttner, 2016; Toruño et al., 2016). However, bacterial effectors also have an important role in the suppression of PTI. Many effectors directly target PRRs and their co-receptors, RLCKs and MAPKs using multiple strategies to ensure suppression (Büttner, 2016; Macho and Zipfel, 2015). Effectors AvrPto, AvrPtoB (HopAB2), HopAO1, and HopF2, are known to act as direct suppressors of PRRs, such as in the case of FLS2 and/or their co-receptors BAK1 (BRI1-ASSOCIATED RECEPTOR KINASE 1) and CERK1 (CHITIN ELICITOR RECEPTOR KINASE 1). Another example are effectors HopAI1 and HopF2 that suppress MAPK signalling by directly modifying these proteins (Büttner, 2016; Macho and Zipfel, 2015; Toruño et al., 2016).

Pst DC3000 T3 effectors also target hormone physiology to cause susceptibility (Kazan and Lyons, 2014). Effectors AvrPto and AvrPtoB (HopAB2) are known to elevate ABA levels to antagonize SA signalling (de Torres-Zabala et al., 2007), to promote ethylene signalling and biosynthesis (Cohn and Martin, 2005), and to target brassinosteroid receptor BAK1 (Cheng et al., 2011; Shan et al., 2008). Effector HopQ1-1 is known to activate the cytokinin pathway to suppress FLS2-mediated defence signalling (Hann et al., 2014). *Pst* DC3000 effector HopB1 acts as a protease that cleaves BAK1 when activated by flg22. Prior to activation, HopB1 constitutively interacts with FLS2. BAK1 is recruited to the FLS2-HopB1 complex upon activation and gets phosphorylated. HopB1 specifically cleaves BAK1 to inhibit FLS2 signalling. HopB1-mediated cleavage of BAK1 leads to enhanced virulence, but not disease resistance (Li et al., 2016).

Effector HopAI1 inhibits the MAPKs in *A. thaliana* when activated by exposure to MAMPs. HopAI1 inactivates MAPKs by removing the phosphate group from phosphothreonine through a unique phosphothreonine lyase activity, which is required for its function. By inhibiting MAPKs, the effector suppresses the reinforcement of cell wall defence and transcriptional activation of PAMP response genes. The MAPKs MPK3 and MPK6 physically interact with HopAI1

indicating that they are direct targets of HopAI1 (Zhang et al., 2007). It is reported that S- nitrosylation modification inhibits its phosphothreonine lyase activity to restore MAPK signalling to trigger HR (Ling et al., 2017).

Prior to the beginning of this PhD project, bioinformatic analysis conducted of the putative promoter regions locating upstream of the *A. thaliana TN* genes resulted in the discovery of three motifs (m1, m2, and m3) recognised by transcription factors, that are conserved among the different *TN* promoters. Point mutations were introduced to each motif to create mutated versions of *promAT1G72940::LUC,* including one bearing the mutations for both m1 and m2 motifs (m1-m2). Effectors AvrPtoB (HopAB2), HopB1, AvrPto and HopQ1-1 are among the 6 candidate effectors that were previously shown to correlate with the upregulation of the WT *promAT1G72940::LUC.* When the WT and mutated versions of *promAT1G72940* were co-expressed with those 4 *Pst* DC3000 effectors into Col-0 protoplasts, the results showed that mutated motifs m1 and m3 do not lead to induction of *promAT1G72940::LUC* in the presence of the selected effectors. However, in *promAT1G72940::LUC* mutated motif2 (m2) the LUC expression is very faintly detected, indicating that the presence of m2 is important for the regulation of promoter *AT1G72940.*

The discovery of motifs that may play a role in controlling the regulation of *TN* promoters upon *Pst* DC3000 effector delivery, as well as the candidate effectors correlated with the positive regulation of expression of *TN* genes upon bacterial infection, led to a search for transcription factors that mediate those transcriptional changes. As previously discussed in the Introduction of this Chapter, transcriptional reprogramming has a very important role in plant defence responses and TFs are key players within signalling pathways responsible to interpret the signal transduction in various ways that lead to a variety of transcriptional changes (Tsuda and Somssich, 2015). Results of a recent study showed that ERF6 TF binds to the promoters of genes *AT1G72920* and *AT1G72940*, suggesting that ERF6 and possibly its homologs ERF5, ERF104, and ERF105 contribute to the expression of these genes in a manner independent of the JA/ethylene/PAD4/ SA network during

ETI (Mine et al., 2018). They also suggest that ERF6 potentially plays an important role in the regulation of expression of *TN* genes *AT1G72920* and *AT1G72940* during plant immunity.

In order to begin elucidating the specific mechanism interconnecting *TN* gene expression, *Pst* DC3000 effector delivery and control of transcriptional regulation upon infection, we decided to perform a large-scale Y1H screening using the putative promoter region of *AT1G72940* as bait to identify potential DNA-protein interactions in a yeast library of 1,965 known (Pruneda-Paz et al., 2014) *A. thaliana* TFs. The binding of ERF6 to the promoter of *AT1G72940* has been tested and confirmed *in planta* using ChIP experiments on transgenic *A. thaliana* ERF6 lines. Therefore, it was suggested that the haploid Y8800 bearing the *ERF6/pDEST22* construct was used as a potential positive control for the interaction with the haploid Y8930 bearing the *promAT1G72940/pMW#3* construct. However, this interaction was not successful when testing the negative and positive controls prior to the large-scale screening.

Since *S. cerevisiae* is a heterologous system for plant protein expression, the confirmed *in planta* interaction does not guarantee that the same interaction is possible in yeast. Plant proteins often undergo post-translational modifications that control their activity and are likely not happening when they are expressed in a heterologous system. ERF6 is reported to be activated through phosphorylation by MPK3 and MPK6 during ETI, when these MAP kinases are active (Meng et al., 2013; Tsuda et al., 2013). If phosphorylation by MAPKs is a prerequisite for ERF6 activation *in planta*, then the lack of DNA-protein interaction between yeast expressed ERF6 and *promAT1G72940* in the diploid *promAT1G72940/pMW#3*(Y8930) x *ERF6/pDEST22*(Y8800) is probably due to the lack of the necessary post-translational modification machinery in yeast.

Table 3.2 **List of available AP2/ERF TF family members in the Y8800 library of *A. thaliana* TFs.**

Gene identifier (AGI)	Clone location (plate-well)	TF family	DNA array	Gene isoform	Coding sequence (bp)
AT1G01250	U09-H08	AP2-EREBP [a,b,c]	specific probe	AT1G01250.1	579
AT1G03800	U05-G12	AP2-EREBP [a,b,c]	no probe	AT1G03800.1	738
AT1G04370	U06-E07	AP2-EREBP [a,b,c]	no probe	AT1G04370.1	402
AT1G06160	U11-F03	AP2-EREBP [a,b,c]	specific probe	AT1G06160.1	735
AT1G12610	U15-C04	AP2-EREBP [a,b,c]	specific probe	AT1G12610.1	630
AT1G12630	U08-E03	AP2-EREBP [a,b,c]	specific probe	AT1G12630.1	579
AT1G12890	U13-E05	AP2-EREBP [a,b,c]	no probe	AT1G12890.1	660
AT1G12980	U20-C11	AP2-EREBP [a,b,c]	no probe	AT1G12980.1	987
AT1G15360	U04-E01	AP2-EREBP [a,b,c]	specific probe	AT1G15360.1	600
AT1G19210	U06-A05	AP2-EREBP [a,b,c]	specific probe	AT1G19210.1	558
AT1G21910	U10-F06	AP2-EREBP [a,b,c]	specific probe	AT1G21910.1	693
AT1G22810	U18-C03	AP2-EREBP [a,b,c]	specific probe	AT1G22810.1	435
AT1G22985	U14-A10	AP2-EREBP [a,b,c]	specific probe	AT1G22985.1	480
AT1G24590	U15-G10	AP2-EREBP [a,b,c]	no probe	AT1G24590.1	921
AT1G25470	U04-E11	AP2-EREBP [a,b]	multiple	AT1G25470.1	864
AT1G28160	U08-E04	AP2-EREBP [a,b,c]	specific probe	AT1G28160.1	738
AT1G28360	U07-G08	AP2-EREBP [a,b,c]	specific probe	AT1G28360.1	570
AT1G28370	U07-F04	AP2-EREBP [a,b,c]	specific probe	AT1G28370.1	501
AT1G33760	U20-B09	AP2-EREBP [a,b,c]	specific probe	AT1G33760.1	555
AT1G36060	U14-H08	AP2-EREBP [a,b,c]	specific probe	AT1G36060.1	945
AT1G43160	U17-D06	AP2-EREBP [a,b,c]	specific probe	AT1G43160.1	579
AT1G44830	U14-C06	AP2-EREBP [a,b,c]	specific probe	AT1G44830.1	636
AT1G49120	U02-E04	AP2-EREBP [a,b]	no probe	AT1G49120.1	990
AT1G50640	U06-G02	AP2-EREBP [a,b,c]	specific probe	AT1G50640.1	678
AT1G53170	U05-C10	AP2-EREBP [a,b,c]	specific probe	AT1G53170.1	558
AT1G53910	U10-C10	AP2-EREBP [a,b,c]	specific probe	AT1G53910.1	1077
AT1G63030	U09-H09	AP2-EREBP [a,b,c]	specific probe	AT1G63030.1	546
AT1G63040	U12-G06	ND	specific Probe	AT1G63040.1	747
AT1G64380	U01-H06	AP2-EREBP [a,b,c]	specific probe	AT1G64380.1	1008
AT1G68550	U03-B11	AP2-EREBP [a,b,c]	multiple	AT1G68550.1	975
AT1G71130	U05-F08	AP2-EREBP [a,b,c]	specific probe	AT1G71130.1	486
AT1G71450	U02-C01	AP2-EREBP [a,b,c]	specific probe	AT1G71450.1	552
AT1G72360	U15-E11	AP2-EREBP [a,b,c]	specific probe	AT1G72360.1	789
AT1G74930	U08-A02	AP2-EREBP [a,b,c]	specific probe	AT1G74930.1	588
AT1G75490	U06-E08	AP2-EREBP [a,b,c]	specific probe	AT1G75490.1	621
AT1G77200	U08-D10	AP2-EREBP [a,b,c]	specific probe	AT1G77200.1	735
AT1G77640	U10-E06	AP2-EREBP [a,b,c]	specific probe	AT1G77640.1	735
AT1G78080	U05-C03	AP2-EREBP [a,b,c]	specific probe	AT1G78080.1	1005
AT1G80580	U01-D01	AP2-EREBP [a,b,c]	specific probe	AT1G80580.1	771
AT2G20350	U06-H06	AP2-EREBP [a,b,c]	specific probe	AT2G20350.1	477
AT2G22200	U10-E01	AP2-EREBP [a,b,c]	specific probe	AT2G22200.1	786
AT2G25820	U14-F10	AP2-EREBP [a,b,c]	specific probe	AT2G25820.1	678
AT2G31230	U03-C09	AP2-EREBP [a,b,c]	specific probe	AT2G31230.1	732
AT2G33710	U07-H10	AP2-EREBP [a,b,c]	specific probe	AT2G33710.1	657
AT2G35700	U13-H10	AP2-EREBP [a,b,c]	specific probe	AT2G35700.1	585
AT2G38340	U04-G03	AP2-EREBP [a,b,c]	specific probe	AT2G38340.1	735
AT2G40340	U10-F08	AP2-EREBP [a,b,c]	multiple	AT2G40340.1	1026
AT2G40350	U10-A03	AP2-EREBP [a,b,c]	multiple	AT2G40350.1	474
AT2G44840	U18-E11	AP2-EREBP [a,b,c]	specific probe	AT2G44840.1	681
AT2G44940	U06-A10	AP2-EREBP [a,b,c]	specific probe	AT2G44940.1	888
AT3G11020	U15-F02	AP2-EREBP [a,b,c]	specific probe	AT3G11020.1	993
AT3G14230	U14-F08	AP2-EREBP [a,b,c]	specific probe	AT3G14230.2	1140
AT3G15210	U10-D10	AP2-EREBP [a,b,c]	specific probe	AT3G15210.1	669
AT3G16280	U01-E12	AP2-EREBP [a,b,c]	specific probe	AT3G16280.1	711
AT3G16770	U05-C06	AP2-EREBP [a,b,c]	specific probe	AT3G16770.1	747
AT3G20310	U03-H08	AP2-EREBP [a,b,c]	specific probe	AT3G20310.1	735
AT3G23220	U17-F11	AP2-EREBP [a,b,c]	specific probe	AT3G23220.1	420
AT3G23230	U11-F04	AP2-EREBP [a,b,c]	specific probe	AT3G23230.1	420
AT3G23240	U04-A08	AP2-EREBP [a,b,c]	specific probe	AT3G23240.1	657
AT3G25890	U01-H07	AP2-EREBP [a,b]	specific probe	AT3G25890.1	999
AT3G50260	U03-G09	AP2-EREBP [a,b,c]	specific probe	AT3G50260.1	462
AT3G57600	U02-E05	AP2-EREBP [a,b,c]	specific probe	AT3G57600.1	834
AT3G60490	U02-E06	AP2-EREBP [a,b,c]	specific probe	AT3G60490.1	771
AT4G06746	U01-H05	AP2-EREBP [a,b,c]	no probe	AT4G06746.1	453
AT4G11140	U07-A03	AP2-EREBP [a,b,c]	specific probe	AT4G11140.1	864
AT4G13620	U05-H11	AP2-EREBP [a,b,c]	no probe	AT4G13620.1	1167
AT4G16750	U05-H02	AP2-EREBP [a,b,c]	specific probe	AT4G16750.1	540
AT4G17490	U17-D07	AP2-EREBP [a,b,c]	specific probe	AT4G17490.1	849
AT4G17500	U07-G03	AP2-EREBP [a,b,c]	specific probe	AT4G17500.1	807
AT4G18450	U17-D11	AP2-EREBP [a,b,c]	specific probe	AT4G18450.1	912
AT4G23750	U14-C01	AP2-EREBP [a,b,c]	specific probe	AT4G23750.1	1032
AT4G25470	U01-A12	AP2-EREBP [a,b,c]	specific probe	AT4G25470.1	651
AT4G25490	U09-D12	AP2-EREBP [a,b,c]	specific probe	AT4G25490.1	642
AT4G27950	U02-E07	AP2-EREBP [a,b,c]	no probe	AT4G27950.1	1008
AT4G28140	U04-B04	AP2-EREBP [a,b,c]	specific probe	AT4G28140.1	879
AT4G31060	U17-B06	AP2-EREBP [a,b,c]	specific probe	AT4G31060.1	564
AT4G32800	U14-D11	AP2-EREBP [a,b,c]	specific probe	AT4G32800.1	666
AT4G34410	U05-A09	AP2-EREBP [a,b,c]	specific probe	AT4G34410.1	807
AT4G36900	U01-C12	AP2-EREBP [a,b,c]	specific probe	AT4G36900.1	591
AT4G39780	U05-E11	AP2-EREBP [a,b,c]	specific probe	AT4G39780.1	819
AT5G05410	U01-E11	AP2-EREBP [a,b,c]	specific probe	AT5G05410.1	1008
AT5G07310	U06-E05	AP2-EREBP [a,b,c]	specific probe	AT5G07310.1	792
AT5G07580	U13-F04	AP2-EREBP [a,b,c]	specific probe	AT5G07580.1	825
AT5G11190	U02-E08	AP2-EREBP [a,b,c]	no probe	AT5G11190.1	570
AT5G11590	U15-C06	AP2-EREBP [a,b,c]	specific probe	AT5G11590.1	711
AT5G13330	U12-E06	AP2-EREBP [a,b,c]	specific probe	AT5G13330.1	639
AT5G13910	U07-A06	AP2-EREBP [a,b,c]	specific probe	AT5G13910.1	636
AT5G18450	U06-D07	AP2-EREBP [a,b,c]	specific probe	AT5G18450.1	924
AT5G18560	U09-H11	AP2-EREBP [a,b,c]	specific probe	AT5G18560.1	1047
AT5G19790	U09-G08	AP2-EREBP [a,b,c]	specific probe	AT5G19790.1	762
AT5G21960	U05-D12	AP2-EREBP [a,b,c]	no probe	AT5G21960.1	651
AT5G25190	U03-E05	AP2-EREBP [a,b,c]	specific probe	AT5G25190.1	546
AT5G25390	U16-E11	AP2-EREBP [a,b,c]	specific probe	AT5G25390.2	570
AT5G25810	U16-H12	AP2-EREBP [a,b,c]	specific probe	AT5G25810.1	657
AT5G44210	U05-F07	AP2-EREBP [a,b,c]	specific probe	AT5G44210.1	603
AT5G47220	U10-F11	AP2-EREBP [a,b,c]	specific probe	AT5G47220.1	732
AT5G47230	U07-F08	AP2-EREBP [a,b,c]	specific probe	AT5G47230.1	903
AT5G51190	U10-H03	AP2-EREBP [a,b,c]	specific probe	AT5G51190.1	666
AT5G51990	U08-F03	AP2-EREBP [a,b,c]	specific probe	AT5G51990.1	675
AT5G52020	U01-H04	AP2-EREBP [a,b,c]	specific probe	AT5G52020.1	699
AT5G53290	U06-G03	AP2-EREBP [a,b,c]	specific probe	AT5G53290.1	1065
AT5G61600	U06-B08	AP2-EREBP [a,b,c]	specific probe	AT5G61600.1	726
AT5G61890	U11-F05	AP2-EREBP [a,b,c]	specific probe	AT5G61890.1	747
AT5G64750	U20-B10	AP2-EREBP [a,b,c]	no probe	AT5G64750.1	1176
AT5G65130	U05-E05	AP2-EREBP [a,b,c]	specific probe	AT5G65130.1	834
AT5G67000	U17-F09	AP2-EREBP [a,b,c]	specific probe	AT5G67000.1	555
AT5G67190	U14-F01	AP2-EREBP [a,b,c]	specific probe	AT5G67190.1	555

The Y1H screening was not successful due to technical complications with the protocol. However, all the different versions of *promAT1G72940* have been successfully subcloned into the yeast expression vector *pMW#3* and transfected into Y8930 for future attempts. Optimization of the β-galactosidase assay to the needs of this specific Y1H screening is suggested before any future attempts. Furthermore, obtaining and subcloning the positive controls used in the initial studies to monitor the effectiveness of expression of vector *pMW#3*-based constructs could also prove useful to identify strong interactions.

One possible way to reduce the size and increase the sensitivity of the experiment would be to limit the initial screening to the AP2/ERF family members available in the yeast library (**Table 3.2**). Nevertheless, the example of ERF6 should be taken into consideration during future Y1H experiments to identify more transcriptional factors that regulate the expression of *TN* genes. We cannot exclude the possibility that other TFs involved in the regulation of *TN* genes also need to undergo post-translational modifications that determine their activity, thus preventing those interactions from occurring in the heterologous yeast system. Similarly, any interactions identified with Y1H should be confirmed *in planta* before drawing any safe conclusions.

4. Investigating the susceptibility of TN inducible expression and knock-out *A. thaliana* lines against the plant pathogen *Pst* DC3000

4.1 Introduction

Two different sets of *A. thaliana* stable transgenic lines for dexamethasone (DEX) inducible overexpression of the *TN* gene *AT1G72940* were previously created and kindly donated for the purposes of this thesis by the group of Prof. Murray Grant (University of Warwick, UK): *promDEX::AT1G72940* and *promDEX::AT1G72940:HA:FLAG* lines. The genetic background of the *AT1G72940* transgenic plants is the *A. thaliana* WT ecotype Col-0. *A. tumefaciens* mediated transformation of the *A. thaliana* Col-0 floral buds was used to deliver the recombinant plasmid vectors bearing the T-DNA cassette. The transgene used to create the *promDEX::AT1G72940* lines included the CDS of gene *AT1G72940* fused to a promoter regulated by the presence of the glucocorticoid dexamethasone, as well as the gene conferring resistance to the antibiotic Hygromycin for the selection of the successfully transformed plants. The transgene used for the creation of *promDEX::AT1G72940:HA:FLAG* lines also included the 3' fusion of *AT1G72940* with the DNA sequences coding for the oligopeptides HA and FLAG at the C' terminal of the expressed protein.

The DEX inducible system (Aoyama and Chua, 1997) is a set of two transcriptional units: the *prom35S::GVG* and the *promDEX::gene-of-interest*. *prom35S::GVG* transcriptional unit is constitutively active and codes for the production of GVG (GAL4-VP16-GR), a synthetic chimeric transcription factor regulated to be activated by a hormone binding domain (HBD) of the rat's glucocorticoid receptor (GR) for dexamethasone. The GVG synthetic TF also includes the GAL4 DNA binding site of the respective yeast TF, and VP16, the

transactivate domain of the herpes viral protein 16. The GVG TF is constitutively expressed but not activated in absence of DEX. When DEX is present it binds on the GR, thus activating GVG. The promoter driving the transcription of our gene of interest (called here *promDEX*) comprises of a minimal 35S CaMV promoter and 6 repeats of the GAL4 upstream activating sequence (UAS). The DEX-activated form of GVG recognises and binds to the GAL4 UAS, thus activating the transcription of our gene of interest. In the absence of DEX, GVG is inactive, so the gene of interest remains inactive.

As previously shown in **Chapter 3**, *AT1G72940* is one of the 3 members of the *A. thaliana TN* gene family whose expression is positively regulated following *Pst* DC3000 infection in *A. thaliana* Col-0 adult plants. Previous published work on the role of TN proteins in plant defence (Nandety et al., 2013) indicates that transient overexpression of *AT1G72940* in *N. benthamiana* resulted in mild HR response. Furthermore, they generated transgenic lines in *A. thaliana* Col-0 with stable overexpression of several TN genes, including *AT1G72940*, which they tested for developmental phenotypes and/or phenotypes resulting in response to bacterial and fungal plant pathogens. Regarding the *AT1G72940* lines, they report no developmental phenotype observed as a result of the overexpression of the transgene or a disease response different to the WT, when the lines are challenged with virulent *Pst* DC3000, but the data are not shown in the study.

This PhD project therefore aimed to investigate and provide further insights on the role of *AT1G72940* in plant immune responses. *promDEX::AT1G72940* and *promDEX::AT1G72940:HA:FLAG* lines were initially created to test the effects of overproduction of the protein AT1G72940 on the defence responses of *A. thaliana* plants when challenged with the virulent bacterial pathogen *Pst* DC3000. Taking into account the data showing HR in response to overexpression of *AT1G72940* in *N. benthamiana* (Nandety et al., 2013) as well as the fact that *TN* genes share similarities to NLRs, whose expression is tightly regulated by the plant cells, the group previously working on this project decided on the creation of inducible overexpressing lines instead of constitutively overexpressing lines.

The creation of *promDEX::AT1G72940* lines was decided in order to avoid potential downsides of C terminal protein tag fusions, that could affect the functionality of AT1G72940 protein. However, since the absence of protein tags does not easily allow for protein detection and/or protein immunoprecipitation, the need for *promDEX::AT1G72940:HA:FLAG* creation arose. Both set of stable transgenic lines were tested for phenotypes when challenged with *Pst* DC3000, which were assessed via bacterial growth colony count and measuring the maximum potential quantum efficiency of PSII in response to infection.

Figures 4.1 and **4.2** show developmental maps generated using the *Arabidopsis* eFP browser (Schmid et al., 2005; Winter et al., 2007) depicting the absolute expression levels of each *TN* gene in different developmental stages and organs of the plant. Genes *AT1G72920* (**Figure 4.1.A**) and *AT1G72940* (**Figure 4.2.A**) have a similar developmental map of expression in normal growth conditions, but in a different magnitude as *AT1G72940* is expressed twice as much as *AT1G72920*. Both show their maximum expression in the seedling stage and an average expression in the rosette leaves and flower stage 12 sepals. Gene *AT1G72930* (**Figure 4.1.B**) has a maximum expression 7-fold higher than *AT1G72920,* which is detected in the rosette leaves and flower stage 15 sepals, and average to high expression in the seedling stage and entire rosette after transition to flowering. Gene *AT1G72950* (**Figure 4.2.B**) has the lowest levels of expression and is mainly expressed in roots.

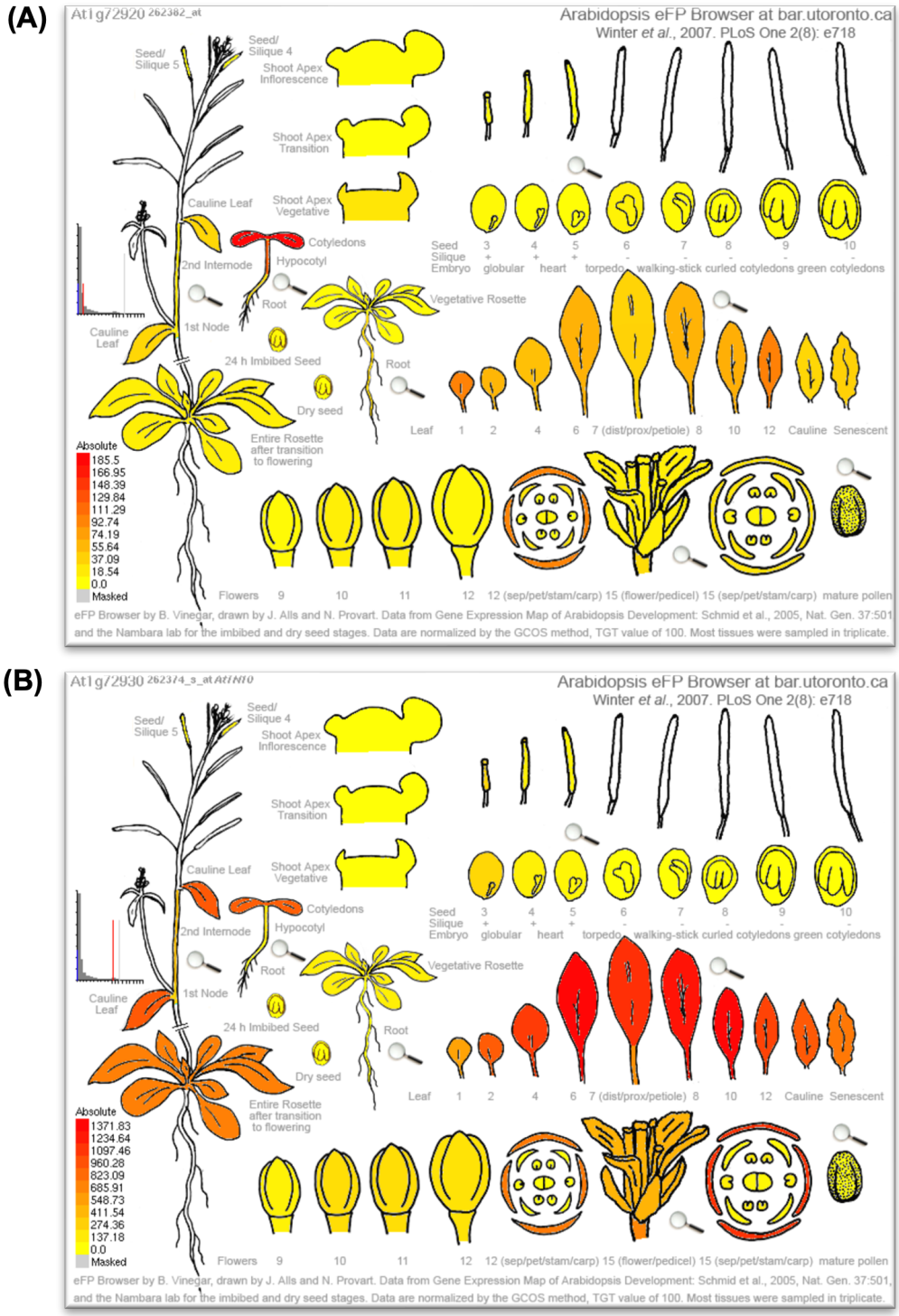

Figure 4.1 **Developmental map of *AT1G72920* and *AT1G72930* expression in *Arabidopsis thaliana* from the *Arabidopsis* eFP browser.**

Colour variations from yellow (0 expression) to red (maximum expression) show the levels of absolute expression of the gene of interest in each developmental stage and/or organ. **(A)** Expression levels of gene *AT1G72920*. Maximum expression detected at the seedling level, average expression in flower stage 12 sepals and low to average expression in the rosette leaves. **(B)** Expression levels of gene *AT1G72930*. Maximum expression detected in the

rosette leaves and flower stage 15 sepals, and average to high expression in the seedling stage and entire rosette after transition to flowering.

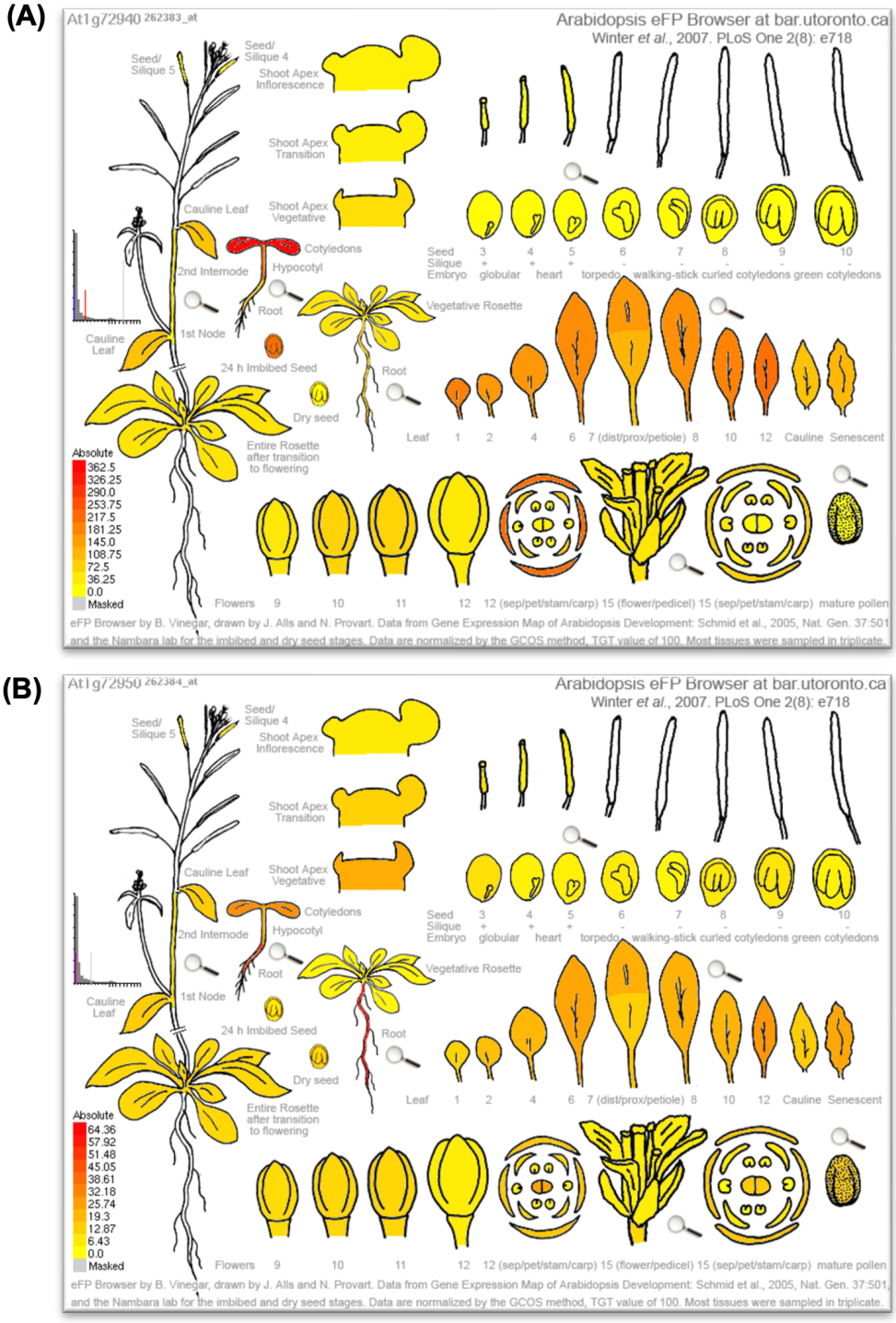

***Figure 4.2* Developmental map of *AT1G72940* and *AT1G72950* expression in *Arabidopsis thaliana* from the *Arabidopsis* eFP browser.**

Colour variations from yellow (0 expression) to red (maximum expression) show the levels of absolute expression of the gene of interest in each developmental stage and/or organ. **(A)** Expression levels of gene *AT1G72940*.

Maximum expression detected at the seedling level and average to expression in flower stage 12 sepals, rosette leaves and 24h imbibed seed. **(B)** Expression levels of gene *AT1G72950*. Maximum expression detected in the roots of seedlings and rosette stage plants, and low to average expression in the rosette leaves, flower stage 12 carpels and shoot apex vegetative stage.

According to the study of Nandety et al. (2013) when they attempted to screen *A. thaliana* single T-DNA knockout lines of *TN* genes for developmental as well as susceptibility phenotypes in response to plant pathogens (e.g., *Pst* DC3000), they did not record any. The absence of susceptibility phenotypes in single T-DNA knockout lines could be attributed to gene redundancy, which would be a likely scenario in the case of our *TN* family of interest, based on the high sequence similarity of the gene family members. Furthermore, the developmental map of *TN* gene expression (**Figures 4.1** and **4.2)** showed that while *TN* genes have diverse basal expression levels and developmental stages or organs they are specialised, they all show average expression levels in the rosette leaves, except *AT1G72930* that shows maximum expression. As pathogen assays are performed in rosette leaves, *TN* gene redundancy could explain the lack of phenotypes in single gene T-DNA mutants. To address this issue, the group of Prof. Murray Grant (University of Warwick, UK) decided to obtain knockout lines of the *TN* locus of interest created with the CRISPR-Cas9 technology. Two CRISPR-Cas9 *TN* K.O. homozygous lines were kindly donated by Prof. Murray Grant (University of Warwick, UK) for the purposes of this thesis.

In this Chapter, the results of immunity related phenotypes in both inducible overexpressing lines of *AT1G72940* and CRISPR-Cas9 *TN* K.O lines are presented when those were challenged with various strains of the bacterial plant pathogen *Pst* DC3000. Furthermore, the expression levels of *AT1G72940* were measured in the *promDEX::AT1G72940* and *promDEX::AT1G72940:HA:FLAG* lines in response to dexamethasone.

Both DEX-inducible and CRISPR-Cas9 *TN* K.O lines were tested for susceptibility phenotypes when challenged with *Pst* DC3000, primarily via bacterial growth colony count. Furthermore, lines were assessed using

chlorophyl fluorescence imaging of the treated leaves post infection, since the rapid suppression of photosynthesis represents one of the earliest physiological responses detected to *Pst* DC3000 (Zabala et al., 2015). The maximum dark-adapted quantum efficiency of PSII photochemistry (F_v/F_m) is related to photoinhibition of PSII resulting by stress factors. Subsequently, we used the changes in F_v/F_m measurements to ask if there were differences between the response of transgenic *AT1G72940* plants and Col-0 to pathogenic *Pst* DC3000.

4.2 Results

4.2.1 Dexamethasone-inducible AT1G72940 A. thaliana stable transgenic lines were tested for susceptibility phenotypes post infection with Pst DC3000.

Four lines of the *promDEX::AT1G72940* transgenic plants were previously selected and kindly donated for the purposes of this PhD project. Those lines are descended from four individual mother plants representing different insertions of the transgene in the Col-0 genome resulting from the transformation of the T0 plants: $T_{1\text{-}1}$, $T_{2\text{-}3}$, $T_{3\text{-}2}$, and $T_{4\text{-}2}$. For the initial experiments of the project, plants of T2 generation of each previously mentioned line were delivered to the author to use and propagate for the collection of T3 generation. Seeds of both T2 and T3 generations were grown in MS media containing Hygromycin to ensure homozygosity of the transgene for the selected lines. Plants of the T3 generation were used for the majority of experiments presented in this chapter, unless stated otherwise.

promDEX::AT1G72940 lines were challenged with *Pst* DC3000 to measure the bacterial growth and the maximum dark-adapted quantum efficiency of the PSII in response to bacterial infection, compared to WT Col-0 plants. As previously described (**Materials and Methods**, **sections 2.4.1** and **2.4.3**), all plants tested were grown for 5 to 6 weeks post germination and on the day prior to infection, rosette leaves number 7, 8 and 9 were identified and surface-painted with 10μM of DEX solution, unless stated otherwise. Leaves were induced with DEX for 16hrs and then infiltrated with *Pst* DC3000 inoculum. Plants used for bacterial growth were infected with a lower bacterial O.D. (0.0002), and the virulent bacteria were allowed to incubate in the leaf apoplast for 3 days prior to isolation, bacterial growth, and colony count. Plants used for measuring the maximum dark-adapted quantum efficiency of PSII were inoculated with higher bacterial O.D. (0.15) and kept in the CF Imager for

24hrs. In addition, plants were alternatively treated with *Pst* DC3000 *hrpA* and mock ($MgCl_2$).

Figure 4.3 shows the changes in the maximum dark-adapted quantum efficiency of the PSII photochemistry (F_v/F_m) recorded by a CF Imager in treated rosette leaves of Col-0 (green curves) and *promDEX::AT1G72940* (red curves) lines T_{1-1} and T_{2-3} Treatments with DEX, *Pst* DC3000 *hrpA,* and DEX+*Pst* DC3000 *hrpA* do not affect PSII, hence the rate remains mostly stable post-infection and for the duration of the experiment, for all tested lines. Figure 4.3.A shows the changes in F_v/F_m rate post-treatments for *promDEX::AT1G72940* T_{1-1} against Col-0 plants. The response of Col-0 leaves shows a similar trend between *Pst* DC3000 and *Pst* DC3000+DEX treatments (F_v/F_m =0.55). *promDEX::AT1G72940* T_{1-1} shows a faster decline of F_v/F_m when treated with *Pst* DC3000+DEX, which eventually reaches a slightly lower value (<0.5) compared to when treated with *Pst* DC3000 (0.6). However, when comparing the response of line T_{1-1} to that of Col-0 when both treated with *Pst* DC3000+DEX, the difference in their lowest F_v/F_m values after 24hrs is approximately 0.05 which makes it not possible to differentiate. **Figure 4.3.B** presents the changes in F_v/F_m rate post-treatments for *promDEX::AT1G72940* T_{2-3} against Col-0 plants. Data show that the decline of F_v/F_m in both *promDEX::AT1G72940* T_{2-3} and Col-0 is the same for *Pst* DC3000 treatment (F_v/F_m =0.65) and *Pst* DC3000+DEX treatment (F_v/F_m =0.6), indicating that the plants have the same response to infection regardless of DEX.

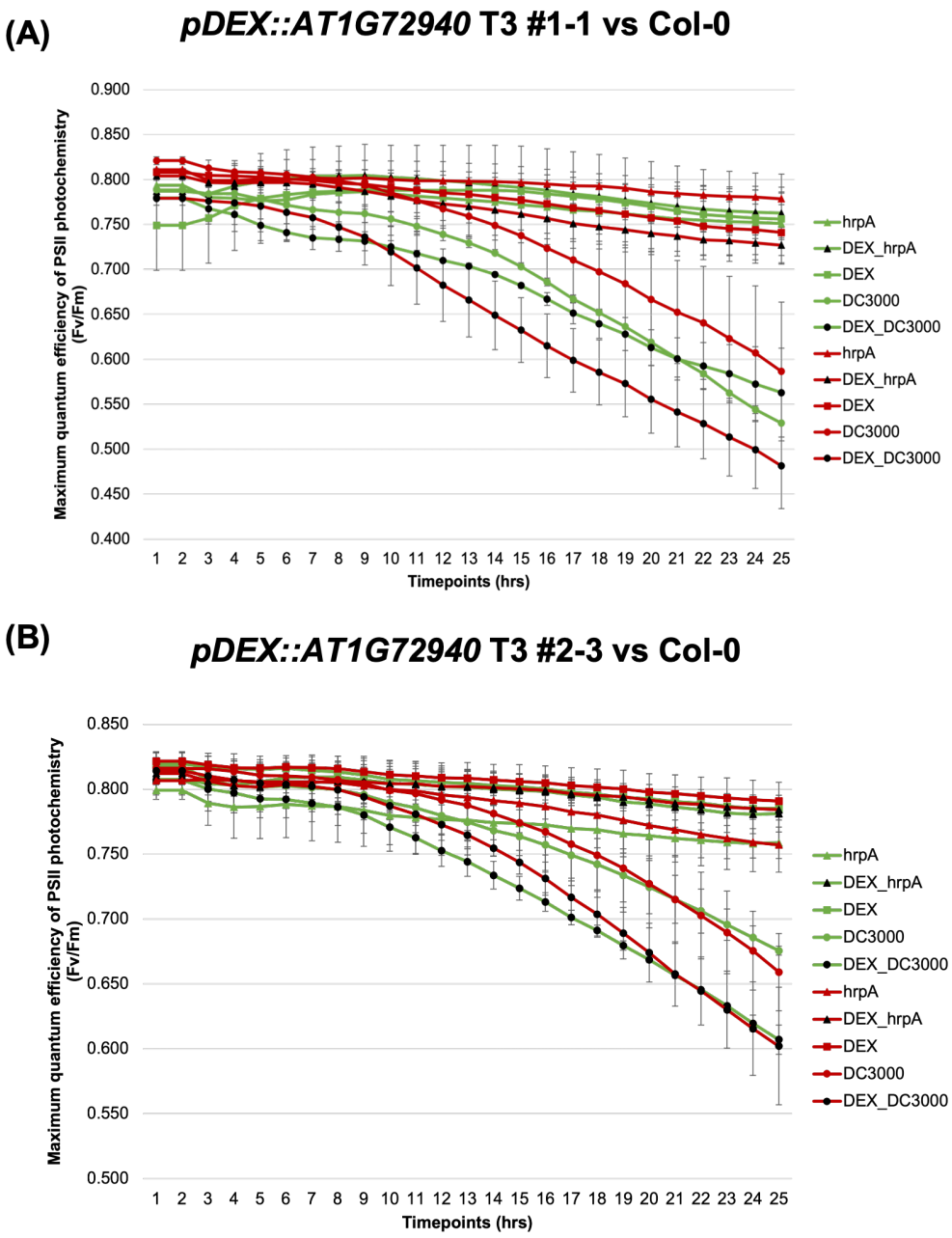

Figure 4.3 **Measuring of the maximum quantum efficiency of the PSII photochemistry of *A. thaliana promDEX::AT1G72940* lines $T_{1\text{-}1}$ and $T_{2\text{-}3}$ post-*Pst* DC3000 challenge.**

Rosette leaves of *promDEX::AT1G72940* $T_{1\text{-}1}$, $T_{2\text{-}3}$ and Col-0 plants were treated with 10µM of DEX and 16hrs later they were infiltrated with *Pst* DC3000 and *Pst* DC3000 *hrpA* (O.D.=0.15). Different leaves were infiltrated only with *Pst* DC3000 and *Pst* DC3000 *hrpA* (O.D.=0.15), and some leaves were only treated with DEX. Treated plants were dark-adapted inside a CF Imager for 1hr and then subjected to pulses of light for 24hrs while PSII chemistry fluorescence was recorded. Charts present the changes in the maximum dark-adapted quantum efficiency of PSII photochemistry (F_v/F_m) rate as recorded in the treated plants. Each data point represents the average F_v/F_m measurements

and the bars the standard deviation, calculated from 3 leaves/treatment. **(A)** F_v/F_m rate of *promDEX::AT1G72940* T_{1-1} against Col-0. *Pst* DC3000 and *Pst* DC3000+DEX treatments have a similar effect on Col-0 F_v/F_m. In *promDEX::AT1G72940* T_{1-1} the rate drops faster and lower when treated with *Pst* DC3000+DEX compared to *Pst* DC3000. **(B)** F_v/F_m rate of *promDEX::AT1G72940* T_{2-3} against Col-0. *promDEX::AT1G72940* T_{2-3} exhibits a similar trend to Col-0 in both *Pst* DC3000 and *Pst* DC3000+DEX treatments. Plants treated with DEX, *Pst* DC3000 *hrpA*, and DEX+ *Pst* DC3000 *hrpA* show a mostly stable F_v/F_m rate post treatment in both **(A)** and **(B)**.

Red: *promDEX::AT1G72940* lines

Green: Col-0

▵ Pst DC3000 hrpA, ▲ DEX+ Pst DC3000 hrpA, ☐ DEX

○ Pst DC3000, ● Pst DC3000+DEX

Figure 4.4 shows the bacterial growth curves at 3DPI resulting from the colony counts in Col-0 and *promDEX::AT1G72940* lines T_{1-1} and T_{2-3}, when treated with DEX and challenged with virulent *Pst* DC3000. Col-0 plants (black column) show an average *Pst* DC3000 growth of 6.5 (log_{10} cfu/cm^2), while and *promDEX::AT1G72940* T_{1-1} (light green column) reaches 5.5, thus showing less susceptibility than Col-0 to virulent *Pst* DC3000 infection. A two-tail t-test assuming unequal variances (due to the small number of biological replicates) determined that the difference in *Pst DC3000* growth between *promDEX::AT1G72940* T_{1-1} and Col-0 is statistically significant, with $p<0.05$. However, these results were not reproduced in further experiments. Additionally, the colony counts at 3DPI for *promDEX::AT1G72940* line T_{2-3} plants showed that their response to *Pst* DC3000 infection is similar to Col-0 (6.5 log_{10} cfu/cm^2) and any differences are not statistically significant.

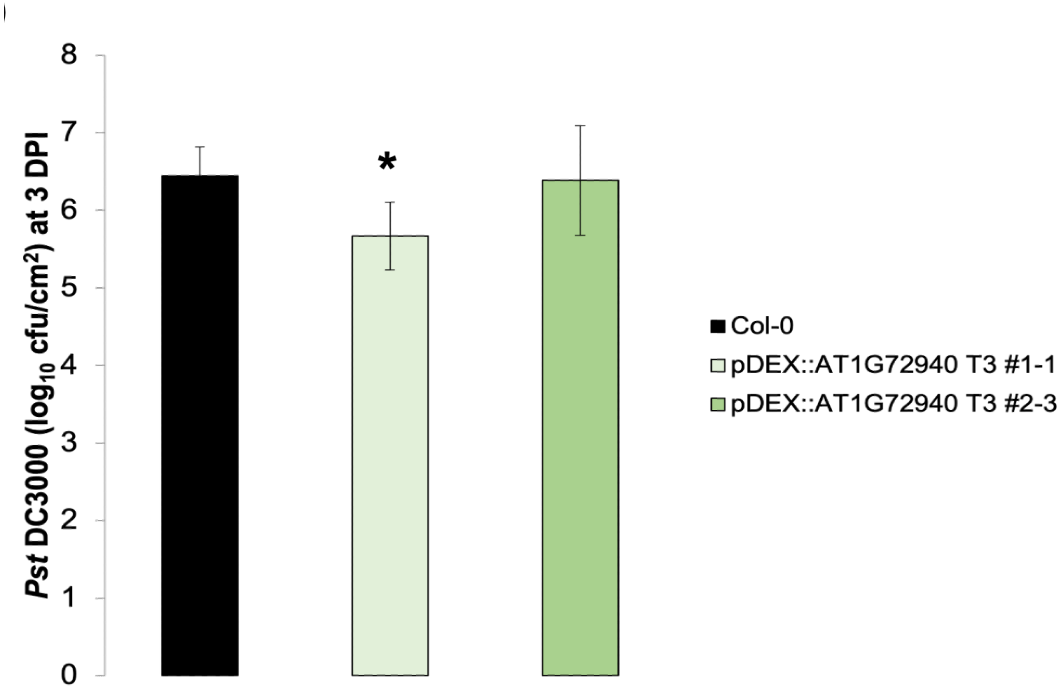

Figure 4.4 **Bacterial growth curves at 3DPI of *A. thaliana promDEX::AT1G72940* lines $T_{1\text{-}1}$ and $T_{2\text{-}3}$ when challenged with virulent *Pst* DC3000.**

Rosette leaves of *promDEX::AT1G72940* $T_{1\text{-}1,}$ $T_{2\text{-}3}$ and Col-0 plants were treated with 10μM of DEX and 16hrs later they were infiltrated with *Pst* DC3000 (O.D.=0.0002). At 3DPI Col-0 plants (black) show an average *Pst* DC3000 growth of 6.5 (log_{10} cfu/cm^2) similar to *promDEX::AT1G72940* $T_{2\text{-}3}$ (green), while *promDEX::AT1G72940* $T_{1\text{-}1}$ (light green) reaches 5.5 (log_{10} cfu/cm^2). Bar charts represent the log10 of the average *Pst* DC3000 colony counts per cm^2 and the bars the standard error, calculated from 6 plants/treatment. One asterisk (*) indicates statistically significant difference to 5%; two asterisks (**) indicate statistically significant difference to 1%. Due to small sample number, a two-tail t-test assuming unequal variances was selected for the statistical analysis.

Figure 4.5 shows the changes in the maximum dark-adapted quantum efficiency of the PSII photochemistry (F_v/F_m) recorded by a CF Imager in treated rosette leaves of Col-0 (green curves) and *promDEX::AT1G72940* (red curves) lines T_{3-2} and T_{4-2} Treatments with DEX, *Pst* DC3000 *hrpA,* and DEX+*Pst* DC3000 *hrpA* do not affect PSII, hence the rate remains mostly stable post-infection and for the duration of the experiment, for all tested lines. **Figure 4.5.A** shows the changes in F_v/F_m rate post-treatments for *promDEX::AT1G72940* T_{3-2} against Col-0 plants. *promDEX::AT1G72940* T_{3-2} exhibits a similar trend to Col-0 for *Pst* DC3000 (F_v/F_m =~0.66) and *Pst* DC3000+DEX treatment (F_v/F_m =0.6). Therefore, there is no detected difference in the F_v/F_m response of *promDEX::AT1G72940* T_{3-2} to that of Col-0 following *Pst* DC3000+DEX treatment. **Figure 4.5.B** presents the changes in F_v/F_m rate post-treatments for *promDEX::AT1G72940* T_{4-2} against Col-0 plants. Data show that both Col-0 and *promDEX::AT1G72940* T_{4-2} respond similarly to *Pst* DC3000 and *Pst* DC3000+DEX treatments (F_v/F_m ranging around 0.65), with *promDEX::AT1G72940* T_{4-2} dropping slightly lower post *Pst* DC3000+DEX treatment (F_v/F_m =0.6).

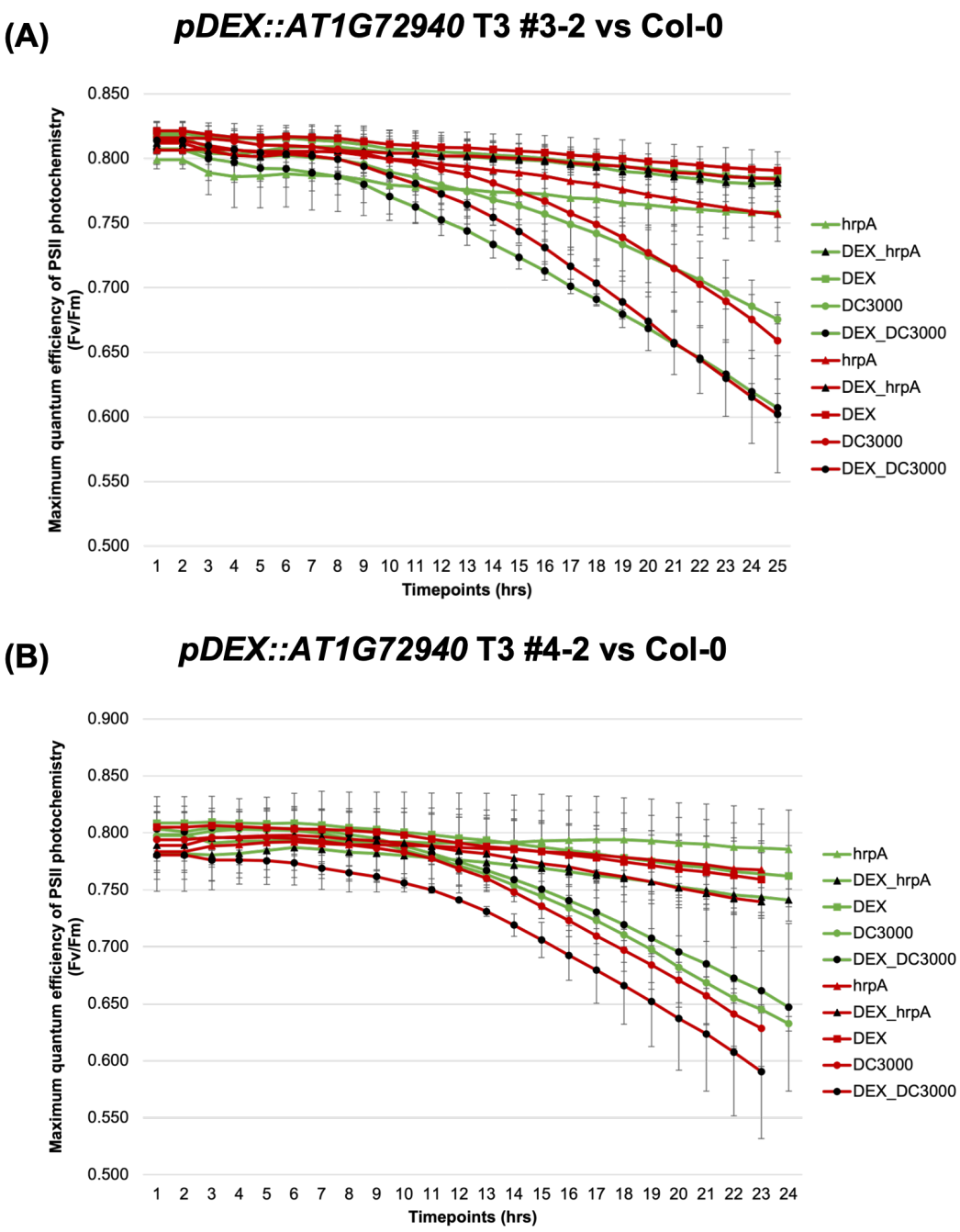

Figure 4.5 **Measuring the maximum quantum efficiency of the PSII photochemistry of *A. thaliana promDEX::AT1G72940* lines $T_{2\text{-}3}$ and $T_{4\text{-}2}$ following *Pst* DC3000 challenge.**

Rosette leaves of *promDEX::AT1G72940* $T_{2\text{-}3}$, $T_{4\text{-}2}$ and Col-0 plants were treated with 10µM of DEX and 16hrs later they were infiltrated with *Pst* DC3000 and *Pst* DC3000 *hrpA* (O.D.=0.15). Different leaves were infiltrated only with *Pst* DC3000 and *Pst* DC3000 *hrpA* (O.D.=0.15), and some leaves were only treated with DEX. Treated plants were dark-adapted inside a CF Imager for 1hr and then subjected to pulses of light for 24hrs while PSII chemistry fluorescence was recorded. Charts present the changes in the maximum dark-adapted quantum efficiency of PSII photochemistry (F_v/F_m) rate as recorded in the treated plants. Each data point represents the average F_v/F_m measurements

and the bars the standard deviation, calculated from 3 leaves/treatment. **(A)** F_v/F_m rate of *promDEX::AT1G72940* T_{2-3} against Col-0. *promDEX::AT1G72940* T_{2-3} exhibits a similar trend to Col-0 both in the case of *Pst* DC3000 and *Pst* DC3000+DEX treatment. **(B)** F_v/F_m rate of *promDEX::AT1G72940* T_{2-3} against Col-0. Both Col-0 and *promDEX::AT1G72940* T_{4-2} show a similar trend in response to *Pst* DC3000 and *Pst* DC3000+DEX treatments, except *promDEX::AT1G72940* T_{4-2} dropping slightly lower when treated with *Pst* DC3000+DEX. Plants treated with DEX, *Pst* DC3000 *hrpA*, and DEX+ *Pst* DC3000 *hrpA* show a mostly stable F_v/F_m rate post treatment in both **(A)** and **(B)**.

Red: *promDEX::AT1G72940* lines

Green: Col-0

▵ Pst DC3000 hrpA, ▲ DEX+ Pst DC3000 hrpA, ☐ DEX

○ Pst DC3000, • Pst DC3000+DEX

Figure 4.6 presents the results of the bacterial growth curves at 3DPI for Col-0 and *promDEX::AT1G72940* lines T_{3-2} and T_{4-2}, when treated with DEX and challenged with virulent *Pst* DC3000. Charts in **(A)** and **(B)** represent the average bacterial growth recorded when combining the results of three independent biological replicates of each experiment. **Figure 4.6.A** shows the results of bacterial growth in the T2 generation of *promDEX::AT1G72940* lines T_{3-2} and T_{4-2} against Col-0. The *Pst* DC3000 colony count in Col-0 plants (black column) shows an average growth of 6.5 ($\log_{10}$ cfu/cm^2). *promDEX::AT1G72940* T_{4-2} (dark green column) responds to *Pst* DC3000 similarly to Col-0, while *promDEX::AT1G72940* T_{3-2} (green column) colony are only ~0.2 higher than Col-0 (~6.7 $\log_{10}$ cfu/cm^2). Those differences were not found to be statistically significant against the *Pst* growth in Col-0, when a two tail t-test assuming unequal variances was used. **Figure 4.6.B** shows that Col-0 plants have an average *Pst* DC3000 growth of 7 ($\log_{10}$ cfu/cm^2) same as *promDEX::AT1G72940* T_{4-2}, while *promDEX::AT1G72940* T_{3-2} counts appear to be slightly lower than Col-0. However, this difference is not statistically significant.

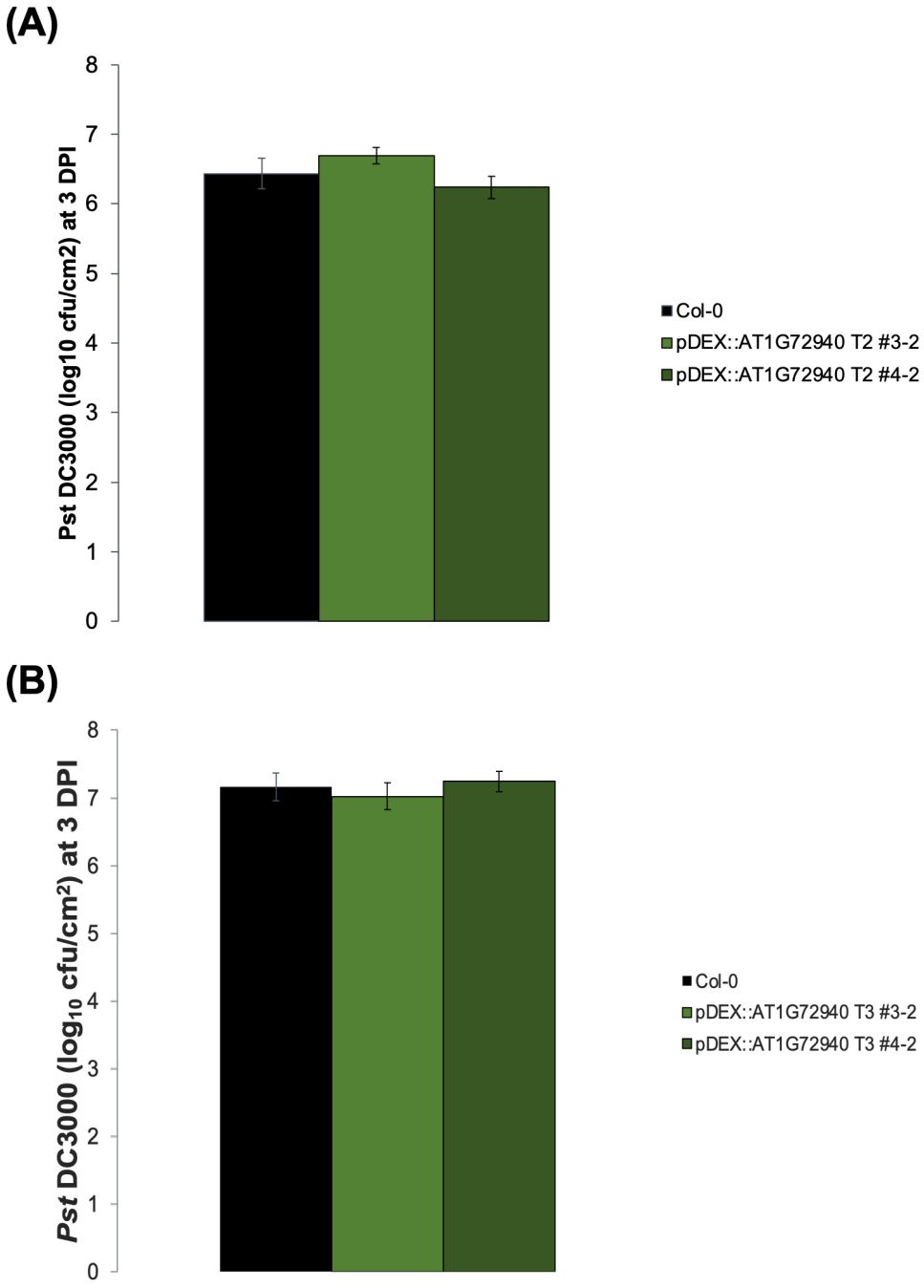

Figure 4.6 **Bacterial growth curves at 3DPI of *A. thaliana promDEX::AT1G72940* lines $T_{3\text{-}2}$ and $T_{4\text{-}2}$ when challenged with virulent *Pst* DC3000.**

Rosette leaves of *promDEX::AT1G72940* $T_{3\text{-}2,}$ $T_{4\text{-}2}$ and Col-0 plants were treated with 10µM of DEX and 16hrs later they were infiltrated with *Pst* DC3000 (O.D.=0.0002). **(A)** Bacterial growth of T2 generation of *promDEX::AT1G72940* $T_{3\text{-}2,}$ $T_{4\text{-}2}$ against Col-0. Col-0 plants (black) show an average *Pst* DC3000 growth of 6.5 ($\log_{10}$ cfu/cm^2) similar to *promDEX::AT1G72940* $T_{4\text{-}2}$ (dark green), while *promDEX::AT1G72940* $T_{3\text{-}2}$ (green) shows ~6.7 ($\log_{10}$ cfu/cm^2). **(B)** Bacterial growth of T3 generation of *promDEX::AT1G72940* $T_{3\text{-}2,}$ $T_{4\text{-}2}$ against Col-0. Col-0 plants (black) show an average *Pst* DC3000 growth of 7 ($\log_{10}$

cfu/cm^2) similar to *promDEX::AT1G72940* $T_{4\text{-}2}$ (dark green), while *promDEX::AT1G72940* $T_{3\text{-}2}$ (green) is slightly lower. Bar charts represent the log10 of the average *Pst* DC3000 colony counts per cm^2 and the bars the standard error, calculated from 6 plants/treatment. The results include the combined data of 3 independent biological replicates. Due to small sample number, a two-tail t-test assuming unequal variances was selected for the statistical analysis, but no statistically significant differences were found.

In a final attempt to assess the impact of *Pst* DC3000 infection on the *promDEX::AT1G72940* lines when those are treated with DEX, a bacterial growth experiment was performed simultaneously at all available lines, using Col-0 plants for reference. **Figure 4.7** presents the results of the bacterial growth curves at 3DPI for Col-0 and *promDEX::AT1G72940* lines $T_{1\text{-}1}$, $T_{2\text{-}3}$, $T_{3\text{-}2}$ and $T_{4\text{-}2}$ when treated with DEX and challenged with virulent *Pst* DC3000. Col-0 plants (black column) show an average *Pst* DC3000 growth of 5.6 (log_{10} cfu/cm^2). All tested *promDEX::AT1G72940* lines show similar colony counts to Col-0, with the exception of line $T_{3\text{-}2}$ where the average counts are approximately 5.5 (log_{10} cfu/cm^2). A two tail t-test assuming unequal variances showed that there is no statistically significant difference in the growth of Pst DC3000 between the *promDEX::AT1G72940* lines and Col-0.

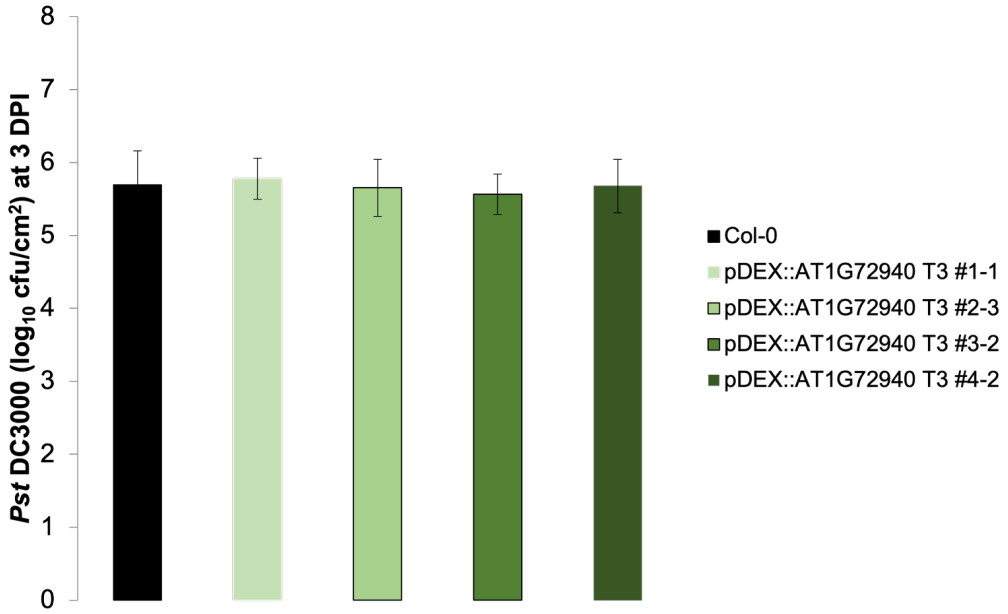

Figure 4.7 **Bacterial growth curves at 3DPI of all four *A. thaliana promDEX::AT1G72940* lines in T3 generation when challenged with virulent *Pst* DC3000.**

Rosette leaves of *promDEX::AT1G72940* $T_{1\text{-}1}$, $T_{2\text{-}3}$, $T_{3\text{-}}$, $T_{4\text{-}2}$ and Col-0 plants were treated with 10μM of DEX and 16hrs later they were infiltrated with *Pst* DC3000 (O.D.=0.0002). Col-0 plants (black) show an average *Pst* DC3000 growth of 5.6 (log_{10} cfu/cm^2). All *promDEX::AT1G72940* lines show similar colony counts to Col-0, with the exception of line $T_{3\text{-}2}$ where the average counts are slightly decreased. The curves represent the log10 of the average *Pst* DC3000 colony counts per cm^2 and the bars the standard deviation, calculated from 6 plants/treatment. Due to small sample number, a two-tail t-test

assuming unequal variances was selected for the statistical analysis, but no statistically significant differences were found.

The lack of recorded evidence to support that the induction of overexpression of *AT1G72940* in *promDEX::AT1G72940* lines causes any impact on the transgenic plants' response to *Pst* DC3000 infection, led to the question of whether DEX treatment is functioning as expected and results to the proper induction of *AT1G72940* transgene. To address this question, we decided to treat the *promDEX::AT1G72940* lines with DEX over a time course of 12hrs and perform RT-q-PCR to detect the levels of *AT1G72940* transcript before and after the induction. Rosette leaf number 8 of 5 to 6-weeks-old Col-0 and *promDEX::AT1G72940* lines $T_{1\text{-}1}$, $T_{2\text{-}3}$, $T_{3\text{-}2}$ and $T_{4\text{-}2}$ (T3 generation) were infiltrated with 30μM of DEX solution. Samples were collected at 0, 6 and 12hrs following DEX treatment from 3 individual plants per line. The detected levels of *AT1G72940* were normalised against the respective levels of the housekeeping gene *α-tubulin*, and the relative expression levels are presented as fold change against the basal expression of *AT1G72940* in the Col-0 sample at 0h (**Figure 4.8).** Due to small sample number, a two-tail t-test assuming unequal variances was selected for the statistical analysis

Figure 4.8.A shows the fold change in relative expression of *AT1G72940* in *promDEX::AT1G72940* lines against Col-0 at 0 and 6hrs post DEX treatment. *AT1G72940* levels at 0hrs vary when compared to Col-0, but the differences are not statistically significant. At 6hrs, the transcript levels of *AT1G72940* are not increased in response to DEX treatment for any of the *promDEX::AT1G72940* lines or Col-0. On the contrary, since we express the fold change against Col-0 at 0hrs, *AT1G72940* levels at 6h post-DEX show a decrease across all lines tested, including Col-0. The decrease in *AT1G72940* expression levels at 6h post-DEX is statistically significant, when compared to Col-0 at 0h; however, it is not significant when the expression of *AT1G72940* in *promDEX::AT1G72940* lines is compared to Col-0 at 6h.

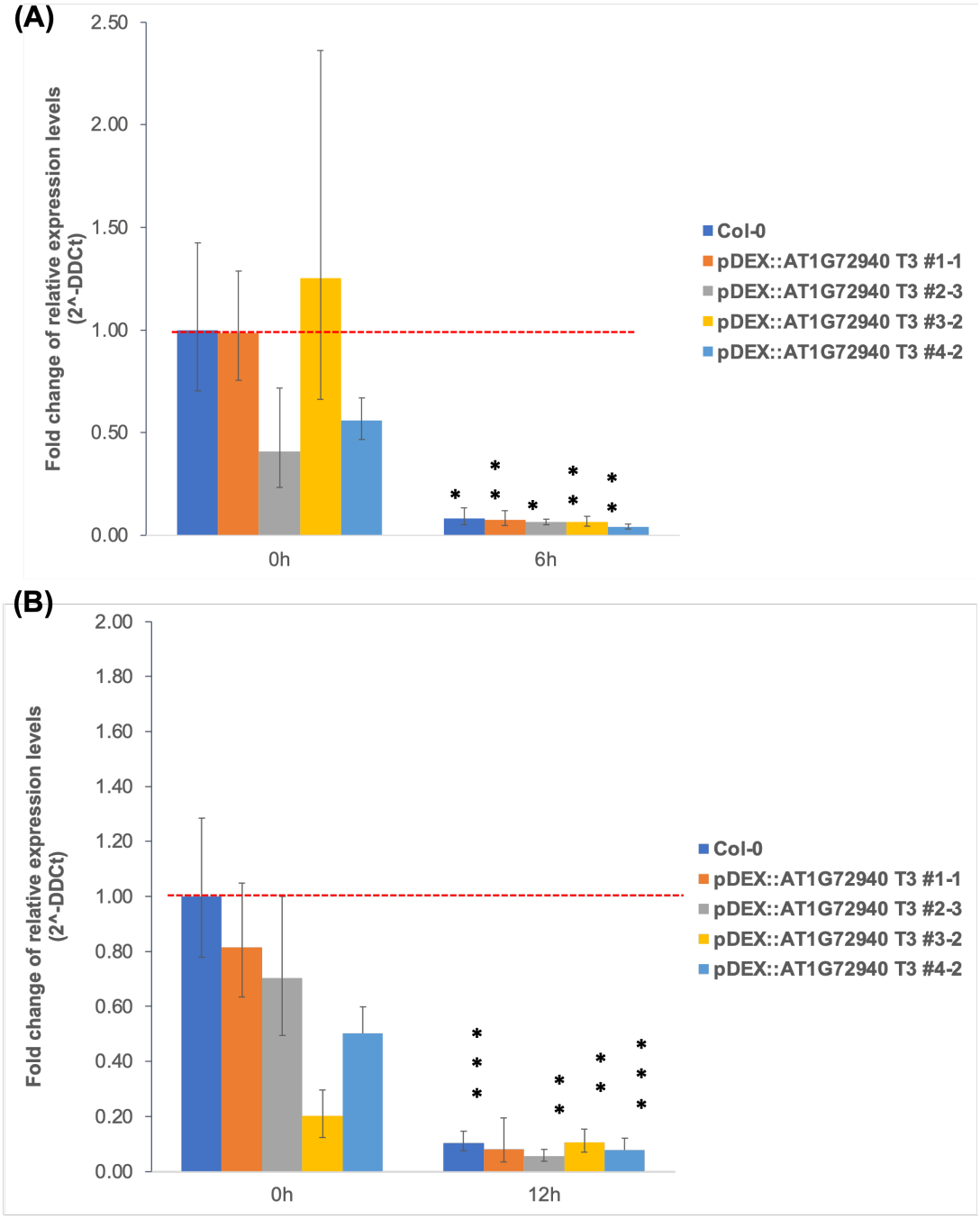

***Figure 4.8* Fold change of the relative expression levels of *AT1G72940* in *A. thaliana promDEX::AT1G72940* transgenic lines post treatment with DEX.**

RT-qPCR was performed on rosette leaf number 8 of 5 to 6-weeks-old Col-0 and *promDEX::AT1G72940* lines $T_{1\text{-}1}$, $T_{2\text{-}3}$, $T_{3\text{-}2}$ and $T_{4\text{-}2}$ (T3 generation)that were infiltrated with 30µM of DEX. Samples were collected at 0, 6 and 12hrs following DEX treatment from 3 individual plants per line. The detected levels of *AT1G72940* were normalised against the housekeeping gene *a-tubulin*, and the relative expression levels are presented as fold change against the basal expression of *AT1G72940* in the Col-0 sample at 0h. Bar heights represent the average fold change in expression of *AT1G72940* gene for each line, calculated from 3 biological replicates. Error bars indicate the 95% confidence interval for the fold change of relative Ct values. One asterisk (*) indicates statistically

significant difference to 5%; two asterisks (**) indicate statistically significant difference to 1%; three asterisks (***) indicate statistically significant difference to 0.1%. Due to small sample number, a two-tail t-test assuming unequal variances was selected for the statistical analysis. **(A)** Fold change of *AT1G72940* expression at 0 and 6hrs post-DEX treatment. *AT1G72940* levels at 0hrs vary when compared to Col-0, but the differences are not statistically significant. At 6hrs, the transcript levels of *AT1G72940* are not increased in response to DEX treatment for any of the *promDEX::AT1G72940* lines or Col-0. The decrease in *AT1G72940* expression levels at 6h post-DEX is statistically significant, when compared to Col-0 at 0h; however, not when the expression is compared to Col-0 at 6h. **(B)** Fold change of *AT1G72940* at 0 and 12hrs post-DEX treatment. *AT1G72940* levels at 0hrs vary when compared to Col-0, but the differences are not statistically significant. At 12hrs, the transcript levels of *AT1G72940* do not show any increase in response to DEX treatment for any of the *promDEX::AT1G72940* lines or Col-0. The decrease in *AT1G72940* expression levels at 12h post-DEX is statistically significant, when compared to Col-0 at 0h; however, not when the expression is compared to Col-0 at 12h.

Figure 4.8.B shows the fold change in relative expression of *AT1G72940* in *promDEX::AT1G72940* lines against Col-0 at 0 and 12hrs post DEX treatment. The results follow a similar trend to the response of the same lines at 6h post-DEX treatment (**Figure 4.8.A).** *AT1G72940* levels at 0hrs vary compared to Col-0, but the differences are not statistically significant. At 12hrs, the transcript levels of *AT1G72940* do not show any increase in response to DEX treatment for any of the *promDEX::AT1G72940* lines or Col-0. The decrease in *AT1G72940* expression levels at 12h post-DEX is statistically significant, when compared to Col-0 at 0h; however, not when the expression is compared to Col-0 at 12h.

Collectively, the results of the RT-q-PCR on *promDEX::AT1G72940* lines $T_{1\text{-}1}$, $T_{2\text{-}3}$, $T_{3\text{-}2}$ and $T_{4\text{-}2}$ (T3 generation) when compared to Col-0 following treatment with DEX over a time course of 12hrs showed that DEX does not induce the transcription of *AT1G72940* in any of the tested *promDEX::AT1G72940* lines, indicating that the transgene is not functional. The decrease observed in the levels of *AT1G72940* transcripts across all tested lines is statistically significant when compared to the expression of *AT1G72940* in Col-0 at 0hr, but not when compared with Col-0 at 6h and 12hrs post-DEX, respectively.

After verifying that *promDEX::AT1G72940* lines were not induced by DEX, we proceeded with the analysis of *promDEX::AT1G72940:HA:FLAG* lines, as in the meantime those were made available for this PhD project by Prof. Murray Grant and his group (University of Warwick). We hypothesised that the transgene was unresponsive to DEX in *promDEX::AT1G72940* lines, so it was decided to check if this was a common issue to all plants generated with the same T-DNA vectors. Additionally, *promDEX::AT1G72940:HA:FLAG* lines carry protein tags on the C' terminal, allowing for protein detection assays to assess AT1G72940 expression.

Figure 4.9 shows the changes of F_v/F_m in treated Col-0 (green measurements) and *promDEX::AT1G72940:HA:FLAG* $T_{1\text{-}2}$ (red measurements) rosette leaves when challenged with *Pst* DC3000. Different leaves were infiltrated only with *Pst* DC3000 and mock (10mM of MgCl2). Images **(A)** to **(E)** show the photoinhibition of PSII (F_v/F_m) as recorded at 0, 1, 6, 12 and 24hrs, respectively. The chart in **Figure 4.9 (F)** presents the changes in F_v/F_m rate as recorded in the treated plants. Mock treatment does not affect PSII, hence the F_v/F_m remains stable. Both Col-0 and *promDEX::AT1G72940:HA:FLAG* line $T_{1\text{-}2}$ when treated with *Pst* DC3000 and *Pst* DC3000+DEX show the same trend of photoinhibition (F_v/F_m=0.6), thus DEX does not affect the photoinhibition response of *promDEX::AT1G72940:HA:FLAG* $T_{1\text{-}2}$ plants to *Pst* DC3000.

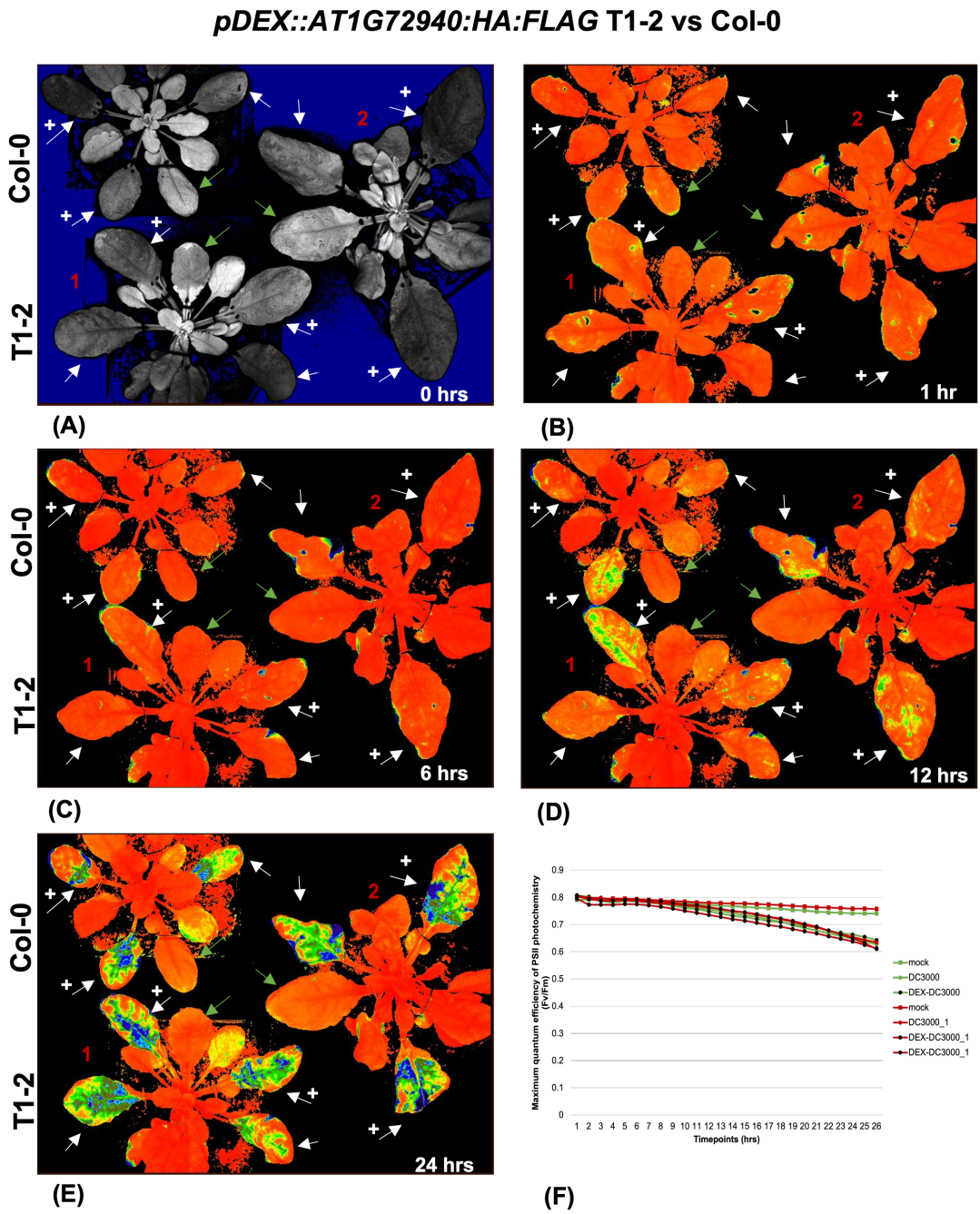

Figure 4.9 **Measuring the maximum quantum efficiency of the PSII photochemistry of *A. thaliana promDEX::AT1G72940:HA:FLAG* line $T_{1\text{-}2}$ post *Pst* DC3000 challenge.**

Rosette leaves of *promDEX::AT1G72940:HA:FLAG* $T_{1\text{-}2}$ and Col-0 plants were treated with 10µM of DEX and 16hrs later they were infiltrated with *Pst* DC3000 (O.D.=0.15). Different leaves were infiltrated only with *Pst* DC3000 and mock (10mM of MgCl2). Treated plants were dark-adapted inside a CF Imager for 1hr and then subjected to pulses of light for 24hrs while PSII chemistry fluorescence was recorded. Images **(A)** to **(E)** show the photoinhibition of PSII (F_v/F_m) as recorded at 0, 1, 6, 12 and 24hrs, respectively. Treated leaves are marked with different arrows: white for *Pst* DC3000, white+ for *Pst* DC3000+DEX, and green for mock. Charts present the

changes in the maximum dark-adapted quantum efficiency of PSII photochemistry (F_v/F_m) rate as recorded in the treated plants. Each data point represents the average F_v/F_m measurements and the bars the standard deviation, calculated from 3 leaves/treatment. **(F)** F_v/F_m rate of *promDEX::AT1G72940:HA:FLAG* T_{1-2} against Col-0. Both Col-0 and *promDEX::AT1G72940:HA:FLAG* T_{1-2} when treated with *Pst* DC3000 and *Pst* DC3000+DEX show the same trend of photoinhibition. Plants treated with mock show a mostly stable F_v/F_m rate post treatment.

Red: *promDEX::AT1G72940:HA:FLAG* lines

Green: Col-0

□ mock ,○ Pst DC3000, • Pst DC3000+DEX

Figure 4.10 shows the changes of F_v/F_m in treated Col-0 (green measurements) and *promDEX::AT1G72940:HA:FLAG* T_{1-3} (red measurements) rosette leaves when challenged with *Pst* DC3000. Different leaves were infiltrated only with *Pst* DC3000 and mock (10mM of MgCl2). Images **(A)** to **(E)** show the photoinhibition of PSII (F_v/F_m) as recorded at 0, 1, 6, 12 and 24hrs, respectively. The chart in **Figure 4.10 (F)** presents the changes in F_v/F_m rate as recorded in the treated plants. Mock treatment does not affect PSII, hence the F_v/F_m remains stable. Both Col-0 and *promDEX::AT1G72940:HA:FLAG* line T_{1-3} when treated with *Pst* DC3000 and *Pst* DC3000+DEX show the same trend of photoinhibition (F_v/F_m=0.6), thus DEX does not affect the photoinhibition response of *promDEX::AT1G72940:HA:FLAG* T_{1-3} plants to *Pst* DC3000.

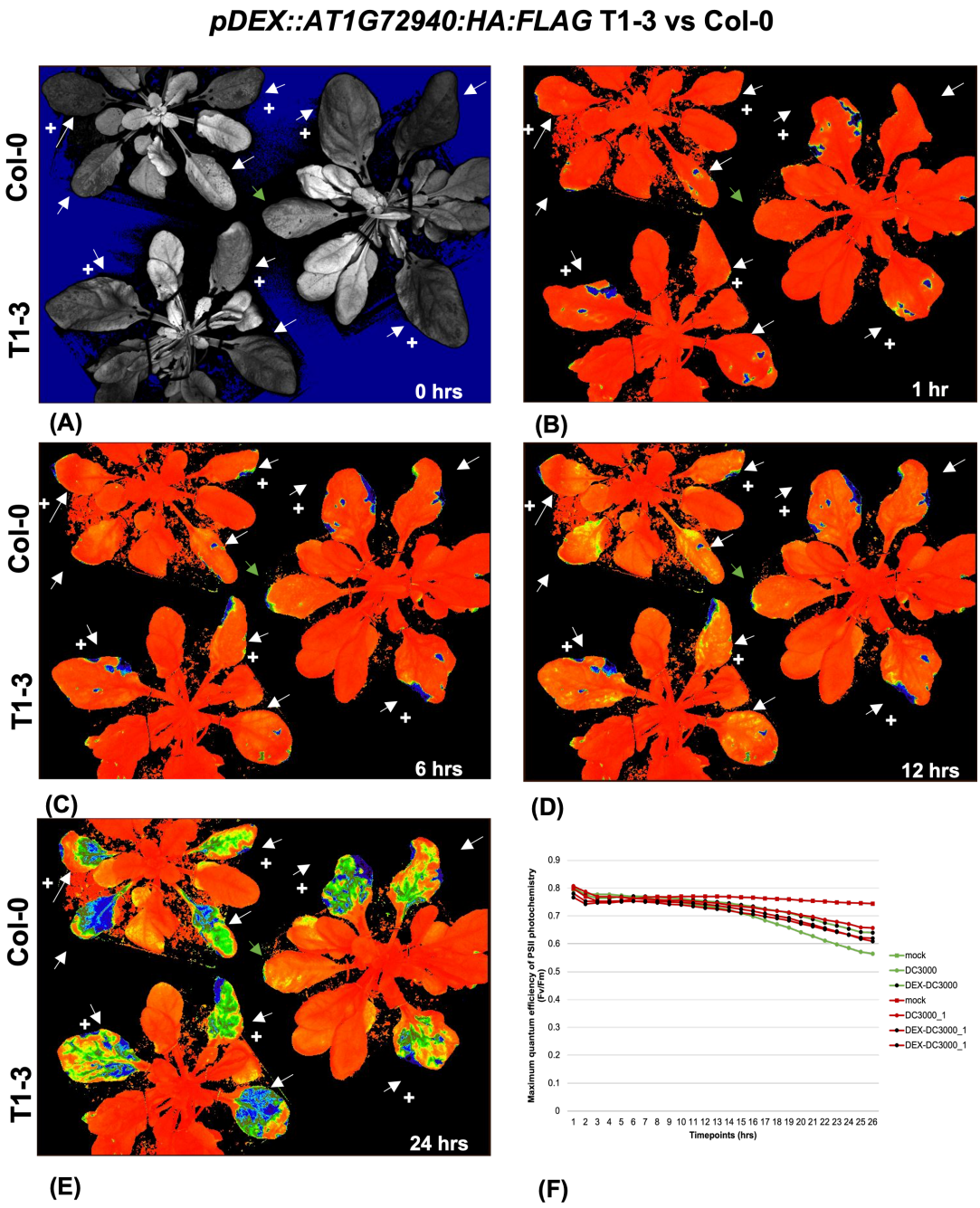

Figure 4.10 **Measuring the maximum quantum efficiency of the PSII photochemistry of *A. thaliana promDEX::AT1G72940:HA:FLAG* line $T_{1\text{-}3}$ post *Pst* DC3000 challenge.**

Rosette leaves of *promDEX::AT1G72940:HA:FLAG* $T_{1\text{-}3}$ and Col-0 plants were treated with 10µM of DEX and 16hrs later they were infiltrated with *Pst* DC3000 (O.D.=0.15). Different leaves were infiltrated only with *Pst* DC3000 and mock (10mM of MgCl2). Treated plants were dark-adapted inside a CF Imager for 1hr and then subjected to pulses of light for 24hrs while PSII chemistry fluorescence was recorded. Images **(A)** to **(E)** show the photoinhibition of PSII (F_v/F_m) as recorded at 0, 1, 6, 12 and 24hrs, respectively. Treated leaves are marked with different arrows: white for *Pst* DC3000, white+ for *Pst* DC3000+DEX, and green for mock. Charts present the

changes in the maximum dark-adapted quantum efficiency of PSII photochemistry (F_v/F_m) rate as recorded in the treated plants. Each data point represents the average F_v/F_m measurements and the bars the standard deviation, calculated from 3 leaves/treatment. **(F)** F_v/F_m rate of *promDEX::AT1G72940:HA:FLAG* T_{1-3} against Col-0. Both Col-0 and *promDEX::AT1G72940:HA:FLAG* T_{1-3} when treated with *Pst* DC3000 and *Pst* DC3000+DEX show the same trend of photoinhibition. Plants treated with mock show a mostly stable F_v/F_m rate post treatment.

Red: *promDEX::AT1G72940:HA:FLAG* lines

Green: Col-0

□ mock ,○ Pst DC3000, • Pst DC3000+DEX

The preliminary results of PSII photoinhibition of *promDEX::AT1G72940:HA:FLAG* lines following DEX+*Pst* DC3000 treatment show that the lines respond similar to Col-0, meaning that DEX does not affect the response of the *promDEX::AT1G72940:HA:FLAG* lines to *Pst* DC3000. **Figure 4.11** shows the relative expression levels of *AT1G72940* resulting of RT-q-PCR analysis of *promDEX::AT1G72940:HA:FLAG* T_{1-2} and T_{1-3} lines post DEX treatment and compared to Col-0 basal gene expression at 0h over a 16hrs time course. *AT1G72940* levels at 0hrs vary when compared to Col-0, but the differences are not statistically significant. At 16hrs, the transcript levels of *AT1G72940* are not increased in response to DEX treatment for any of the *promDEX::AT1G72940:HA:FLAG* lines or Col-0. The decrease in *AT1G72940* expression levels at 16h post-DEX is statistically significant for *promDEX::AT1G72940:HA:FLAG* line T_{1-3}, when compared to Col-0 at 0h; however, not when the expression is compared to Col-0 at 16h.

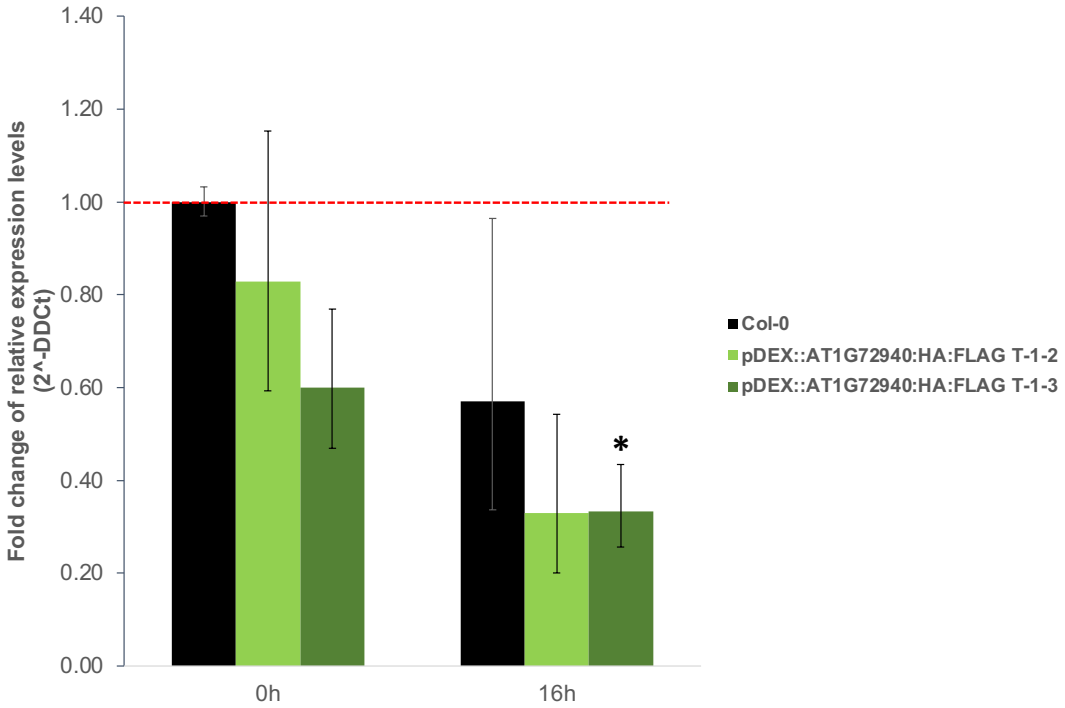

***Figure 4.11* Relative expression levels of *AT1G72940* in *A. thaliana promDEX::AT1G72940:HA:FLAG* transgenic lines post treatment with DEX.**

RT-qPCR was performed on rosette leaf number 8 of 5 to 6-weeks-old Col-0 and *promDEX::AT1G72940:HA:FLAG* lines $T_{1\text{-}2}$ and $T_{1\text{-}3}$ that were infiltrated with 30µM of DEX. Samples were collected at 0 and 16hrs following DEX treatment from 3 individual plants per line. The detected levels of *AT1G72940* were normalised against the housekeeping gene *a-tubulin*, and the relative expression levels are presented as fold change against the basal expression of *AT1G72940* in the Col-0 sample at 0h. Bar heights represent the average fold change in expression of *AT1G72940* gene for each line, calculated from 3 biological replicates. Error bars indicate the 95% confidence interval for the fold change of relative Ct values. One asterisk (*) indicates statistically significant difference to 5%; two asterisks (**) indicate statistically significant difference to 1%; three asterisks (***) indicate statistically significant difference to 0.1%. Due to small sample number, a two-tail t-test assuming unequal variances was selected for the statistical analysis. *AT1G72940* levels at 0hrs vary when compared to Col-0, but the differences are not statistically significant. At 16hrs, the transcript levels of *AT1G72940* are not increased in response to DEX treatment for any of the *promDEX::AT1G72940:HA:FLAG* lines or Col-0. The decrease in *AT1G72940* expression levels at 16h post-DEX is statistically significant for *promDEX::AT1G72940:HA:FLAG* line $T_{1\text{-}3}$, when compared to Col-0 at 0h; however, not when the expression is compared to Col-0 at 16h.

4.2.2 *Arabidopsis thaliana CRISPR-Cas9 TIR-NB locus deletion lines were tested for susceptibility phenotypes post infection with various Pst DC3000 strains*

Two lines of the CRISPR-Cas9 *TN* K.O. plants were previously selected for homozygosity of the *TN* locus deletion and kindly donated for the purposes of this thesis. The homozygosity of the lines was verified through genotyping PCR by the group of Prof. Murray Grant (University of Warwick, UK) before the start of this PhD project. According to the information given to the author, six genes were deleted from the *TN* locus using the CRISPR-Cas9 technology, including genes *AT1G72920, AT1G72930, AT1G72940*, and *AT1G72950*.

CRISPR-Cas9 *TN* K.O. lines 2 and 11 were challenged with *Pst* DC3000 to measure the bacterial growth and the maximum dark-adapted quantum efficiency of the PSII in response to bacterial infection, compared to WT Col-0 plants. As previously described in the **Materials and Methods** (**Sections 2.4.1** and **2.4.3**), all plants tested were grown for 5 to 6 weeks post germination. Rosette leaves number 7, 8 and 9 were identified and infiltrated with *Pst* DC3000 inoculum. Plants used for bacterial growth were infected with a lower bacterial O.D. (0.001), and the bacteria were allowed to incubate in the leaf apoplast for 3 days prior to isolation, bacterial growth, and colony count. Plants used for measuring the maximum dark-adapted quantum efficiency of PSII were inoculated with higher bacterial O.D. (0.15) and kept in the CF Imager for 24hrs. In addition, those plants included treatments with *Pst* DC3000 *hrpA* and mock ($MgCl_2$).

Figure 4.12 shows the results of the bacterial growth curves at 3DPI for Col-0 and CRISPR-Cas9 *TN* K.O. lines 2 and 11, when challenged with virulent *Pst* DC3000. Charts in **(A)** and **(B)** represent two biological replicates of the experiment with different outcomes. In **Figure 4.12.A** the *Pst* DC3000 colony count in Col-0 plants (black column) shows an average growth of 7.3 (log_{10} cfu/cm^2). Line 2 (light grey column) responds to *Pst* DC3000 similarly to Col-0, while line 11 (dark grey column) appears to be less susceptible to infection

than Col-0, with a colony count of ~6.5 (log_{10} cfu/cm^2), and that difference is statistically significant. However, these results were not reproduced in further experiments. **Figure 4.11 (B)** shows the representative bacterial growth for CRISPR-Cas9 *TN* K.O. #2 and #11, with both lines and Col-0 plants having the same average *Pst* DC3000 growth. The collective results of all the biological replicates performed during this PhD project showed that there is no difference in the response of CRISPR-Cas9 *TN* K.O. #2 and #11 to *Pst* DC3000 infection when compared to Col-0.

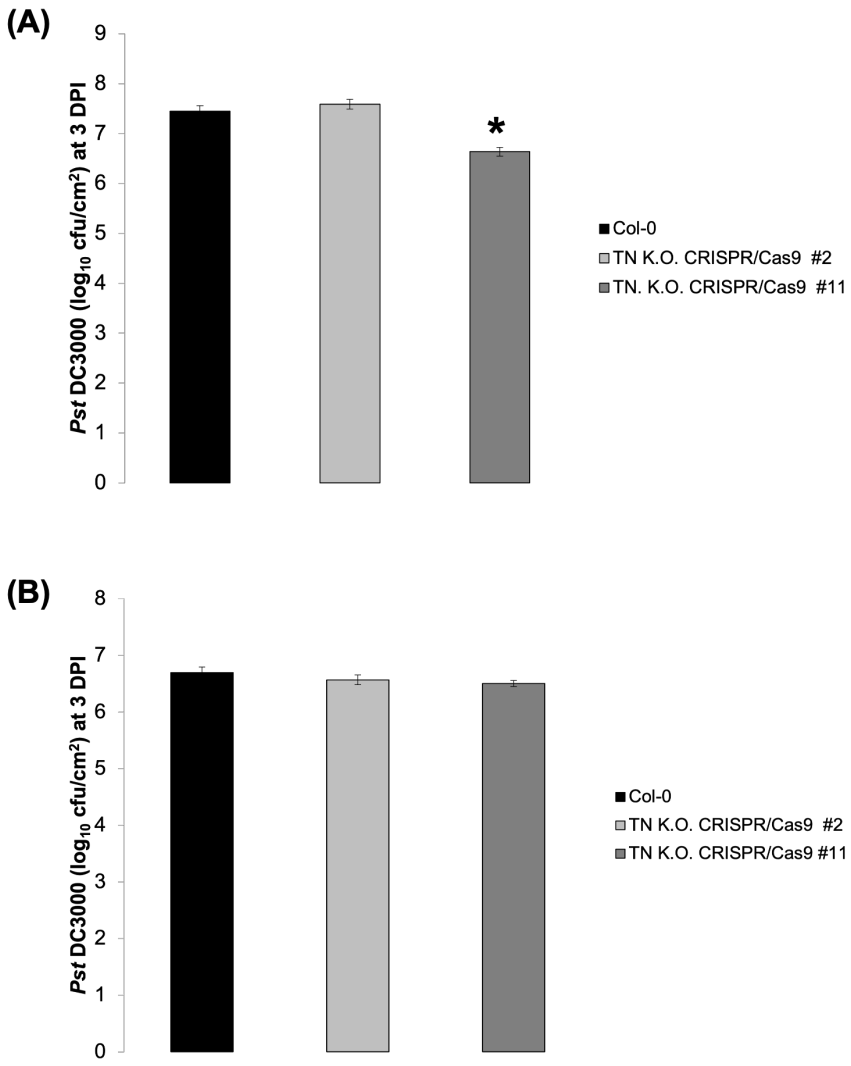

***Figure 4.12* Bacterial growth curves at 3DPI of *A. thaliana* CRISPR-Cas9 *TN* K.O lines 2 and 11 when challenged with virulent *Pst* DC3000.**

Pst DC3000 bacterial growth curves at 3DPI comparing colony counts between Col-0 and homozygous CRISPR-Cas9 *TN* K.O lines 2 and 11. Rosette leaves number 7, 8 and 9 of 5 to 6-weeks-old plants were infiltrated with *Pst* DC3000

(O.D.=0.001). Due to small sample number, a two-tail t-test assuming unequal variances was selected for the statistical analysis. One asterisk (*) indicates statistically significant difference to 5%. Charts in (A) and (B) represent two biological replicates of the experiment. (A) Col-0 plants (black) show an average *Pst* DC3000 growth of 7.3 (log_{10} cfu/cm^2) similar to CRISPR-Cas9 *TN* K.O #2 (light grey), while CRISPR-Cas9 *TN* K.O #11 (dark) shows a lower count of ~6.5. (B) Both Col-0 plants and CRISPR-Cas9 *TN* K.O #2 and #11 show an average *Pst* DC3000 growth of 6.7 (log_{10} cfu/cm^2). Bar heights represent the log10 of the average *Pst* DC3000 colony counts per cm^2 and the error bars the standard deviation, calculated from 6 plants/treatment.

Figure 4.13 presents the changes of F_v/F_m in treated Col-0 (green measurements) and CRISPR-Cas9 *TN* K.O line 11 (red measurements) rosette leaves when challenged with *Pst* DC3000. Different leaves were infiltrated with *Pst* DC3000 *hrpA* and mock (10mM of MgCl2). Images **(A)** to **(E)** show the photoinhibition of PSII (F_v/F_m) as recorded at 0, 1, 6, 12 and 24hrs, respectively. The chart in **Figure 4.13.F** presents the changes in F_v/F_m rate as recorded in the treated plants. *Pst* DC3000 *hrpA* and mock treatments are not expected to affect PSII, hence the F_v/F_m remains mostly stable for the duration of the experiment. Both Col-0 and CRISPR-Cas9 *TN* K.O line 11 when treated with *Pst* DC3000 show the same trend of photoinhibition (F_v/F_m=0.6), thus CRISPR-Cas9 *TN* K.O #11 does not respond different to Col-0 in terms of photoinhibition when infected with *Pst* DC3000.

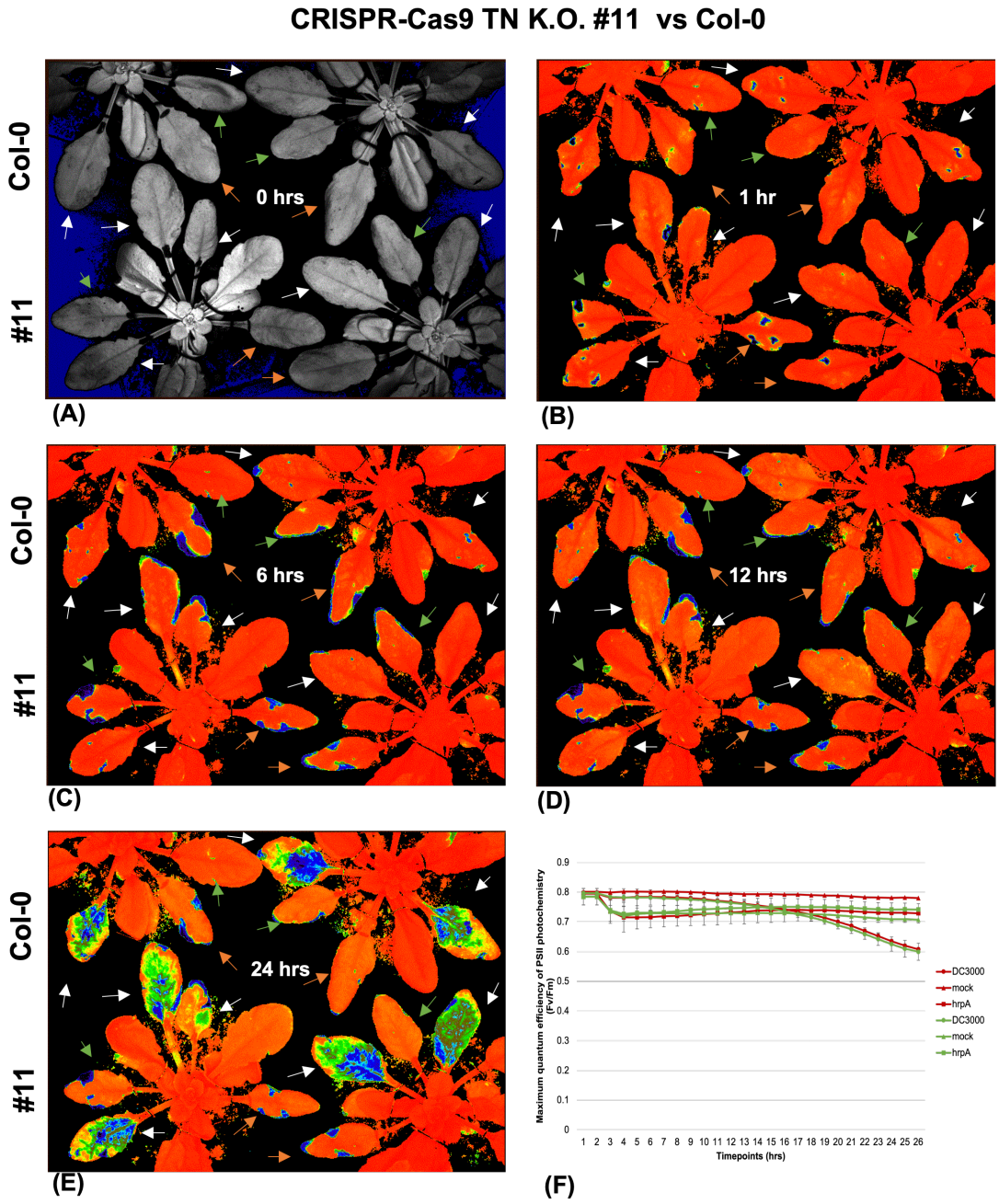

Figure 4.13 **Measuring the maximum quantum efficiency of the PSII photochemistry of *A. thaliana* CRISPR-Cas9 *TN* K.O line 11 post *Pst* DC3000 challenge.**

Rosette leaves of CRISPR-Cas9 *TN* K.O line 11 and Col-0 plants were infiltrated with either *Pst* DC3000, *Pst* DC3000 *hrpA* (O.D.=0.15) or mock (10mM of $MgCl_2$). Treated plants were dark-adapted inside a CF Imager for 1hr and then subjected to pulses of light for 24hrs while PSII chemistry fluorescence was recorded. Images **(A)** to **(E)** show the photoinhibition of PSII (F_v/F_m) as recorded at 0, 1, 6, 12 and 24hrs, respectively. Treated leaves are marked with different arrows: white for *Pst* DC3000, orange for *Pst* DC3000 *hrpA*, and green for mock. Charts present the changes in the maximum dark-

adapted quantum efficiency of PSII photochemistry (F_v/F_m) rate as recorded in the treated plants. Each data point represents the average F_v/F_m measurements and the bars the standard deviation, calculated from 3 leaves/treatment. **(F)** F_v/F_m rate of CRISPR-Cas9 *TN* K.O #11 against Col-0. Both Col-0 and CRISPR-Cas9 *TN* K.O #11 when treated with *Pst* DC3000 show the same trend of photoinhibition. Plants treated with *Pst* DC3000 *hrpA* and mock show a mostly stable F_v/F_m rate post-treatment.

Red: CRISPR-Cas9 *TN* K.O lines

Green: Col-0

∆ mock, , □ Pst DC3000 hrpA,○ Pst DC3000

The PSII photoinhibition of CRISPR-Cas9 *TN* K.O line 2 was also assessed upon *Pst* DC3000 infection with two independent experiments. **Figure 4.14** presents the changes of F_v/F_m in treated Col-0 (green measurements) and CRISPR-Cas9 *TN* K.O #2 (red measurements) rosette leaves when challenged with *Pst* DC3000. Images **(A)** to **(E)** show the photoinhibition of PSII (F_v/F_m) as recorded at 0, 1, 6, 12 and 24hrs, respectively. The chart in **Figure 4.14.F** presents the changes in F_v/F_m recorded in the treated plants. *Pst* DC3000 *hrpA* and mock treatments are not expected to affect PSII, hence the F_v/F_m remains mostly stable for the duration of the experiment. Both Col-0 and CRISPR-Cas9 *TN* K.O #2 when treated with *Pst* DC3000 show the same trend of photoinhibition (F_v/F_m=0.7), therefore CRISPR-Cas9 *TN* K.O #2 does not respond different to Col-0 in terms of photoinhibition when infected with *Pst* DC3000.

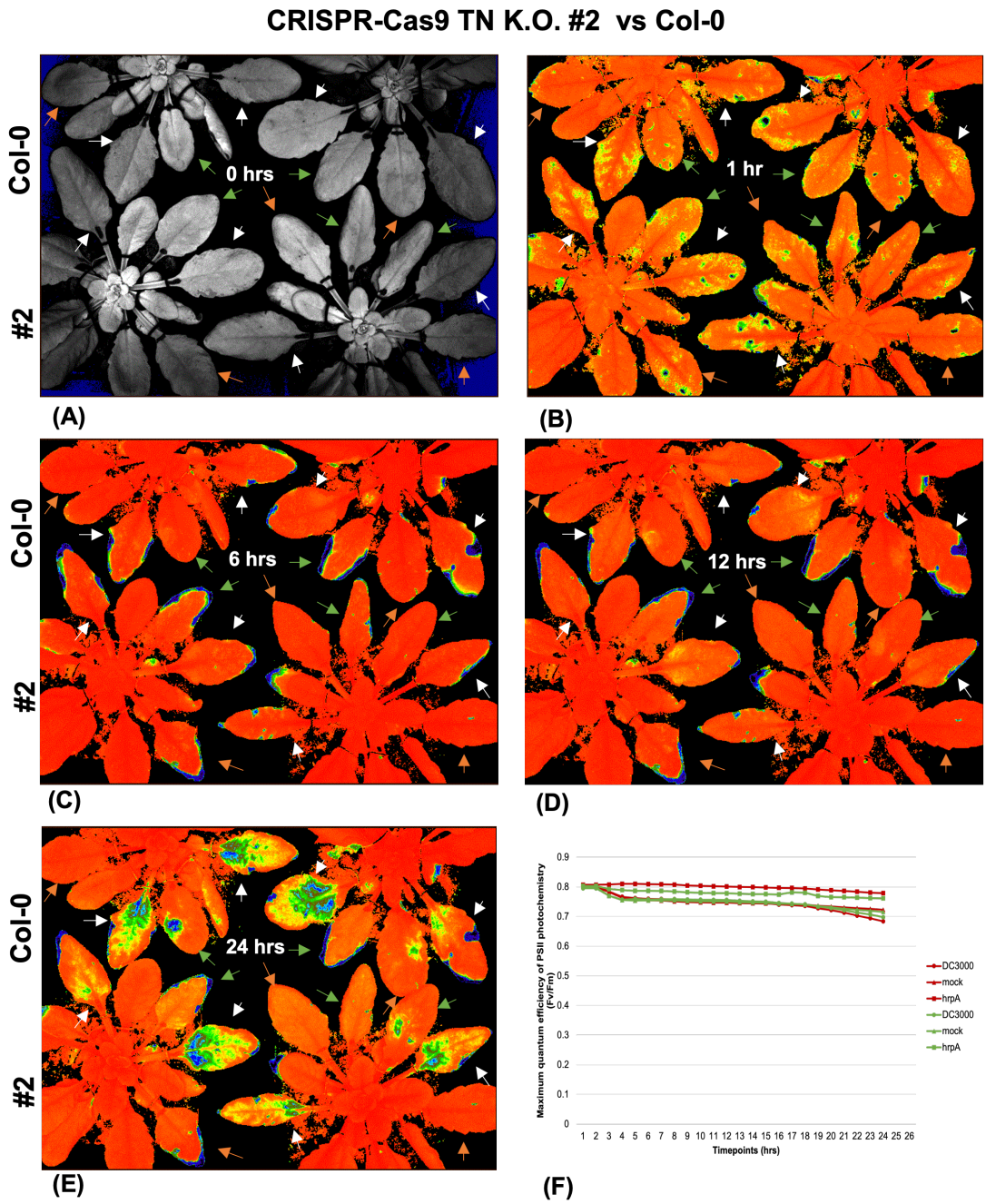

Figure 4.14 **Measuring the maximum quantum efficiency of the PSII photochemistry of *A. thaliana* CRISPR-Cas9 *TN* K.O line 2 post *Pst* DC3000 challenge – Biological replicate 1.**

Rosette leaves of CRISPR-Cas9 *TN* K.O line 2 and Col-0 plants were infiltrated with either *Pst* DC3000, *Pst* DC3000 *hrpA* (O.D.=0.15) or mock (10mM of $MgCl_2$). Treated plants were dark-adapted inside a CF Imager for 1hr and then subjected to pulses of light for 24hrs while PSII chemistry fluorescence was recorded. Images **(A)** to **(E)** show the photoinhibition of PSII (F_v/F_m) as recorded at 0, 1, 6, 12 and 24hrs, respectively. Treated leaves are marked with different arrows: white for *Pst* DC3000, orange for *Pst* DC3000 *hrpA*, and green for mock. Charts present the changes in the maximum dark-adapted quantum efficiency of PSII photochemistry (F_v/F_m) rate as recorded in the treated

plants. Each data point represents the average F_v/F_m measurements and the bars the standard deviation, calculated from 3 leaves/treatment. **(F)** F_v/F_m rate of CRISPR-Cas9 *TN* K.O #2 against Col-0. Both Col-0 and CRISPR-Cas9 *TN* K.O #2 when treated with *Pst* DC3000 show the same trend of photoinhibition. Plants treated with *Pst* DC3000 *hrpA* and mock show a mostly stable F_v/F_m rate post-treatment.

Red: CRISPR-Cas9 *TN* K.O lines

Green: Col-0

▵ mock, ☐ Pst DC3000 hrpA,○ Pst DC3000

Figure 4.15 presents the changes of F_v/F_m in treated Col-0 (green measurements) and CRISPR-Cas9 *TN* K.O #2 (red measurements) rosette leaves when challenged with *Pst* DC3000. Images **(A)** to **(E)** show the photoinhibition of PSII (F_v/F_m) as recorded at 0, 1, 6, 12 and 24hrs, respectively. The chart in **Figure 4.15.F** presents the changes in F_v/F_m recorded in the treated plants. Mock treatment is not expected to affect PSII, hence the F_v/F_m remains mostly stable for the duration of the experiment. Both Col-0 and CRISPR-Cas9 *TN* K.O #2 when treated with *Pst* DC3000 show the same trend of photoinhibition (F_v/F_m=0.65). Collectively, the results of both biological replicates show that CRISPR-Cas9 *TN* K.O #2 does not respond different to Col-0 in terms of photoinhibition when infected with *Pst* DC3000.

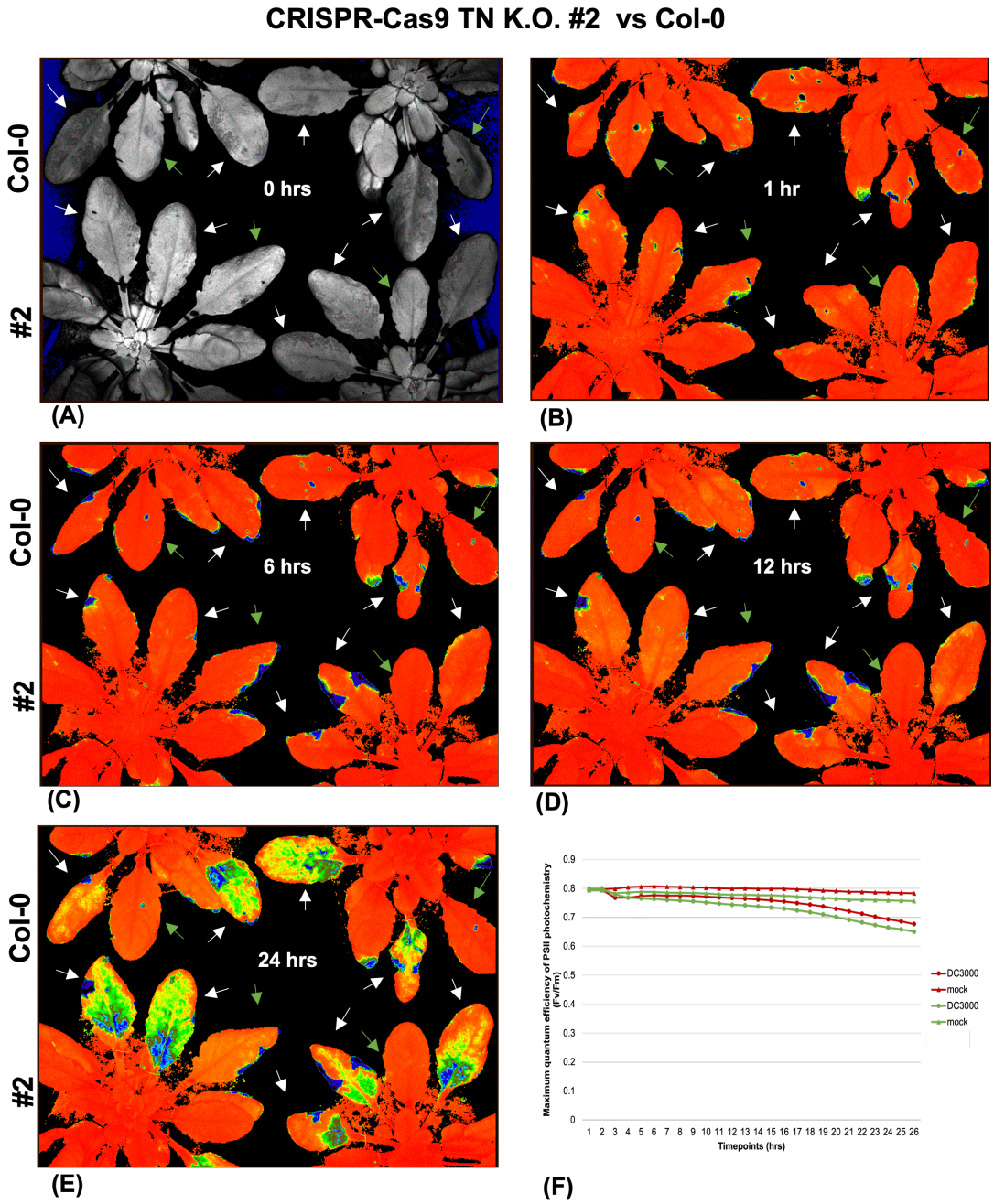

Figure 4.15 **Measuring the maximum quantum efficiency of the PSII photochemistry of *A. thaliana* CRISPR-Cas9 *TN* K.O line 2 post *Pst* DC3000 challenge – Biological replicate 2.**

Rosette leaves of CRISPR-Cas9 *TN* K.O line 2 and Col-0 plants were infiltrated with either *Pst* DC3000 or mock (10mM of $MgCl_2$). Treated plants were dark-adapted inside a CF Imager for 1hr and then subjected to pulses of light for 24hrs while PSII chemistry fluorescence was recorded. Images **(A)** to **(E)** show the photoinhibition of PSII (F_v/F_m) as recorded at 0, 1, 6, 12 and 24hrs, respectively. Treated leaves are marked with different arrows: white for *Pst* DC3000 and green for mock. Charts present the changes in the maximum dark-adapted quantum efficiency of PSII photochemistry (F_v/F_m) rate as

recorded in the treated plants. Each data point represents the average F_v/F_m measurements and the bars the standard deviation, calculated from 3 leaves/treatment. **(F)** F_v/F_m rate of CRISPR-Cas9 *TN* K.O #2 against Col-0. Both Col-0 and CRISPR-Cas9 *TN* K.O #2 when treated with *Pst* DC3000 show the same trend of photoinhibition. Plants treated with mock show a mostly stable F_v/F_m rate post-treatment.

Red: CRISPR-Cas9 *TN* K.O lines

Green: Col-0

∆ mock, ○ Pst DC3000

We further investigated the susceptibility of the knockout lines to infection using the available avirulent *Pst* DC3000 strains expressing effectors avrRPS4 and avrRPM1, both of which trigger ETI via well studied mechanisms. **Figure 4.16** presents the results of the bacterial growth curves for Col-0 and CRISPR-Cas9 *TN* K.O. lines 2 and 11, when challenged with different *Pst* DC3000 strains. In **Figure 4.16.A,** all plants were inoculated with virulent *Pst* DC3000 bacteria expressing an empty vector (EV) and avirulent *Pst* DC3000 bacteria expressing the effector avrRPS4. At 3DPI, the colony counts post *Pst* DC3000 EV treatment for both Col-0 and CRISPR-Cas9 *TN* K.O. lines show an average bacterial growth of 7.5 (log_{10} cfu/cm^2). When infected with *Pst* DC3000 avrRPS4, both Col-0 and CRISPR-Cas9 *TN* K.O. lines show an average bacterial growth of approximately 5.5 (log_{10} cfu/cm^2).

Similarly, in **Figure 4.16.B** plants were inoculated with virulent *Pst* DC3000 bacteria expressing an empty vector (EV) and avirulent *Pst* DC3000 bacteria expressing the effector avrRPM1. At 3DPI, when infected with *Pst* DC3000 EV both Col-0 and CRISPR-Cas9 *TN* K.O. lines show an average bacterial growth of 7.7 (log_{10} cfu/cm^2). *Pst* DC3000 avrRPM1 treatment for all plants resulted in an average bacterial growth of 5.5 (log_{10} cfu/cm^2). Finally, to identify a potential earlier response to infection, we tested Col-0 and CRISPR-Cas9 *TN* K.O. lines with avirulent *Pst* DC3000 avrRPM1 bacteria at 1, 2 and 3DPI. **Figure 4.16.C** shows that both CRISPR-Cas9 *TN* K.O. lines resulted in the same average bacterial growth to Col-0, for each respective day of sampling.

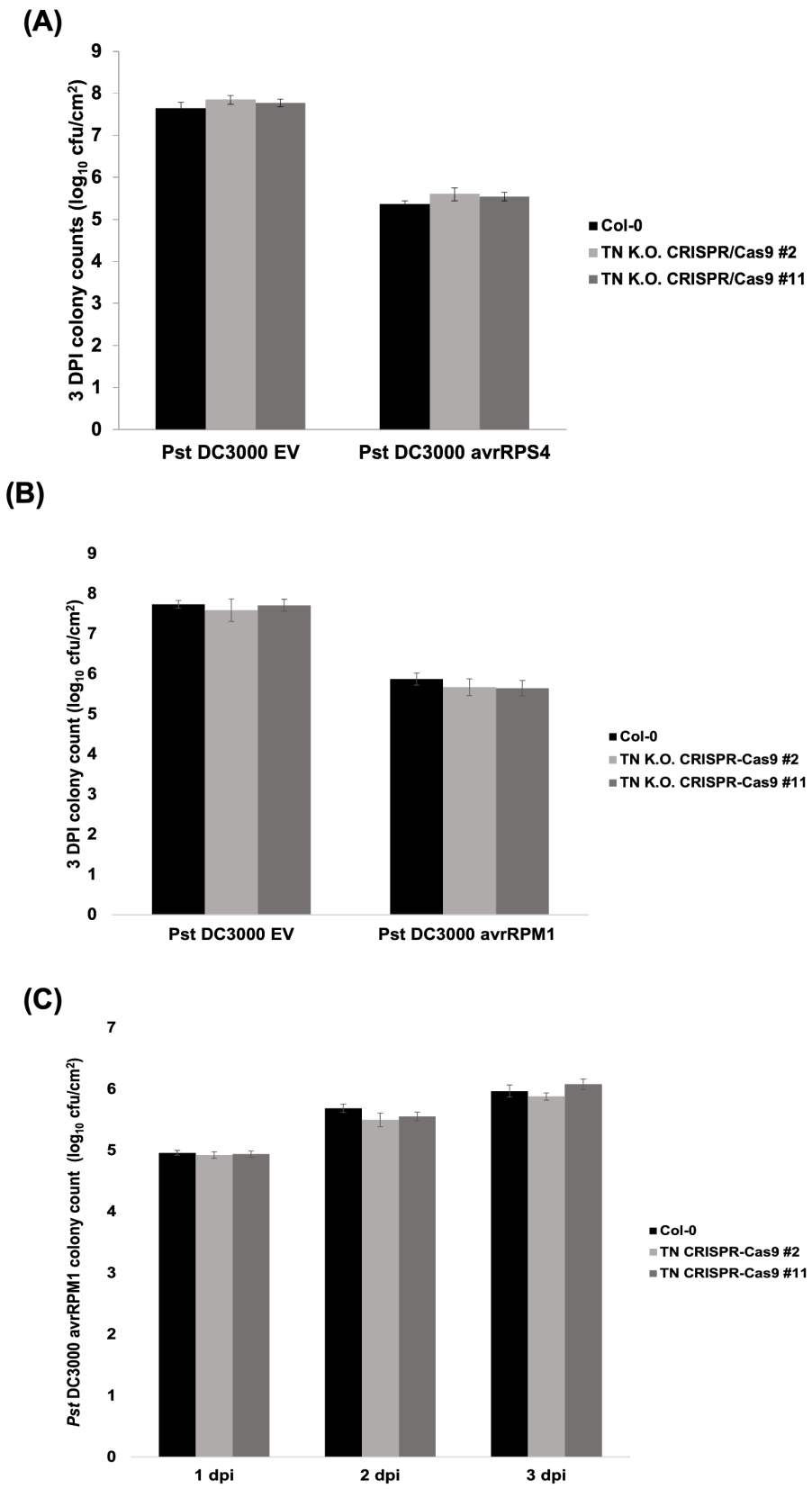

Figure 4.16 **Bacterial growth curves of *A. thaliana* CRISPR-Cas9 *TN* K.O lines 2 and 11 when challenged with different *Pst* DC3000 strains.**

Pst DC3000 bacterial colony counts between Col-0 and homozygous CRISPR-Cas9 *TN* K.O lines 2 and 11. Rosette leaves number 7, 8 and 9 of 5 to 6-weeks-

old plants were infiltrated with different *Pst* DC3000 strains (O.D.= 0.001). Due to small sample number, a two-tail t-test assuming unequal variances was selected for the statistical analysis. **(A)** Plants were inoculated with virulent *Pst* DC3000 bacteria expressing an empty vector (EV) and avirulent *Pst* DC3000 bacteria expressing the effector avrRPS4. At 3DPI, when infected with *Pst* DC3000 EV both Col-0 and CRISPR-Cas9 *TN* K.O lines show an average bacterial growth of 7.5 (log_{10} cfu/cm^2). When infected with *Pst* DC3000 avrRPS4, both Col-0 and CRISPR-Cas9 *TN* K.O lines show an average bacterial growth of 5.5 (log_{10} cfu/cm^2). **(B)** Plants were inoculated with virulent *Pst* DC3000 bacteria expressing an empty vector (EV) and avirulent *Pst* DC3000 bacteria expressing the effector avrRPM1. At 3DPI, when infected with *Pst* DC3000 EV both Col-0 and CRISPR-Cas9 *TN* K.O lines show an average bacterial growth of 7.7 (log_{10} cfu/cm^2). When infected with *Pst* DC3000 avrRPM1, both Col-0 and CRISPR-Cas9 *TN* K.O lines show an average bacterial growth of 5.5 (log_{10} cfu/cm^2). **(C)** Plants were inoculated with avirulent *Pst* DC3000 avrRPM1. Bacteria were harvested at 1, 2 and 3DPI. Both Col-0 and CRISPR-Cas9 *TN* K.O lines showed the same average bacterial growth for each respective day of sampling. Bar heights represent the log10 of the average *Pst* DC3000 colony counts per cm^2 and the error bars the standard deviation, calculated from 6 plants/treatment.

To summarise, CRISPR-Cas9 *TN* K.O. lines 2 and 11 show approximately the same bacterial colony counts as Col-0, when infected with *Pst* DC3000 (EV), *Pst* DC3000 avrRPS4, and *Pst* DC3000 avrRPM1, meaning that the knockout mutant is neither more susceptible nor more resistant to said *Pst* strains than the wild type plants. A two-tail t-test assuming unequal variances verified that any observed differences in the bacterial growth between Col-0 and the CRISPR-Cas9 *TN* K.O. lines 2 and 11, are not statistically significant for any of the *Pst* DC3000 strains.

4.3 Discussion

This Chapter presented the results of testing *Pst DC3000* infection on the dexamethasone-inducible overexpressing *promDEX::AT1G72940* and *promDEX::AT1G72940:HA:FLAG* stable transgenic *A. thaliana* lines, as well as the *CRISPR-Cas9 TN* locus homozygous knockout lines, in order to detect if overexpression of *AT1G72940* or deletion of the *TN* locus affected the outcome. Both knockout and inducible overexpressing plants were challenged with various strains of the pathogenic *Pst DC3000* bacteria and their response to infection was measured against the wild type *A. thaliana* Col-0 plants via bacterial growth colony counts and measuring the maximum dark-adapted quantum efficiency of PSII photochemistry. Finally, the DEX-inducible overexpressing *promDEX::AT1G72940* and *promDEX::AT1G72940:HA:FLAG* lines were assessed for the relative expression of *AT1G72940* before and after induction with dexamethasone via RT-q-PCR.

When *promDEX::AT1G72940* lines $T_{1\text{-}1,}$ $T_{2\text{-}3,}$ $T_{3\text{-}2}$ and $T_{4\text{-}2}$ were treated with dexamethasone and infected with *Pst DC3000* to measure the bacterial growth against Col-0, the collective results of colony counts at 3DPI for all lines are similar to Col-0; any detected differences where not found to be statistically significant and if they were, the results were not reproduced in other biological replicates of the experiment. When assessing the response of *promDEX::AT1G72940* lines to *Pst* DC3000 as recorded by the impact of infection to PSII photoinhibition (F_v/F_m), the collective results showed that treatment with DEX does not affect differently the suppression of PSII in any of the tested lines when those are challenged with *Pst* DC3000, in comparison to plants not treated with DEX and Col-0 in the same conditions. Any differences recorded in individual experiments were in most cases minor and not reproducible in the biological replicates. Those findings suggest that if DEX induces the overexpression of *AT1G72940* in the tested *promDEX::AT1G72940* lines, protein AT1G72940 does not have a detectable

impact to the plant's response to virulent *Pst* DC3000 infection, as the transgenic plants behave similarly to the WT Col-0 plants.

Similarly, *promDEX::AT1G72940:HA:FLAG* lines $T_{1\text{-}2}$ and $T_{1\text{-}3}$ were assessed for their response to *Pst* DC3000 as recorded by the impact of infection to PSII photoinhibition (F_v/F_m). The results showed that DEX treatment does not affect differently the suppression of PSII in *promDEX::AT1G72940:HA:FLAG* plants when those are challenged with *Pst* DC3000, in comparison to plants not treated with DEX and Col-0 in the same conditions.

The lack of recorded differences in the response between DEX-induced stable transgenic plants of *promDEX::AT1G72940* and *promDEX::AT1G72940:HA:FLAG* lines and WT Col-0 plants, when challenged with *Pst* DC3000, suggested that the inducible transgenic lines may not respond to dexamethasone. We addressed this hypothesis by measuring the relative expression levels of *AT1G72940* in the inducible overexpressing transgenic plants before and after DEX treatment, in comparison to the basal gene expression of Col-0. In a time course of 6 and 12hrs post induction for *promDEX::AT1G72940* lines and 16hrs post induction for *promDEX::AT1G72940:HA:FLAG* lines, RT-q-PCR showed that there is no increase in the detected *AT1G72940* transcript levels between the treated and untreated transgenic plants and Col-0. Therefore, it was concluded that these plants are not induced by dexamethasone.

The RT-q-PCR findings suggest that the T3 generation of *promDEX::AT1G72940* lines $T_{1\text{-}1,}$ $T_{2\text{-}3,}$ $T_{3\text{-}2}$ and $T_{4\text{-}2}$, as well as *promDEX::AT1G72940:HA:FLAG* lines $T_{1\text{-}2}$ and $T_{1\text{-}3}$ do not respond to dexamethasone treatment. Those results are in line with the findings of bacterial growth and PSII photoinhibition experiments presented in this chapter, as the lack of successful DEX induction is expected to result in the *promDEX::AT1G72940* and *promDEX::AT1G72940:HA:FLAG* transgenic plants behaving as WT Col-0 plants.

As previously described in **Section 4.1**, the dexamethasone inducible system is based in two components: the first component that controls the overexpression of the chimeric GVG transcription factor under *prom35S CaMV*, and the second component that contains the GVG binding sites flanked by a minimal *prom35S CaMV* to control the overexpression of the gene of interest (Aoyama and Chua, 1997). The chimeric GVG transcription factor can activate the transcription of the gene of interest by binding on the promoter driving its expression only after induction with the glucocorticoid dexamethasone. The GVG inducible system has been widely used in the study of effector proteins from plant pathogens, thus allowing for controlled *in planta* expression of effectors whose constitutive expression would be otherwise toxic or lethal for the plant (Geng and Mackey, 2011). One example is the DEX-inducible expression of AvrRPM1 T3SS effector of *Pst DC3000* in *A. thaliana* Col-0 plants (Al-Daoude et al., 2005; Andersson et al., 2006; Kim et al., 2009, 2005; Kourtchenko et al., 2007; Mackey et al., 2003, 2002; Nimchuk et al., 2000). The induction of AvrRPM1 in transgenic *promDEX:AvrRPM1-HA* Col-0 plants induces rapid and strong cell death, similar to HR caused by *Pst DC3000* bacteria expressing AvrRPM1. However, when working with GVG transgenic lines, potential silencing of the GVG system must be taken into consideration.

Silencing of the GVG inducible system is one of the most serious issues encountered in stably transgenic dexamethasone-inducible plants (Geng and Mackey, 2011). It is often observed that the inducible transgene is successfully expressed in the T1 or T2 generations of some transgenic lines, but its expression is silenced in the following generations. Silencing of GVG system has been often correlated to the presence of other transgenes driven by *prom35S CaMV* in the same lines (Geng and Mackey, 2011). It is still unclear how this silencing occurs, but one possible cause suggested is post-transcriptional silencing deriving by the presence of more than one transgene driven by *prom35S CaMV.* However, assuming that the original (or a modified version) *pTA7001* vector described by Aoyama and Chua (1997) was used for the generation of *promDEX::AT1G72940* and

promDEX::AT1G72940:HA:FLAG transgenic plants, then we can not safely attribute GVG silencing to the presence of another *prom35S CaMV.*

Different factors can contribute to the silencing of GVG system. For example, high transcriptional levels of the GVG TF can lead to post-transcriptional gene silencing (PTGS) (Schubert et al., 2004) or non-specific binding, which either leads to the inactivation of the system or can cause strong developmental effects to *A. thaliana* and other plants (Amirsadeghi et al., 2007; Andersen et al., 2003; Kang et al., 1999; Ouwerkerk et al., 2001). RNA silencing has been reported in cases that the transcript levels of a transgene exceed a threshold specific for each gene (Schubert et al., 2004). Silencing due to excessive transcript levels is responsible for transgene expression variability observed among lines deriving from different transformation events. Therefore, the RNA sensing mechanism eliminates RNA corresponding to excessively transcribed genes, including transgenes, as a defence mechanism.

Despite the fact that we did not observe any developmental effects in the transgenic *promDEX::AT1G72940* and *promDEX::AT1G72940:HA:FLAG* lines, post-transcriptional gene silencing due to high GVG expression levels is one possibility to consider. Additionally, since the GVG system has been extensively used in our lab, we cannot exclude the possibility of mutations occurring in either component of the dual system during plasmid replication. It is possible that one or more mutations occurring in the GVG transcriptional unit could halt the production of GVG or result in a mutated version that is not activated by dexamethasone. Similarly, mutations occurring in the GVG binding site on the second transcriptional unit could potentially prevent the activation of our gene of interest.

Regarding the CRISPR-Cas9 knockout lines of the TN locus containing our genes of interest, when lines 2 and 11 were infected with *Pst DC3000* to measure the bacterial growth against Col-0, the collective results of colony counts at 3DPI for both CRISPR-Cas9 *TN* K.O. lines 2 and 11 are similar to Col-0. Furthermore, when the same lines were assessed for their response to *Pst* DC3000 as recorded by the impact of infection to PSII photoinhibition

(F_v/F_m), the results showed that the absence of *TN* genetic locus does not affect differently the suppression of PSII in either line when those are challenged with *Pst* DC3000, in comparison to the WT Col-0 plants in the same conditions. However, the results also suggest that the *Pst* DC3000 infection was not entirely successful in some of the occasions, hence a repetition of the experiment is required before we draw any conclusions.

However, since we confirmed in **Chapter 3** that the expression of *TN* genes is triggered post *Pst* DC3000 infection and appears to be correlated to the delivery of specific *Pst* DC3000 effector proteins, we decided to further investigate the susceptibility of the knockout lines to infection using the available avirulent *Pst* DC3000 strains expressing effectors AvrRPS4 and AvrRPM1. The results of the bacterial growth at 3DPI showed that no significant difference is observed in the response of CRISPR-Cas9 *TN* K.O. lines compared to Col-0 when infected with either the avirulent *Pst* DC3000 avrRPS4 or *Pst* DC3000 avrRPM1. Both lines were further tested for bacterial growth colony counts at 1, 2 and 3DPI against Col-0, when challenged with *Pst* DC3000 avrRPM1. Our findings showed that CRISPR-Cas9 *TN* K.O. and Col-0 plants show the same response to *Pst* DC3000 avrRPM1 as recorded at each individual day for the duration of infection.

Collectively, our findings indicate that there is no significant difference detected in terms of susceptibility to infection between the CRISPR-Cas9 *TN* K.O lines 2 and 11 and Col-0, when those are challenged with either virulent *Pst* DC3000 or the avirulent strains *Pst* DC3000 avrRPS4 and *Pst* DC3000 avrRPM1. Taking these results into account, we hypothesized that the absence of the *TN* genetic locus from *A. thaliana* may be redundant regarding defence responses of the plant to pathogenic bacteria.

Studies from different model organisms give a broader definition of what is considered genetic redundancy. Some examples include genes that derived from convergent evolution encoding enzymes with the same function (Pickett and Meeks-Wagner, 1995), redundant biochemical pathways due to interconnected metabolic networks (Weintraub, 1993), and genes from the

same family (paralogs) that maintain a level of similar functionality (Kempin et al., 1995). Genetic redundancy recently is mostly referring to the latter definition, where multiple copies of a gene with overlapping functions derive from a duplication event. Plants have a high rate of whole genome duplication events, although most duplicates end up with loss of function (pseudogenes) (Panchy et al., 2016). Duplicates can survive selection for extended periods of time due to slow genetic drift (Panchy et al., 2016), or they are retained through neo-functionalization due to a new, adaptive function and/or selection on existing functions through gene dosage increase (Ohno, 1970).

Regarding our *TN* genes of interest (*AT1G72920, AT1G72930, AT1G72940*, and *AT1G72950*), a study on the origin of *TN* and *TX* genes by Meyers et al. (2002) examined their genomic context and phylogenetic relationships. They found complex clusters of *TN* and *TX* genes and *TNL* genes that were duplicated to multiple locations in the genome. Although the reason for the mixed clusters and conserved duplications of *TN*, *TX*, and *TNL* genes is unclear, it is hypothesized that selection keeps alleles of those two types of genes together as functional unit (Meyers et al., 2002). Furthermore, their findings suggest that some of the most closely related in sequence context genes have different expression patterns. They found that genes *AT1G72930* and *AT1G72940* are most closely related to nearby genes *AT1G72910* and *AT1G72920,* which is likely attributed to a recent genomic duplication event. However, they identified a poor gene expression for genes *AT1G72910* and *AT1G72920,* while *AT1G72930* and *AT1G72940* were expressed in most of the tested libraries. They suggest that different expression patterns in recently duplicated genes may indicate divergent functions, or a loss of function of these genes due to relaxed selection of the duplicated copies (Meyers et al., 2002).

Our CRISPR-Cas9 knockout lines cover only 6 genes of the respective *TN* locus, including genes *AT1G72910, AT1G72920, AT1G72930, AT1G72940*, and *AT1G72950.* Nevertheless, as presented in **Figure 1.7** (Meyers et al., 2002) this *TN* locus is a cluster of several *TN* and some *TNL* genes arranged in different orientations. Even though our *TN* genes of interest are completely

removed from the locus, the possibility that the arrangement of these gene clusters is favoured by selection to retain functionality suggests that partial removal of the *TN* locus may not result to a detectable phenotype. Thus, we cannot safely exclude the possibility that the function of our *TN* genes of interest is not partially or fully replaced by the function of other genes in the same locus. We can consider the possibility that multiple copies of *TN* genes with similar function are employed by the plant to enhance its defence against *Pst* DC3000 infection, but in cases where the expression of those genes is silenced the impact may not be detectable. One more possibility to consider is that the *Pst* DC3000 strains tested were not suitable to reveal the part of our *TN* genes of interest to immunity and a different approach should instead be followed.

5. Generation of new *TN* constitutively expressing *A. thaliana* lines and their characterisation.

5.1 Introduction

In Chapter 4 we analysed and presented the results of *Pst* DC3000 infection on two different sets of *A. thaliana* plants transformed with the *AT1G72940* transgene under the regulation of a dexamethasone-inducible promoter. Our findings suggested that the glucocorticoid DEX is not efficiently inducing the expression of *AT1G72940* in neither of the tested sets of transgenic plants, thus compromising the outcome of any experimental procedures aim to assess the role of AT1G72940 protein in the plant's defence response to pathogenic *Pst* DC3000 infection. Moreover, the CRISPR-Cas9 *TN* K.O. lines did not respond differently than WT Col-0 plants when challenged with various strains of *Pst* DC3000, suggesting that the sole absence of the *TN* genetic locus does not have a significant visible impact to *A. thaliana*'s susceptibility against *Pst* DC3000 bacterial infection.

Along with the fact that the knockout lines did not successfully provide new information regarding the role of *TN* genes in plant immunity, the lack of functional overexpression *TN* lines did not allow for any safe conclusions to be drawn on the matter. Therefore, new stable transgenic *A. thaliana* plants facilitating the overexpression of the *TN* genes of interest were generated. Taking into account the previously published work on *TN* genes (Nandety et al., 2013), the creation of both constitutively overexpressing and inducible overexpressing lines was deemed necessary. In addition, to overcome potential issues arising by the DEX inducible system, the use of both DEX and estradiol (ESTR) inducible systems was employed.

In this Chapter the necessary tools for the generation of functional *A. thaliana* TN transgenic plants are presented, as well as the selection of homozygous lines when possible. All overexpressing lines selected for immunity experiments in this Chapter are assessed with RT-q-PCR to verify elevated transcript levels and immunoblotting to verify the presence and overexpression of the respective protein. Due to time limitations, only preliminary results of bacterial growth experiments of the selected transgenic *TN* lines when challenged with *Pst* DC3000 are presented.

5.2 Results

5.2.1 Creating the tools for the generation of new A. thaliana TN transgenic plants for constitutive and inducible overexpression and selection of homozygous lines

The initial plan was to utilise the technology of the Golden Gate assembly, as well as the available modules supplied in the MoClo Plant Tool Kit and the GG Plant Parts Kit (Engler et al., 2014, 2012), to create a variety of L2 vectors containing T-DNAs of the *TN* genes of interest (*AT1G72920, AT1G72930, AT1G72940*, and *AT1G72950*) under the regulation of different promoters and with a combination of different protein tags. However, due to technical complications and time limitations, only genes *AT1G72940* and *AT1G72950* made it to L2 constructs. **Table 5.1** lists the different combinations of promoters, genes, and tags used to generate the T-DNA vectors for this PhD project.

The creation of the tools used to generate the new *A. thaliana TN* transgenic plants for constitutive and inducible overexpression has been previously described in detail in **Section 2.5.3.3** of the **Materials and Methods**. The *TN* genes were amplified for Golden Gate assembly using as template the recombinant plasmid vectors donated by Prof. Murray Grant (see plasmids No. 15-18, **Table 2.3**). Those constructs were generated and used by the Grant group to create the DEX inducible *A. thaliana TN* lines analysed in **Chapter 4** of this thesis, and they contain GG domesticated sequences of each *TN* gene.

Table 5.1 **List of T-DNA constructs of *TN* genes planned for Golden Gate assembly to create *A. thaliana TN* transgenic plants for constitutive and inducible overexpression.**

Each L2 construct contains the following transcriptional units between the left and right T-DNA borders, for the respective gene: 1) *promoter::TNgene:tag*. Promoters used were the constitutive *prom35S CaMV*, and the inducible *promDEX* (dexamethasone) and *promESTR* (estradiol). C′ terminal protein tags used were GFP, 6 repeats of HA (6HA), and 3 repeats of FLAG (3FLAG). Transcriptional units for each *TN* gene were generated with all possible combinations among promoters and tags; 2) pFAST-R plant selection cassette; 3) GVG or LexA transactivators, for DEX-inducible or ESTR-inducible systems, respectively.

Final GG Level 2 (T-DNA) constructs
AT1G72940
prom35S::AT1G72940:GFP/pICSL4723[pFAST-R]
prom35S::AT1G72940:6HA/pICSL4723[pFAST-R]
prom35S::AT1G72940:3FLAG/pICSL4723[pFAST-R]
promDEX::AT1G72940:GFP/pICSL4723[pFAST-R + GVG]
promDEX::AT1G72940:6HA/pICSL4723[pFAST-R + GVG]
promDEX::AT1G72940:3FLAG/pICSL47232[pFAST-R +GVG]
promESTR::AT1G72940:GFP/pICSL4723[pFAST-R + LexA]
promESTR::AT1G72940:6HA/pICSL4723[pFAST-R + LexA]
promESTR::AT1G72940:3FLAG/pICSL4723[pFAST-R + LexA]
AT1G72950
prom35S::AT1G72950:GFP/pICSL4723[pFAST-R]
prom35S::AT1G72950:6HA/pICSL4723[pFAST-R]
prom35S::AT1G72950:3FLAG/pICSL4723[pFAST-R]
promDEX::AT1G72950:GFP/pICSL4723[pFAST-R + GVG]
promDEX::AT1G72950:6HA/pICSL4723[pFAST-R + GVG]
promDEX::AT1G72950:3FLAG/pICSL47232[pFAST-R +GVG]
promESTR::AT1G72950:GFP/pICSL4723[pFAST-R + LexA]
promESTR::AT1G72950:6HA/pICSL4723[pFAST-R + LexA]
promESTR::AT1G72950:3FLAG/pICSL4723[pFAST-R + LexA]

The L0 assembly reactions for genes *AT1G72920* and *AT1G72930* never had a successful outcome, even after several attempts and optimisation steps and despite the fact that the initial amplification from the pre-existing constructs was successful. Gene *AT1G72920* was one of the priorities for this PhD project, together with *AT1G72940*, as they are both induced significantly in response to *Pst* DC3000 infection (see **Figure 3.4**) and both their promoters are bound by the TF ERF6 (Mine et al., 2018), which is likely activated during ETI by MPK3 and MPK6. However, gene *AT1G72920* underwent multiple subcloning attempts but was not successfully introduced into the L0 vector *pAGM1287*. Collectively, more than 100 colonies were screened through colonies PCR to identify a recombinant *AT1G72920* clone. Two colonies that showed a PCR product were sequenced and proven to bear multiple point mutations and/or lacking the full gene sequence. Furthermore, they suggested the presence of genomic sequence instead of CDS. The creation of *AT1G72920* T-DNA vectors was not further pursued due to the inability of generating a L0 *AT1G72920* recombinant vector that would allow for Golden Gate assembly. Likewise, the subcloning of gene *AT1G72930* into *pAGM1287* failed to produce successful recombinant L0 clones, thus it was not further attempted.

Figure 5.1 shows the PCR products resulting from the amplification of *TN* genes of interest from the recombinant plasmid vectors containing the respective subcloned sequences that had been domesticated for Golden Gate assembly. *A. thaliana* genes *AT1G72920, AT1G72930, AT1G72940* and *AT1G72950* were amplified using primer pairs VN989/VN990, VN991/VN992, VN993/VN994, and VN995/VN996, respectively. All primer pairs introduce the appropriate recognition sites for GG cloning, flanking either ends of the *TN* genes, to create “CDS1 no-stop” modules to meet the specifications of the MoClo Plant Tool Kit for 5’ promoter fusion and 3’ protein tag fusions. When the PCR-amplified products were analysed with agarose gel electrophoresis, the MWs of the respective bands showed that the original recombinant plasmids likely contain the CDS of genes *AT1G72920* (830 bp), *AT1G72930* (530 bp) and *AT1G72940* (1,140 bp), and the genomic sequence of gene

AT1G72950 (1,583 bp). The PCR products were then subcloned into the Level-0 Acceptor *pAGM1287* through BpiI digestion and T4 Ligation.

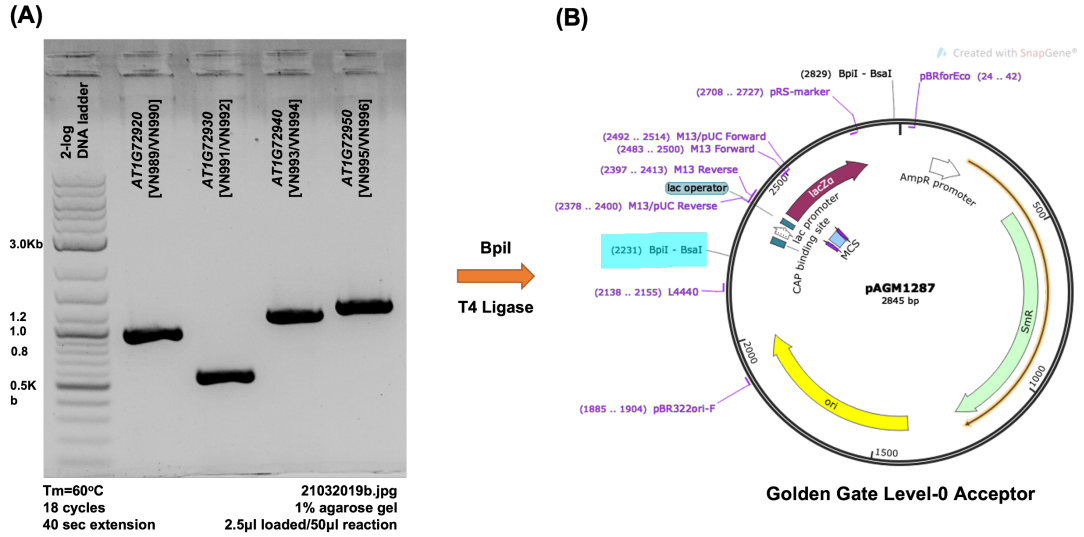

***Figure 5.1* Amplification of *A. thaliana TN* genes *AT1G72920, AT1G72930, AT1G72940* and *AT1G72950* and subcloning into the Golden Gate Level-0 Acceptor vector *pAGM1287*.**

The *A. thaliana TN* genes of interest were PCR-amplified from previously made recombinant plasmid vectors, where the subcloned sequences have been domesticated for Golden Gate assembly. Genes *AT1G72920, AT1G72930, AT1G72940* and *AT1G72950* were amplified using primer pairs VN989/VN990, VN991/VN992, VN993/VN994, and VN995/VN996, respectively. All primer pairs used were designed to introduce the appropriate recognition sites for GG cloning. (A) The PCR products were run in agarose gel electrophoresis to verify product specificity and the respective molecular weights. (B)The PCR products were cleaned, digested with BpiI, and ligated into BpiI site of the *pAGM1287* L0 vector (highlighted in turquoise). Level-0 recombinant vectors confer resistance to Spectinomycin, and recombinant colonies can be identified with Xgal/IPTG blue/white selection.

The subcloning of gene *AT1G72950* into the *pAGM1287* L0 Acceptor produced recombinant *AT1G72950/pAGM1287* vectors and the presence of the genomic sequence of *AT1G72950* was verified with sequencing. Sequencing of *AT1G72950/pAGM1287* colonies with Level-0 primers (see **Table 2.10**) showed that the original construct (*pTA70002-GG/promDEX::AT1G72950*, **Table 2.3**) contained the genomic sequence of

AT1G72950 and it is seemingly fine, although the sequencing did not cover the full length of the gene.

The assembly and selection of L1 and L2 clones followed the same procedure as for gene *AT1G72940,* which will be described later on this section. However, sequencing of L1 and L2 recombinant vectors revealed the presence of an additional codon (TTC) at the 3' end of *AT1G72950* sequence, prior to the GG fusion site between the gene and the 3' tag. The extra codon does not affect the open reading frame between the two parts; however, it will code for an additional amino acid that is not naturally present in the WT AT1G72950 protein. The creation of L1 and L2 modules preceded the full sequence analysis, hence most of the L2 T-DNA vectors are available for future use. However, the creation of *A. thaliana* stable transgenic *AT1G72950* overexpression lines was postponed for future project work, as it was not deemed a priority at the time, given the limited time and the low *AT1G72950* expression levels detected in the RT-q-PCR post-*Pst* DC3000 infection (see **Figure 3.4**).

Gene *AT1G72940* was successfully introduced into the *pAGM1287* L0 Acceptor. Sequencing of several *AT1G72940/pAGM1287* colonies revealed that the original construct (*pTA70002-GG/promDEX::AT1G72940,* **Table 2.3**) contained the CDS of *AT1G72940*, however it carried a non-silent point mutation that would cause an amino acid change (leucine to phenylalanine) at the N-terminal of the predicted protein. The PCR-amplification and subcloning of *AT1G72940* into *pAGM1287* was modified and repeated and the newly produced clones were also sequenced. The sequencing results showed the mutation is neither a domestication result nor a result of the recent PCR amplification, as it appears in all the clones and different PCR conditions tested for *AT1G72940*, suggesting that it pre-existed in the template clone.

The results of site-directed mutagenesis performed on the *AT1G72940/pAGM1287* clone to invert the point mutation back into Leucine-coding triplet are presented in **Figure 5.2.** Three different pairs of mutagenesis primers were designed and tested for their efficiency on plasmid

AT1G72940/pAGM1287 (**Figure 5.2.A**). Pairs VN1068/VN1069 and VN1066/VN1067 successfully amplified the whole *AT1G72940/pAGM1287* recombinant vector. The PCR products were digested with DpnI to eliminate the template plasmid and then transformed into *E. coli* competent cells to propagate. Colonies PCR verifying the presence of *AT1G72940* was performed in the resulted recombinant clones (**Figure 5.2.B)**. Ten different colonies (marked in red) were selected and sequenced to identify the clones with the inverted mutation, and seven out of ten had successfully inverted the mutation. Clone *AT1G72940/pAGM1287* #1 was selected for the assembly of *AT1G72940* into Level-1 transcriptional units.

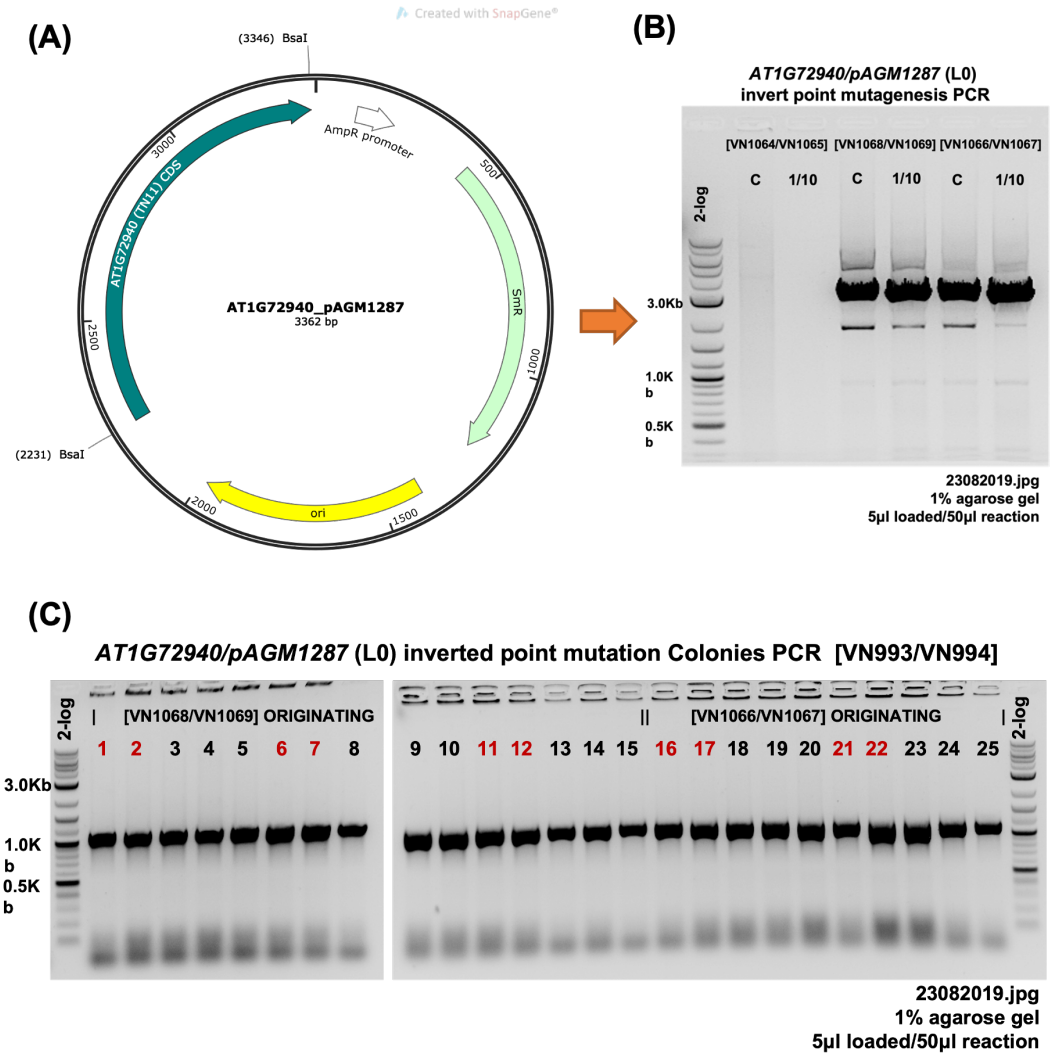

Figure 5.2 **Site-directed mutagenesis of *AT1G72940/pAGM1287* aiming to invert the point mutation carried over from the template clones.**

Site-directed mutagenesis was applied to *AT1G72940/pAGM1287* recombinant vector to invert the mutation result**ing** to an amino acid change in the putative AT1G72940 protein, converting Leucine into Phenylalanine. **(A)** *pAGM1287* vector containing the mutated *AT1G72940***. (B)** Testing of three different sets of primer pairs used to invert the point mutation back to the WT codon, by amplification of the whole mutated *AT1G72940/pAGM1287* vector. The PCR products of pairs VN1068/VN1069 and VN1066/VN1067 were digested with DpnI to eliminate the template plasmid and then transformed into *E. coli* competent cells to propagate. **(C)** Colonies PCR to identify the presence of *AT1G72940* in the recombinant clones. Colonies marked with red colour were selected and sequenced to verify the inversion of the point mutation on gene *AT1G72940*.

Figures 5.3, **5.4** and **5.5** present the maps of the Level-1 assembled transcriptional units of *AT1G72940* with different promoters and protein tags. **Figure 5.3** shows the assembly of Level-0 modules containing the parts of *prom35S CaMV*, *AT1G72940*, *GFP*, *3xFLAG* repeats, *6xHA* repeats and *3'UTR+AtACT2* terminator into the L1P1 acceptor *pICH47732.* The following recombinant vectors containing the transcriptional units for constitutive overexpression of *AT1G72940* were generated: *prom35S::AT1G72940:GFP:AtACT2ter/pICH47732* (**Figure 5.3.A)**, *prom35S::AT1G72940:FLAG:AtACT2ter/pICH47732* (**Figure 5.3.B)**, and *prom35S::AT1G72940:HA:AtACT2ter/pICH47732* (**Figure 5.3.C)**.

Figure 5.4 shows the assembly of Level-0 modules containing the parts of *promDEX*, *AT1G72940*, *GFP*, *3xFLAG* repeats, *6xHA* repeats and *3'UTR+AtACT2* terminator into the L1P1 acceptor *pICH47732.* The following recombinant vectors containing the transcriptional units for dexamethasone-inducible overexpression of *AT1G72940* were generated: *promDEX::AT1G72940:GFP:AtACT2ter/pICH47732* (**Figure 5.4.A)**, *promDEX::AT1G72940:FLAG:AtACT2ter/pICH47732* (**Figure 5.4.B)**, and *promDEX::AT1G72940:HA:AtACT2ter/pICH47732* (**Figure 5.4.C)**.

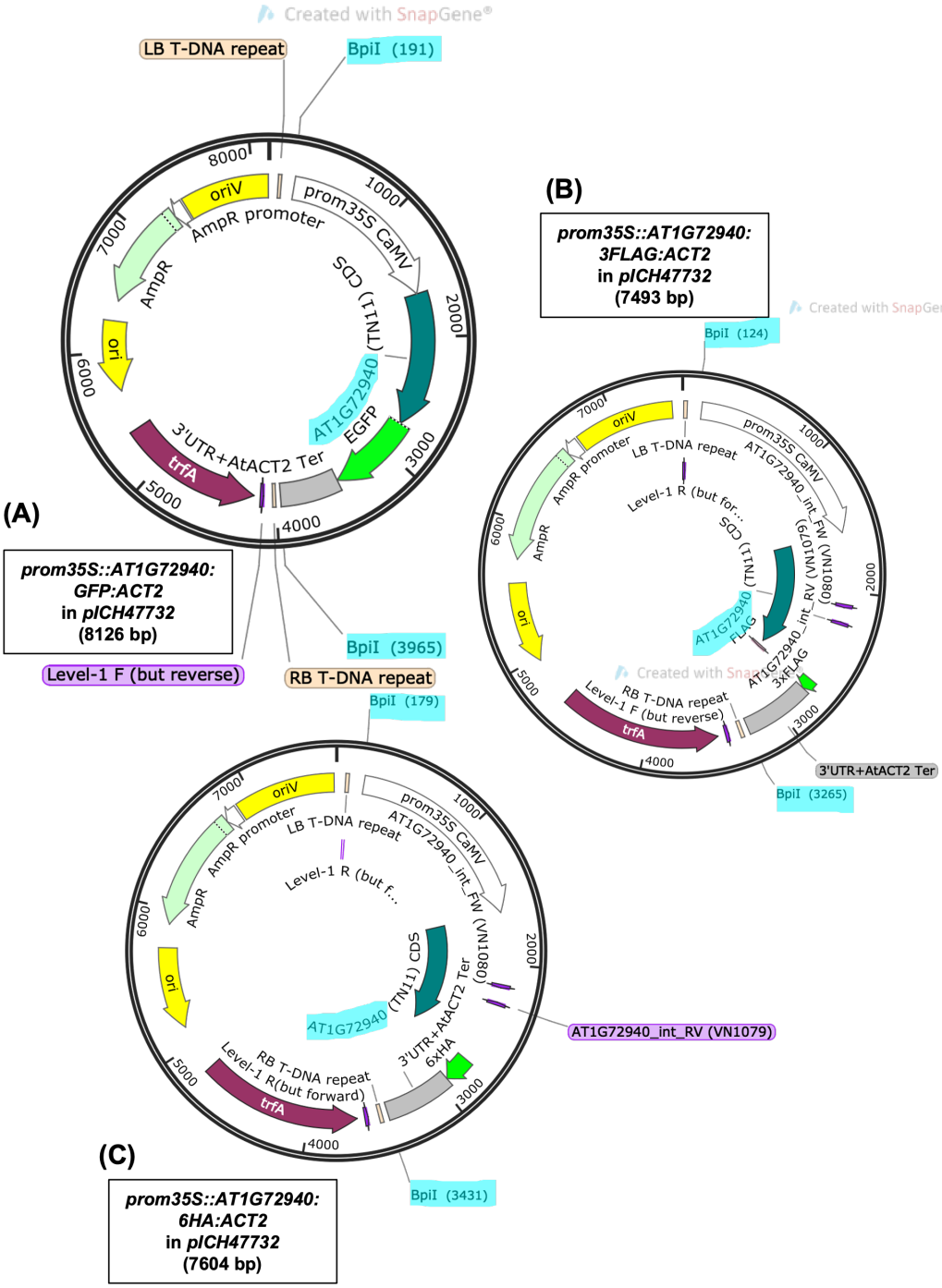

***Figure 5.3* Level-1 Golden Gate assembly of construct *prom35S::AT1G72940* fused with the sequences coding for protein tags GFP, FLAG and HA.**

Level-0 modules containing the parts of *prom35S CaMV*, *AT1G72940*, *GFP*, *3xFLAG* repeats, *6xHA* repeats and *3'UTR+AtACT2* terminator were assembled using BsaI into the L1P1 acceptor *pICH47732* to create the following transcriptional units: **(A)** *prom35S::AT1G72940:GFP:AtACT2ter/pICH47732*, **(B)** *prom35S::AT1G72940:FLAG:AtACT2ter/pICH47732*, **(C)** and *prom35S::AT1G72940:HA:AtACT2ter/pICH47732*. The recombinant L1P1 vectors confer resistance to ampicillin and colonies can be further selected on

Xgal/IPTG. L1P1 constructs can be subcloned to L2 vectors using BpiI (highlighted in turquoise).

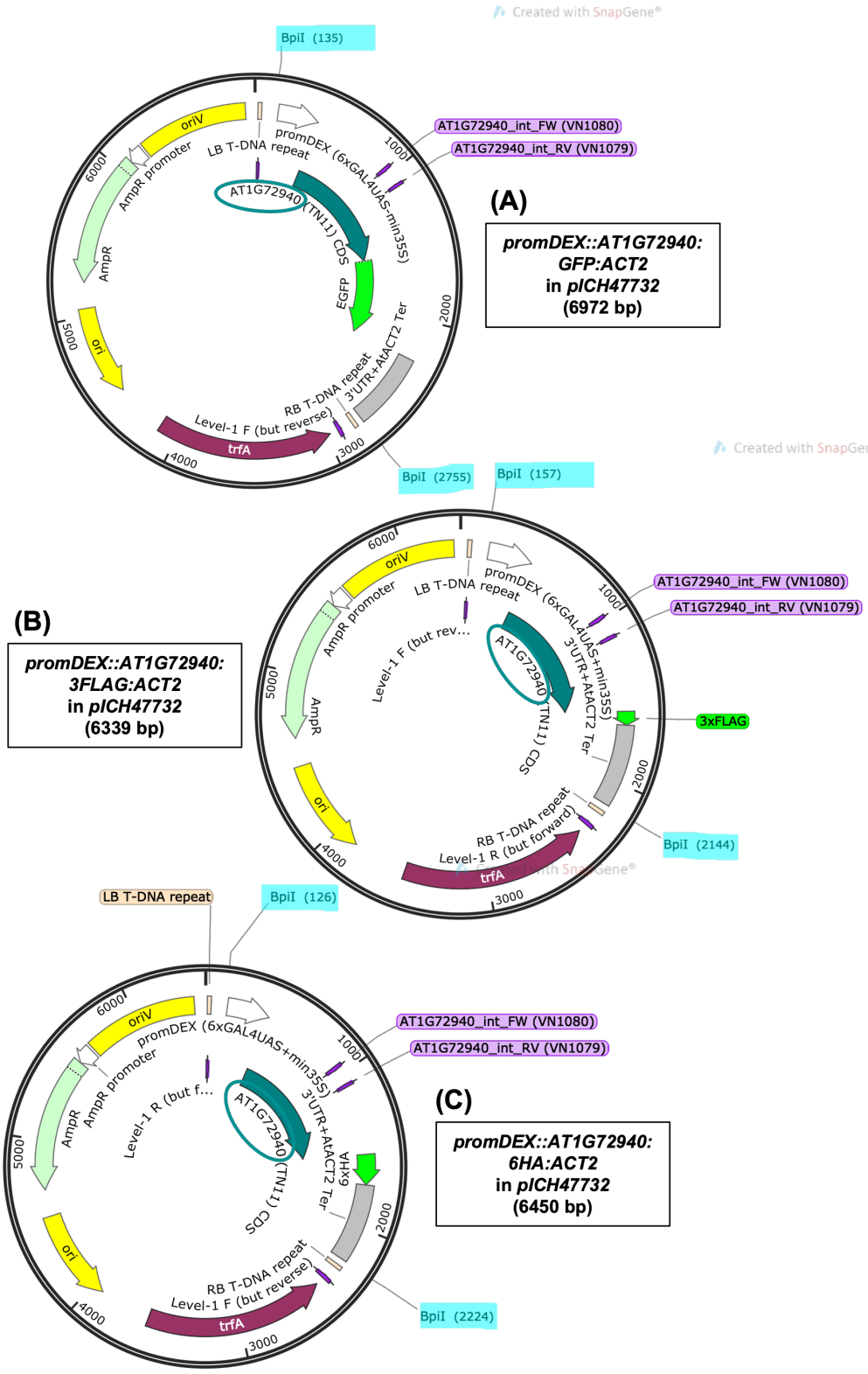

***Figure 5.4* Level-1 Golden Gate assembly of construct *promDEX::AT1G72940* fused with the sequences coding for protein tags GFP, FLAG and HA.**

Level-0 modules containing the parts of *promDEX, AT1G72940, GFP, 3xFLAG* repeats, *6xHA* repeats and *3'UTR+AtACT2* terminator were assembled using BsaI into the L1P1 acceptor *pICH47732* to create the following transcriptional units: *promDEX::AT1G72940:GFP:AtACT2ter/pICH47732* **(A),** *promDEX::AT1G72940:FLAG:AtACT2ter/pICH47732* **(B),** and *promDEX::AT1G72940:HA:AtACT2ter/pICH47732* **(C).** The recombinant L1P1 vectors confer resistance to ampicillin and colonies can be further selected on Xgal/IPTG. L1P1 constructs can be subcloned to L2 vectors using BpiI (highlighted in turquoise).

Likewise, **Figure 5.5** shows the assembly of Level-0 modules containing the parts of *promESTR*, *AT1G72940*, *GFP*, *3xFLAG* repeats, *6xHA* repeats and *3'UTR+AtACT2* terminator into the L1P1 acceptor *pICH47732.* The following recombinant vectors containing the transcriptional units for estradiol-inducible overexpression of *AT1G72940* were created: *promESTR::AT1G72940:GFP:AtACT2ter/pICH47732* (**Figure 5.5.A)**, *promESTR::AT1G72940:FLAG:AtACT2ter/pICH47732* (**Figure 5.5.B)**, and *promESTR::AT1G72940:HA:AtACT2ter/pICH47732* (**Figure 5.5.C)**. Successful clones of all L1P1 were selected with colonies PCR and verified with sequencing, before proceeding to L2 T-DNA assembly.

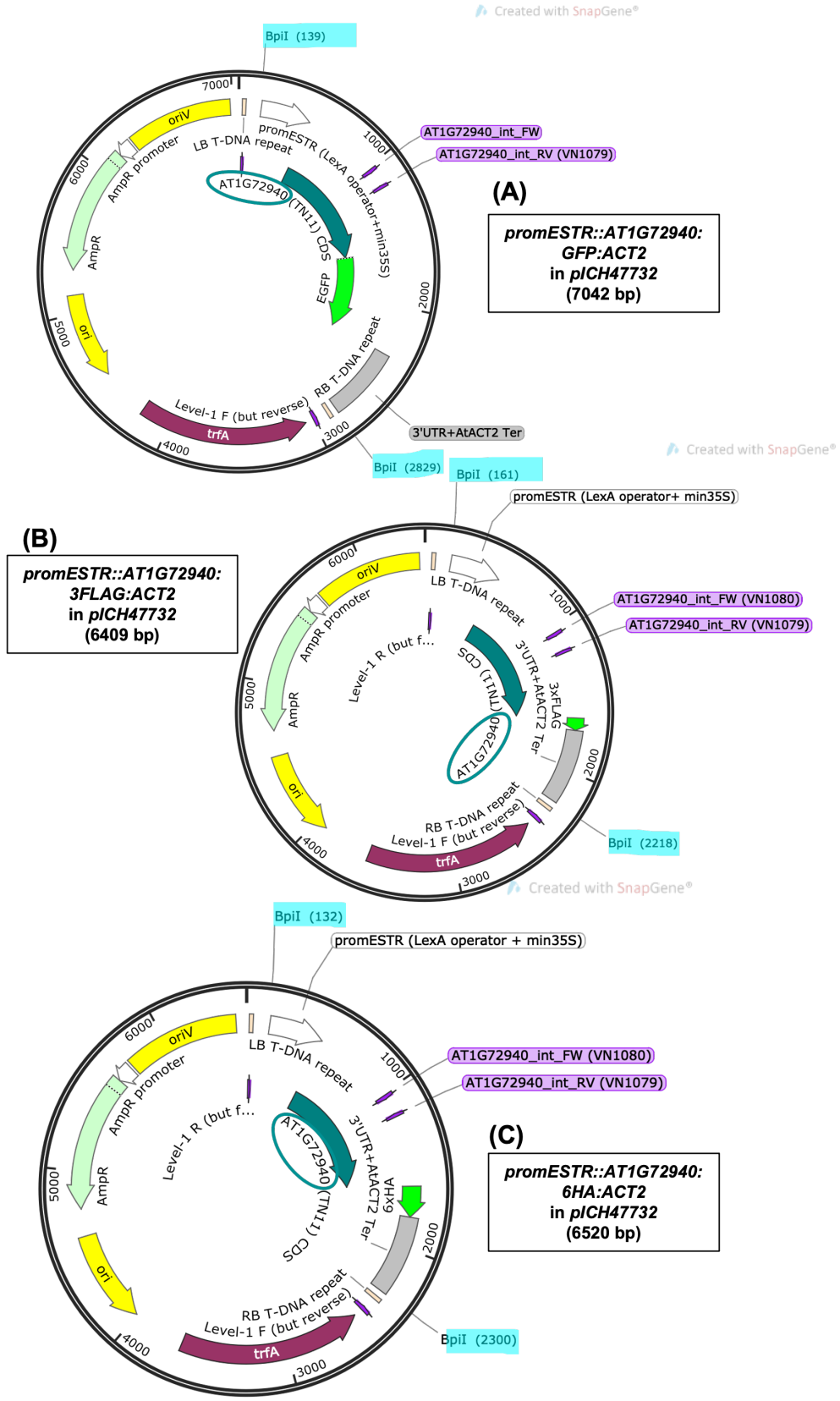

Figure 5.5 **Level-1 Golden Gate assembly of construct *promESTR::AT1G72940* fused with the sequences coding for protein tags GFP, FLAG and HA.**

Level-0 modules containing the parts of *promESTR*, *AT1G72940*, *GFP*, *3xFLAG* repeats, *6xHA* repeats and *3'UTR+AtACT2* terminator were assembled using BsaI into the L1P1 acceptor *pICH47732* to create the following transcriptional units: *promESTR::AT1G72940:GFP:AtACT2ter/pICH47732* **(A),** *promESTR::AT1G72940:FLAG:AtACT2ter/pICH47732* **(B),** and *promESTR::AT1G72940:HA:AtACT2ter/pICH47732* **(C).** The recombinant L1P1 vectors confer resistance to ampicillin and colonies can be further selected on Xgal/IPTG. L1P1 constructs can be subcloned to L2 vectors using BpiI (highlighted in turquoise).

The Level-2 T-DNAs were created by the assembly of either two L1 modules in the case of constructs made for constitutive overexpression or three L1 modules for the constructs of inducible overexpression. **Figure 5.6** presents the assembly of modules *prom35S::AT1G72940:tag* (L1P1) and *pFAST-R* (L1P2) together with an end link for two L1 parts, into the T-DNA borders of the L2 vector *pICSL4723.* The assembly resulted into the generation of the following recombinant T-DNA vectors: *prom35S::AT1G72940:GFP:ACT2/pICSL4723[pFAST-R]* (**Figure 5.6.A)**, *prom35S::AT1G72940:FLAG:ACT2/pICSL4723[pFAST-R]* (**Figure 5.6.B)**, and *prom35S::AT1G72940:HA:ACT2/pICSL4723[pFAST-R]* (**Figure 5.6.C)**.

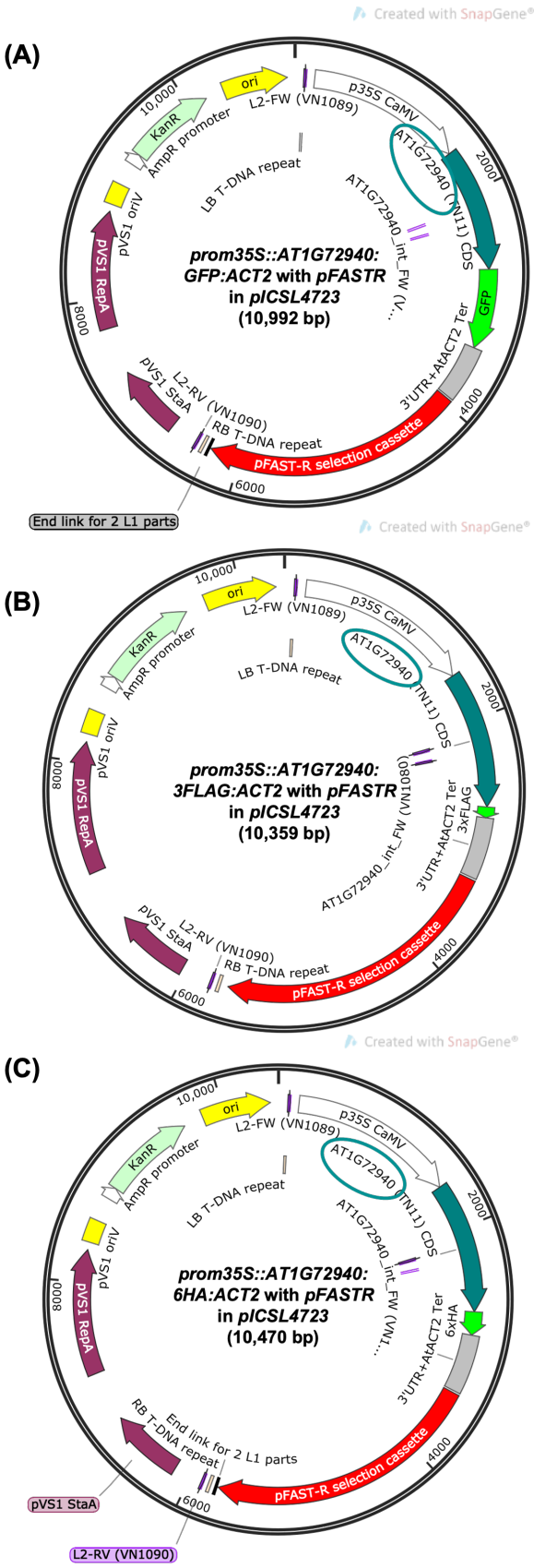

Figure 5.6 **Level-2 Golden Gate assembly of *prom35S::AT1G72940* constructs with the *pFAST-R* marker for plant selection into the T-DNA cassette.**

Level-1 modules containing the *prom35S::AT1G72940:tag* (L1P1) and *pFAST-R* (L1P2) transcriptional units and an end link for L1 parts were assembled using BpiI into the L2 acceptor *pICSL4723* to create the following T-DNA units: *prom35S::AT1G72940:GFP:ACT2/pICSL4723[pFAST-R]* **(A)**, *prom35S::AT1G72940:FLAG:ACT2/pICSL4723[pFAST-R]* **(B)**, and *prom35S::AT1G72940:HA:ACT2/pICSL4723[pFAST-R]* **(C)**. The recombinant L2 vectors confer resistance to kanamycin. Plants transformed with L2 T-DNAs can be selected for the presence of the transgene via the FAST-R red fluorescence (RFP) at the seed level.

Similarly, **Figure 5.7** shows the maps of the L2 vectors generated by the assembly of modules *promDEX::AT1G72940:tag* (L1P1), *pFAST-R* (L1P2) and *prom35S::GVG* (L1P3) together with an end link for three L1 parts, into the T-DNA borders of vector *pICSL4723.* The following T-DNA vectors were created: *promDEX::AT1G72940:GFP:ACT2/pICSL4723[pFAST-R + GVG]* **(Figure 5.7.A)**, *promDEX::AT1G72940:FLAG:ACT2/pICSL4723[pFAST-R + GVG]* **(Figure 5.7.B)**, and *promDEX::AT1G72940:HA:ACT2/pICSL4723[pFAST-R + GVG]* **(Figure 5.7.C)**. Finally, **Figure 5.8** presents the results of the assembly of modules *promESTR::AT1G72940:tag* (L1P1), *pFAST-R* (L1P2) and *prom35S::LexA* (L1P3) together with an end link for three L1 parts, into the T-DNA borders of the L2 vector *pICSL4723.* The assembly resulted into the generation of the following recombinant T-DNA vectors: *promESTR::AT1G72940:GFP:ACT2/pICSL4723[pFAST-R + LexA]* **(Figure 5.8.A)**, *promESTR::AT1G72940:FLAG:ACT2/pICSL4723[pFAST-R + LexA]* **(Figure 5.8.B)**, and *promESTR::AT1G72940:HA:ACT2/pICSL4723[pFAST-R + LexA]* **(Figure 5.8.C)**.

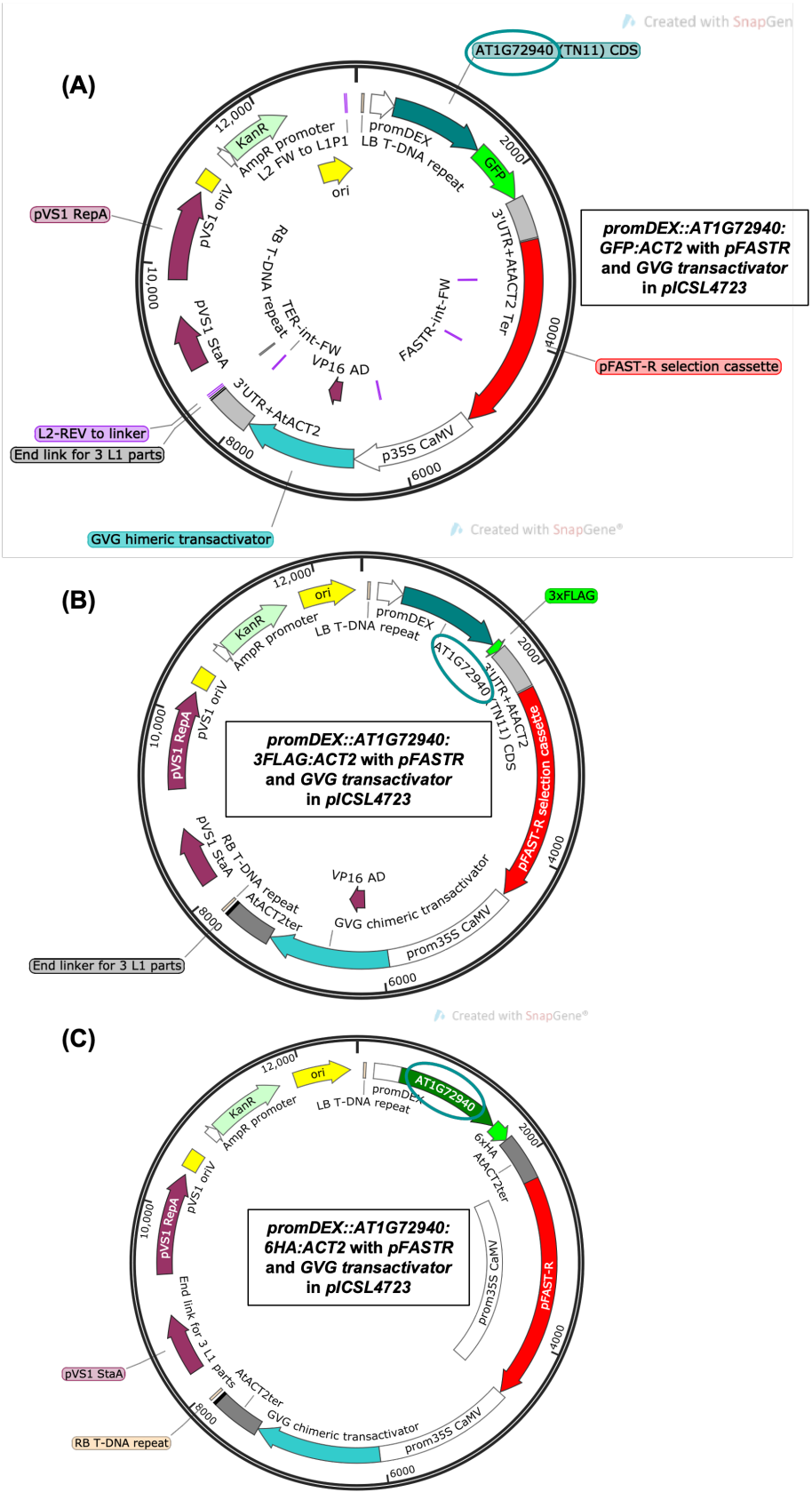

Figure 5.7 **Level-2 Golden Gate assembly of *promDEX::AT1G72940* constructs with the *pFAST-R* marker for plant selection and *GVG* transactivator into the T-DNA cassette.**

Level-1 modules containing the *promDEX::AT1G72940:tag* (L1P1), *pFAST-R* (L1P2) and *prom35S::GVG* (L1P3) transcriptional units, and an end link for L1 parts were assembled using BpiI into the L2 acceptor *pICSL4723* to create the following T-DNA units: *promDEX::AT1G72940:GFP:ACT2/pICSL4723[pFAST-R + GVG]* **(A)**, *promDEX::AT1G72940:FLAG:ACT2/pICSL4723[pFAST-R + GVG]* **(B)**, and *promDEX::AT1G72940:HA:ACT2/pICSL4723[pFAST-R + GVG]* **(C)**. The recombinant L2 vectors confer resistance to kanamycin. Plants transformed with L2 T-DNAs can be selected for the presence of the transgene via the FAST-R red fluorescence (RFP) at the seed level.

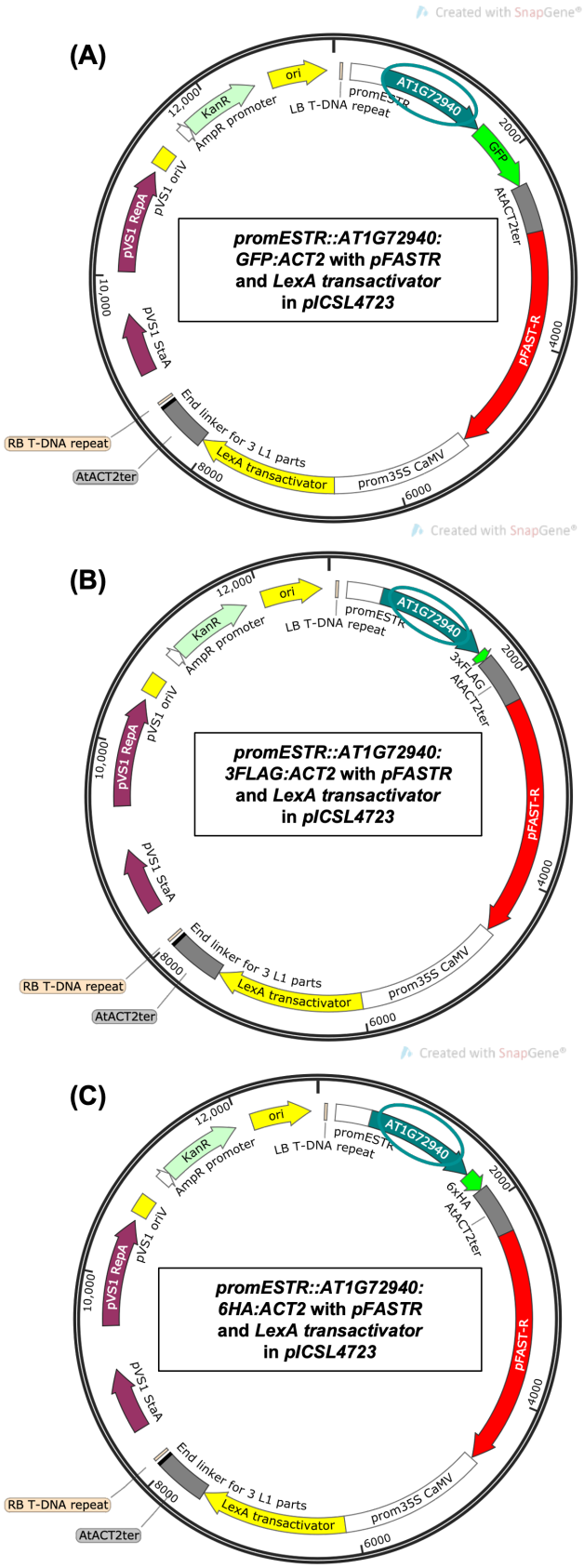

Figure 5.8 **Level-2 Golden Gate assembly of *promESTR::AT1G72940* constructs with the *pFAST-R* marker for plant selection and *LexA* transactivator into the T-DNA cassette.**

Level-1 modules containing the *promESTR::AT1G72940:tag* (L1P1), *pFAST-R* (L1P2) and *prom35S::LexA* (L1P3) transcriptional units, and an end link for L1 parts were assembled using BpiI into the L2 acceptor *pICSL4723* to create the following T-DNA units: *promESTR::AT1G72940:GFP:ACT2/pICSL4723[pFAST-R + LexA]* **(A)**, *promESTR::AT1G72940:FLAG:ACT2/pICSL4723[pFAST-R + LexA]* **(B)**, and *promESTR::AT1G72940:HA:ACT2/pICSL4723[pFAST-R + LexA]* **(C)**. The recombinant L2 vectors confer resistance to kanamycin. Plants transformed with L2 T-DNAs can be selected for the presence of the transgene via the FAST-R red fluorescence (RFP) at the seed level.

Successful clones of all L2 *AT1G72940* T-DNA modules were selected after three different sets of colonies PCR checking for the presence of all required L1 parts and verified with sequencing. *Agrobacterium tumefaciens* cells were transfected with the selected L2 T-DNA vectors to prepare for *A. thaliana* stable transformation. *A. tumefaciens* recombinant colonies for each different T-DNA were selected and tested with PCR for the presence of gene *AT1G72940,* as presented in **Figure 5.9.B**. No PCR products were detected in the colonies resulted after transformation with constructs *promDEX::AT1G72940:HA:ACT2/pICSL4723[pFAST-R + GVG]* and *promESTR::AT1G72940:HA:ACT2/pICSL4723[pFAST-R + LexA]*. **Figure 5.9.A** shows different levels of extracted plasmid per construct, which could explain the lack of significant PCR product yield in **Figure 5.9.B.**

The successful *A. tumefaciens* constructs were used to transform the floral buds of WT *A. thaliana* Col-0 (generation T0). The following transgenic *A. thaliana* plants were produced for constitutive overexpression of *AT1G72940*: *prom35S::AT1G72940:GFP, prom35S::AT1G72940:FLAG,* and *prom35S::AT1G72940:HA.* For dexamethasone-inducible and estradiol-inducible overexpression of *AT1G72940*, the following transgenic plants were generated: *promDEX::AT1G72940:GFP, promDEX::AT1G72940:FLAG, promDEX::AT1G72940:HA promESTR::AT1G72940:GFP, promESTR::AT1G72940:FLAG,* and *promESTR::AT1G72940:HA.*

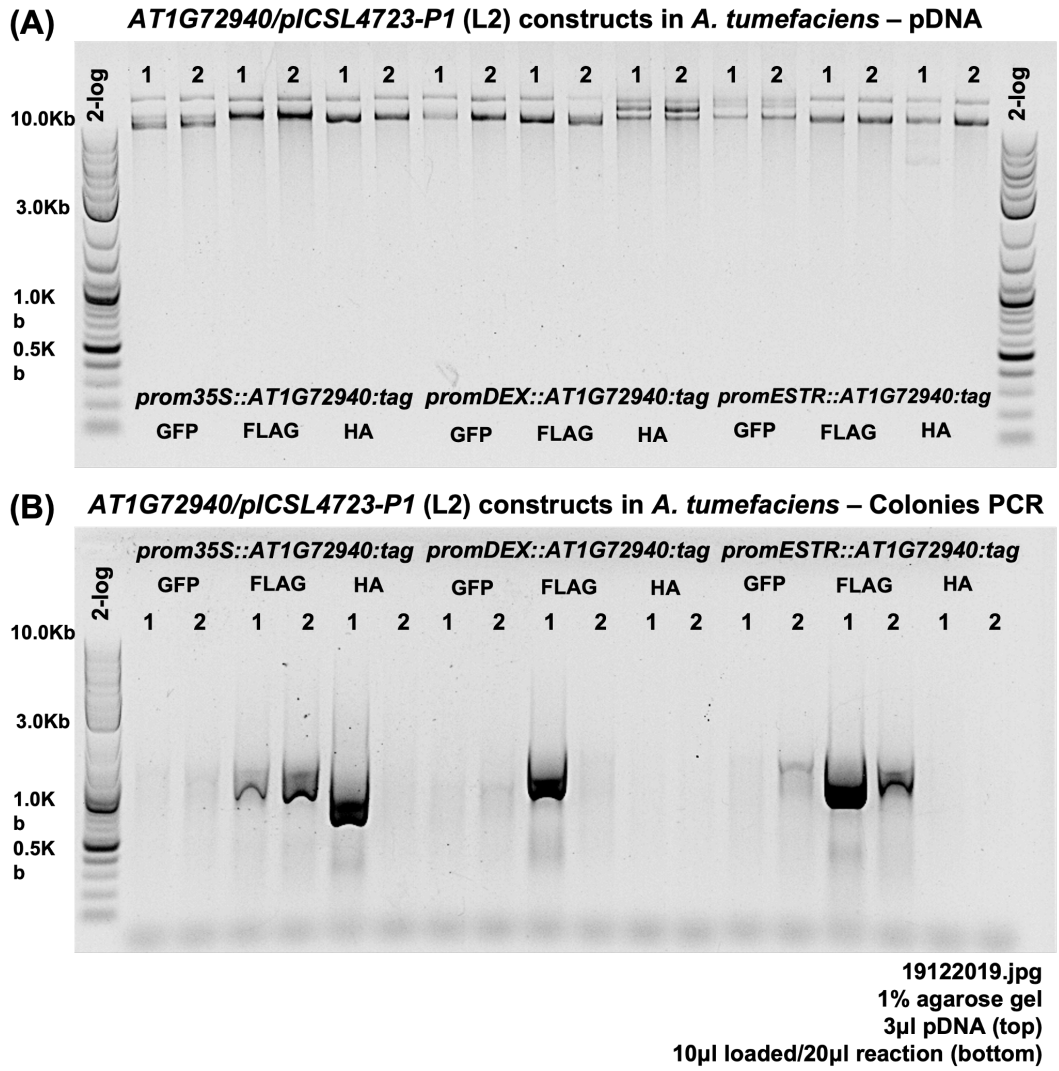

Figure 5.9 **PCR verifying the presence of the *AT1G72940* T-DNAs in *Agrobacterium tumefaciens* prior to *A. thaliana* transformation.**

A. tumefaciens competent cells were transfected with the L2 vectors containing the 9 different *AT1G72940* T-DNAs and 2 colonies per construct were selected. **(A)** plasmid DNA of the *AT1G72940/pICSL4723* constructs was extracted from the respective *A. tumefaciens* clones and analysed with agarose gel electrophoresis. All L2 recombinant vectors exceed the 10Kb in size, hence the bands are visible above the highest MW of the ladder (2-log). **(B)** Extracted *AT1G72940/pICSL4723* plasmids were used as a PCR template for the amplification of *AT1G72940* gene. All GFP constructs give a low product yield for *AT1G72940,* possibly due to low plasmid yield. The *HA*-tagged *AT1G72940* constructs for *promDEX* and *promESTR*, resulted in no detected PCR product.

Figure 5.10 presents as an example of the process of selection of the T1 and T2 generations of transgenic *A. thaliana AT1G72940* seeds, using the red fluorescence of the *pFAST-R* cassette embedded in the transgenes. The expression of the FAST marker at the specific stage of dry seeds in dormancy

allowed to differentiate between transgenic and WT seeds, based on the RFP fluorescence. Due to time limitations, the selection and analysis of the estradiol-inducible *AT1G72940* transgenic seeds was not pursued as part of this PhD project. Furthermore, it was suggested that the dexamethasone inducible lines should be prioritised, since the preliminary experiments preceding this PhD projected were conducted on DEX-inducible plants. Thus we proceeded with the selection of the constitutively overexpressed and dexamethasone-inducible transgenic seeds.

Figure 5.10.A shows the selection of *prom35S::AT1G72940:GFP* T1 generation, which descends from the transformed T0 *A. thaliana* Col-0 plants. **Figure 5.10.Ai** shows that the T1 generation contains mostly WT seeds (dark, non-fluorescent) and only a few transformed fluorescent seeds. Transformed T1 seeds are picked up gently with tweezers under a UV fluorescence stereoscope (**Figure 5.10.Aii**) and collected into an Eppendorf tube for future use (**Figure 5.10.Aiii**). Each transformed T1 seed is a product of one (or more) different T-DNA insertions in the Col-0 genome. Selected T1 seeds (right picture) were grown into the mother plants of each different line for the respective transgene. The descended transgenic lines are hereafter named after the number (n) of the mother plant (T1-n), following the preferred notation of the lab. T1 seeds of *prom35S::AT1G72940:HA* plants were not fluorescent at all, showing that the T0 transformation was unsuccessful.

Figure 5.10.B shows the selection of T2 generation of *prom35S::AT1G72940:GFP* transgenic seeds, descending by each selected T1-n mother plant (line). The pictures show that the majority of T2 seeds are fluorescent, hence transgenic. T1-n plants are usually heterozygous (one copy of the T-DNA), which results to the ratio of 3:1 transgenic (fluorescent) to WT (non-fluorescent) seeds in the T2 generation, as observed in the presented pictures. From the selected T2 fluorescent seeds, 1 in 3 is expected to be homozygous for the transgene.

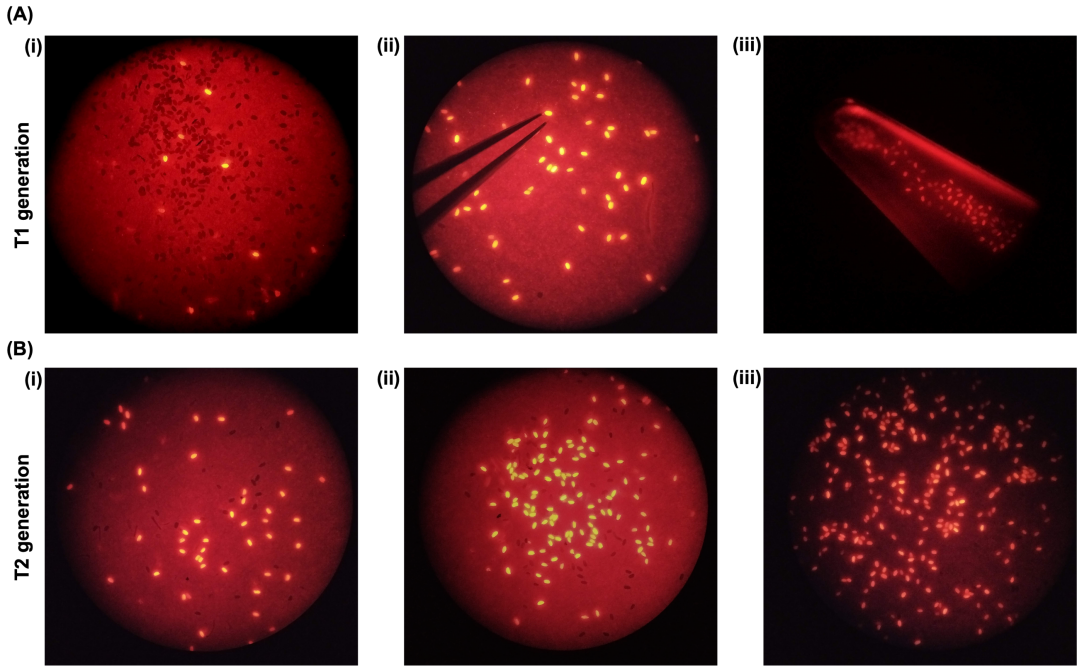

Figure 5.10 **Example of the selection of transgenic *A. thaliana AT1G72940* seeds of T1 and T2 generation through *pFAST-R* red fluorescence.**

The RFP fluorescence of the FAST marker allows the identification of transgenic *A. thaliana* seeds. **(A)** Selection of T1 generation of ***prom35S::AT1G72940:GFP*** transgenic seeds. The T1 generation contains mostly WT seeds (dark, non-fluorescent) and only a few (usually heterozygous) transformed fluorescent seeds **(i)**. Transformed T1 seeds are picked up gently with tweezers under a UV fluorescence stereoscope **(ii)** and collected into an Eppendorf tube for future use **(iii)**. **(B)** Selection of T2 generation of ***prom35S::AT1G72940:GFP*** transgenic seeds. Each panel **(i)** to **(iii)** shows the selection of T2 seeds from a different mother plant (line). T1-n plants are usually heterozygous, which results to an expected ratio of 3:1 transgenic (fluorescent) to WT (non-fluorescent) seeds in the T2 generation. From the selected T2 fluorescent seeds, 1 in 3 is expected to be homozygous for the transgene.

When growing the selected T2 seeds, six seedlings from each line were randomly chosen to propagate for the generation of T3 seeds and to identify the homozygous plants among them. Regarding the T2 transgenic lines of the constitutively overexpressing *prom35S::AT1G72940:GFP* and *prom35S::AT1G72940:FLAG* plants, as well as the inducible overexpressing *promDEX::AT1G72940:GFP* and *promDEX::AT1G72940:FLAG* plants, no developmental differences were observed at the seedling stage when compared to Col-0 (data not shown). However, **Figure 5.11** shows the developmental variation of the selected T2 plants as observed at 8 weeks post germination. Within each line of the T2 *prom35S::AT1G72940:GFP* (**Figure 5.11.A)** and *prom35S::AT1G72940:FLAG GFP* (**Figure 5.11.B** and **C)** some plants behave like Col-0 whereas other plants show delayed development with late flowering, increased number of rosette leaves and multiple central stems.

pFAST-R examination of the T3 seeds (**Figure 5.12**) produced by each individual plant shown in **Figure 5.11** showed that the developmental phenotype observed is not related to the heterozygosity or homozygosity of the T-DNA insertion of the developmentally delayed plants. **Figure 5.11.A** presents the development of six transgenic plants originating from *prom35S::AT1G72940:GFP* line T1-2. As shown in **Figure 5.11.A(iii),** plants #1 (homozygous, +/+) and #3 (heterozygous, +/-) have the same developmental phenotype, but different number of transgene copies. **Figure 5.11.B** shows six plants of *prom35S::AT1G72940:FLAG* line T1-1. As shown in **Figure 5.11.B(iii)-(iv)** plants #4 (homozygous, +/+) and #6 (heterozygous, +/-), respectively, have the same developmental phenotype, but different number of transgene copies. **Figure 5.11.C** presents six transgenic plants of *prom35S::AT1G72940:FLAG* line T1-4. **Figure 5.11.C(iii)** shows that plants #1(homozygous, +/+) and #3(homozygous, +/+) are both homozygous for the insertion, but have different developmental phenotypes.

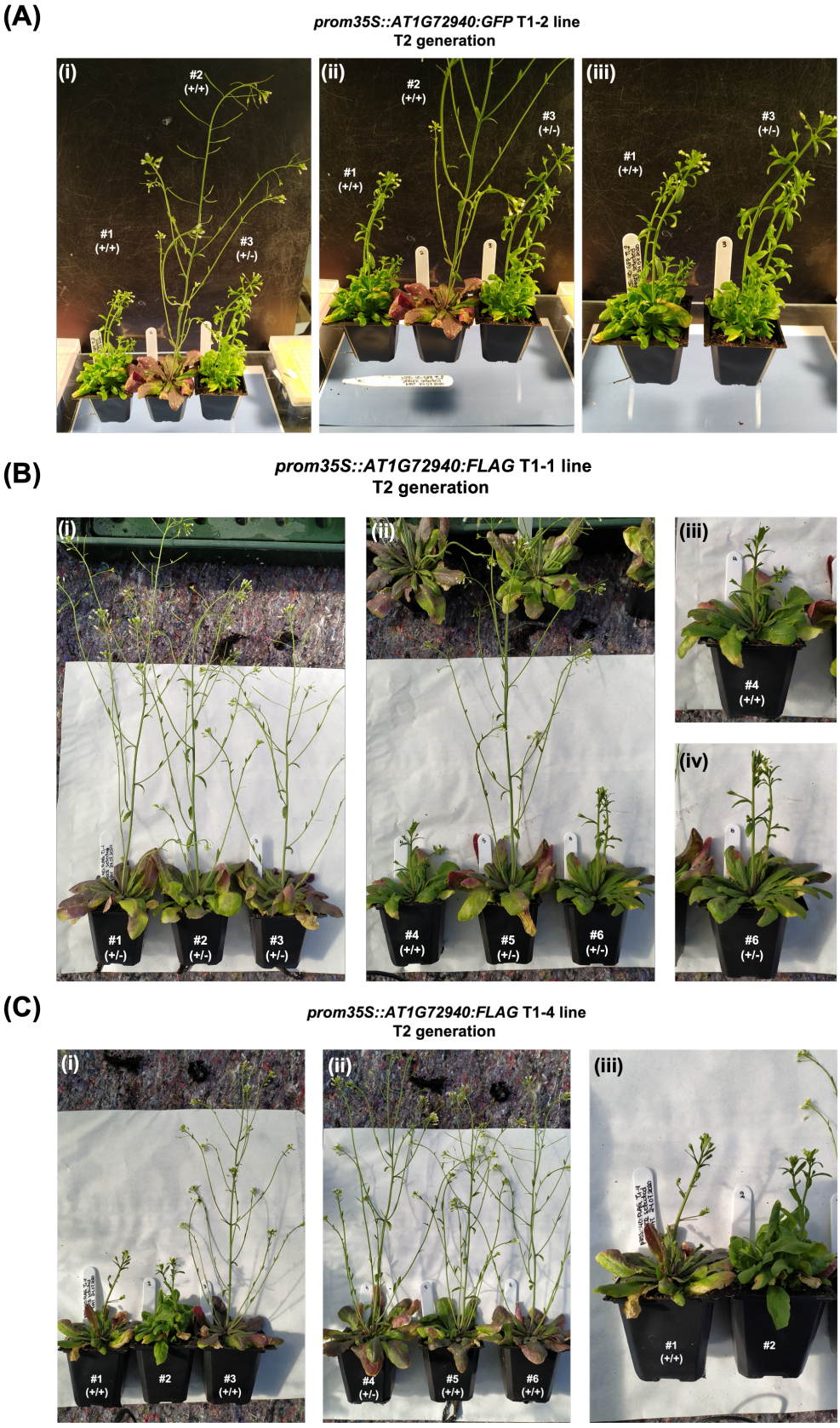

Figure 5.11 **Developmental variations of selected transgenic *prom35S::AT1G72940* lines in T2 generation are independent to the homozygosity or heterozygosity of each plant.**

Of the *pFAST-R* selected T2 seeds for each T1-n mother plant, 6 seedlings per T1-n line were randomly chosen to grow and propagate for the identification of the homozygous plants among them. *prom35S::AT1G72940:GFP* and *prom35S::AT1G72940:FLAG* seedlings do not show different growth than Col-0. However, at 8 weeks post-germination a developmental variation of delayed flowering, increased number of rosette leaves and multiple stems is observed among plants within each T1-n line. **(A) (i)** and **(ii)** T2 *pFAST-R* selected plants of *prom35S::AT1G72940:GFP* line T1-2**. (iii)**Plants #1(+/+) and #3(+/-) have the same developmental phenotype, but different number of transgene copies. **(B) (i)** and **(ii)** T2 *pFAST-R* selected plants of *prom35S::AT1G72940:FLAG* line T1-1. **(iii)** and **(iv)** Plants #4(+/+) and #6(+/-), respectively, have the same developmental phenotype, but different number of transgene copies. **(C) (i)** and **(ii)** T2 *pFAST-R* selected plants of *prom35S::AT1G72940:FLAG* line T1-4. **(iii)** Plants #1(+/+) and #3(+/+) are both homozygous for the transgene but have different developmental phenotypes.

n: number of line, (+/-): heterozygous for the T-DNA insertion, (+/+): homozygous for the T-DNA insertion

The *pFAST-R* assessment of T3 seeds (**Figure 5.12**) provided information on the heterozygocity/homozygocity of both T2 and T3 plants in terms of the transgene in question. T3 seeds that were 100% fluorescent are homozygous and are descending from a homozygous T2 plant, whereas T3 seeds with a ratio of 3:1 transgenic (fluorescent) to WT (non-fluorescent) are descending from a heterozygous T2 plant and still segregating. A full list with information on the homozygosity/heterozygosity of each generation of the transgenic *AT1G72940* plants is provided in **Section 7.5**.

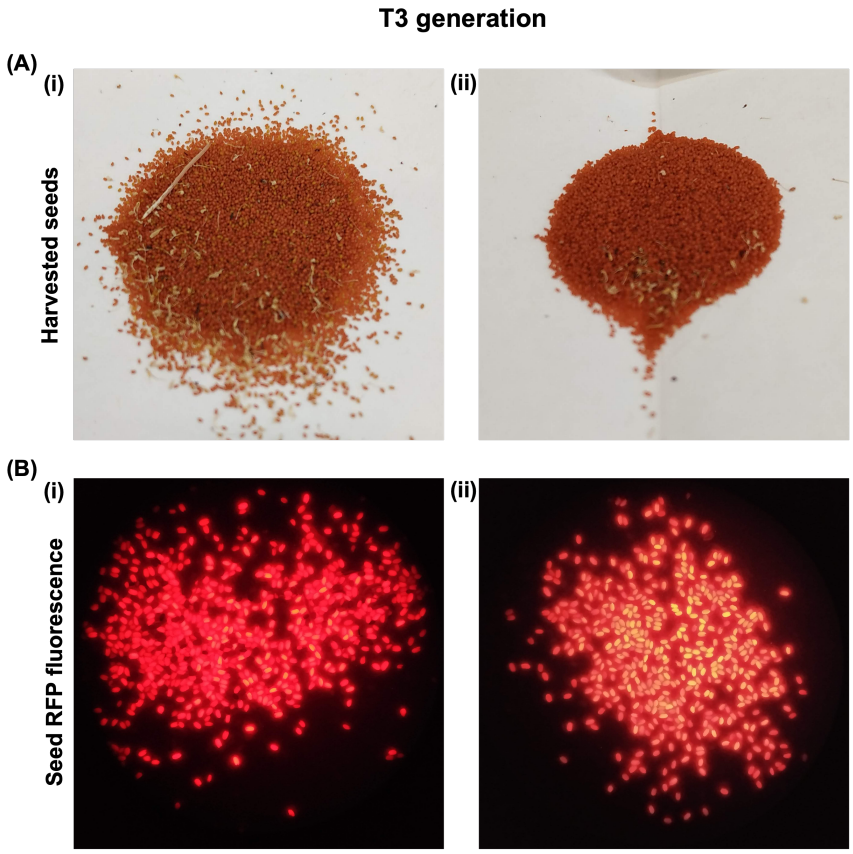

Figure 5.12 **Example of the selection of T3 generation of transgenic *A. thaliana AT1G72940* seeds using the *pFAST-R* red fluorescence.**

T3 Seeds were collected individually for each of the 6 selected T2 plants grown from the respective T1-n mother plant. Each seed batch was examined in the UV fluorescence stereoscope for the *pFAST-R* red fluorescence. T3 seeds that were 100% fluorescent are homozygous and are descending from a homozygous T2 plant, whereas T3 seeds with a ratio of 3:1 transgenic (fluorescent) to WT (non-fluorescent) are descending from a heterozygous T2 plant and still segregating**. (A**) T3 seed collection and cleaning. Homozygous T3 seeds are bright red even in the optical light. **(B)** Strong RFP fluorescence of homozygous T3 seeds as observed in the UV fluorescence stereoscope.

In conclusion, *AT1G72940* was the only *TN* gene that was successfully subclones and transformed into Col-0 plants, iv various combinations of promoters and C' terminal tags. Despite multiple attempts, gene *AT1G72920* was not successfully subcloned, and gene *AT1G72950* was but didn't move forward with. The pFAST-R selection verified that the transformation of Col-0 plants with the *AT1G72940* T-DNA vectors was successful for all constructs except *prom35S::AT1G72940:HA,* which didn't produce any fluorescent seeds. Selection up to T3 generation of *prom35S* and *promDEX* transgenic

seeds led to the identification of both homozygous and heterozygous lines for each different *AT1G72940* transgene, to be used for further characterisation experiments. Phenotyping of the selected T2 plants for each construct showed that any developmental phenotypes observed are not connected to the homozygosity/heterozygosity of the plant, the transgene itself, or multiple T-DNA insertions in the genome as the same developmental phenotype is randomply observed across all the different lines and/or transgenes.

5.2.2 Testing the expression levels of the new transgenic *A. thaliana* AT1G72940 constitutively expressing lines using immunoblotting assays and RT-q-PCR

The selected T2 and T3 generations of *A. thaliana* constitutively and inducible overexpressing transgenic lines were tested for AT1G72940 expression via immunoblotting assays (western blots) and RT-q-PCR in various developmental stages. For the immunoblotting assays, crude protein extracts were generated, analysed with SDS PAGE electrophoresis, and transferred on activated PVDF membranes for detection via western blotting. PVDF membranes were incubated with the appropriate antibodies and then with a chemiluminescent substrate for HRP. Tagged proteins were visualised via exposure of the HRP signal on X-ray film. For GFP-tagged proteins, we used an α-GFP-HRP conjugated antibody diluted 1:10,000 in milk-TBST (5% w/v). FLAG-tagged proteins were detected via a primary rabbit polyclonal α-FLAG® antibody (diluted 1:5,000 in 5% w/v milk-TBST) and secondary α-rabbit-HRP conjugated antibody diluted 1:10,000 in milk-TBST (5% w/v). The expected MW for AT1G72940:GFP is ~73KDa and for AT1G72940:FLAG is ~48KDa. Col-0 seedlings were generally used as negative control.

Figure 5.13 shows the results of AT1G72940 protein detection in 15-days-old seedlings of constitutively overexpressing *prom35S::AT1G72940:GFP* and *prom35S::AT1G72940:FLAG* T2 lines (**Figure 5.13.Ai)**, as well as DEX-inducible overexpressing *promDEX::AT1G72940:GFP* (**Figure 5.13.Aii)** and *promDEX::AT1G72940:FLAG* (**Figure 5.13.Aiii)** T2 lines. *prom35S::GFP* stable transgenic line was kindly donated by Dr. Ana Dominguez-Ferreras (University of Warwick, UK) as a potential positive control for GFP detection. In **Section 5.2.1** we presented that T2 seeds are segregating, so they were selected via *pFAST-R* fluorescence. 1 in 3 selected plants is homozygous (+/+), so we consider T2 plants mainly heterozygous (+/-).

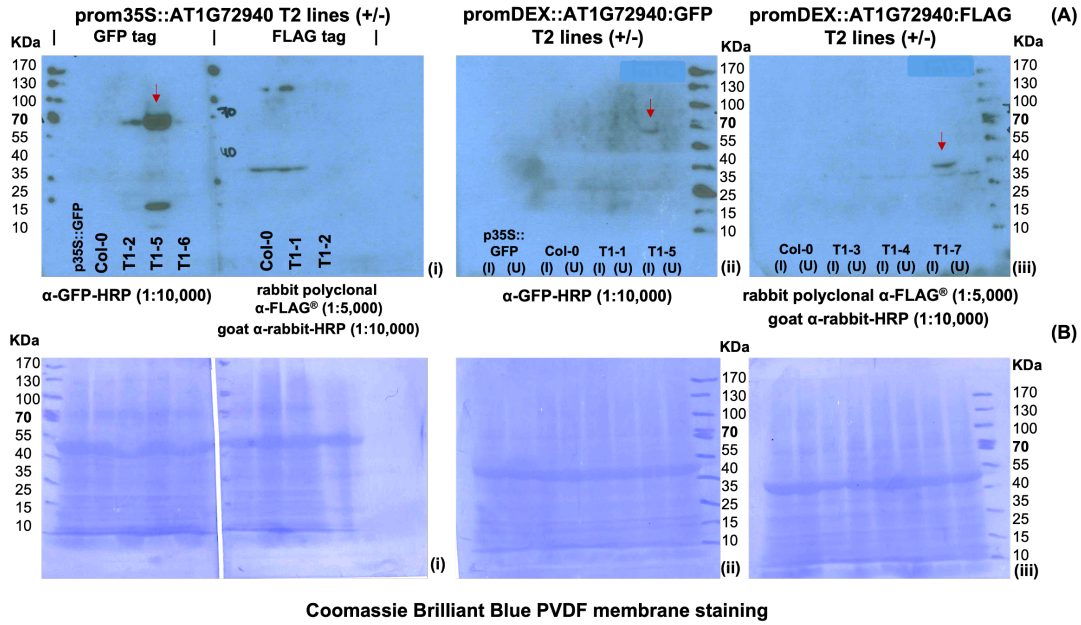

Figure 5.13 **Immunoblot detection of protein AT1G72940 in 15 days old seedings of *A. thaliana AT1G72940* transgenic T2 lines.**

Ten *pFAST-R*-selected T2 seedlings of 15 days old were used for crude protein extraction, analysed with SDS PAGE electrophoresis and transferred on activated PVDF membranes for immunoblot detection (western blotting). Expected MW for AT1G72940:GFP is ~73KDa and for AT1G72940:FLAG is ~48KDa. Col-0 seedlings were used as negative control and *p35S::GFP* as a potential positive control for GFP detection. **(A)** Visualisation of extracted tagged proteins on X-ray film following O/N exposure. **(Ai)** *prom35S::AT1G72940:GFP* T2 lines T1-2, T1-5 and T1-6, and *prom35S::AT1G72940:FLAG* T2 lines T-1 and T1-2 were tested for AT1G72940 expression. Only *prom35S::AT1G72940:GFP* line T1-5 shows a strong signal (red arrow) coinciding with the 70KDa band of the protein ladder. The lower signal in line T1-5 is probably free GFP. **(Aii)** Dexamethasone-induced overexpressing *promDEX::AT1G72940:GFP* T2 lines T1-1 and T1-5 were tested for AT1G72940 expression, after treatment with 30μM of DEX solution or mock (water) for the untreated samples. DEX-induced (I) line T1-5 shows a weak signal (red arrow) coinciding with the 70KDa band of the protein ladder, as opposed to uninduced (U) T1-5 seedlings. **(Aiii)** Dexamethasone-induced overexpressing *promDEX::AT1G72940:FLAG* T2 lines T1-3, T1-4 and T1-7 were tested for AT1G72940 expression, after treatment with 30μM of DEX solution or mock (water) for the untreated samples. DEX-induced (I) line T1-7 shows a weak signal (red arrow) coinciding with the 40KDa band of the protein ladder, as opposed to uninduced (U) T1-7 seedlings. **(B)** Staining of PVDF membranes post X-ray film exposure with Coomassie Brilliant Blue solution to verify the successful transfer or proteins on the membrane. Membranes in **(i), (ii)** and **(iii)** correspond to the respective X-ray films of **(A).**

(+/-): heterozygous for the T-DNA insertion,

(+/+): homozygous for the T-DNA insertion

Of the tested T2 heterozygous *prom35S::AT1G72940:GFP* seedlings (**Figure 5.13.Ai)**, only line T1-5 shows a strong signal (red arrow) coinciding with the 70KDa band of the protein ladder, while T1-2 and T1-6 show a weaker signal at the same size, which may originate by overflown T1-5 protein extract to the adjacent wells. On the contrary, *prom35S::AT1G72940:FLAG* T2 tested lines did not produce any FLAG signal at the expected size. For the dexamethasone-induced overexpressing lines, seedlings were treated with 30μM of DEX solution or mock (water) for the untreated samples. **Figure 5.13.Aii** shows that of the *promDEX::AT1G72940:GFP* T2 lines, the induced sample of line T1-5 shows a weak signal (red arrow) coinciding with the 70KDa band of the protein ladder, while uninduced (U) T1-5 seedlings do not show any GFP signal. Similarly, **Figure 5.13.Aiii** shows that of the *promDEX::AT1G72940:FLAG* T2 lines, only DEX-induced (I) line T1-7 shows a weak signal (red arrow) coinciding with the 40KDa band of the protein ladder, while uninduced (U) T1-7 seedlings do not show FLAG signal. Staining of the PVDF membranes with Coomassie Brilliant Blue (**Figure 5.13.B)** following protein transfer and film exposure, showed that the proteins were successfully transferred and bound on the membranes.

The experiment was repeated for the T2 constitutively overexpressed lines *prom35S::AT1G72940:GFP* T1-2, T1-5, and T1-6 as well as *prom35S::AT1G72940:FLAG* T1-1 and T1-2. **Figure 5.14.A** shows the results of AT1G72940 detection in 15-days-old seedlings of *prom35S::AT1G72940:GFP* and *prom35S::AT1G72940:FLAG* T2 lines. Consistent with the previous results, *prom35S::AT1G72940:GFP* line T1-5 shows the GFP signal (red arrow) at the 70KDa band of the protein ladder. *prom35S::AT1G72940:FLAG* T2 lines did not produce any FLAG signal at the expected size. Staining of the PVDF membrane with Ponceau S solution verified the successful transfer or proteins on the membrane.

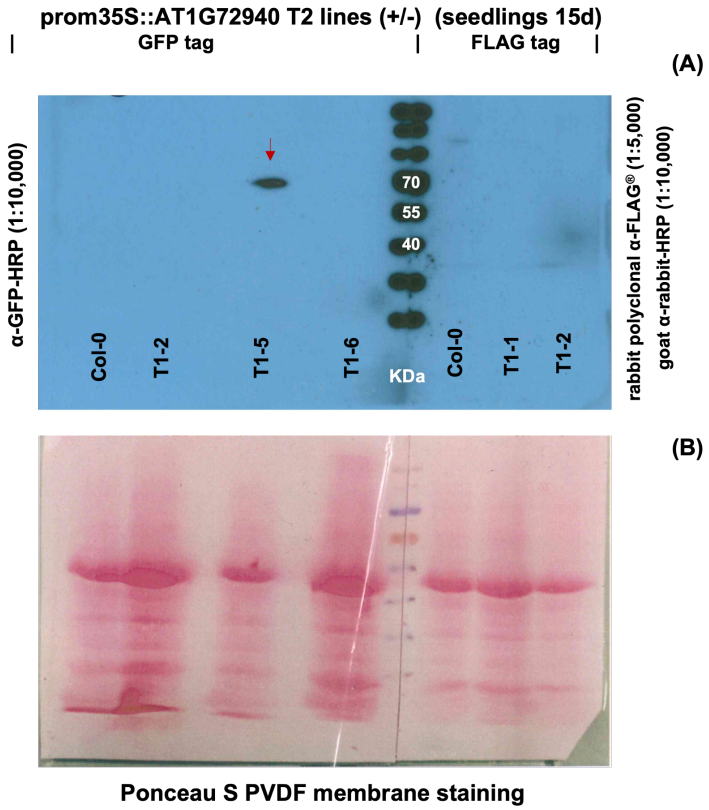

Figure 5.14 **Immunoblot detection of protein AT1G72940 in 15 days old seedings of transgenic *A. thaliana AT1G72940* constitutively overexpressing T2 lines.**

Ten *pFAST-R* selected T2 seedlings of 15 days old were used for crude protein extraction, analysed with SDS PAGE electrophoresis and transferred on activated PVDF membranes for immunoblot detection (western blotting). Expected MW for AT1G72940:GFP is ~73KDa and for AT1G72940:FLAG is ~48KDa. Col-0 seedlings were used as negative control. **(A)** Visualisation of extracted tagged proteins on X-ray film following O/N exposure. *prom35S::AT1G72940:GFP* T2 lines T-2, T1-5 and T1-6, and *prom35S::AT1G72940:FLAG* T2 lines T-1 and T1-2 were tested for AT1G72940 expression. Only *prom35S::AT1G72940:GFP* line T1-5 shows the GFP signal (red arrow) coinciding with the 70KDa band of the protein ladder. *prom35S::AT1G72940:FLAG* T2 lines did not produce any FLAG signal at the expected size. **(B)** Staining of the PVDF membrane post X-ray film exposure with Ponceau S solution to verify the successful transfer or proteins on the membrane.

(+/-): heterozygous for the T-DNA insertion

(+/+): homozygous for the T-DNA insertion

The homozygous batches of seeds were selected for the T3 generation of all tested lines, except for *prom35S::AT1G72940:GFP* line T1-5 which was still segregating at T3 generation. Plants from line T1-5 were selected based on

their *pFAST-R* fluorescence for all experiments thereafter. T3 seedlings of 6 days old from *prom35S::AT1G72940:GFP* lines were tested to ask if protein AT1G72940 could be detected (**Figure 5.15.A)**. Consistent with the results of the respective lines in T2 generation, protein AT1G72940:GFP is detected in *prom35S::AT1G72940:GFP* line T1-5 (+/-), but not in the homozygous lines T1-2 and T1-6. Staining of the SDS PAGE gel with Coomassie Brilliant Blue showed that there is sufficient amount of crude protein extract for all samples (**Figure 5.15.C)**. Coomassie staining of the SDS PAGE gel used for the western blot after the protein transfer (**Figure 5.15.D**), showed that the transfer was successful, which was also verified by Coomassie staining of the PVDF membrane post film exposure (**Figure 5.15.B).**

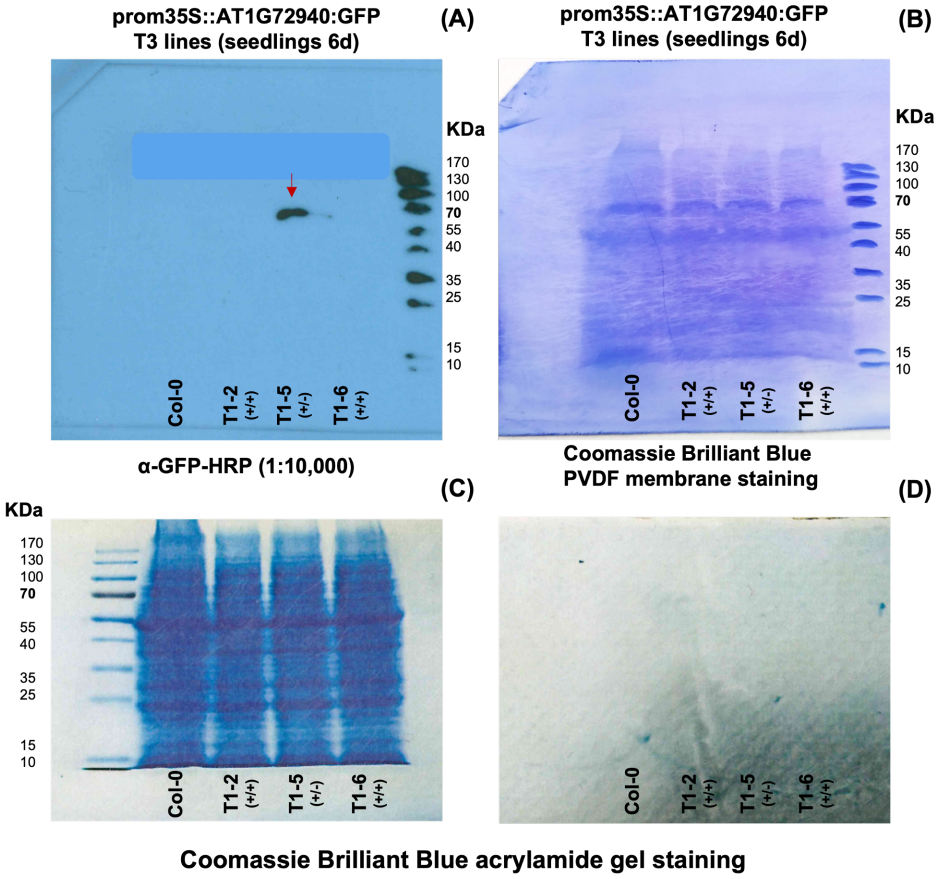

***Figure 5.15*Immunoblot detection of protein AT1G72940 in 6 days old seedings of transgenic *prom35S::AT1G72940:GFP A. thaliana* T3 lines.**

Ten homozygous 6 days old T3 generation seedlings of *prom35S::AT1G72940:GFP* lines T1-2 and T1-6 and the heterozygous line T1-5 (*pFAST-R* selected) were used for crude protein extraction, analysed with SDS PAGE electrophoresis and transferred on activated PVDF membranes for

immunoblot detection (western blotting). The expected MW for AT1G72940:GFP is ~73KDa. Col-0 seedlings were used as negative control. **(A**) Visualisation of extracted tagged proteins on X-ray film following O/N exposure. *prom35S::AT1G72940:GFP* lines T-2, T1-5 and T1-6 were tested for AT1G72940 expression. Only *prom35S::AT1G72940:GFP* line T1-5 shows the GFP signal (red arrow) coinciding with the 70KDa band of the protein ladder. **(B)** Staining of the PVDF membrane post X-ray film exposure with Coomassie Brilliant Blue solution to verify the successful transfer or proteins on the membrane. **(C)** Coomassie Brilliant Blue staining of a second SDS PAGE gel, to visualise the efficiency of crude extraction. Only 1/3 of the total protein extract used for the western blot was loaded for Coomassie staining. **(D)** SDS PAGE gel used for western blotting stained with Coomassie Brilliant Blue solution post transfer. The image shows that there are no detectable traces of proteins on the gel, so the transfer on the PVDF membrane (B) was successful.

(+/-): heterozygous for the T-DNA insertion

(+/+): homozygous for the T-DNA insertion

Figure 5.16 presents the results of AT1G72940 protein detection in the T3 generation of the transgenic lines constitutively overexpressing *AT1G72940,* in various developmental stages. We analysed the abundance of protein AT1G72940 expressed in homozygous plants of T3 *prom35S::AT1G72940:GFP* and *prom35S::AT1G72940:FLAG* lines, and the heterozygous line *prom35S::AT1G72940:GFP* T1-5 at 18 days (18d) and 5 weeks (5w) post germination. The crude protein extract of 6 days old *prom35S::AT1G72940:GFP* T1-5 seedlings was used as a previously tested positive control for GFP detection (see **Figure 5.15**). Protein extract of a FLAG-tagged spCAS9 protein (donated by Claudia Payacan-Ortiz, PhD, University of Warwick) was used as a positive control for FLAG detection.

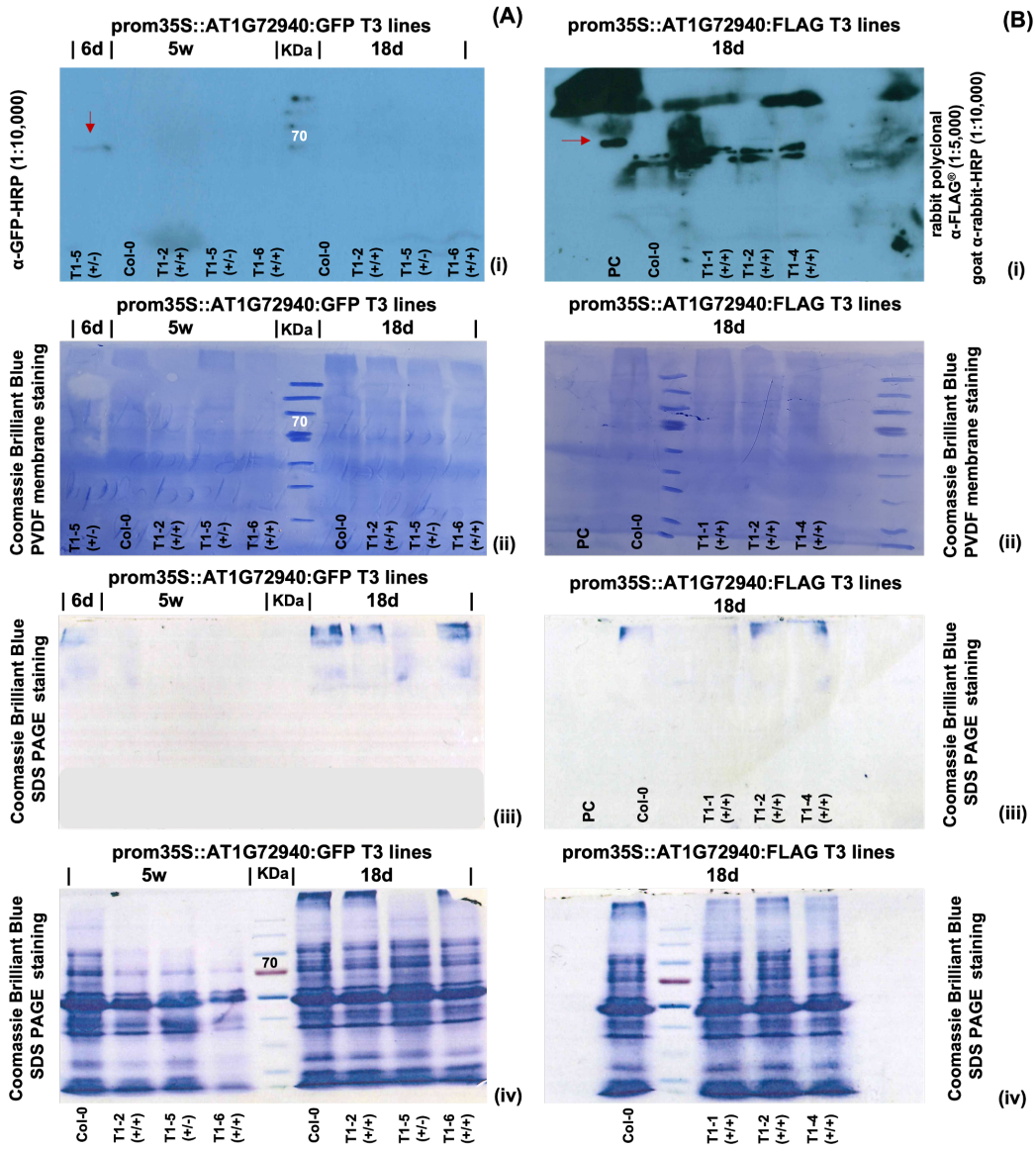

Figure 5.16 **Immunoblot detection of protein AT1G72940 in various developmental stages of the T3 generation of transgenic *A. thaliana AT1G72940* overexpressing lines.**

Homozygous plants of T3 *prom35S::AT1G72940:GFP* and *prom35S::AT1G72940:FLAG* lines, and the heterozygous line *prom35S::AT1G72940:GFP* T1-5 (*pFAST-R* selected) at 18 days (18d) and 5 weeks (5w) post germination were used for crude protein extraction. Protein extracts were analysed with SDS PAGE electrophoresis and transferred on activated PVDF membranes for immunoblot detection (western blotting). The expected MW for AT1G72940:GFP is ~73KDa and for AT1G72940:FLAG is ~48KDa. Col-0 plants were used as negative control. The crude protein extract of *prom35S::AT1G72940:GFP* line T1-5 (6 days old seedlings) was used as a previously tested positive control for GFP detection. Protein extract of a FLAG-tagged spCAS9 protein (donated by Claudia Payacan-Ortiz, PhD, University of Warwick) was used as a positive control for FLAG detection. **(Ai)** Visualisation of extracted tagged proteins on X-ray film following O/N

exposure of constitutively overexpressing *prom35S::AT1G72940:GFP* lines tested for AT1G72940 expression. Protein AT1G72940 is faintly detected (red arrow) in the control *prom35S::AT1G72940:GFP* line T1-5 (6d), but not in lines T1-2, T1-5 and T1-6 at 18d and 5w post germination. **(Bi**) Visualisation of extracted tagged proteins on X-ray film following 1hr exposure of constitutively overexpressing *prom35S::AT1G72940:FLAG* lines tested for AT1G72940 expression. Protein spCAS9 is detected (red arrow) in the positive control. Protein AT1G72940 is not detected in any of the tested *prom35S::AT1G72940:FLAG* lines at 18d post germination. **(Aii)** and **(Bii)** show the staining of the PVDF membranes post X-ray film exposure with Coomassie Brilliant Blue solution to verify the successful transfer of proteins on the membranes. Membranes correspond to the respective X-ray films in **(Ai)** and **(Bi). (Aiii)** and **(Biii)** SDS PAGE gels used for western blotting stained with Coomassie Brilliant Blue solution post transfer. The images show that there are no detectable traces of of proteins on the gel, so the transfer on the PVDF membranes was successful. Gels correspond to the respective PVDF membranes in **(Aii)** and **(Bii). (Aiv)** and **(Biv)** show the Coomassie Brilliant Blue staining of the extra SDS PAGE gels, to visualise the efficiency of crude extraction. Only 1/3 of the total protein extract used for the western blot was loaded for Coomassie staining. Gels correspond to the respective samples in **(Ai**) and **(Bi)**.

(+/-): heterozygous for the T-DNA insertion

(+/+): homozygous for the T-DNA insertion

Figure 5.16.Ai shows that AT1G72940 is faintly detected (red arrow) in the control *prom35S::AT1G72940:GFP* line T1-5 (6d), but not in lines T1-2, T1-5 and T1-6 at 18d and 5w post germination. **Figure 5.16.Bi** shows that protein spCAS9 is detected (red arrow) in the positive control, however AT1G72940 is not detected in any of the tested *prom35S::AT1G72940:FLAG* lines at 18d post germination. The detection of spCAS9 in the positive control rules out the possibility of a dysfunctional α-FLAG® antibody. **Figure 5.16** images **(Aii)** to **(Aiv)** and **(Bii)** to **(Biv)** show that there was sufficient amount of crude protein extract and that the transfer of proteins on the PVDF membrane was successful. The results show that protein AT1G7940 is borderline detected in the crude protein extract at an early developmental stage (6 days) of *prom35S::AT1G72940:GFP* line T1-5, but not in older seedlings (18 days) or adult plants (5 weeks). The results for the remaining *prom35S::AT1G72940:GFP* lines and *prom35S::AT1G72940:FLAG* lines are consistent with the previous western blots showing no detection of protein AT1G7940 in any of the developmental stages tested.

The lack of successful detection of protein AT1G7940 in the majority of the constitutively and inducible overexpressed *AT1G7940* transgenic lines led to RT-q-PCR analysis of the *AT1G72940* transcript levels in the same lines and/or developmental stages of the transgenic plants. Primer pair [VN1153/VN1154] was designed to detect the *AT1G72940* transcript levels in both WT and transgenic *A. thaliana AT1G72940* overexpressing plants, as it amplifies a small region at 3' end of the transcript that detects both endogenous and transgene-deriving transcripts. This pair of primers was chosen specifically to detect *AT1G72940* mRNAs at all *AT1G72940* transgenic lines, regardless of the tag used. The ability to detect the endogenous mRNAs allows us to compare the transcript levels in *AT1G72940* transgenic lines to the basal *AT1G72940* expression and determine whether there is overexpression. It is also designed to allow comparison between induced and uninduced plants of the inducible *promDEX::AT1G72940* lines, by detecting just the basal gene expression in the uninduced plants and the total expression of the endogenous gene and the transgene in the induced plants. Using primers that detect only the specific transgenes would allow us to measure the level of the transgene expression and genotype between different transgenes, but we wouldn't be able to compare against Col-0. The primers were first tested with normal PCR instead of RT-q-PCR, using as template the L2 T-DNA vectors used to generate the transgenic *AT1G72940* plants to verify they are functional (**Figure 5.17**).

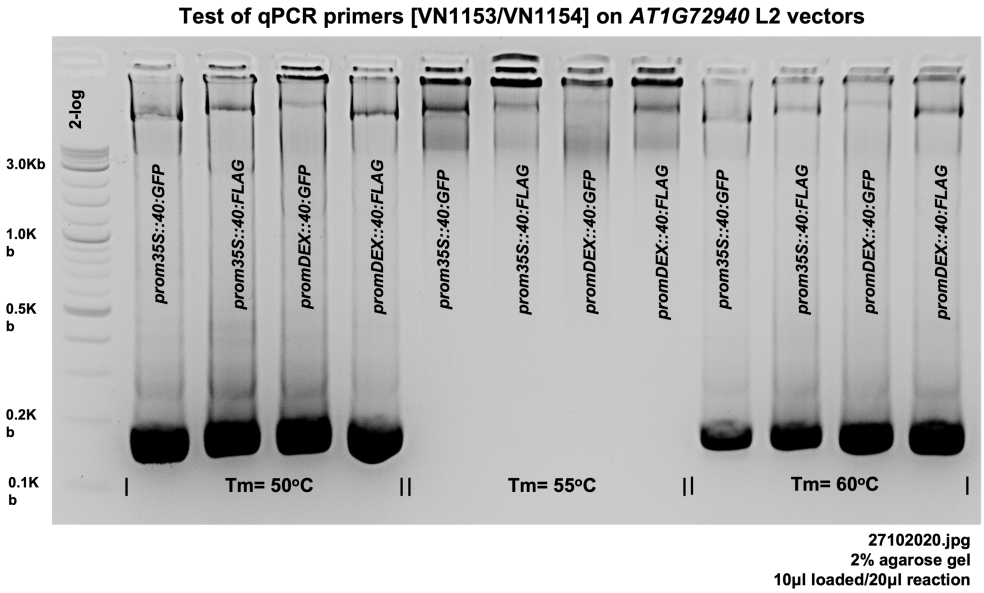

Figure 5.17 **Testing of primers pair designed for RT-q-PCR expression analysis of transgenic *A. thaliana AT1G72940* overexpressing lines.**

Primer pair [VN1153/VN1154] was designed to detect the *AT1G72940* transcript levels in the *A. thaliana AT1G72940* overexpressing lines. The primers were tested with normal PCR using as template the L2 T-DNA vectors used to generate the transgenic *AT1G72940* plants: *prom35S::AT1G72940:GFP:ACT2/pICSL4723[pFAST-R],* *prom35S::AT1G72940:FLAG:ACT2/pICSL4723[pFAST-R],* *promDEX::AT1G72940:GFP:ACT2/pICSL4723[pFAST-R + GVG],* and *promDEX::AT1G72940:FLAG:ACT2/pICSL4723[pFAST-R + GVG].* The expected size of the amplicon is 184bp (cDNA). Tm was tested at 50°C, 55°C and 60°C to identify the appropriate annealing temperature. Amplification of *AT1G72940* was successful at 50°C and 60°C. Tm= 60°C was selected for the RT-q-PCR to increased annealing specificity of the primers.

Additionally, prior to RT-q-PCR we genotyped and verified the expression of transcripts *AT1G72940:GFP* and *AT1G72940:FLAG* in the respective *prom35S::AT1G72940:GFP* lines and *prom35S::AT1G72940:FLAG* lines, using normal PCR amplification of the cDNA prepared for the RT-q-PCR reactions. Primer pairs [VN1145/VN1146] and [VN1147/VN1147] are designed to amplify different areas covering the sequence between gene *AT1G72940* and the *GFP* tag, thus ensuring the detection of *AT1G72940* transcripts originating only from the transgene and not the endogenous copy of the gene. In a similar manner, primers [VN1149/VN1150] are designed to

specifically amplify the area covering the sequence between *AT1G72940* and the *FLAG* tag.

In **Figure 5.18** *pFAST-R* selected plants of T2 and T3 generations of *prom35S::AT1G72940:GFP* and *prom35S::AT1G72940:FLAG* lines were tested with RT-q-PCR at 6 days (6d) and 6 weeks (6w) post germination for the presence of *AT1G72940* transcripts expressed only by the transgenes. The results verify the expression of *AT1G72940:GFP* and *AT1G72940:FLAG* transcripts at the respective samples and developmental stages tested. Col-0 did not generate any PCR product, verifying that primer pairs [VN1145/VN1146], [VN1147/VN1147] and [VN1149/VN1150] are specific to the transgene transcripts. Additionally, the results verified that each tested line is expressing the appropriate transgene, and that the transcription of the transgene is active in both generations and developmental stages.

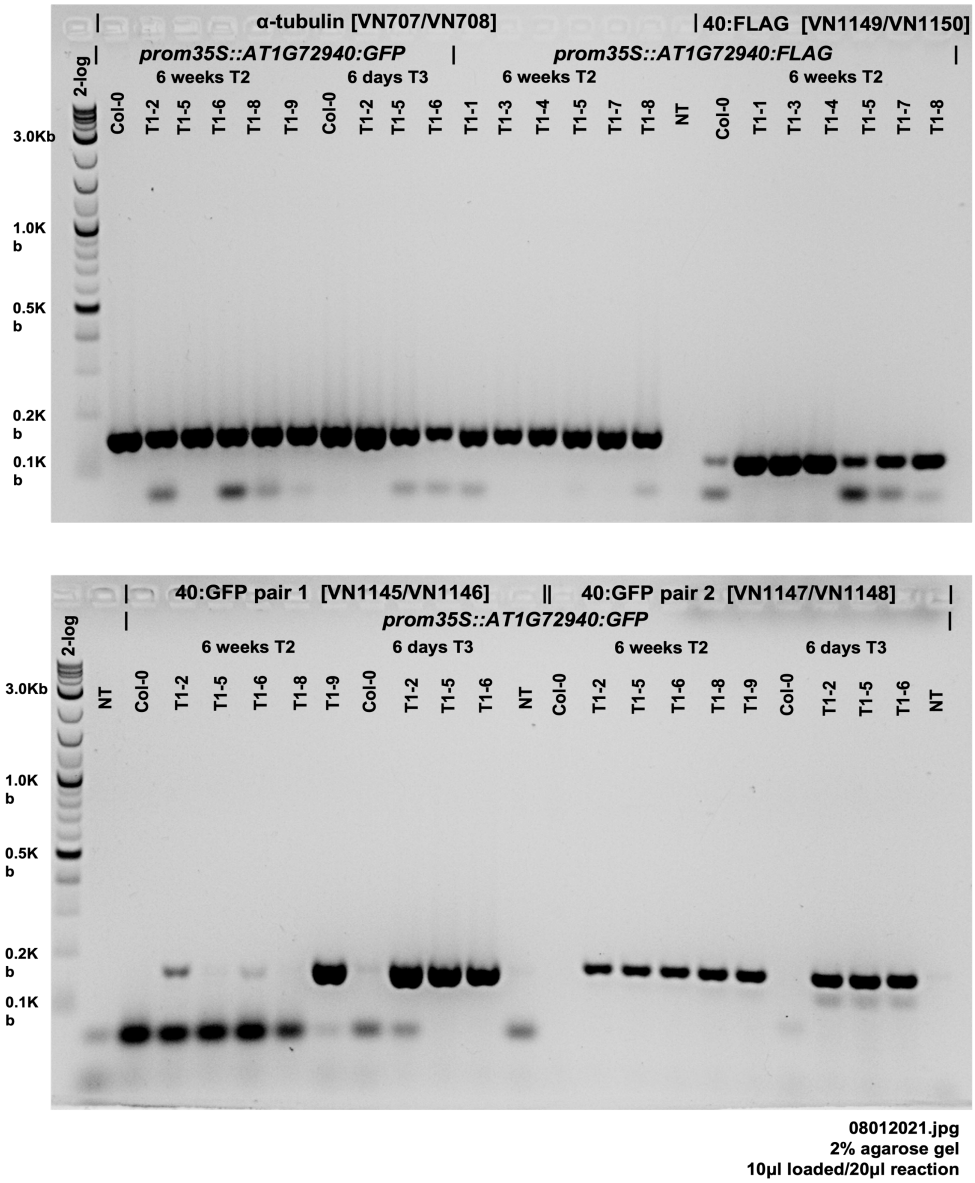

***Figure 5.18* PCR detection of *AT1G72940* transcript in transgenic *A. thaliana* *AT1G72940* overexpressing lines in different developmental stages.**

pFAST-R selected plants of T2 and T3 generations of *prom35S::AT1G72940:GFP* and *prom35S::AT1G72940:FLAG* lines were tested with RT-q-PCR at 6 days (6d) and 6 weeks (6w) post germination for the presence of *AT1G72940* transcripts expressed only by the transgenes. α-tubulin housekeeping gene was amplified to ensure equal levels of cDNA template generated in all tested samples. Primer pairs [VN1145/VN1146] and [VN1147/VN1147] are designed to amplify different areas covering the sequence between gene *AT1G72940* and the *GFP* tag, thus ensuring the detection of *AT1G72940* transcripts originating only from the transgene and not the endogenous copy of the gene. Likewise, primers [VN1149/VN1150] are designed to specifically amplify the area covering the sequence between *AT1G72940* and the *FLAG* tag. Col-0 and non-template (NT) samples were used as a negative control for the reaction. The results show the expression of *AT1G72940:GFP* and *AT1G72940:FLAG* transcripts at the respective samples and developmental

stages tested. Pair [VN1147/VN1147] generates more stable results than [VN1145/VN1146] for the detection of *AT1G72940:GFP* transcripts. Col-0 did not generate any PCR product, showing primer pairs [VN1145/VN1146], [VN1147/VN1147] and [VN1149/VN1150] are specific to the transgene transcripts.

In **Figure 5.19** we used RT-q-PCR to determine the relative expression levels of *AT1G72940* transcript in the T2 generation of the constitutively and inducible overexpressing *A. thaliana AT1G72940* adult plants. *AT1G72940* transcripts were amplified using RT-q-PCR primers pair [VN1153/VN1154] that detects all *AT1G72940* transcripts (endogenous and transgene-deriving). *AT1G72940* Ct values were normalised against the Ct values of the housekeeping gene *α-tubulin*. The relative expression levels of *AT1G72940* for each sample are presented as fold change (2^-ΔΔCt) of the basal expression of *AT1G72940* in the Col-0 sample. A two-tail t-test assuming unequal variances was used for the statistical analysis of the results and, unless stated otherwise, the statistically significant differences were calculated against the expression of *AT1G72940* in the Col-0 sample.

Figure 5.19.A shows the fold change of the relative expression levels of *AT1G72940* in 6-weeks-old *prom35S::AT1G72940:GFP* lines T1-2, T1-5, T1-6, T1-8 and T1-9, and *prom35S::AT1G72940:FLAG* lines T1-1, T1-2, T1-4, T1-5, T1-7 and T1-8, against Col-0. Each sample represents leaves originating from 3 plants within the same line. With the exception of *prom35S::AT1G72940:GFP* T1-5, the fold changes observed in the expression of *AT1G72940* for the other *prom35S::AT1G72940:GFP* lines tested are not statistically significant, when compared to basal *AT1G72940* in Col-0. The fold changes observed in the expression of *AT1G72940* for *prom35S::AT1G72940:FLAG* lines T1-1, T1-2, T1-4, and T1-5 were found to be statistically significant when compared to basal *AT1G72940* in Col-0, however not for *prom35S::AT1G72940:FLAG* T1-7 and T1-8. Collectively, the results showed that the detected increase in *AT1G72940* transcripts is much lower in *prom35S::AT1G72940:GFP* than in *prom35S::AT1G72940:FLAG* adult plants of T2 generation.

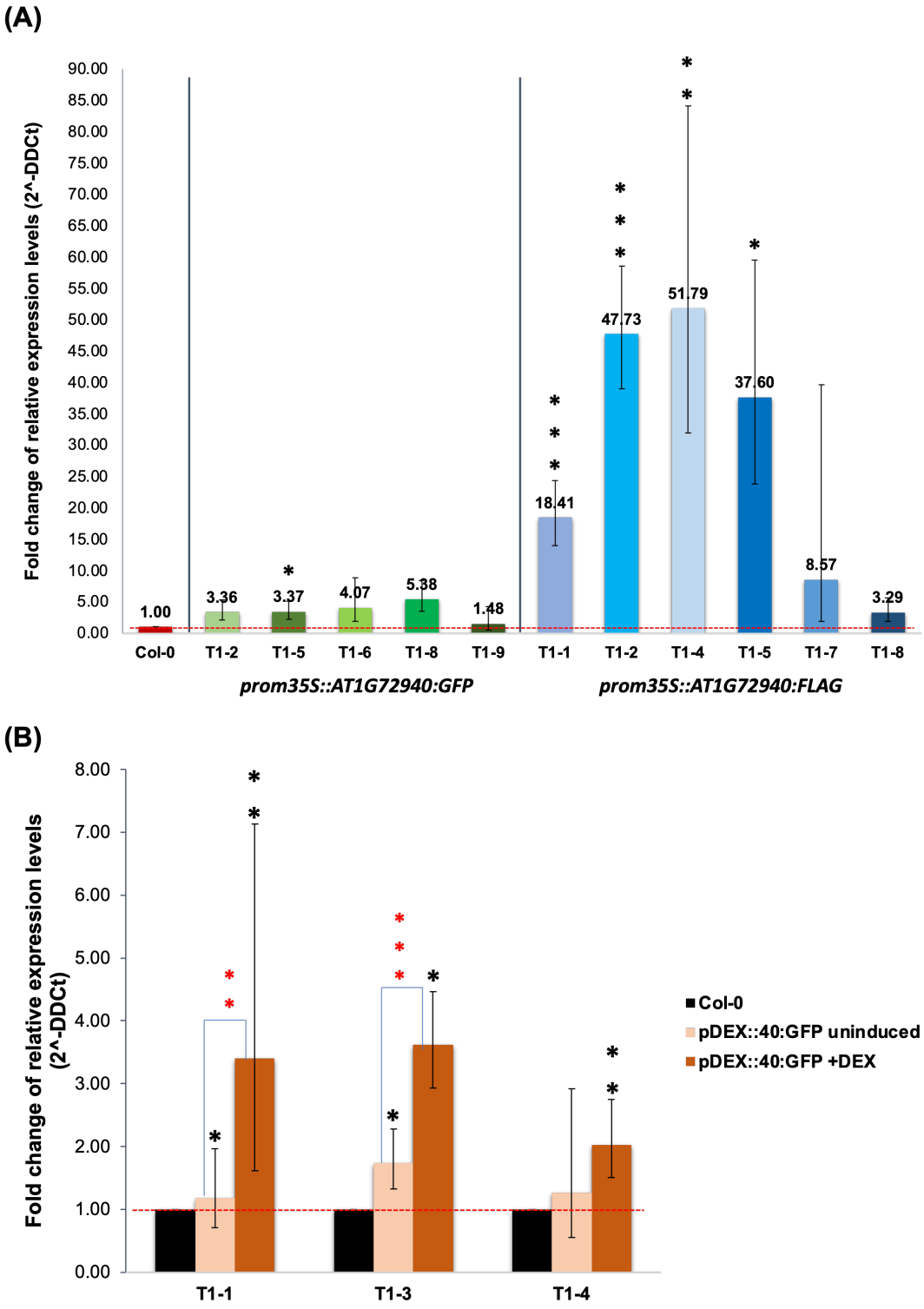

Figure 5.19 **Fold change of relative *AT1G72940* expression measured in the T2 generation of 6-week-old plants of the constitutively and inducible overexpressing *A. thaliana AT1G72940* transgenic lines.**

AT1G72940 transcripts were amplified using RT-q-PCR primers pair [VN1153/VN1154] that detects both the endogenous and the transgene-deriving transcripts. *AT1G72940* Ct values were normalised against the Ct values of the housekeeping gene *a-tubulin*, and the relative expression levels

are presented as fold change against the basal expression of *AT1G72940* in the Col-0 sample. Bar heights represent the average fold change ($2^{-\Delta\Delta Ct}$) in *AT1G72940* expression for each transgenic line, calculated from 3 plants per line. Error bars indicate the 95% confidence intervals for the fold change of relative Ct values. A two-tail t-test assuming unequal variances was selected for the statistical analysis. One asterisk (*) indicates statistically significant difference to 5%; two asterisks (**) indicate statistically significant difference to 1%; three asterisks (***) indicate statistically significant difference to 0.1%.**(A)** 6-weeks-old *prom35S::AT1G72940:GFP* lines T1-2, T1-5, T1-6, T1-8 and T1-9, and *prom35S::AT1G72940:FLAG* lines T1-1, T1-2, T1-4, T1-5, T1-7 and T1-8 were analysed with RT-q-PCR for *AT1G72940* expression levels against Col-0. **(B)** 6-weeks-old *promDEX::AT1G72940:GFP* lines T1-1, T1-3, and T1-4 were analysed with RT-q-PCR for *AT1G72940* expression levels against Col-0, with and without induction with DEX. Induced leaves were infiltrated with 30μM of DEX solution and samples were collected 16hrs later. Black asterisk indicate statistically significant differences in expression detected when Col-0 expression is used for reference; red asterisks indicate statistically significant differences in expression detected when the expression of the uninduced sample is used for reference.

Figure 5.19.B shows the fold change of the relative *AT1G72940* expression levels measured in 6-weeks-old *promDEX::AT1G72940:GFP* lines T1-1, T1-3, and T1-4 against Col-0, with and without dexamethasone treatment. Induced leaves were infiltrated with 30μM of DEX solution and samples were collected 16hrs later. Each measurement is the average of 3 biological replicates analysed per treatment, each biological replicate being a pool of leaves originating from 2 plants within the same line. Uninduced leaves for all tested lines already show higher *AT1G72940* transcript levels when compared to Col-0, and the difference is statistically significant for *promDEX::AT1G72940:GFP* lines T1-1 and T1-3, but not for T1-4. Leaves treated with DEX show an average 3 to 4-fold change for *promDEX::AT1G72940:GFP* lines T1-1 and T1-3, and 2-fold for *promDEX::AT1G72940:GFP* line T1-4 slightly lower. The significance of the increase in expression of *AT1G72940* was assessed also within each line (red asterisks), and it was found to be statistically significant post-DEX treatment for *promDEX::AT1G72940:GFP* T1-1 and T1-3, when compared to the uninduced samples, respectively, but not for *promDEX::AT1G72940:GFP* T1-4 .Collectively, the results show that the transcript levels of *AT1G72940* in T2 generation *promDEX::AT1G72940:GFP* adult plants are increased in

response to dexamethasone induction, and the increase is significant, albeit moderately low.

Figure 5.20 shows the fold change of the relative *AT1G72940* expression levels in different developmental stages of the T2 and T3 generations of the constitutively overexpressing *A. thaliana AT1G72940* transgenic lines. 6-days-old seedlings of T3 *prom35S::AT1G72940:GFP* lines, and 6-weeks-old *prom35S::AT1G72940:GFP* and *prom35S::AT1G72940:FLAG* lines were analysed to detect *AT1G72940* expression levels against Col-0. At 6 days of growth, *AT1G72940* expression is significantly increased in all T3 *prom35S::AT1G72940:GFP* lines, when compared to Col-0. However, at 6 weeks of growth, only *prom35S::AT1G72940:FLAG* lines T1-1, T1-2, T1-4, and T1-5 show any significant difference in *AT1G72940* expression against Col-0. Collectively, the results show that that the transcript levels of *AT1G72940* in T3 generation of *prom35S::AT1G72940:GFP* early developmental stages (6 days) are significantly higher compared to Col-0, but at 6 weeks they drop back to basal gene expression.

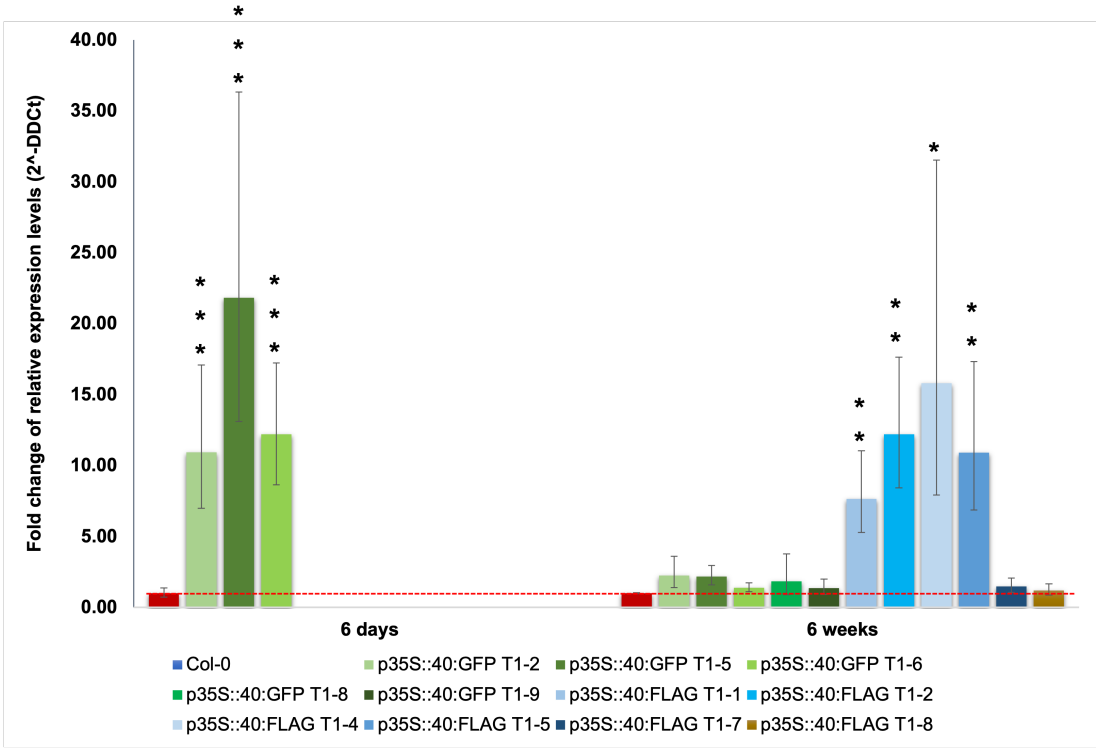

Figure 5.20 **Fold change of the relative expression levels of *AT1G72940* in different developmental stages of the T3 and T2 generations of the constitutively overexpressing *A. thaliana AT1G72940* transgenic lines.**

6-days-old seedlings of T3 *prom35S::AT1G72940:GFP* lines T1-2, T1-5 and T1-6, and rosette leaf number 8 of 6-weeks-old *prom35S::AT1G72940:GFP* lines T1-2, T1-5, T1-6, T1-8 and T1-9, and *prom35S::AT1G72940:FLAG* lines T1-1, T1-2, T1-4, T1-5, T1-7 and T1-8 were analysed to detect *AT1G72940* expression levels against Col-0 using RT-q-PCR. *AT1G72940* transcripts were amplified using RT-q-PCR primers pair [VN1153/VN1154] that detects both the endogenous and the transgene-deriving transcripts. *AT1G72940* Ct values were normalised against the Ct values of the housekeeping gene *a-tubulin*, and the relative expression levels are presented as fold change against the basal expression of *AT1G72940* in the Col-0 sample. Bar heights represent the average fold change ($2^{-\Delta\Delta Ct}$) in *AT1G72940* expression for each transgenic line, calculated from 3 plants per line. Error bars indicate the 95% confidence intervals for the fold change of relative Ct values. A two-tail t-test assuming unequal variances was selected for the statistical analysis. One asterisk (*) indicates statistically significant difference to 5%; two asterisks (**) indicate statistically significant difference to 1%; three asterisks (***) indicate statistically significant difference to 0.1%. At 6 days of growth, *AT1G72940* expression is significantly increased in all T3 *prom35S::AT1G72940:GFP* lines, when compared to Col-0. At 6 weeks of growth, only *prom35S::AT1G72940:FLAG* lines T1-1, T1-2, T1-4, and T1-5 show any significant difference in *AT1G72940* expression against Col-0.

(+/-): heterozygous for the T-DNA insertion

(+/+): homozygous for the T-DNA insertion

Figure 5.21 shows the fold change of the relative *AT1G72940* expression levels in different developmental stages of the T3 transgenic *A. thaliana* lines constitutively overexpressing *AT1G72940*. *prom35S::AT1G72940:GFP* lines T1-2, T1-5 and T1-6 at 6 days (seedlings), 18 days (older seedlings) and 5 weeks old (rosette leaves #8), and *prom35S::AT1G72940:FLAG* lines T1-1, T1-2 and T1-4 at 18 days (older seedlings) were analysed to detect *AT1G72940* expression levels against Col-0. At 6 days of growth, *AT1G72940* expression is significantly increased in all T3 *prom35S::AT1G72940:GFP* lines tested, when compared to Col-0, whereas at 18 days of growth *AT1G72940* expression for the same lines is already decreased to <5-fold change, albeit still significantly higher than Col-0. At 5 weeks of growth, *AT1G72940* levels in *prom35S::AT1G72940:GFP* lines T1-2, T1-5 and T1-6 are reduced to Col-0 levels of basal expression, and no statistically significant difference in *AT1G72940* expression is observed. At 18 days of growth, *AT1G72940* expression is significantly increased in all T3 *prom35S::AT1G72940:FLAG* lines tested, when compared to Col-0. Collectively, the results show that the transcript levels of *AT1G72940* in T3 generation of *prom35S::AT1G72940:GFP* early developmental stages (6 days) are significantly higher compared to Col-0, but they decrease almost 15-20 fold by the 18th day of growth and drop back to basal *AT1G72940* expression by the 5th week of growth, consistent with the findings shown in **Figure 5.19.A** and **Figure 5.20**. On the contrary, T3 *prom35S::AT1G72940:FLAG* lines show significantly increased *AT1G72940* expression when compared to Col-0 at 18 days of growth.

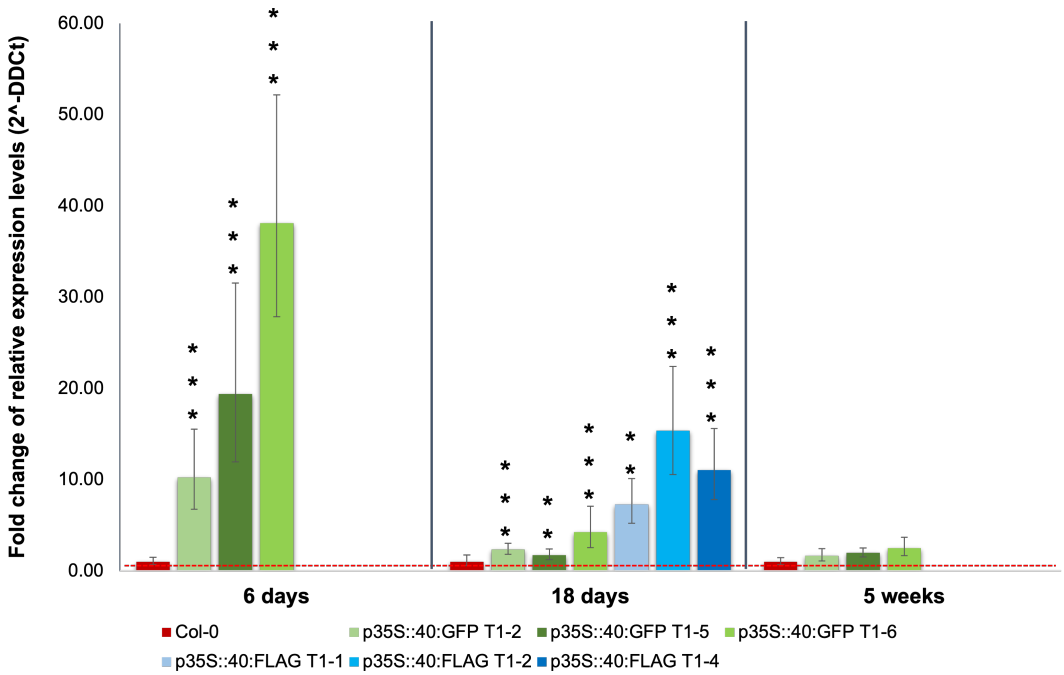

Figure 5.21 **Fold change of relative expression levels of *AT1G72940* in different developmental stages of the T3 constitutively overexpressing *A. thaliana AT1G72940* transgenic lines.**

T3 *prom35S::AT1G72940:GFP* lines T1-2, T1-5 and T1-6 at 6 days (seedlings), 18 days (older seedlings) and 5 weeks old (rosette leaf #8), and T3 *prom35S::AT1G72940:FLAG* lines T1-1, T1-2 and T1-4 at 18 days (older seedlings) were analysed to detect *AT1G72940* expression levels against Col-0 leaves using RT-q-PCR. *AT1G72940* Ct values were normalised against the Ct values of the housekeeping gene *a-tubulin*, and the relative expression levels are presented as fold change against the basal expression of *AT1G72940* in the Col-0 sample. Bar heights represent the average fold change ($2^{-\Delta\Delta Ct}$) in *AT1G72940* expression for each transgenic line, calculated from 3 plants per line. Error bars indicate the 95% confidence intervals for the fold change of relative Ct values. A two-tail t-test assuming unequal variances was selected for the statistical analysis. One asterisk (*) indicates statistically significant difference to 5%; two asterisks (**) indicate statistically significant difference to 1%; three asterisks (***) indicate statistically significant difference to 0.1%.. At 6 days of growth, *AT1G72940* expression is significantly increased in all T3 *prom35S::AT1G72940:GFP* lines tested, when compared to Col-0, whereas at 18 days of growth *AT1G72940* expression for the same lines is decreased to <5-fold change, however still significantly higher than Col-0; at 5 weeks of growth, no statistically significant difference in *AT1G72940* expression is observed. At 18 days of growth, *AT1G72940* expression is significantly increased in all T3 *prom35S::AT1G72940:FLAG* lines tested, when compared to Col-0.

5.2.3 Preliminary results of Pst DC3000 infection on selected A. thaliana AT1G72940 constitutively overexpressing lines

In parallel to identifying the expression levels of the different generations and various developmental stages of the *A. thaliana AT1G72940* constitutively overexpressing lines, *prom35S::AT1G72940:GFP* lines T1-2, T1-5 and T1-6, as well as *prom35S::AT1G72940:FLAG* lines T1-1, T1-2 and T1-4 were used in preliminary experiments assessing the bacterial growth following *Pst* DC3000 infection. **Figure 5.22** presents the results of the bacterial growth curves for Col-0 and *pFAST-R* selected heterozygous T2 plants of *prom35S::AT1G72940:GFP* and *prom35S::AT1G72940:FLAG* transgenic lines, when challenged with *Pst* DC3000. Plants of each genotype were infiltrated with virulent Pst DC3000 bacteria (O.D.= 0.001). Due to small sample number, a two-tail t-test assuming unequal variances was selected for the statistical analysis. At 3DPI, Col-0 plants show an average bacterial growth of 7.6 (log_{10} cfu/cm^2). All tested lines are more susceptible to *Pst* DC3000 than Col-0, and the differences observed are statistically significant, except for *prom35S::AT1G72940:GFP* T1-5 and *prom35S::AT1G72940:FLAG* T1-1.

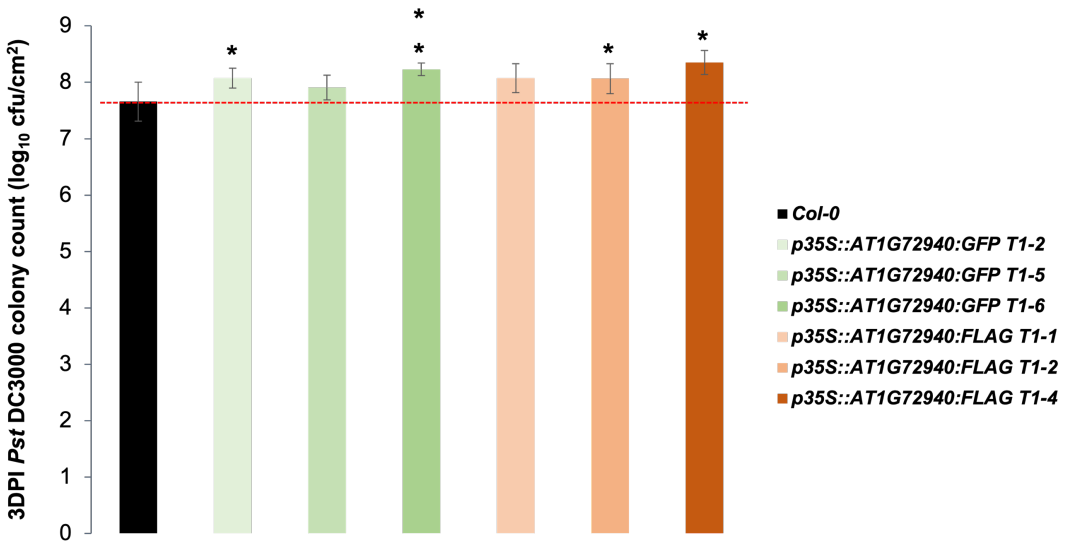

Figure 5.22 **Bacterial growth curves of T2 *A. thaliana AT1G72940* constitutively overexpressing lines when challenged with *Pst* DC3000.**

Pst DC3000 bacterial colony counts between Col-0 and *pFAST-R* selected heterozygous T2 plants of *prom35S::AT1G72940:GFP* lines T1-2, T1-5, and T1-6 and *prom35S::AT1G72940:FLAG* lines T1-1, T1-2, and T1-4. Rosette leaves number 7, 8 and 9 of 6-weeks-old plants were infiltrated with *Pst* DC3000 (O.D.= 0.001). All tested lines are more susceptible to *Pst* DC3000 than Col-0 and the differences observed are statistically significant, except for *prom35S::AT1G72940:GFP* T1-5 and *prom35S::AT1G72940:FLAG* T1-1. Bar charts represent the log10 of the average *Pst* DC3000 colony counts per cm^2 and the bars the standard error, calculated from 6 plants/treatment. One asterisk (*) indicates statistically significant difference to 5%; two asterisks (**) indicate statistically significant difference to 1%. Due to small sample number, a two-tail t-test assuming unequal variances was selected for the statistical analysis.

.

Figure 5.23 presents the results of the bacterial growth curves generated by the colony counts on 6 days old seedlings of Col-0 and the T3 generation of homozygous *prom35S::AT1G72940:GFP* lines T1-2 and T1-6, and heterozygous line T1-5, as well as *prom35S::AT1G72940:FLAG* lines T1-1, T1-2 and T1-4. Strains *Pst* DC3000 and *Pst* DC3000 *hrC* were used to challenge the overexpressing transgenic lines and Col-0. At 2DPI, when infected with *Pst* DC3000, Col-0 seedlings show an average bacterial growth of 8.6 (log_{10} cfu/10 seedlings) and they appear to be more susceptible to infection than any of the transgenic lines tested. When infected with *Pst* DC3000 *hrC,* Col-0 seedlings show an average bacterial growth of 6.5 (log_{10} cfu/10 seedlings) and appear to be less susceptible to infection than any of the transgenic lines tested. Collectively, the differences observed in the bacterial growth between the transgenic lines and Col-0 were found to be statistically significant. However, more replicates are required to draw conclusions, as this contradicts the results shown in **Figure 5.22,** where *prom35S::AT1G72940:GFP* lines and *prom35S::AT1G72940:FLAG* lines are more susceptible than Col-0 upon *Pst* DC3000 infection.

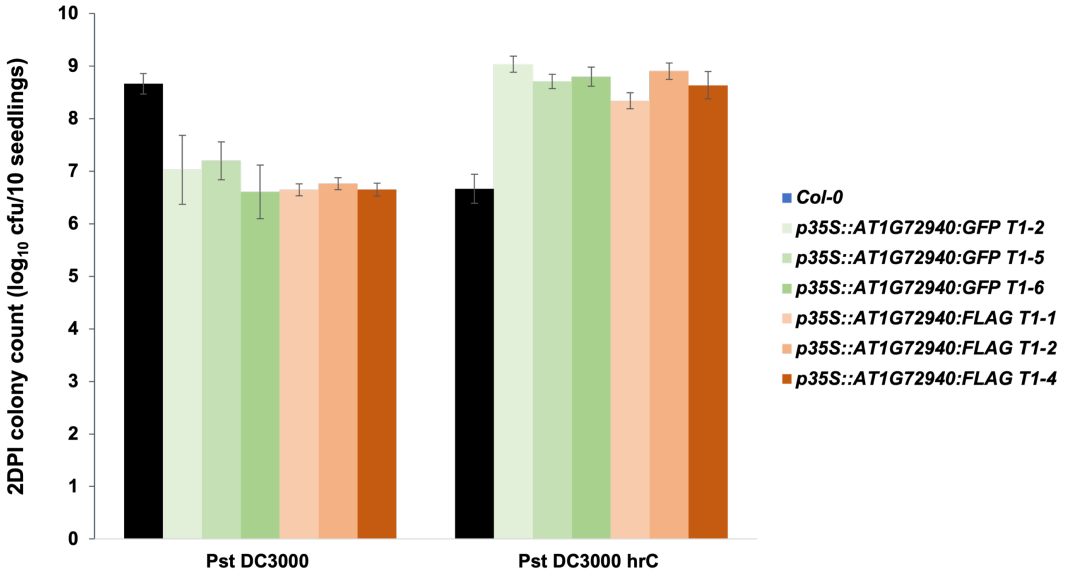

Figure 5.23 **Bacterial growth curves on 6 days old seedlings of T3 *A. thaliana AT1G72940* constitutively overexpressing lines when challenged with different strains of *Pst* DC3000.**

6 days old seedlings of the T3 generation of homozygous *prom35S::AT1G72940:GFP* lines T1-2 and T1-6, and heterozygous line T1-5, as well as the homozygous *prom35S::AT1G72940:FLAG* lines T1-1, T1-2 and T1-4 were used to measure *Pst* DC3000 bacterial growth colony counts against Col-0. Strains *Pst* DC3000 and *Pst* DC3000 *hrC* were used to challenge all plants. Seedlings were submerged for 1hr in the inoculum of each *Pst* DC3000 strain (O.D.= 0.01), washed and allowed the bacteria to grow for 48hrs. At 2DPI, when infected with *Pst* DC3000, Col-0 seedlings appear to be more susceptible to infection than any of the transgenic lines tested. When infected with *Pst* DC3000 *hrC,* Col-0 seedlings appear to be less susceptible to infection than any of the transgenic lines tested. Collectively, the differences observed in the bacterial growth between the transgenic lines and Col-0 were found to be statistically significant, so notation with asterisks was redundant. Bar charts represent the log10 of the average *Pst* DC3000 colony counts per 10 seedlings and the bars the standard deviation, calculated from 40 seedlings/treatment. Due to small sample number, a two-tail t-test assuming unequal variances was selected for the statistical analysis.

The bacterial growth in seedlings was repeated once more for 6 days old seedlings of Col-0 and the T3 generation of homozygous *prom35S::AT1G72940:GFP* lines T1-2 and T1-6, and heterozygous line T1-5. (**Figure 5.24).** Strains *Pst* DC3000 and *Pst* DC3000 *hrC* were used to challenge the overexpressing transgenic lines and Col-0. At 2DPI, when infected with *Pst* DC3000, there are no statistically significant differences between the bacterial growth in Col-0 and *prom35S::AT1G72940:GFP* lines.

When infected with *Pst* DC3000 *hrC, prom35S::AT1G72940:GFP* lineT1-6 is more susceptible to infection than Col-0, and the difference is statistically significant. Collectively, the results do not come in line with **Figure 5.23,** so more biological replicates are required before we draw conclusions.

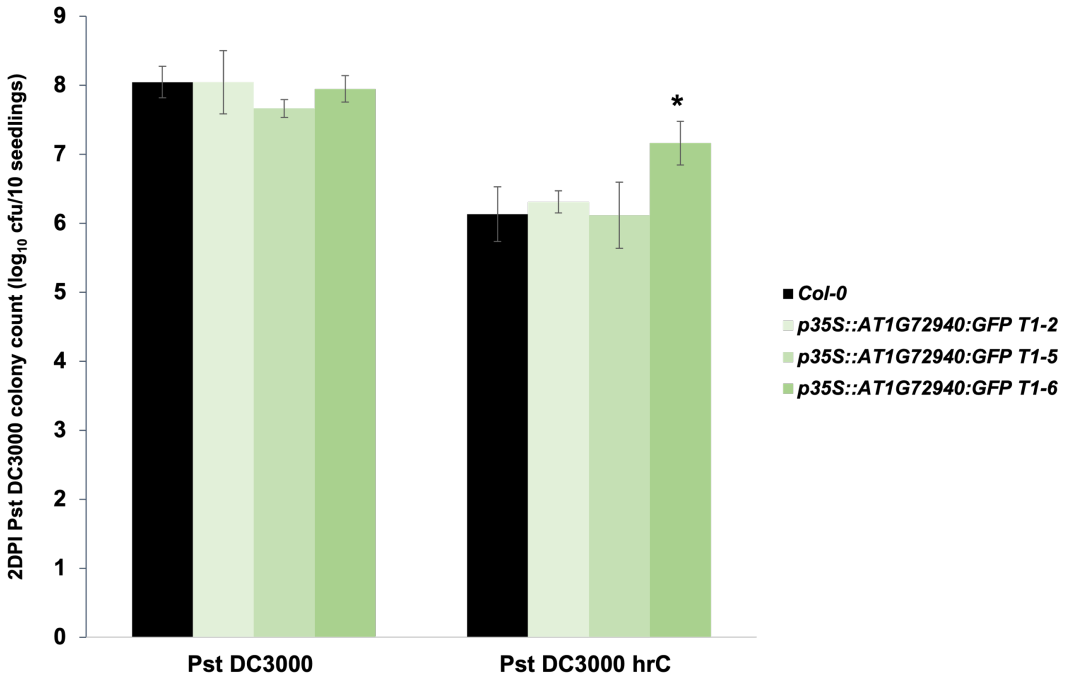

Figure 5.24 **Bacterial growth curves on 6 days old seedlings of T3 *A. thaliana p35S::AT1G72940:GFP* lines when challenged with different strains of *Pst* DC3000.**

6 days old seedlings of the T3 generation of homozygous *prom35S::AT1G72940:GFP* lines T1-2 and T1-6, and heterozygous line T1-5 were used to measure *Pst* DC3000 bacterial growth colony counts against Col-0. Strains *Pst* DC3000 and *Pst* DC3000 *hrC* were used to challenge all plants Seedlings were submerged for 1hr in the inoculum of each *Pst* DC3000 strain (O.D.= 0.01), washed and allowed the bacteria to grow for 48hrs. At 2DPI, when infected with *Pst* DC3000, there are no statistically significant differences between the bacterial growth in Col-0 and *prom35S::AT1G72940:GFP* lines. When infected with *Pst* DC3000 *hrC, prom35S::AT1G72940:GFP* lineT1-6 is more susceptible to infection than Col-0, and the difference is statistically significant. Bar charts represent the log10 of the average *Pst* DC3000 colony counts per 10 seedlings and the bars the standard deviation, calculated from 40 seedlings/treatment. One asterisk (*) indicates statistically significant difference to 5%; two asterisks (**) indicate statistically significant difference to 1%. Due to small sample number, a two-tail t-test assuming unequal variances was selected for the statistical analysis.

5.3 Discussion

In **Chapter 5** we aimed to generate and characterise new *A. thaliana* transgenic lines for constitutive and inducible overexpression of the *TN* genes of interest, as essential tools required to study the role of the *Arabidopsis TN* family in plant immunity and defence against the bacterial pathogen *Pst* DC3000. The impact of Covid-19 pandemic on laboratory research together with time gaps between *A. thaliana* generations compromised the ability to achieve the generation of transgenic lines for all *TN* genes, as well as the selection and characterisation of more transgenic lines for *AT1G72940*. Covid-19 pandemic led to the loss of all plant material grown before the lockdowns and set back the propagation of seeds thereafter, as plants were neglected due to the fact that access to the greenhouse was prohibited. Furthermore, limited availability of space for plant growth and money for high-throughput experiments, such as RNA sequencing and mass spectrometry, impacted many of the original targets and limited the number of biological replicates per experiment that could be achieved before the end of this PhD project.

As presented in **Section 5.2.1**, the attempt to subclone and express the *TN* genes of interest in *A. thaliana* stable transgenic lines was successful only for *AT1G72940*. Using the Golden Gate technology and the available plant tools and plant parts kits (Engler et al., 2014, 2012) gene *AT1G72940* was eventually subcloned into the final T-DNA vectors that facilitated the transformation of *A. thaliana* Col-0 plants to produce the various constitutively and inducible overexpressing lines. Gene *AT1G72950* was subcloned twice into GG vectors using different PCR products amplified by the original recombinant clones (not produced by the author). However, sequencing analysis revealed the presence of an additional codon in the 3' of the gene, which does not affect the reading frame but would result in the production of one extra amino acid missing from the WT protein, halting the production of *AT1G72950* stable transgenic overexpressing lines. The subcloning of genes *AT1G72920* and *AT1G72930* was attempted multiple times and proven unsuccessful.

Mutations discovered in the sequences of *AT1G72940* and *AT1G72950* when the newly made Level-0 and L1 GG clones were sequenced, indicate that the mutations are deriving from the original recombinant clones and they are not a product of the new PCR amplifications, as they are consistent after different amplification attempts. The presence of mutations give rise to the possibility of further sequence issues existing that could potentially halt the cloning process of the remaining *TN* genes. However, taking into account the lack of specific information on the cloning strategy and sequencing of the DNA templates used for the production of the original recombinant *TN* vectors, it is unclear if the new subcloning failed due to compatibility issues of the GG cloning and/or the viability of transformed *E. coli* cells, or due to unknown issues (such as mutations) carried over from the original clones.

Consequently, to produce the remaining *TN* stable *A. thaliana* overexpressing plants it is proposed that the future subcloning of genes *AT1G72920, AT1G72930* and *AT1G72950* is attempted via the amplification of the respective CDS from newly produced cDNA, or via the use of the genomic DNA sequences. Alternatively, synthesized copies of the gene sequences could also be used.

Stable transgenic *A. thaliana* plants *prom35S::AT1G72940:GFP* and *prom35S::AT1G72940:FLAG* were generated to facilitate the constitutively activated transcription of *AT1G72940*, which were designed to result in increased levels of AT1G72940 protein. Transient overexpression of AT1G72940 protein resulted in mild HR in *Nicotiana benthamiana* (Nandety et al., 2013) and at the time, there were no published information available on the effect of *AT1G72940* overexpression on stable transgenic *A. thaliana* plants. To avoid the possibility of AT1G72940 accumulation deleterious effects that could compromise the viability and development of the overexpressing plants, we generated dexamethasone-inducible and estradiol-inducible overexpressing lines. Stable transgenic *A. thaliana* plants *promDEX::AT1G72940:GFP* and *promDEX::AT1G72940:FLAG* were partially analysed, however the respective estradiol-inducible plants were produced but

not used in this PhD project due to time limitations and the need for comparable results with the previously made *promDEX::AT1G72940* and *promDEX::AT1G72940:HA:FLAG* lines that we analysed in **Chapter 4**.

5.3.1 Regulation of AT1G72940 transgene expression and the ability to detect AT1G72940 protein could be attributed to multiple factors

Analysis of the expression profile of *AT1G72940* transcripts through RT-q-PCR and AT1G72940 protein via western blotting of the previously mentioned plants raised some interesting topics for discussion. Protein AT1G72940 was detected via western blotting in crude extracts of early developmental stages (15-days-old) of *prom35S::AT1G72940:GFP* line T1-5 seedlings (T2 generation), but not in any of the remaining tested lines. It was also detected at lower amounts in 6-day-old seedlings of line T1-5 (T3 generation), but not in 18-day-old seedlings. Protein AT1G72940 was not detected in adult plants (5 -weeks-old) of any of the tested *prom35S::AT1G72940:GFP* lines in either T2 or T3 generations.

Non-detection of protein AT1G72940 in older seedlings and adult overexpressing plants suggested that it would be useful to measure the levels of *AT1G72940* transcription in the respective developmental stages and generations. The fold change of relative expression levels of *AT1G72940* generated with RT-q-PCR showed that, while *AT1G72940* transcript levels are significantly increased at early developmental stages (6-days-old) of all tested overexpressing *prom35S::AT1G72940:GFP* lines when compared to the WT, *AT1G72940* expression is visibly decreased (15 to 20-fold down) in older seedlings (18-days-old), and is almost levelled to Col-0 basal *AT1G72940* expression in adult plants (5-weeks-old). For *prom35S::AT1G72940:GFP* line T1-5, these findings are consistent with the detection of protein AT1G72940 only at 6-days-old seedlings, but fail to explain the lack of detected protein in *prom35S::AT1G72940:GFP* line T1-2 and T1-6. It should be noted that *prom35S::AT1G72940:GFP* line T1-5 is still segregating at T3 generation as opposed to *prom35S::AT1G72940:GFP* lines T1-2 and T1-6 (homozygous),

however AT1G72940 protein was not detected in them at 15-days-old seedlings in either T2 (heterozygous) or T3 (homozygous) stage.

AT1G72940 detection in *prom35S::AT1G72940:FLAG* plants was unsuccessful at all lines and developmental stages tested. Relative expression levels of *AT1G72940* showed that *AT1G72940* transcript levels are significantly increased at both older seedlings (18-days-old) and adult plants (5-weeks-old) for 4 out of the 6 tested overexpressing *prom35S::AT1G72940:FLAG* lines, compared to WT. The RT-q-PCR in the case of *prom35S::AT1G72940:FLAG* plants is therefore inconsistent with a lack of AT1G72940 protein detection in the same lines. Initially, we hypothesized that our α-FLAG® primary polyclonal antibody may have not been properly functional, so a different primary monoclonal α-FLAG® was tested on the same samples without any success (data not shown). We further tested the antibody by using as a positive control for FLAG detection a previously tested FLAG-tagged SpCAS9 protein (donated by Claudia Payacan-Ortiz, PhD). The results verified that our α-FLAG® primary polyclonal antibody was functional since the signal for SpCAS9 was successfully detected in the western blot, therefore the lack of AT1G72940 protein detection in *prom35S::AT1G72940:FLAG* lines is not attributed to the antibody.

5.3.1.1 Epigenetic silencing at the transcriptional and/or post-transcriptional level could affect AT1G72940 expression in the selected A. thaliana AT1G72940 overexpressing and inducible lines.

The *35S CaMV* promoter has been extensively used to drive constitutive expression of transgenes in many plants, including *A. thaliana*, facilitating plant biologists' attempt to uncover gene function (Amack and Antunes, 2020). Overexpression of a gene of interest in *A. thaliana* Col-0 background (wild type plants) can potentially result in phenotypes that provide important information regarding the function of the gene product. Employment of the regulatory

functions of *prom35S CaMV* has proven very useful, as it drives high levels of gene expression and can result in ectopic expression of the desirable protein in plants (Amack and Antunes, 2020). However, the variability in *prom35S CaMV* expression patterns observed among and within tissues of a plant species, as well as under different environmental conditions, should be taken into consideration when working with overexpressing transgenes (Schnurr and Guerra, 2000). A number of studies over the years have shown that *prom35S CaMV*-driven transgene expression can differ in plants, indicating that the promoter is not always constitutive and cannot ensure stable and high transgene expression in all parts of the plant, or regardless of the environmental conditions (Kiselev et al., 2021).

In addition, protein concentration resulting from transgene expression may vary significantly from the endogenous levels, which could affect the interaction of the protein with endogenous genetic factors. It has been observed that high levels of transgene expression that significantly differ from the endogenous levels of some proteins, can be deleterious for the plant (Jung et al., 2008; Lee et al., 2003; S. Li et al., 2014). Toxicity can derive from the accumulation of the protein itself or the protein's activity. Another possibility is that overexpression of the gene of interest may also activate the plant's gene silencing mechanisms, a side effect that can halt gene expression, especially in the subsequent generations (Rajeevkumar et al., 2015).

Epigenetic silencing describes the natural phenomenon where modifications of DNA, RNA, or histone proteins regulate the expression of genes, as a defence mechanism employed by host genomes against transposable elements and viral infection. Furthermore, it is responsible for regulating the expression of duplicate gene family members, while it also acts by silencing transgenes (Rajeevkumar et al., 2015). The molecular mechanism underlying epigenetic silencing has not been entirely elucidated yet, however it is suggested that it acts in two levels: transcriptional gene silencing (TGS) and post-transcriptional gene silencing. Over the last three decades there have been many reports of segregating transgenic plants deviating from the Mendelian ratios, indicating transgene instabilities (Charrier et al., 2000;

Stroud et al., 2013; Weinhold et al., 2013). The proposed reasons behind these instabilities were silencing of transcription due to promoter methylation, condensation of chromatin and/or post-transcriptional degradation of transcripts via diverse mechanisms (Fagard and Vaucheret, 2000).

Transgene silencing can occur in two different ways. One of them is when the transgene is silenced due to its position next to negatively-regulated host DNA or chromosomal location (Matzke et al., 2000). The second is known as homology-dependent gene silencing (HDGS), a type of epigenetic regulation occurring when multiple copies of the same or homologous sequence are introduced in a genome. TGS and PTGS are both types of HDGS that have been observed in transgenic plants (Jauvion et al., 2012). When it comes to TGS, genes that interact and share high levels of homology in promoter regions are highly methylated. On the other hand, PTGS requires high homology between the sequences of interacting genes which leads to sequence-specific transcript turnover in the cytosol. The level of homology between the transgene and endogenous gene, the complexity of the host genome, the genomic position of two transgenes are a few examples of factors that can influence HDGS. Additionally, increase of transcript levels above a gene-specific threshold induces specific degradation of homologous transcripts (Rajeevkumar et al., 2015).

In PTGS cases of epigenetic silencing, constitutive transcription does not result to accumulation of transcripts (Vaucheret et al., 1997). When transgenes and endogenous genes share high homology, PTGS is responsible for silencing both types of transcripts. Such cases occur when a plant is transformed with another copy of the same gene, which can also lead to silencing of the endogenous gene (Rajeevkumar et al., 2015). Homologous transcripts that derive from both the transgene and the endogenous gene have the potential to form double-stranded RNA (dsRNA), which is used as a template by RNA-directed RNA polymerase (RdRP). Transcription of dsRNA by RdRP would result in antisense RNAs, which could target complementary transcripts for degradation by dsRNA-specific RNases (Bond and Baulcombe, 2015).

The results from evaluating the expression levels of *AT1G72940* stable overexpressing *A. thaliana* transgenic lines presented in this chapter showed that the *AT1G72940* transcript is detected in high levels only at the early developmental stages of the *prom35S::AT1G72940:GFP* plants (6 days). Non-detection of the transcript at later developmental stages of all tested lines indicates that the transgene may undergo epigenetic silencing as the plants grow older, or not expressed in all types of plant cells and/or tissues despite the use of 35S CaMV promoter. Overexpressing transgenic plants tend to accumulate higher levels of transcripts deriving from the transgene expression between the seedling and adult stages of plants.

The expression profile of *prom35S::AT1G72940:FLAG* plants showed that *AT1G72940* transcript levels remain significantly high from the seedling stage until adulthood for at least half of the tested lines, however protein AT1G72940 is not detected at any tested developmental stage. This outcome suggests that half of the tested lines do not undergo TGS since the levels of transcription remain high as the plants grow older. One possibility is that the lines selected for *prom35S::AT1G72940:FLAG* do not exhibit very high transgene expression compared to *prom35S::AT1G72940:GFP* lines, thus the cumulative transcript levels do not exceed the gene-specific threshold that would trigger PTGS.

5.3.1.2 Long non-coding RNAs located between TN genes in the Arabidopsis locus could be responsible for regulating expression in the absence of pathogens, thus affecting the expression of AT1G72940 transgene

Another emerging factor of gene silencing is long non-coding RNAs (lncRNAs). They are defined as transcripts longer than 200bp that lack coding potential and are therefore unable to construct a full-length protein, which makes them different than mRNA (Kapranov et al., 2007). Plant genomes produce thousands of lncRNAs from intergenic, intronic or coding regions

(Wang and Chekanova, 2017). Most lncRNAs are classified based on their relationships to protein-coding genes: long intergenic ncRNAs (lincRNAs), lncRNAs produced from introns (incRNAs), and antisense RNAs and natural antisense transcripts (NATs), which are transcribed from the antisense strand of genes. The expression levels of incRNAs and NATs differ depending on the tissue and they also change in response to biotic or abiotic stress, indicating that they are subjected to dynamic regulation and have a role in the regulation of development and stress responses (Liu et al., 2012).

While their role is not fully elucidated, emerging evidence over the recent years support that lncRNAs function in gene silencing, flowering time control, root organogenesis, seedling photomorphogenesis, abiotic stress responses, and reproduction (Wang and Chekanova, 2017). lncRNAs affect gene regulation through a variety of complex mechanisms. They can serve as precursors to small RNAs (smRNAs) or act as decoys that mimic the DNA or RNA targets of regulatory proteins and microRNAs. In plants, lncRNAs have an important role in epigenetic silencing through siRNA-dependent DNA methylation (RdDM), which acts as a repressor of transcription of transposons and repetitive sequences (Wang and Chekanova, 2017).

Figure 5.25 shows three lncRNAs that have been identified in the same genetic locus as our *TN* genes of interest (Araport11, TAIR). The figure shows that lncRNAs *AT1G09343.1, AT1G09353.1*, and *AT1G09357.1* are transcribed from the antisense strand and are located in the intergenic regions between our *TN* genes of interest. *AT1G09343.1* lncRNA is positioned between genes *AT1G72910* and *AT1G72920, AT1G09353.1* lncRNA is positioned between genes *AT1G72930* and *AT1G72940,* and *AT1G09357.1* lncRNA is positioned between genes *AT1G72940* and *AT1G72950*. Even though there is no information available on the function of those lncRNAs, according to TAIR there are several mutant lines available for T-DNA insertions on *AT1G09353.1 and AT1G09357.1* genomic regions. Analysis of those mutant lines could potentially provide useful information on the role of those lncRNAs and whether they function in regulatory mechanisms that control the expression of our *TN* genes of interest. As previously discussed in

Chapter 4, this *TN* locus is a cluster of several *TN* and some *TNL* genes arranged in different orientations and this arrangement is potentially selected to favour functionality (Meyers et al., 2002). Consequently, we cannot exclude the possibility that the position of those lncRNAs could be part of the *TN* regulatory mechanism. One of the possible scenarios to consider is that they may function to control the expression levels of the flanking *TN* genes via PTGS.

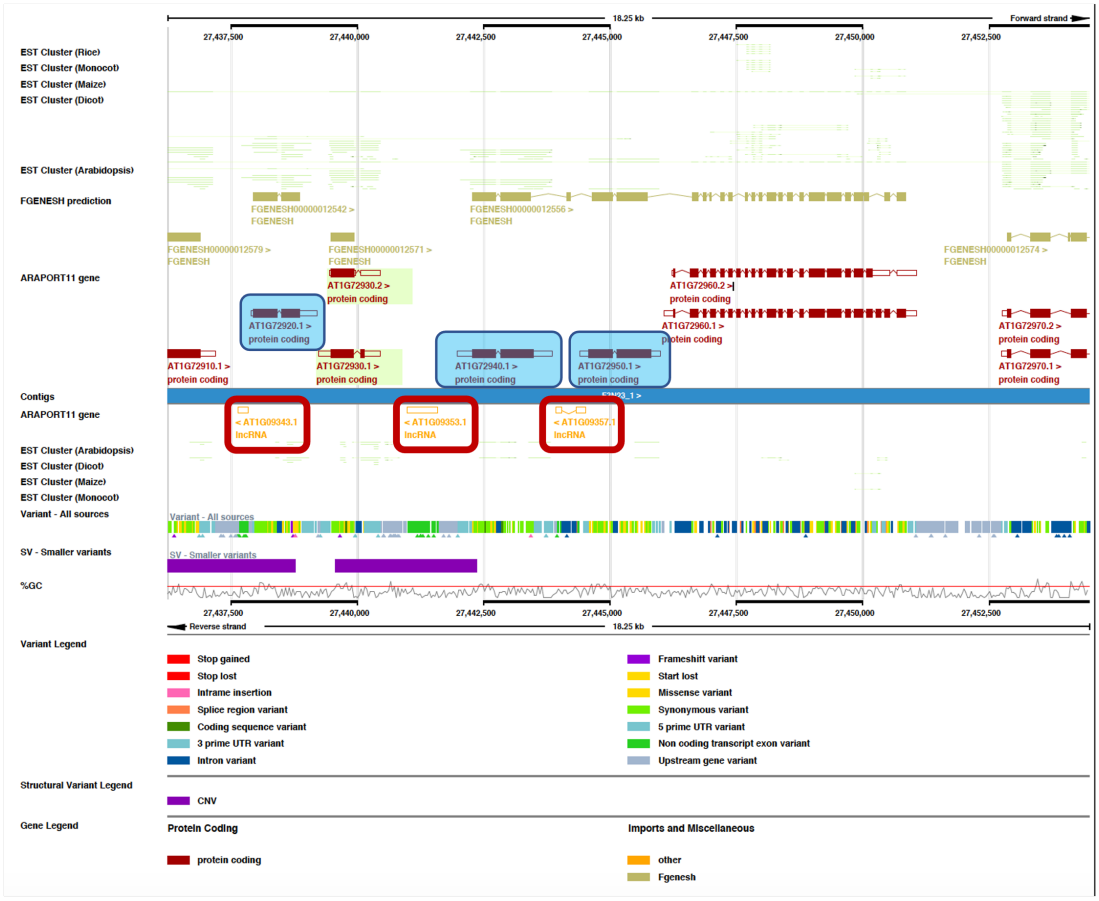

***Figure 5.25* Long non-coding RNAs identified in the *TN* locus of *A. thaliana* genome.**

Three long non-coding RNAs (lncRNAs, red boxes) have been found in the Araport11 genome release (TAIR), located in the same *A. thaliana* genetic locus as our *TN* genes of interest. According to TAIR, they are all transcribed from the antisense strand than the *TN* genes (blue boxes). DNA sequences coding for lncRNAs *AT1G09343.1*, *AT1G09353.1*, and *AT1G09357.1* are located in the intergenic regions between our *TN* genes of interest and are marked on the figure with red boxes. *AT1G09343.1* lncRNA is positioned between genes *AT1G72910* and *AT1G72920*, *AT1G09353.1* lncRNA is positioned between genes *AT1G72930* and *AT1G72940*, and *AT1G09357.1* lncRNA is positioned between genes *AT1G72940* and *AT1G72950*.

5.3.1.3 Epigenetic silencing at the protein level could affect AT1G72940 protein detection in the selected A. thaliana AT1G72940 overexpressing and inducible lines.

Protein synthesis is the most energy-costly process of the cells and its regulation is strictly controlled even in the cases of extreme environmental conditions (Edwards et al., 2012). Regulation of protein synthesis in many cases is happening in the transcriptional level, which is why a constitutive promoter has been selected for overexpression of *AT1G72940.* As we have already discussed in this section, post-transcriptional regulation of transcripts can control if a protein will be synthesized. Epigenetic silencing may be partially the reason why we were unable to detect protein AT1G72940 in older seedlings or adult *prom35S::AT1G72940:GFP* and *prom35S::AT1G72940:FLAG* plants. However, non-detection of the protein at those developmental stages could also potentially be attributed to protein turnover due to post-translational modifications.

Plants have evolved to regulate protein synthesis and turnover in different environmental conditions and developmental stages, balancing the energy cost depending on the importance of each respective protein through a combination of transcriptional, post-transcriptional, translational and post-translational mechanisms (Nelson and Millar, 2015). Post-translational modification of a protein affect, among other things, its stability. Phosphorylation is one of the most studied forms of post-translational modifications that affect stability of proteins in plants, such as the PSII proteins D1 and D2 (Koivuniemi et al., 1995). Non-enzymatic modifications of proteins that occur during oxidative stress can cause changes in protein structure and folding which ultimately lead to protein degradation. Extensive oxidation often leads to the formation of protein aggregates with loss of function that can be proven deleterious for the cells (Nelson and Millar, 2015). It is still unclear why some proteins are degrading in a faster rate than others and how that accelerated turnover rate is connected to post-translational modifications. In some cases, fast protein turnover is attributed to removal of damaged proteins

(Koivuniemi et al., 1995), whereas in other cases a short protein half-life would allow for rapid response to changing environmental factors (Yang et al., 2010).

Protein degradation in the cytosol and the nucleus mainly occurs through the ubiquitin proteasome system (UPS), when E1, E2 and E3 ligases tag proteins with ubiquitin for degradation (Nelson and Millar, 2015). When a polyubiquitin chain is formed following multiple cycles of ubiquitination, the proteasome gets the signal for degradation. The proteasome is a large protein complex that changes under biotic stress, offering plants a level for flexibility in terms of the rate and extend of protein degradation (Sun et al., 2013).

5.3.1.4 Technical limitations could affect protein AT1G72940 detection

We should consider the possibility that the use of crude protein extraction has limitations to protein detection, due to the fact that the whole pool of proteins extracted is used to detect one protein of interest. In the cases that the protein of interest is not abundant or overrepresented in the cells, crude protein extraction may not be the best approach. When young seedlings (6 days old) are used for protein extraction, it is possible that the small size and large number of seedlings used allow for more concentrated protein extract that can fit the SDS PAGE gel loading capacity. Furthermore, when seedlings are used, we are extracting protein from all developed types of plant cells. However, extraction from adult plants is limited to crude extract of one or two leaves per sample. When the protein of interest is not abundant in the leaf cells, detection may become challenging in the crude extract, as the protein concentration is diluted by the presence of other proteins.

Therefore, before drawing conclusions, we propose that detection of protein AT1G72940 in *prom35S::AT1G72940:GFP* and *prom35S::AT1G72940:FLAG* transgenic plants should be attempted by protein extraction and immunoprecipitation (IP) from both seedlings and adult plants. Detection of AT1G72940 after IP would be informative of the abundance of the protein in the transgenic lines and the developmental stage it can be detected. While

non-detection of AT1G72940 post IP would be indicative of non-production, low detected levels could suggest that AT1G72940 synthesis is heavily regulated by the plant, or that the protein is degraded. Inhibiting the activity of the proteasome would be a reasonable approach to address post-translational modifications of AT1G72940. If the protein is detected through IP, then a mass spectrometry analysis would potentially provide with more information regarding potential targets or interactors of AT1G72940, that could give more insight on the role of AT1G72940 in plant immunity.

5.3.2 Preliminary results of Pst DC3000 bacterial colony counts in AT1G72940 overexpressing lines are inconsistent with AT1G72940 protein detection

Regarding the results of the bacterial growth on *prom35S::AT1G72940:GFP* and *prom35S::AT1G72940:FLAG* plants following *Pst* DC3000 infection, the data deriving from only one biological repeat are not sufficient to draw any conclusions yet. The preliminary results in adult plants showed that all tested lines, with the exception of *prom35S::AT1G72940:GFP* line T1-5, are more susceptible to infection compared to Col-0 and that difference is statistically significant. However, the lack of AT1G72940 protein detection at the same developmental stage raises the question of whether the recorded susceptibility of the transgenic plants to *Pst* DC3000 is correlated to the expression of the transgene. Our initial hypothesis speculated that specific bacterial-delivered effectors upregulate the TN genes as a virulent mechanism aiming to dampen NLR- mediated resistance. We hypothesized that TNs could potentially form heterodimers with full length TNLs, thus acting as negative regulators of immunity by preventing TNLs from effector recognition and disrupting ETI. However, in the absence of AT1G72940 protein that scenario seems unlikely in the overexpressing *AT1G72940* lines.

One possible explanation would be the recently discovered potential of plant TIR domains as NAD+ hydrolases required for immune signal transduction (Horsefield et al., 2019; Wan et al., 2019). It is speculated that the compounds generated by plant TIR NAD+ consumption may be signalling downstream

immune components (Wan et al., 2019). Plant TIR NADse activity produces the compounds NAM, ADPR, and v-cADPR (variant cADPR), which is a different compound with unknown chemical structure that has a near identical HPLC retention time and molecular mass to the product of an archaeal TIR, TcpO (Essuman et al., 2018; Wan et al., 2019). v-cADPR was also detected after activation of RBA1 upon recognition of the *Pst* DC3000 effector HopBA1 (Wan et al., 2019). Activated TIRs in planta did not require EDS1 or NRG1, which are known signalling components downstream of TIR containing proteins (Wan et al., 2019), indicating that v-cADPR accumulation occurs upstream of both known signalling mechanisms initiated by TIR proteins and HR.

Similar to other NAD+-deriving compounds, v-cADPR could also exhibit signalling properties (Grant et al., 2000; Marcec et al., 2019). Since the production of v-cADPR is so far known to be correlated to TIR enzymatic function, it can serve as a biomarker for plant TIR activity. Nevertheless, there is still not enough evidence to support if it is sufficient to trigger cell death and defence, since it is still to be detected *in planta* (Horsefield et al., 2019). It is speculated that EDS1- being a downstream component of TIR-proteins signalling – would make a reasonable target of v-cADPR signal transduction, but it is yet to be investigated how v-cADPR is implicated in plant immune responses.

It is possible that the lack of AT1G72940 protein detection in *prom35S::AT1G72940:GFP* and *prom35S::AT1G72940:FLAG* lines does not necessarily show that the protein was never produced and/or being active. AT1G72940 expression levels that are higher than the normal levels of the protein outside of *Pst* DC3000 infection state, may cause elevated NAD+ hydrolase activity of the protein's TIR domain, which could lead to accumulation of v-cADPR. However, exceeded v-cADPR threshold in absence of bacterial infection may be perceived and regulated by the plant through other mechanisms, such as rapid protein turnover of AT1G72940 caused by post-translational modifications. Since little is known for v-cADPR activity and the role of AT1G72940 in plant defence, we are not yet able to explain how

this mechanism works. However, future experiments measuring the v-cADPR concentration in *prom35S::AT1G72940:GFP* and *prom35S::AT1G72940:FLAG* prior and after infection with *Pst* DC3000 could provide with useful information.

6. Summary of conclusions and future work

A transcriptomic analysis conducted by (Lewis et al., 2015) showed that the expression of a group of genes from the *A. thaliana TN* family gets upregulated in Col-0 adult plants when those are challenged with virulent *Pst* DC3000 bacteria, between 5 and 9 hrs post infection. *TN* genes *AT1G72920, AT1G72940* and *AT1G72950* are upregulated in response to virulent *Pst* DC3000, but not in response to treatments with the mutant strain *Pst* DC3000 *hrpA*, mock solution ($MgCl_2$) or other types of biotic (e.g. *Botrytis cinerea*) or abiotic stresses (e.g. high light, drought). The transcription levels of genes *AT1G72920* and *AT1G72940* and their responses were confirmed via RT-q-PCR analysis of *A. thaliana* Col-0 plants at the same developmental stage, following the same treatments and environmental conditions. Data on gene *AT1G72950* were not confirmed, as its expression levels upon virulent *Pst* DC3000 infection were not found as differentially expressed as for genes *AT1G72920* and *AT1G72940.*

The transcriptional response of *TN* genes to virulent *Pst* DC3000 infection but not to *Pst* DC3000 *hrpA*, a mutant strain that is unable to deliver bacterial effectors to the plant, suggested that there is a potential correlation between effector delivery and transcriptional reprogramming of genes *AT1G72920, AT1G72940* and *AT1G72950.* We used the promoters of those genes fused to the luciferase reporter gene in a protoplast-based screening of 22 *Pst* DC3000 effectors to identify the specific effectors correlated to *TN* gene upregulation. *promTN::LUC* constructs when co-expressed with *Pst* DC3000 effectors HopQ1-1, HopAI1, HopB1, AvrPto, HopF2 and HopAB2 (AvrPtoB) in protoplasts, showed induction of LUC expression compared to an the empty vector. Effectors HopAO1 and AvrRPT2 showed repression of TN promoters at almost every replicate. All six candidate effectors have been reported to play key roles in multiple pathways that affect the plant's defence responses to infection, mainly by targeting and suppressing PRRs and their co-receptors, RLCKs and MAPKs (Büttner, 2016; Macho and Zipfel, 2015). Therefore, it is

suggested that *Pst* DC3000 effectors HopQ1-1, HopAI1, HopB1, AvrPto, HopF2 and HopAB2 (AvrPtoB) and their correlation to *TN* promoter regulation should be further pursued with *in planta* experiments, to try and elucidate their role in *TN* gene response upon *Pst* DC3000 infection.

A bioinformatic analysis conducted prior to the beginning of this project resulted in the discovery of three motifs (m1, m2, and m3) putatively recognised by transcription factors, that are conserved among the different *TN* promoters. By introducing point mutations on these motifs for *promAT1G72940::LUC* constructs and co-expressing them with the candidate *Pst* DC3000 effectors in protoplasts, we identified that in *promAT1G72940::LUC* mutated motif2 (m2) the LUC expression is borderline detected, indicating that the presence of m2 is important for the regulation of promoter *AT1G72940.*

To address the question of which transcription factors potentially regulate the *TN* promoters upon *Pst* DC3000 infection, a large-scale Y1H screening was performed using the putative promoter region of *AT1G72940* as bait to identify potential DNA-protein interactions in a yeast library of 1,965 known *A. thaliana* TFs (Pruneda-Paz et al., 2014). The screening was unsuccessful due to technical complications, but the tools to facilitate future work were generated. The transcription factor ERF6 has been proven *in planta* to bind to promoters of genes *AT1G72920* and *AT1G72940*, suggesting that ERF6 and possibly its homologs ERF5, ERF104, and ERF105 contribute to the expression of these genes in a manner independent of the JA/ethylene/PAD4/ SA network during ETI (Mine et al., 2018). A list of AP2/ERF transcription factors available in the yeast library was generated, as suggested potential targets for future Y1H screenings. However, it is noted that the ERF6 x *promAT1G72940* interaction did not work in the heterologous yeast system, possibly because ERF6 is activated *in planta* during ETI by MPK3- and MPK6-mediated post-translational phosphorylation (Meng et al., 2013; Tsuda et al., 2013). Therefore, should the Y1H screening be pursued again in future experiments, the acquisition of a verified positive control for DNA-protein interactions in this system, is deemed necessary.

In parallel to identifying the molecular mechanisms underlying the transcriptional reprogramming of *TN* genes upon *Pst* DC3000 infection, the functionality of *TN* proteins in plant immune responses was also investigated. The dexamethasone inducible *AT1G72940* overexpressing *A. thaliana* transgenic lines (kindly donated by Prof. Murray Grant) were assessed following infection with virulent *Pst* DC3000 in a dual manner: bacterial growth colony counts and measuring of the maximum dark-induced quantum efficiency of the PSII photochemistry (F_v/F_m). Both experiments showed that none of the tested lines shows any significant difference in their response to *Pst* DC3000 infection than the wild type plants (Col-0), when induced with dexamethasone.

RT-q-PCR analysis of *promDEX::AT1G72940* and *promDEX::AT1G72940:HA:FLAG* lines up to 12 and 16hrs post induction with 30μM of DEX, respectively, revealed that there is no recorded increase in *AT1G72940* transcript levels when compared with Col-0 basal gene expression, suggesting that these plants are not induced by dexamethasone. Since silencing of the GVG inducible system is an issue often encountered in stably transgenic dexamethasone-inducible plants (Geng and Mackey, 2011), we hypothesized that those lines do not respond to DEX due to post-transcriptional gene silencing (PTGS). Alternatively, mutations have occurred in either component of the GVG system after multiple series of plasmid replication.

In a similar approach to study of the inducible overexpressing lines, knockout lines of the *TN* locus we analysed, where genes *AT1G72910, AT1G72920, AT1G72930, AT1G72940* and *AT1G72950* have been removed with the CRISPR-Cas9 technology. Single T-DNA knockout lines of *TN* genes were previously screened for developmental and susceptibility phenotypes in response to plant pathogens with no success (Nandety et al., 2013), possibly due to gene redundancy. The CRISPR-Cas9 *TN* knockout lines were tested post-infection with virulent *Pst* DC3000 and the avirulent strains *Pst* DC3000 AvrRPS4 and *Pst* DC3000 AvrRPM1 that trigger ETI. Collectively, the findings

showed that there is no significant difference detected in terms of susceptibility to infection between the CRISPR-Cas9 *TN* K.O and Col-0 plants, when those are challenged with either virulent *Pst* DC3000 or the avirulent strains *Pst* DC3000 AvrRPS4 and *Pst* DC3000 AvrRPM1. Since these CRISPR-Cas9 K.O. did not cover the entire *TN* locus, which is a functionality-favoured cluster of variably arranged *TN* and *TNL* genes (Meyers et al., 2002), we hypothesized that partial removal of the locus may not result to a detectable phenotype due to functional redundancy.

Finally, Golden Gate assembly was used to produced new tools to generate constitutively and inducible overexpressed *TN* stable *A. thaliana* transgenic lines, aiming to study the functionality of TN proteins in plant defence responses. Due to time limitations, technical issues with the cloning and the Covid-19 pandemic, generation of transgenic lines was completed successfully only for *AT1G72940.* We generated a set of various constitutively and inducible overexpressed lines for *AT1G72940*, which we selected up to T3 generation and tested for their transcriptional and protein levels via RT-q-PCR and western blotting. Despite the importance of *AT1G72920*, after many failed attempts to subclone the CDS using GG assembly, it was not further pursued in this PhD project.

Protein AT1G72940 was detected via western blotting in crude extracts of early developmental stages of *prom35S::AT1G72940:GFP* line T1-5 (T2 generation), but not in any of the other tested lines. It was also detected at lower amounts in 6-day-old seedlings of line T1-5 (T3 generation), but not at 18-day-old seedlings. Protein AT1G72940 was not detected in adult plants (5 -weeks-old) of any of the tested *prom35S::AT1G72940:GFP* lines. Relative expression levels of *AT1G72940* generated with RT-q-PCR showed that, while *AT1G72940* transcript levels are significantly increased at early developmental stages (6-day-old) of the overexpressing *prom35S::AT1G72940:GFP* lines compared to the WT, they are already decreased by 15 to 20-fold in older seedlings (18-day-old) and return to basal gene expression in adult plants (5-week-old). These findings are consistent with the detection of protein AT1G72940 only at 6-day-old seedlings of T3

prom35S::AT1G72940:GFP line T1-5, but fail to explain the lack of detected protein in the remaining lines.

AT1G72940 detection in *prom35S::AT1G72940:FLAG* plants was unsuccessful at all lines and developmental stages tested. Relative expression levels of *AT1G72940* showed that *AT1G72940* transcript levels are significantly increased at both older seedlings (18-days-old) and adult plants (5-weeks-old) of at least 3 out of the 6 tested overexpressing *prom35S::AT1G72940:FLAG* lines, compared to the WT. The RT-q-PCR data on the *prom35S::AT1G72940:FLAG* plants are not consistent with the lack of AT1G72940 protein detection in the same lines.

We hypothesized that in the overexpressing *AT1G72940* stable transgenic lines, *AT1G72940* may be subjected to epigenetic silencing, that can either occur from transgene silencing or the expression of long non-coding RNAs locating at the same *TN* locus. Another possibility is that the lack of AT1G72940 protein detection in older seedlings and adult plants of *prom35S::AT1G72940:GFP* and *prom35S::AT1G72940:FLAG* transgenic lines is due to protein turnover caused by post-translational modifications. Use of protein immunoprecipitation experiments will potentially help to identify if protein AT1G72940 is present at very low levels in older transgenic plants or is not detected at all.

The preliminary results of bacterial growth on *prom35S::AT1G72940:GFP* and *prom35S::AT1G72940:FLAG* adult plants following *Pst* DC3000 infection showed that all tested lines, with the exception of *prom35S::AT1G72940:GFP* line T1-5, are more susceptible to infection compared to Col-0 and that difference is statistically significant. However, the lack of AT1G72940 protein detection at the same developmental stage and the data resulting from one biological replicate are not sufficient evidence to conclude on whether the recorded susceptibility of the transgenic plants to *Pst* DC3000 is correlated to the expression of the transgene.

Future work should focus on identifying protein AT1G72940 in the existing overexpressing lines via protein IP. More lines should be selected and tested to generate lines with strong expression. Positive results in protein IP could be encouraging for mass spectrometry experiments prior and after infection with *Pst* DC3000, to identify other protein components that interact with AT1G72940. Additionally, if protein AT1G72940 is identified in the overexpressing lines, metabolomic experiments measuring the abundance of v-cADPR compound post infection with *Pst* DC3000 could serve as biomarker for the protein's TIR domain activity. Bacterial growth analysis in the already tested overexpressing lines should be repeated to obtain more biological replicates and identify whether the difference in colony counts recorder in this thesis are reproducible and statistically significant. RNA-sequencing data generated from wild type Col-0 plants, the CRISPR-Cas9 TN K.O. lines and the overexpressing *AT1G72940* lines prior and after *Pst* DC3000 infection could provide insight on the transcriptional level based on the differentially expressed genes identified in each genotype and treatment.

In conclusion, this PhD project confirmed that *A. thaliana TN* genes *AT1G72920* and *AT1G72940* are upregulated in response to *Pst* DC3000 infection. The specific mechanism underlying this upregulation still remains unknown, however important tools were generated and characterise to facilitate future work. The specific effectors implicated in the transcriptional reprogramming of *AT1G72920* and *AT1G72940* have been identified but need to be verified *in planta*. Y1H expression vectors were generated to screen for transcription factors responsible for the regulation of *AT1G72940* promoter*,* as well as identifying the specific promoter motifs responsible for this regulation. Most importantly, constitutively overexpression and inducible *A. thaliana* lines were generated, selected and characterised for *AT1G72940* expression to facilitate with immunity assays and high-throughput experiments that can elucidate the role of *AT1G72940* in plant immunity.

7. Appendix: Supplementary information

7.1 Maps of Cloning Vectors

5.D. pGEM®-T Easy Vector Map and Sequence Reference Points

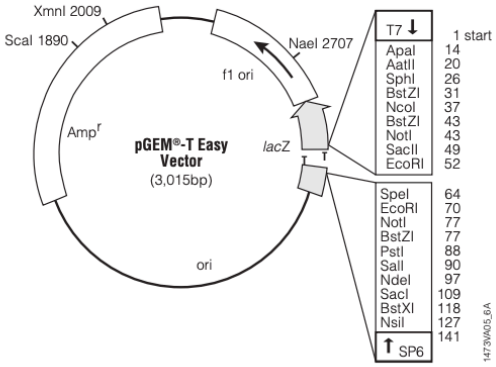

pGEM®-T Easy Vector sequence reference points:

T7 RNA polymerase transcription initiation site	1
multiple cloning region	10–128
SP6 RNA polymerase promoter (–17 to +3)	139–158
SP6 RNA polymerase transcription initiation site	141
pUC/M13 Reverse Sequencing Primer binding site	176–197
lacZ start codon	180
lac operator	200–216
β-lactamase coding region	1337–2197
phage f1 region	2380–2835
lac operon sequences	2836–2996, 166–395
pUC/M13 Forward Sequencing Primer binding site	2949–2972
T7 RNA polymerase promoter (–17 to +3)	2999–3

Note: Inserts can be sequenced using the pUC/M13 Forward Primer (Cat.# Q5601) or pUC/M13 Reverse Primer (Cat.# Q5421).

***Figure 7.1 pGEM®-T-Easy* Cloning Vector (Promega, UK).**

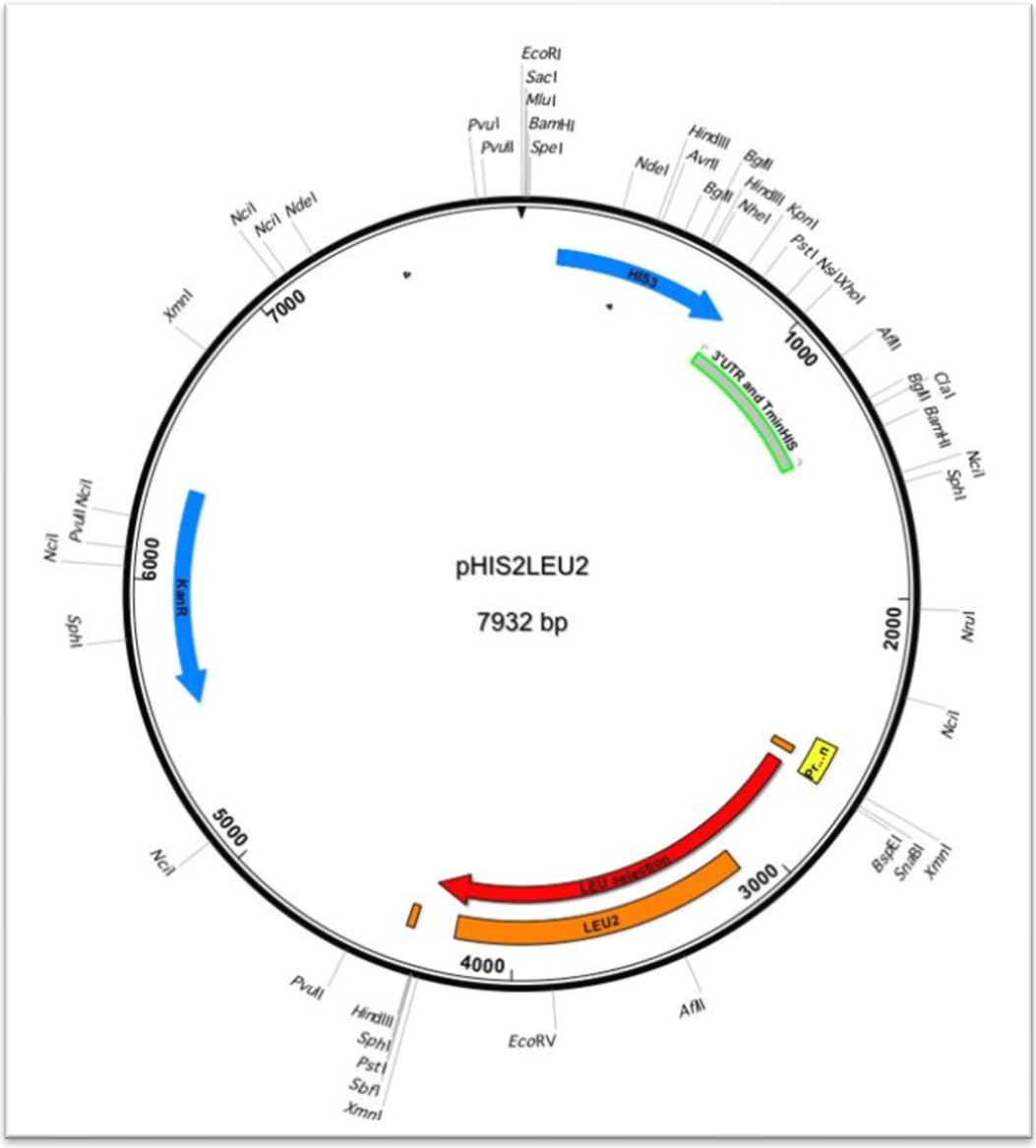

Figure 7.2 pHIS3LEU2 **Cloning vector/ Yeast Expression Vector as described by Davies, S. (2013).**

The vector includes a MCS for classical cloning based on Type II restriction enzymes located upstream of the HIS3 reporter gene, encoding for the amino acid Histidine. It was initially selected as the yeast expression vector to create the bait constructs for the Y1H screening of this PhD project, using the recognition sites for SacI and MluI to subclone promAT1G72940 (WT, m1, m2, m3, m1-2) versions. When transforming the EV into Y8930 and using SC-His to check for autoactivation of HIS3, the yeast was growing in the absence of Histidine. The addition of 3AT was unsuccessful to suppress the growth of pHIS3LEU2/Y8930 in SC-His media. pHIS3LEU2 was therefore excluded from the Y1H experiments since then. However, this vector has been successfully used for Y1H experiments in other PhD projects in our lab (Nippe, 2019), indicating the possibility of a problematic plasmid stock.

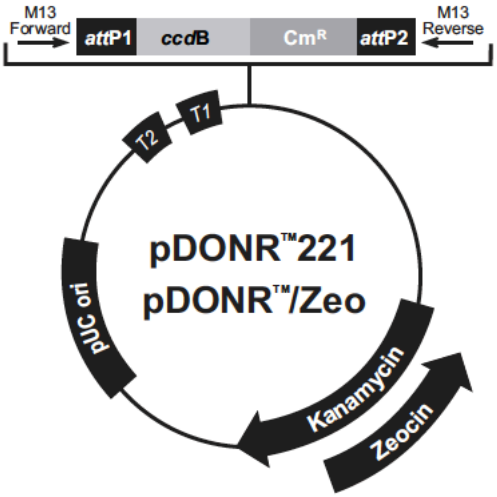

Comments for:	pDONR™221 4761 nucleotides	pDONR™/Zeo 4291 nucleotides
*rrn*B T2 transcription termination sequence (c):	268-295	268-295
rmB T1 transcription termination sequence (c):	427-470	427-470
M13 Forward (-20) priming site:	537-552	537-552
*att*P1:	570-801	570-801
*ccd*B gene (c):	1197-1502	1197-1502
Chloramphenicol resistance gene (c):	1825-2505	1847-2506
*att*P2 (c):	2753-2984	2754-2985
M13 Reverse priming site:	3026-3042	3027-3043
Kanamycin resistance gene:	3155-3964	---
EM7 promoter (c):	---	3486-3552
Zeocin resistance gene (c):	---	3111-3485
pUC origin:	4085-4758	3615-4288

(c) = complementary strand

invitrogen™

***Figure 7.3 pDONR™-Zeo* Cloning Vector (Invitrogen™/ThermoFisher Scientific).**

The vector contains the recombination sites *att*P1 and *att*P2 flanking the *ccdB/Cm*^{R} genes, which makes it a Gateway® compatible donor vector suitable for conventional BP clonase reactions with DNA fragments flanked by the *att*B1 and *att*B2 recombination sites. The *pDONR™-Zeo* vector was used to create entry clones containing the *promAT1G72940* (WT, m1, m2, m3, m1-2) versions for Gateway® cloning.

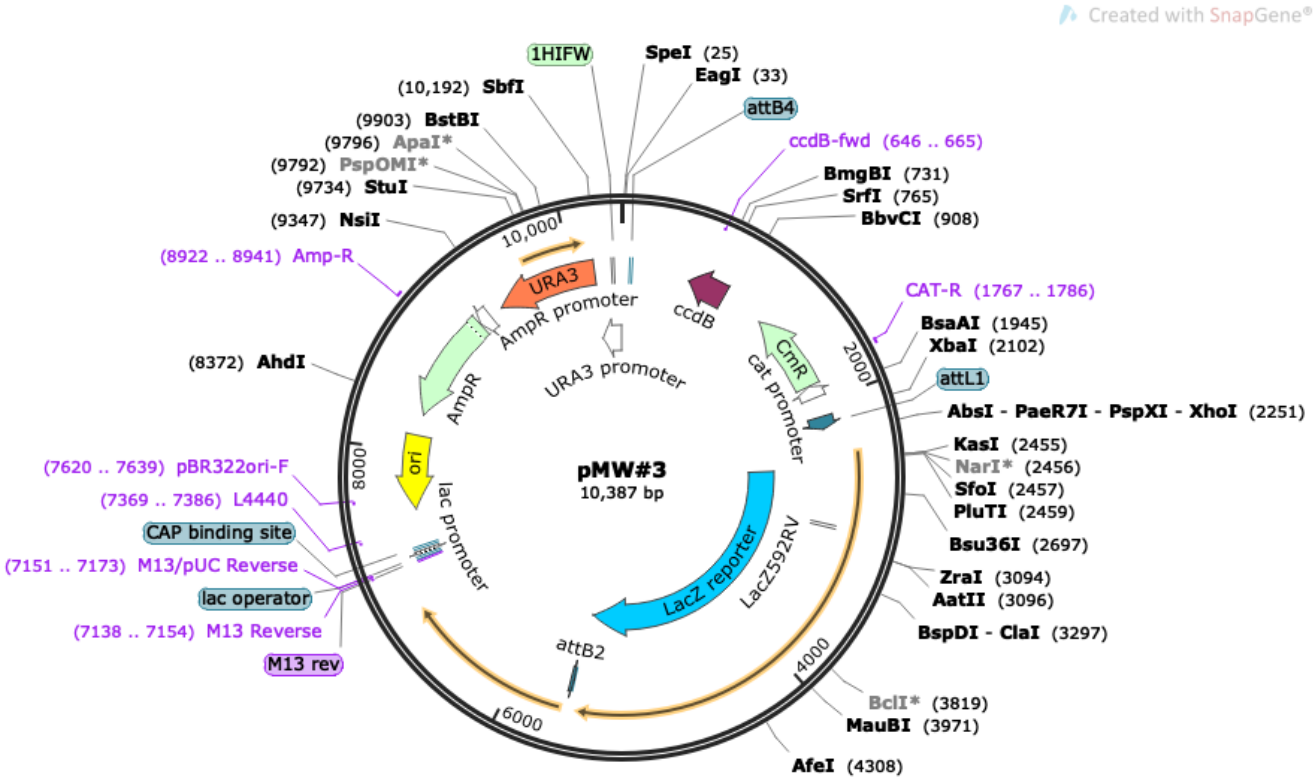

***Figure 7.4 pDONR™-Zeo* Cloning Vector (Invitrogen™/ThermoFisher Scientific).**

The vector contains the recombination sites *att*P1 and *att*P2 flanking the *ccdB/Cm*^{R} genes, which makes it a Gateway® compatible donor vector suitable for conventional BP clonase reactions with DNA fragments flanked by the *att*B1 and *att*B2 recombination sites. The *pDONR™-Zeo* vector was used to create entry clones containing the *promAT1G72940* (WT, m1, m2, m3, m1-2) versions for Gateway® cloning.

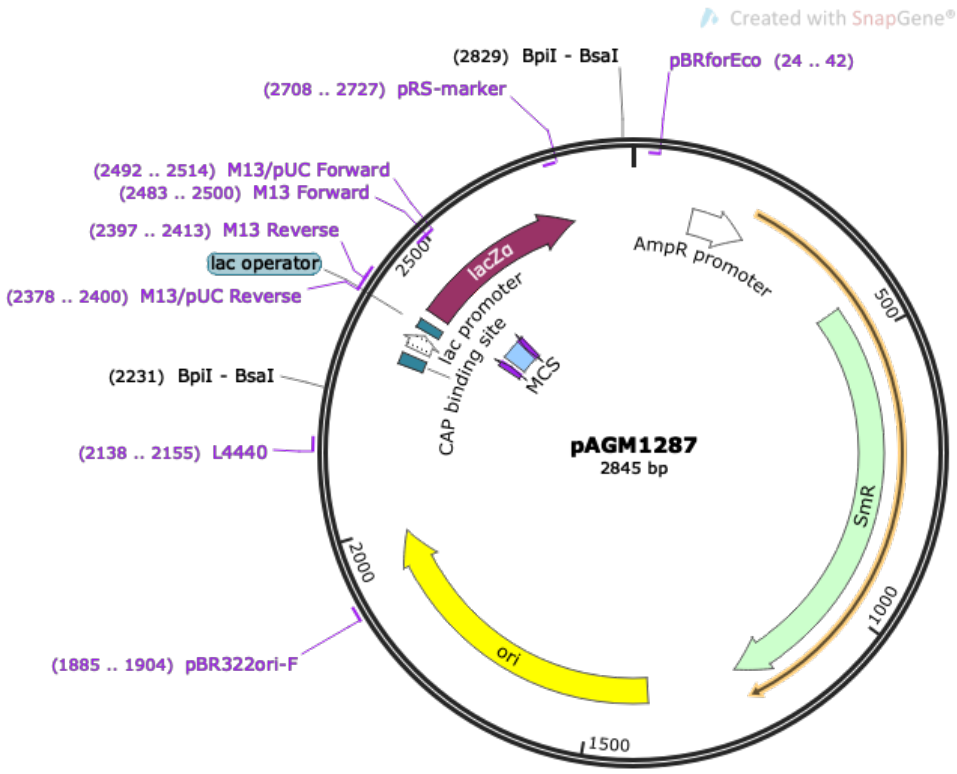

***Figure 7.5 pAGM1287* Golden Gate Level-0 Acceptor Vector for CDS1 no stop modules.**

Vector supplied as part of the MoClo Plant Tool Kit (Engler et al., 2014). Position F2 in plate. Suitable for GG reactions using the restriction enzyme BpiI. Vector confers resistance to the antibiotic Spectinomycin (Sm^R) and allows for blue/white selection (*lacZa*) of the recombinant colonies in the presence of Xgal/IPTG. Suitable for subcloning of CDS1 fragments lacking a stop codon, thus allowing for 3' end fusions of DNA fragments coding for protein tags. *pAGM1287* was used for the creation of the L0 constructs of *TN* genes CDS.

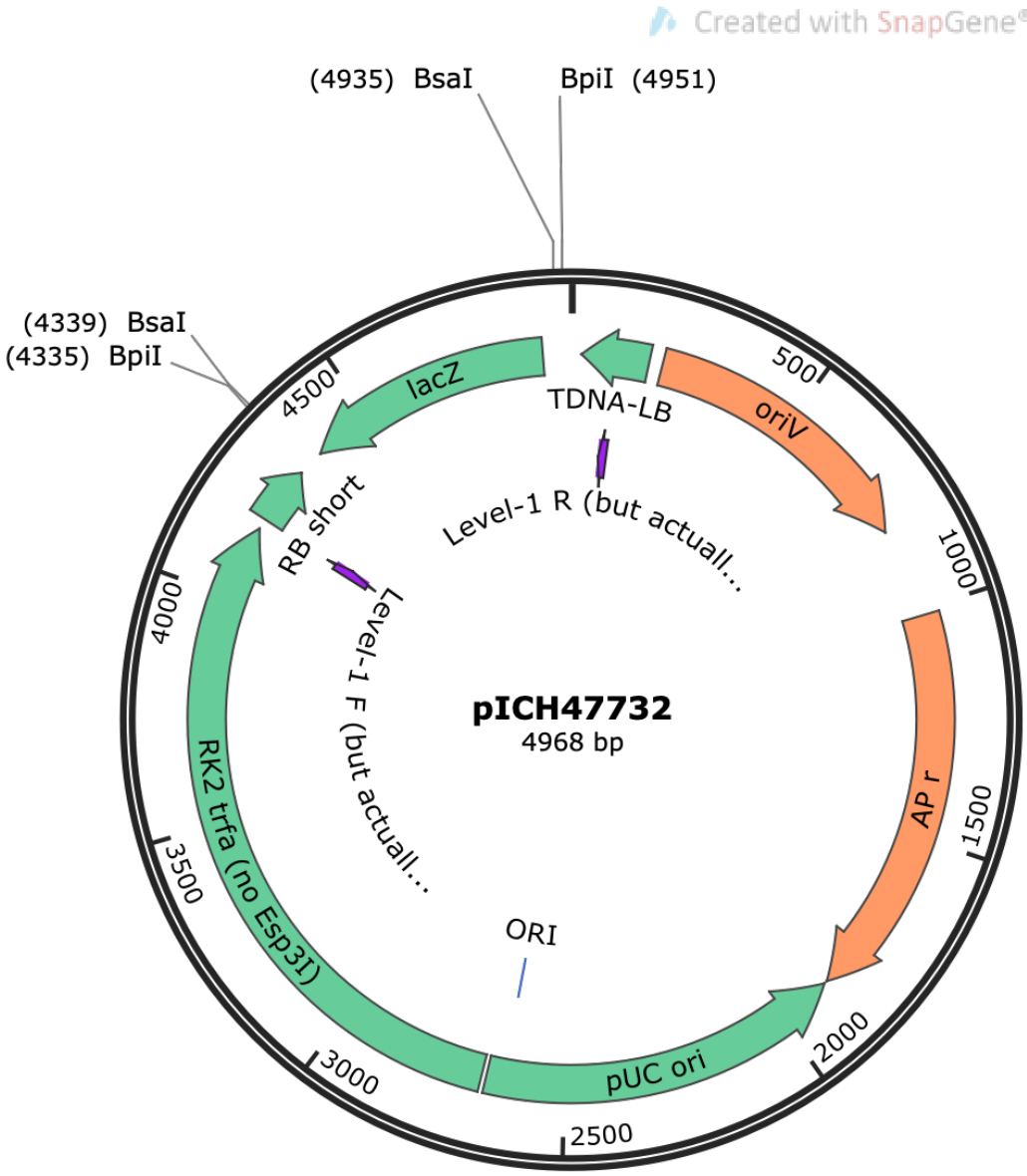

***Figure 7.6 pICH47732* Golden Gate Level 1 Position 1 (L1P1) Acceptor.**

Vector supplied as part of the MoClo Plant Tool Kit (Engler et al., 2014). Suitable for GG reactions using the restriction enzyme BsaI. Vector confers resistance to the antibiotic Ampicillin and allows for blue/white selection (*lacZa*) of the recombinant colonies in the presence of Xgal/IPTG. Vector was used for the creation of the L1 transcription units of *TN* genes.

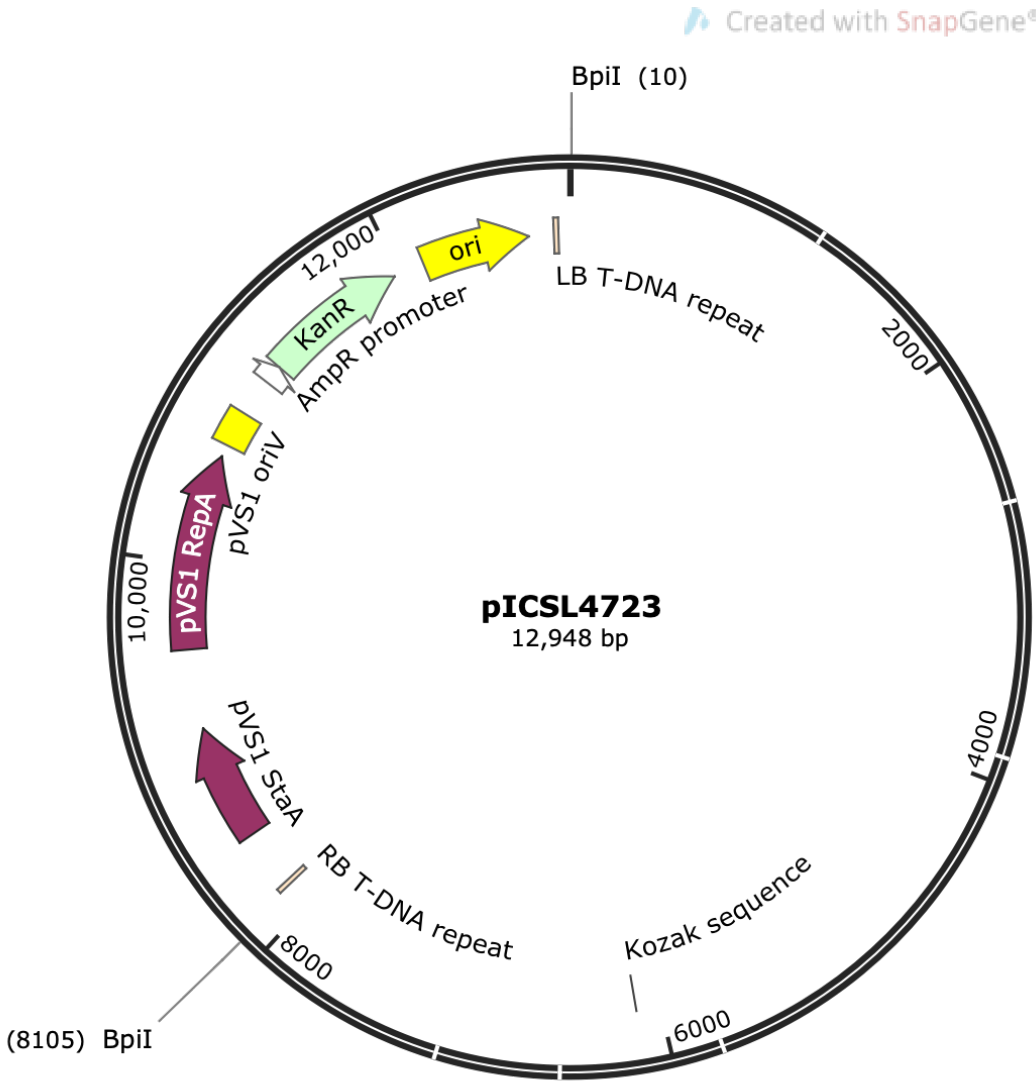

Figure 7.7 *pICSL4723* Golden Gate L2 Acceptor.

Vector supplied as part of the MoClo Plant Tool Kit (Engler et al., 2014). Suitable for GG reactions using the restriction enzyme BpiI. Vector confers resistance to the antibiotic Kanamycin (KanR). Vector was used for the assembly of the L1 transcription units of *TN* genes into the T-DNA cassette for plant transformation.

7.2 Sequences of genetic loci of interest

Hereafter are presented the differences identified with sequencing analysis in promoter *AT1G72940* sequence, depending on each motif mutation.

T : domestication of the promoter for Golden Gate assembly

AAT: mutation in motif 1

TTA: mutation in motif 2

ATC: mutation in motif 3

Red text: 5' UTR region

Yellow text: exon region

ATG: start codon of *AT1G72940*

Promoter AT1G72940

aggttctgcttgtggcagacgacgttactaaggttaaacagttagaagctcttgcagatgatttcagc
agttttggtcctgggagtgttgttatcATCACTACAGACAACAAGGGGTTGTTGAATTCTTATGGTAT
AAAAGAAGTCTACGAAGTTGAGAATTTGAAGTTTTGTGGAATCTTACGATCATTGGGCTTTAAAAAGA
GAGCTGCTGCGTTCCAGCGGGCTTTGTGTAGAGCAAATAGTTTTGCCACGGAATGTTTTTGTTGTCAA
AGTAGTAGTATATCTGGTTATGGGAAAGTGACAGATTCAGTTAATTAAGTTTAAATTCCTTAGTCACA
TGCACTAAGTTAGCTAAACTTAATAAGATGTGTGGCTAGGGGTGTAAAACAAATATCACTCTTCATTA
AATTAAGTAATATACACTTTTTTTTCCTTATCAAATCTGTGTTTGAGTTATAACCTAAATGTTTGTTG
TGTGTCTCTTTCAAGTCTATATTTTCTTAAAAACAAAGTTTGTATAATTTCTTGGGATTCCCATGACC
ATTTGTTCTTTGAATACCCGAATTCTCAAAGGCAGTTTGGTTGTCAAATAAAGATTACACAATTTATA
AAAAAAGATTTGTGTATTTGGGAGGGTTTTTGATGTTTGGACATGCCCAATAAAATTAAAAATTAATA
CAGGAGACACAAAGTCGCAaactttccaaagttggaatctacatatgtctaaaacagagaagaaaagc
ttttaaacttttacatgatgatcctccaataatagtaatagtgtaatggtactatactactacagtt
caaagccactgatttatgctttttgggtacgtggaagatttcaatcacagacaaacgtaattaaatca
tttattggaaaatgtgagtcaagctgaataaacttgatgcacacgaatagatatgaaagaaattgggt
tgatcaacaaaaaaacaagccgacaaaaactgaatcttatgatctttttcgtccgtcagtttcaacc
attcgtttgatcggataatcaaaaccagcaaatgccaataatacacaccagaaaaggtaagatgataa
ttttt**gttcgttagtagtattttattattatcatgctcatcattttcttactttggcggcccatcttt**
tctcttcccctctttctgagtagtttagcaaaacagaagctgacaagaaaaaaatagaacatgcctgg
aaatacacaattacaccactttagcaggaT**gactatgggagtctctaatcaatgcacatgctttattc**
agttcaactactctctagtggtctataaatatccttgagtcctttatttctattactcatcatactta
agttctcaatagagagaatcaaaaatcaaaATG

Promoter AT1G72940 – motif 1 mutated

aggttctgcttgtggcagacgacgttactaaggttaaacagttagaagctcttgcagatgatttcagc
agttttggtcctgggagtgttgttatcATCACTACAGACAACAAGGGGTTGTTGAATTCTTATGGTAT
AAAAGAAGTCTACGAAGTTGAGAATTTGAAGTTTTGTGGAATCTTACGATCATTGGGCTTTAAAAAGA
GAGCTGCTGCGTTCCAGCGGGCTTTGTGTAGAGCAAATAGTTTTGCCACGGAATGTTTTTGTTGTCAA
AGTAGTAGTATATCTGGTTATGGGAAAGTGACAGATTCAGTTAATTAAGTTTAAATTCCTTAGTCACA
TGCACTAAGTTAGCTAAACTTAATAAGATGTGTGGCTAGGGGTGTAAAACAAATATCACTCTTCATTA
AATTAAGTAATATACACTTTTTTTTCCTTATCAAATCTGTGTTTGAGTTATAACCTAAATGTTTGTTG
TGTGTCTCTTTCAAGTCTATATTTTCTTAAAAACAAAGTTTGTATAATTTCTTGGGATTCCCATGACC
ATTTGTTCTTTGAATACCCGAATTCTCAAAGGCAGTTTGGTTGTCAAATAAAGATTACACAATTTATA
AAAAAAGATTTGTGTATTTGGGAGGGTTTTTGATGTTTGGACATGCCCAATAAAATTAAAAATTAATA
CAGGAGACACAAAGTCGCAaactttccaaagttggaatctacatatgtctaaaacagagaagaaaagc

ttttaaacttttacatgatgatcctccaataatagtaatagtgtaatggtactatactactacagtt
caaagccactgatttatgctttttgggtacgtggaagatttcaatcacagacaaacgtaattaaatca
tttattggaaaatgtgagtcaagctgaataaacttgatgcacacgaatagatatgaaagaaattgggt
tgatcaacaaaaaaacaagccgacaaaaactgaatcttatgatctttttcgtccgtcagtttcaacc
attcgtttgatcggataatcaaaaccagcaaatgccaataatacacaccagaaaaggtaagatgataa
ttttt**gttcgttagtagtattttattattatcatgctcatcattttcttactttggc**AAT**ccatcttt**
tctcttcccctctttctgagtagtttagcaaaacagaagctgacaagaaaaaaatagaacatgcctgg
aaatacacaattacaccactttagcagga**T**gactatgggagtctctaatcaatgcacatgctttattc
agttcaactactctctagtggtctataaatatccttgagtcctttatttctattactcatcatactta
agttctcaatagagagaatcaaaaatcaa**a**ATG

Promoter AT1G72940 – motif 2 mutated

aggttctgcttgtggcagacgacgttactaaggttaaacagttagaagctcttgcagatgatttcagc
agttttggtcctgggagtgttgttatcATCACTACAGACAACAAGGGGTTGTTGAATTCTTATGGTAT
AAAAGAAGTCTACGAAGTTGAGAATTTGAAGTTTTGTGGAATCTTACGATCATTGGGCTTTAAAAAGA
GAGCTGCTGCGTTCCAGCGGGCTTTGTGTAGAGCAAATAGTTTTGCCACGGAATGTTTTTGTTGTCAA
AGTAGTAGTATATCTGGTTATGGGAAAGTGACAGATTCAGTTAATTAAGTTTAAATTCCTTAGTCACA
TGCACTAAGTTAGCTAAACTTAATAAGATGTGTGGCTAGGGGTGTAAAACAAATATCACTCTTCATTA
AATTAAGTAATATACACTTTTTTTTCCTTATCAAATCTGTGTTTGAGTTATAACCTAAATGTTTGTTG
TGTGTCTCTTTCAAGTCTATATTTTCTTAAAAACAAAGTTTGTATAATTTCTTGGGATTCCCATGACC
ATTTGTTCTTTGAATACCCGAATTCTCAAAGGCAGTTTGGTTGTCAAATAAAGATTACACAATTTATA
AAAAAAGATTTGTGTATTTGGGAGGGTTTTTGATGTTTGGACATGCCCAATAAAATTAAAAATTAATA
CAGGAGACACAAAGTCGCAaactttccaaagttggaatctacatatgtctaaaacagagaagaaaagc
ttttaaacttttacatgatgatcctccaataatagtaatagtgtaatggtactatactactacagtt
caaagccactgatttatgctttttgggtacgtggaagatttcaatcacagacaaacgtaattaaatca
tttattggaaaatgtgagtcaagctgaataaacttgatgcacacgaatagatatgaaagaaattgggt
tgatcaacaaaaaaacaagccgacaaaaactgaatcttatgatctttttcgt**TTA**tcagtttcaacc
attcgtttgatcggataatcaaaaccagcaaatgccaataatacacaccagaaaaggtaagatgataa
ttttt**gttcgttagtagtattttattattatcatgctcatcattttcttactttggcggcccatcttt**
tctcttcccctctttctgagtagtttagcaaaacagaagctgacaagaaaaaaatagaacatgcctgg
aaatacacaattacaccactttagcagga**T**gactatgggagtctctaatcaatgcacatgctttattc
agttcaactactctctagtggtctataaatatccttgagtcctttatttctattactcatcatactta
agttctcaatagagagaatcaaaaatcaa**a**ATG

Promoter AT1G72940 – motif 3 mutated

aggttctgcttgtggcagacgacgttactaaggttaaacagttagaagctcttgcagatgatttcagc
agttttggtcctgggagtgttgttatcATCACTACAGACAACAAGGGGTTGTTGAATTCTTATGGTAT
AAAAGAAGTCTACGAAGTTGAGAATTTGAAGTTTTGTGGAATCTTACGATCATTGGGCTTTAAAAAGA
GAGCTGCTGCGTTCCAGCGGGCTTTGTGTAGAGCAAATAGTTTTGCCACGGAATGTTTTTGTTGTCAA
AGTAGTAGTATATCTGGTTATGGGAAAGTGACAGATTCAGTTAATTAAGTTTAAATTCCTTAGTCACA
TGCACTAAGTTAGCTAAACTTAATAAGATGTGTGGCTAGGGGTGTAAAACAAATATCACTCTTCATTA
AATTAAGTAATATACACTTTTTTTTCCTTATCAAATCTGTGTTTGAGTTATAACCTAAATGTTTGTTG
TGTGTCTCTTTCAAGTCTATATTTTCTTAAAAACAAAGTTTGTATAATTTCTTGGGATTCCCATGACC
ATTTGTTCTTTGAATACCCGAATTCTCAAAGGCAGTTTGGTTGTCAAATAAAGATTACACAATTTATA
AAAAAAGATTTGTGTATTTGGGAGGGTTTTTGATGTTTGGACATGCCCAATAAAATTAAAAATTAATA
CAGGAGACACAAAGTCGCAaactttccaaagttggaatctacatatgtctaaaacagagaagaaaagc
ttttaaacttttacatgatgatcctccaataatagtaatagtgtaatggtactatactactacagtt
caaagccactgatttatgctttttgggtacgtggaagatttcaatcacagacaaacgtaattaaatca
tttattggaaaatgtgagtcaagctgaataaacttgatgcacacgaatagatatgaaagaaattgggt
tgatcaacaaaaaaacaagccgacaaaaactgaatcttatgatctttttcgtccgtcagtttcaacc
attcgtttgatcggataatcaaaaccagcaaatgccaataatacacaccagaaaaggtaagatgataa
ttttt**gttcgttagtagtattttattattatcatgctcatcattttcttactttggcggcccatcttt**
tctcttcccctctttctgagtagtttagcaaaacagaa**ATC**gacaagaaaaaaatagaacatgcctgg
aaatacacaattacaccactttagcagga**T**gactatgggagtctctaatcaatgcacatgctttattc
agttcaactactctctagtggtctataaatatccttgagtcctttatttctattactcatcatactta
agttctcaatagagagaatcaaaaatcaa**a**ATG

Promoter AT1G72940 – motif 1 and 2 mutated

aggttctgcttgtggcagacgacgttactaaggttaaacagttagaagctcttgcagatgatttcagc
agttttggtcctgggagtgttgttatcATCACTACAGACAACAAGGGGTTGTTGAATTCTTATGGTAT
AAAAGAAGTCTACGAAGTTGAGAATTTGAAGTTTTGTGGAATCTTACGATCATTGGGCTTTAAAAAGA
GAGCTGCTGCGTTCCAGCGGGCTTTGTGTAGAGCAAATAGTTTTGCCACGGAATGTTTTTGTTGTCAA
AGTAGTAGTATATCTGGTTATGGGAAAGTGACAGATTCAGTTAATTAAGTTTAAATTCCTTAGTCACA
TGCACTAAGTTAGCTAAACTTAATAAGATGTGTGGCTAGGGGTGTAAAACAAATATCACTCTTCATTA
AATTAAGTAATATACACTTTTTTTTCCTTATCAAATCTGTGTTTGAGTTATAACCTAAATGTTTGTTG
TGTGTCTCTTTCAAGTCTATATTTTCTTAAAAACAAAGTTTGTATAATTTCTTGGGATTCCCATGACC
ATTTGTTCTTTGAATACCCGAATTCTCAAAGGCAGTTTGGTTGTCAAATAAAGATTACACAATTTATA
AAAAAAGATTTGTGTATTTGGGAGGGTTTTTGATGTTTGGACATGCCCAATAAAATTAAAAATTAATA
CAGGAGACACAAAGTCGCAaactttccaaagttggaatctacatatgtctaaaacagagaagaaaagc
ttttaaacttttacatgatgatcctccaataatagtaatagtgtaatggtactatactactacagtt
caaagccactgatttatgctttttgggtacgtggaagatttcaatcacagacaaacgtaattaaatca
tttattggaaaatgtgagtcaagctgaataaacttgatgcacacgaatagatatgaaagaaattgggt
tgatcaacaaaaaaacaagccgacaaaaactgaatcttatgatctttttcgtTTAtcagtttcaacc
attcgtttgatcggataatcaaaaccagcaaatgccaataatacacaccagaaaaggtaagatgataa
ttttt**gttcgttagtagtattttattattatcatgctcatcattttcttactttggcAAT**ccatcttt
tctcttcccctctttctgagtagtttagcaaaacagaagctgacaagaaaaaaatagaacatgcctgg
aaatacacaattacaccactttagcagga**T**gactatgggagtctctaatcaatgcacatgctttattc
agttcaactactctctagtggtctataaatatccttgagtcctttatttctattactcatcatactta
agttctcaatagagagaatcaaaaatcaaaATG

7.3 Primers for sequencing

Table 7.1 **List of information for all primers used to sequence recombinant plasmids in this thesis.**

VN998	**prom20seqR2**	CTGTAGTAGTGTATTACTATTATTGGAGG	Primer to sequence backwards from ATG the promoter AT1G72920 in the prom20::LUX constructs of M.G. group
VN999	**prom30seqR1**	CATTTTGATTTTTGATTCTCAATGAGTGAT	Primer to sequence backwards from ATG the promoter AT1G72930 in the prom30::LUX constructs of M.G. group
VN1000	**prom30seqR2**	GTGGTGTCAATAGATGATTTTGTAGTATGG	Primer to sequence backwards from ATG the promoter AT1G72930 in the prom30::LUX constructs of M.G. group
VN1001	**prom40seqR1**	CATTTTGATTTTTGATTCTCTCTATTGAGAACT	Primer to sequence backwards from ATG the promoter AT1G72940 in the prom40::LUX constructs of M.G. group
VN1002	**prom40seqR2**	GCATAAATCAGTGGCTTTGAACTGT	Primer to sequence backwards from ATG the promoter AT1G72940 in the prom40::LUX constructs of M.G. group
VN1003	**prom40seqR3**	TTCTCAACTTCGTAGACTTCTTTTA	Primer to sequence backwards from ATG the promoter AT1G72940 in the prom40::LUX constructs of M.G. group
VN1004	**prom40seqR4**	TCCCTCTTCAAAACCAAAGAGAATTCT	Primer to sequence backwards from ATG the promoter AT1G72940 in the prom40::LUX constructs of M.G. group
VN1005	**prom50seqR1**	CATTTCATTGATTCTAAAGAGAAATGG	Primer to sequence backwards from ATG the promoter AT1G72920 in the prom50::LUX constructs of M.G. group
VN1006	**prom50seqR2**	TAGATTCCAACTTTGAGCTATGAAC	Primer to sequence backwards from ATG the promoter AT1G72920 in the prom50::LUX constructs of M.G. group

VN1053	**1HIFW**	GTTCGGAGATTACCGAATCAA	5' sequencing primer for pMW#3 Y1H destination vector, AddGene common sequencing Primers
VN1054	**LacZ592RV**	ATGCGCTCAGGTCAAATTCAGA	3' sequencing primer for pMW#3 Y1H destination vector, AddGene common sequencing Primers
VN1061	**pMW3_RV1**	TGTTGCAACGAACAGGTCAC	Reverse primer for sequencing inserts upstream of b-gal gene in vector pMW#3
VN1062	**pMW3_RV2**	GCCTCGAGGTCGACAGATC	Reverse primer for sequencing inserts upstream of b-gal gene in vector pMW#3
VN1063	**pMW3_FW**	ACCAATCTAAGTCTGTGCTCC	Forward primer for sequencing inserts upstream of b-gal gene in vector pMW#3
VN1070	**p35S_3'_FW**	ATGACGCACAATCCCACTATC	Internal primer at the 3' of promoter 35S CaMV to sequence fused genes downstream
VN1071	**p35S_FW**	TCTGAGCTTAACAGCACAGTTGC	Forward primer at the 5' of promoter 35S CaMV to PCR/ sequence downstream
VN1072	**p35S_RV**	TGTAAATGTAATTGTAATGTTG	Reverse primer at the 3' of promoter 35S CaMV to PCR/ sequence upstream
VN1073	**3FLAG_int_RV**	TCGAGGTCATGGTCCTTATAGTC	Internal reverse primer at the 3xFLAG tag to PCR/ sequence upstream
VN1074	**6HA_int_RV**	AACGTCATATGGATACAATCCTG	Internal reverse primer at the 6xHA tag to PCR/ sequence upstream
VN1075	**GFP_5'_RV**	TCGCCGTCCAGCTCGACCAG	5' reverse primer at the GFP tag to PCR/ sequence fusions upstream
VN1076	**3'UTR-ACT2_RV**	TGTGAATGGAACACATGTAACG	Reverse primer at the 3' of the 3'UTR+ACT2 terminator to PCR/ sequence fusions upstream

VN1077	**pDEX_FW**	GGAGAGCTTGCATGCCGGTC	Forward primer at the 5' of promoter DEX (induced by dexamethasone) to PCR/ sequence downstream
VN1078	**pESTR_FW**	GGAGCTTGGGCTGCAGGTCG	Forward primer at the 5' of promoter ESTR (induced by estradiol) to PCR/ sequence downstream
VN1079	**AT1G72940_int_RV**	AGCTAAAGCTGATCTACCATTG	Internal Reverse primer of AT1G72940 CDS to PCR/ sequence upstream
VN1080	**AT1G72940_int_FW**	TGACTGTTACAACAATAAGCAATGG	Internal Forward primer of AT1G72940 CDS to PCR/ sequence downstream
VN1081	**AT1G72950_int_RV**	AGCTGATCTACCATTGCCTC	Internal Reverse primer of AT1G72950 gen to PCR/ sequence upstream
VN1082	**AT1G72950_int_FW**	ATGACTCGAAGATGGTCGAAG	Internal Forward primer of AT1G72950 gen to PCR/ sequence downstream
VN1083	**M13-F**	GTTGTAAAACGACGGCCAGT	
VN1084	**M13-R**	CACAGGAAACAGCTATGACC	
VN1085	**Level_0 F**	CGTTATCCCCTGATTCTGTGGATAAC	Forward primer for sequencing inserts in Level-0 Golden Gate vectors (suggested by the kit - doesn't work very well)
VN1086	**Level_0 R**	GTCTCATGAGCGGATACATATTTGAATG	Reverse primer for sequencing inserts in Level-0 Golden Gate vectors (suggested by the kit - doesn't work very well)
VN1087	**Level_1 F**	GAACCCTGTGGTTGGCATGCACATAC	Forward primer for sequencing inserts in Level-1 Golden Gate vectors (**labelled as FW but is** reverse)
VN1088	**Level_1 R**	CTGGTGGCAGGATATATTGTGGTG	Reverse primer for sequencing inserts in Level-1 Golden Gate vectors (**labelled as RV but is forward)**

VN1089	**Level_2 F**	GTGGTGTAAACAAATTGACGC	Forward primer for sequencing inserts in Level-2 Golden Gate vectors
VN1090	**Level_2 R**	GGATAAACCTTTTCACGCCC	Reverse primer for sequencing inserts in Level-2 Golden Gate vectors
VN1091	**Level-0_UA Fwd**	TTACGGTTCCTGCACTCTGTG	Forward primer for sequencing inserts in Level-0 Universal acceptor Golden Gate vector
VN1092	**Level-0_UA_Rev**	GCTTATGTCCACTGGGTTCGT	Reverse primer for sequencing inserts in Level-0 Universal acceptor Golden Gate vector
VN1093	**L0-F2-seq**	GTGAGCGAGGAAGCGGAAG	Forward primer for sequencing inserts in Level-0 Golden Gate vectors
VN1094	**L0-R2-seq**	TGCCACCTGACGTCTAAG	Reverse primer for sequencing inserts in Level-0 Golden Gate vectors (
VN1139	**L2-fw to L1P1**	ACCTCTGACTTGAGCGTCGA	Forward primer designed on the GG L2 vector backbone to verify the presence of the L1P1 insert in L2 constructs by PCR or sequencing
VN1140	**35S-internal_rev**	CTTTGATCTTCTGAGACTGTATC	Reverse primer designed on the promoter 35S CaMV to verify the presence of the L1P1 insert in L2 constructs by PCR or sequencing
VN1141	**TER-internal_fw**	TAGCTCTGAGTGATCGAATTG	Forward primer designed on the 3'UTR+terminator part to verify the presence of the L1P2 insert in L2 constructs by PCR or sequencing
VN1142	**FASTR-internal_rev**	CTGCCGATGATATCGTGATG	Reverse primer designed on the 5' end of the pFASTR cassette to verify the presence of this L1P2 insert in L2 constructs by PCR or sequencing

VN1143	**FASTR-internal_fw**	CATCTACAACGTCAAGATCAGA	Forward primer designed on the 3' end of the pFASTR cassette to verify the presence of this L1P2 insert in L2 constructs by PCR or sequencing
VN1144	**L2-rev to linker**	TATATCCTGTCAAACACTGATAG	Reverse primer designed on the GG L2 vector backbone to verify the presence of the L1P- insert in L2 constructs by PCR or sequencing

7.4 Full list of cloning constructs described in Chapter 5

Parts used from the Golden Gate Plant Tool Kit to assemble the following constructs are included in **Table 7.2**:

Table 7.2 **List of information on the different Golden Gate parts used for the generation of the transcriptional units and T-DNA vectors of *TN* genes.**

Name	Description
p35SCaMV/pICH51266	Constitutive expression promoter – ppH2 to CDS1
pDEX/Level-0	Promoter induced by Dexamethasone
pESTR/Level-0	Promoter induced by Estradiol – LexA pEST to CDS1
GFP/Level-0	GFP C-terminal tag
3xFLAG/pICSL50007	FLAG C-terminal tag -ppA8
6xHA/pICSL50009	HA C-terminal tag -ppB8
3' UTR + Terminator	Act2 terminator – ppA12
Linker-L1/pICH41744	Linker of 2 Level-1 parts into Level-2 – PTC5
Linker-L1/pICH41766	Linker of 3 Level-1 parts into Level-2 – PTD5
pAGM1287	Level-0 empty vector without stop codon
pICH47732	Level-1-Position-1 empty vector – PTB3
pICSL4723	Level-2 vector, contains the T-DNA LB and RB cassette for plant transformation
pFAST-R/pICSL70008	Plant selection cassette, expresses RFP protein in the seed stage – ppE11
35S::XVEreceptor	Receptor for estradiol
35S::GVGreceptor	Receptor for Dexamethasone
pJOG130	Works both as an entry vector for GateWay and a Level-1 vector for Golden Gate

Table 7.3 **Constructs subcloned in GG Level 0 vectors.**

Level 0 constructs
AT1G72940/pAGM1287 [CDS synthesised – mutation inverted]
AT1G72950/pAGM1287 [genomic]

Table 7.4 **List of *TN* gene transcriptional units assembled in GG Level 1 vectors.**

Level 1 constructs
AT1G72940
p35SCaMV::AT1G72940:GFP/pICH47732
p35SCaMV::AT1G72940:6HA/pICH47732
p35SCaMV::AT1G72940:3FLAG/pICH47732
pDEX::AT1G72940:GFP/pICH47732
pDEX::AT1G72940:6HA/pICH47732
pDEX::AT1G72940:3FLAG/pICH47732
pESTR::AT1G72940:GFP/pICH47732
pESTR::AT1G72940:6HA/pICH47732
pESTR::AT1G72940:3FLAG/pICH47732
AT1G72950
p35SCaMV::AT1G72950:GFP/pICH47732
p35SCaMV::AT1G72950:6HA/pICH47732
p35SCaMV::AT1G72950:3FLAG/pICH47732
pDEX::AT1G72950:GFP/pICH47732
pDEX::AT1G72950:6HA/pICH47732
pDEX::AT1G72950:3FLAG/pICH47732
pESTR::AT1G72950:GFP/pICH47732
pESTR::AT1G72950:6HA/pICH47732
pESTR::AT1G72950:3FLAG/pICH47732

Table 7.5 **List of of GG Level-2 vectors containing the different Level-1 transcriptional units required for each construct.**

Level 2 constructs
AT1G72940
p35SCaMV::AT1G72940:GFP/pICSL4723[pFAST-R]
p35SCaMV::AT1G72940:6HA/pICSL4723[pFAST-R]
p35SCaMV::AT1G72940:3FLAG/pICSL4723[pFAST-R]
pDEX::AT1G72940:GFP/pICSL4723[pFAST-R]
pDEX::AT1G72940:6HA/pICSL4723[pFAST-R]
pDEX::AT1G72940:3FLAG/pICSL47232[pFAST-R]
pESTR::AT1G72940:GFP/pICSL4723[pFAST-R]
pESTR::AT1G72940:6HA/pICSL4723[pFAST-R]
pESTR::AT1G72940:3FLAG/pICSL4723[pFAST-R]
AT1G72950
p35SCaMV::AT1G72950:GFP/pICSL4723[pFAST-R]
p35SCaMV::AT1G72950:6HA/pICSL4723[pFAST-R]
p35SCaMV::AT1G72950:3FLAG/pICSL4723[pFAST-R]
pDEX::AT1G72950:GFP/pICSL4723[pFAST-R]
pDEX::AT1G72950:6HA/pICSL4723[pFAST-R]
pDEX::AT1G72950:3FLAG/pICSL4723[pFAST-R]
pESTR::AT1G72950:GFP/pICSL4723[pFAST-R]
pESTR::AT1G72950:6HA/pICSL4723[pFAST-R]
pESTR::AT1G72950:3FLAG/pICSL4723[pFAST-R]

Table 7.6 **List of GG Level-2 T-DNA constructs transformed into A. *tumefaciens* for the generation of the *A. thaliana* transgenic lines described in Chapter 5.**

Level 2 constructs (*A. tumefaciens*)
AT1G72940
p35SCaMV::AT1G72940:GFP/pICSL4723[pFAST-R]
p35SCaMV::AT1G72940:6HA/pICSL4723[pFAST-R]
p35SCaMV::AT1G72940:3FLAG/pICSL4723[pFAST-R]
pDEX::AT1G72940:GFP/pICSL4723[pFAST-R]
pDEX::AT1G72940:6HA/pICSL4723[pFAST-R]
pDEX::AT1G72940:3FLAG/pICSL47232[pFAST-R]
pESTR::AT1G72940:GFP/pICSL4723[pFAST-R]
pESTR::AT1G72940:6HA/pICSL4723[pFAST-R]
pESTR::AT1G72940:3FLAG/pICSL4723[pFAST-R]
AT1G72950
p35SCaMV::AT1G72950:GFP/pICSL4723[pFAST-R]
p35SCaMV::AT1G72950:6HA/pICSL4723[pFAST-R]
p35SCaMV::AT1G72950:3FLAG/pICSL4723[pFAST-R]
pDEX::AT1G72950:GFP/pICSL4723[pFAST-R]
pDEX::AT1G72950:6HA/pICSL4723[pFAST-R]
pDEX::AT1G72950:3FLAG/pICSL4723[pFAST-R]
pESTR::AT1G72950:GFP/pICSL4723[pFAST-R]
pESTR::AT1G72950:6HA/pICSL4723[pFAST-R]
pESTR::AT1G72950:3FLAG/pICSL4723[pFAST-R]

7.5 Full list of transgenic *A. thaliana* lines described in Chapter 5

Table 7.7 **Full list of stable transgenic *A. thaliana* lines created for overexpression and inducible expression of *AT1G72940*, including the ones characterised in Chapter 5:**

AT1G72940 transgenic lines in Col-0 background												
T1 generation (Different T-DNA insertions - mother plants selected from the seeds produced by the transformed T0 plants)												
Transgene	Originating clone	Lines obtained	Lines selected	Selection	Genetic status	Box	Position	Volume	Date collected	q-RT-PCR	Western blot	
p35SCaMV::AT1G72940:GFP	p35SCaMV::AT1G72920:GFP/pICSL4723 GV3101 #2 [pFAST-R selection cassette]	T1-1 to T1-9	T1-2/T1-5/T1-6/ T1-8/T1-9	pFAST-R	heterozygous	T1 lines of AT1G72940 constructs (green bottom, transparent top)			Jul-20			
p35SCaMV::AT1G72940:6HA	p35SCaMV::AT1G72920:6HA/pICSL4723 GV3101 #1 [pFAST-R selection cassette]	no seeds transformed										
p35SCaMV::AT1G72940:3FLAG	p35SCaMV::AT1G72920:FLAG/pICSL4723 GV3101 #2 [pFAST-R selection cassette]	T1-1 to T1-15	T1-1/ T1-2/ T1-4/ T1-5/ T1-7 T1-8/ T1-9/ T1-11/ T1-12/ T1-13		heterozygous				Jul-20			
pDEX::AT1G72940:GFP	pDEX::AT1G72920:GFP/pICSL4723 GV3101 #2 [pFAST-R selection cassette + GVG cassette]	T1-1 to T1-15	T1-1/ T1-4/ T1-5/ T1-8/ T1-9/ T1-11/ T1-12/ T1-13/ T1-14		heterozygous				Jul-20			
pDEX::AT1G72940:6HA	pDEX::AT1G72920:6HA/pICSL4723 GV3101 #2 [pFAST-R selection cassette + GVG cassette]	not selected										
pDEX::AT1G72940:3FLAG	pDEX::AT1G72920:FLAG/pICSL4723 GV3101 #1 [pFAST-R selection cassette + GVG cassette]	T1-1 to T1-21	T1-3/ T1-4/ T1-7		heterozygous				Jul-20			
pESTR::AT1G72940:GFP	pESTR::AT1G72920:GFP/pICSL4723 GV3101 #2 [pFAST-R selection cassette + LexA cassette]	not selected										
pESTR::AT1G72940:6HA	pESTR::AT1G72920:6HA/pICSL4723 GV3101 #1 [pFAST-R selection cassette + LexA cassette]	not selected										
pESTR::AT1G72940:3FLAG	pESTR::AT1G72920:FLAG/pICSL4723 GV3101 #1 [pFAST-R selection cassette + LexA cassette]	not selected										

T2 generation (plants selected from the seeds produced by each mother T1 plant)												
Transgene	**T1 selected line**	**T2 plant**	**Phenotype (adult)**	**Selection**	**Genetic status**	**Box**	**Position**	**Volume**	**Date collected**	**q-RT-PCR (adult, pooled)**	**Western blot (seedlings)**	**Western blot (adult, pooled)**
p35SCaMV::AT1G72940:GFP	T1-2	1	short, several stems, delayed flowering		homozygous (+/+)	**AT1G72940 lines pFAST-R selected (transparent)**			Oct-20	4-5 fold change of transcript levels	protein not detected (crude extraction)	protein not detected (crude extraction)
		2	like Col-0		homozygous (+/+)				Oct-20			
		3	short, several stems, delayed flowering		heterozygous (+/-)				Oct-20			
		4	like Col-0		homozygous (+/+)				Oct-20			
		5	like Col-0		homozygous (+/+)				Oct-20			
		6	like Col-0		homozygous (+/+)				Oct-20			
	T1-5	1			heterozygous (+/-)				Oct-20	4-5 fold change of transcript levels	protein detected (crude extraction)	protein not detected (crude extraction)
		2			heterozygous (+/-)				Oct-20			
		3			heterozygous (+/-)				Oct-20			
		4			heterozygous (+/-)				Oct-20			
		5			heterozygous (+/-)				Oct-20			
		6			heterozygous (+/-)				Oct-20			
	T1-6	1			heterozygous (+/-)				Oct-20	4-5 fold change of transcript levels	protein maybe detected (crude extraction)	protein not detected (crude extraction)
		2			homozygous (+/+)				Oct-20			
		3			homozygous (+/+)				Oct-20			
		4			homozygous (+/+)				Oct-20			
		5			heterozygous (+/-)				Oct-20			
		6			heterozygous (+/-)				Oct-20			
	T1-8	1								5-10 fold change of transcript levels		
		2										
		3										
		4										
		5										
		6										
	T1-9	1								4-5 fold change of transcript levels		
		2										
		3										
		4										
		5										
		6										

p35SCaMV::AT1G72940:FLAG	T1-1	1	like Col-0	PFAST-R	heterozygous (+/-)			Oct-20	15-20 fold change of transcript levels	protein not detected (crude extraction) not sure the antibody worked	protein not detected (crude extraction) not sure the antibody worked
		2	like Col-0		heterozygous (+/-)			Oct-20			
		3	like Col-0		heterozygous (+/-)			Oct-20			
		4	short, several stems, delayed flowering		homozygous (+/+)			Oct-20			
		5	like Col-0		heterozygous (+/-)			Oct-20			
		6	short, several stems, delayed flowering		heterozygous (+/-)			Oct-20			
	T1-2	1			homozygous (+/+)			Oct-20	45-50 fold change of transcript levels	protein not detected (crude extraction) not sure the antibody worked	protein not detected (crude extraction) not sure the antibody
		2			homozygous (+/+)			Oct-20			
		3			homozygous (+/+)			Oct-20			
		4			homozygous (+/+)			Oct-20			
		5			heterozygous (+/-)			Oct-20			
		6			homozygous (+/+)			Oct-20			
	T1-4	1	short, several stems, delayed flowering		homozygous (+/+)			Oct-20	50-55 fold change of transcript levels	protein not detected (crude extraction) not sure the antibody worked	protein not detected (crude extraction) not sure the antibody worked
		2	short, several stems, delayed flowering					Oct-20			
		3	like Col-0		homozygous (+/+)			Oct-20			
		4	like Col-0		heterozygous (+/-)			Oct-20			
		5	like Col-0		homozygous (+/+)			Oct-20			
		6	like Col-0		homozygous (+/+)			Oct-20			

8. References

Aarts, N., Metz, M., Holub, E., Staskawicz, B.J., Daniels, M.J., Parker, J.E., 1998. Different requirements for EDS1 and NDR1 by disease resistance genes define at least two R gene-mediated signaling pathways in Arabidopsis. Proc. Natl. Acad. Sci. U. S. A. 95, 10306–10311. https://doi.org/10.1073/pnas.95.17.10306

Agrios, G.N. (1997) Plant Pathology. (San Diego: Academic Press).

Adachi, H., Contreras, M., Harant, A., Wu, C.H., Derevnina, L., Sakai, T., Duggan, C., Moratto, E., Bozkurt, T.O., Maqbool, A., Win, J., Kamoun, S., 2019a. An N-terminal motif in NLR immune receptors is functionally conserved across distantly related plant species. Elife 8, 1–31. https://doi.org/10.7554/eLife.49956

Adachi, H., Derevnina, L., Kamoun, S., 2019b. NLR singletons, pairs, and networks: evolution, assembly, and regulation of the intracellular immunoreceptor circuitry of plants. Curr. Opin. Plant Biol. 50, 121–131. https://doi.org/10.1016/j.pbi.2019.04.007

Al-Daoude, A., de Torres Zabala, M., Ko, J.-H., Grant, M., 2005. RIN13 Is a Positive Regulator of the Plant Disease Resistance Protein RPM1. Plant Cell 17, 1016–1028. https://doi.org/10.1105/tpc.104.028720

Alexandratos, N., Bruinsma, J., 2012. World agriculture towards 2030 / 2050. The 2012 Revision. ESA Working Paper No . 12-03, June 2012.

Alizon, S., de Roode, J.C., Michalakis, Y., 2013. Multiple infections and the evolution of virulence. Ecol. Lett. 16, 556–567. https://doi.org/10.1111/ele.12076

Amack, S.C., Antunes, M.S., 2020. CaMV35S promoter – A plant biology and biotechnology workhorse in the era of synthetic biology. Curr. Plant Biol. 24, 100179. https://doi.org/10.1016/j.cpb.2020.100179

Amirsadeghi, S., McDonald, A.E., Vanlerberghe, G.C., 2007. A glucocorticoid-inducible gene expression system can cause growth defects in tobacco. Planta 226, 453–463. https://doi.org/10.1007/s00425-007-0495-1

Anagnostakis, S.L., 1987. Chestnut blight : the classical problem of an introduced pathogen. Stable URL : https://www.jstor.org/stable/3807741 JSTO 79, 23–37.

Andersen, S.U., Cvitanich, C., Hougaard, B.K., Roussis, A., Grønlund, M., Jensen, D.B., Frøkjær, L.A., Jensen, E.Ø., 2003. The glucocorticoid-inducible GVG system causes severe growth defects in both root and shoot of the model legume *Lotus japonicus*. Mol. Plant-Microbe Interact. 16, 1069–1076. https://doi.org/10.1094/MPMI.2003.16.12.1069

Andersson, M.X., Kourtchenko, O., Dangl, J.L., Mackey, D., Ellerström, M., 2006. Phospholipase-dependent signalling during the AvrRpm1- and AvrRpt2-induced disease resistance responses in *Arabidopsis thaliana*. Plant J. 47, 947–959.

Aoyama, T., Chua, N.-H., 1997. A glucocorticoid-mediated transcriptional induction system in transgenic plants, The Plant Journal.

Asai, T., Tena, G., Plotnikova, J., Willmann, M.R., Chiu, W.-L., Gomez-Gomez, L., Boller, T., Ausubel, F.M., Sheen, J., 2002. MAP kinase signalling cascade in *Arabidopsis* innate immunity. Nature 415, 977–983. https://doi.org/10.1038/415977a

Bacete, L., Mélida, H., Miedes, E., Molina, A., 2018. Plant cell wall-mediated immunity: cell wall changes trigger disease resistance responses. Plant J. 93, 614–636. https://doi.org/10.1111/tpj.13807

Baggs, E., Dagdas, G., Krasileva, K. V., 2017. NLR diversity, helpers and integrated domains: making sense of the NLR IDentity. Curr. Opin. Plant Biol. 38, 59–67. https://doi.org/10.1016/j.pbi.2017.04.012

Baker, N.R., 2008. Chlorophyll fluorescence: a probe of photosynthesis in vivo. Annu. Rev. Plant Biol. 59, 89–113. https://doi.org/10.1146/annurev.arplant.59.032607.092759

Barragan, A.C., 2021. OUP accepted manuscript. Plant Cell 814–831. https://doi.org/10.1093/plcell/koaa002

Baulcombe, D., 2004. RNA silencing in plants. Nature 431, 356–363. https://doi.org/10.1038/nature02874

Baumgarten, A., Cannon, S., Spangler, R., May, G., 2003. Genome-level evolution of resistance genes in *Arabidopsis thaliana*. Genetics 165, 309–319. https://doi.org/10.1093/genetics/165.1.309

Bayless, A.M., Nishimura, M.T., 2020. Enzymatic functions for Toll/Interleukin-1 receptor domain proteins in the plant immune system. Front. Genet. 11, 1–16. https://doi.org/10.3389/fgene.2020.00539

Béné, C., Bakker, D., Chavarro, M.J., Even, B., Melo, J., Sonneveld, A., 2021. Global assessment of the impacts of COVID-19 on food security. Glob. Food Sec. 31. https://doi.org/10.1016/j.gfs.2021.100575

Berrocal-Lobo, M., Molina, A., Solano, R., 2002. Constitutive expression of ETHYLENE-RESPONSE-FACTOR1 in *Arabidopsis* confers resistance to several necrotrophic fungi. Plant J. 29, 23–32. https://doi.org/https://doi.org/10.1046/j.1365-313x.2002.01191.x

BERTANI, G., 1951. Studies on lysogenesis. I. The mode of phage liberation by lysogenic *Escherichia coli.* J. Bacteriol. 62, 293–300. https://doi.org/10.1128/JB.62.3.293-300.1951

Bethke, G., Unthan, T., Uhrig, J.F., Pöschl, Y., Gust, A.A., Scheel, D., Lee, J., 2009. Flg22 regulates the release of an ethylene response factor substrate from MAP kinase 6 in *Arabidopsis thaliana* via ethylene signaling. Proc. Natl. Acad. Sci. 106, 8067 LP – 8072. https://doi.org/10.1073/pnas.0810206106

Bi, G., Zhou, Z., Wang, W., Li, L., Rao, S., Wu, Y., Zhang, X., Menke, F.L.H., Chen, S., Zhou, J.M., 2018. Receptor-like cytoplasmic kinases directly link diverse pattern recognition receptors to the activation of mitogen-activated protein kinase cascades in *Arabidopsis*. Plant Cell 30, 1543–1561. https://doi.org/10.1105/tpc.17.00981

Birkenbihl, R.P., Liu, S., Somssich, I.E., 2017. Transcriptional events defining plant immune responses. Curr. Opin. Plant Biol. 38, 1–9. https://doi.org/10.1016/j.pbi.2017.04.004

Bonardi, V., Cherkis, K., Nishimura, M.T., Dangl, J.L., 2012. A new eye on NLR proteins: Focused on clarity or diffused by complexity? Curr. Opin. Immunol. 24, 41–50. https://doi.org/10.1016/j.coi.2011.12.006

Bonardi, V., Tang, S., Stallmann, A., Roberts, M., Cherkis, K., Dangl, J.L., Bonardi, V., Tang, S., Stallmann, A., Roberts, M., Cherkis, K., Dangl, J.L., 2017. Correction: Expanded functions for a family of plant intracellular immune receptors beyond specific recognition of pathogen effectors (Proceedings of the National Academy of Sciences of the United States of America (2011) 108 (16463-16468) DOI: 10.1073/p. Proc. Natl. Acad. Sci. U. S. A. 114, E108. https://doi.org/10.1073/pnas.1620070114

Bond, D.M., Baulcombe, D.C., 2015. Epigenetic transitions leading to heritable, RNA-mediated de novo silencing in *Arabidopsis thaliana*. Proc. Natl. Acad. Sci. U. S. A. 112, 917–922. https://doi.org/10.1073/pnas.1413053112

Botella, M.A., Parker, J.E., Frost, L.N., Bittner-eddy, P.D., Beynon, J.L., 1998. Three genes of the *Arabidopsis*. Society 10, 1847–1860.

Burch-Smith, T.M., Schiff, M., Caplan, J.L., Tsao, J., Czymmek, K., Dinesh-Kumar, S.P., 2007. A novel role for the TIR domain in association with pathogen-derived elicitors. PLoS Biol. 5, 0501–0514. https://doi.org/10.1371/journal.pbio.0050068

Büttner, D., 2016. Behind the lines–actions of bacterial type III effector proteins in plant cells. FEMS Microbiol. Rev. 40, 894–937. https://doi.org/10.1093/femsre/fuw026

Cai, R., Lewis, J., Yan, S., Liu, H., Clarke, C.R., Campanile, F., Almeida, N.F., Studholme, D.J., Lindeberg, M., Schneider, D., Zaccardelli, M., Setubal, J.C., Morales-Lizcano, N.P., Bernal, A., Coaker, G., Baker, C., Bender, C.L., Leman, S., Vinatzer, B.A., 2011. The plant pathogen *Pseudomonas syringae* pv. *tomato* is genetically monomorphic and under strong selection to evade tomato immunity. PLoS Pathog. 7. https://doi.org/10.1371/journal.ppat.1002130

Callaway, E. (2016). Devastating wheat fungus appears in Asia for first time. Nature 532, 421–422. (doi:10. 1038/532421a)

Cambiagno, D.A., Nota, F., Zavallo, D., Rius, S., Casati, P., Asurmendi, S., Alvarez, M.E., 2018. Immune receptor genes and pericentromeric transposons as targets of common epigenetic regulatory elements. Plant J. 96, 1178–1190. https://doi.org/https://doi.org/10.1111/tpj.14098

Cannon, S.B., Zhu, H., Baumgarten, A.M., Spangler, R., May, G., Cook, D.R., Young, N.D., 2002. Diversity, Distribution, and Ancient Taxonomic Relationships Within the TIR and Non-TIR NBS-LRR Resistance Gene Subfamilies. J. Mol. Evol. 54, 548–562. https://doi.org/10.1007/s0023901-0057-2

Cesari, S., 2018. Multiple strategies for pathogen perception by plant immune receptors. New Phytol. 219, 17–24. https://doi.org/10.1111/nph.14877

Césari, S., Kanzaki, H., Fujiwara, T., Bernoux, M., Chalvon, V., Kawano, Y., Shimamoto, K., Dodds, P., Terauchi, R., Kroj, T., 2014. The NB - LRR proteins RGA 4 and RGA 5 interact functionally and physically to confer disease resistance . EMBO J. 33, 1941–1959. https://doi.org/10.15252/embj.201487923

Cesari, S., Thilliez, G., Ribot, C., Chalvon, V., Michel, C., Jauneau, A., Rivas, S., Alaux, L., Kanzaki, H., Okuyama, Y., Morel, J.B., Fournier, E., Tharreau, D., Terauchi, R., Kroj, T., 2013. The rice resistance protein pair RGA4/RGA5 recognizes the *Magnaporthe oryzae* effectors AVR-Pia and AVR1-CO39 by direct binding. Plant Cell 25, 1463–1481. https://doi.org/10.1105/tpc.112.107201

Chai, J., Shi, Y., 2014. Apoptosome and inflammasome: Conserved machineries for caspase activation. Natl. Sci. Rev. 1, 101–118. https://doi.org/10.1093/nsr/nwt025

Chang, C., Yu, D., Jiao, J., Jing, S., Schulze-Lefert, P., Shen, Q.H., 2013. Barley MLA immune receptors directly interfere with antagonistically acting transcription factors to initiate disease resistance signaling. Plant Cell 25, 1158–1173. https://doi.org/10.1105/tpc.113.109942

Charrier, B., Scollan, C., Ross, S., Zubko, E., Meyer, P., 2000. Co-silencing of homologous transgenes in tobacco. Mol. Breed. 6, 407–419. https://doi.org/10.1023/A:1009672714835

Chen, F., Hu, Y., Vannozzi, A., Wu, K., Cai, H., Qin, Y., Mullis, A., Lin, Z., Zhang, L., 2017. The WRKY transcription factor family in model plants and crops. CRC. Crit. Rev. Plant Sci. 36, 311–335. https://doi.org/10.1080/07352689.2018.1441103

Chen, L., Zhang, L., Yu, D., 2010. Wounding-induced WRKY8 is involved in basal defense in *Arabidopsis*. Mol. Plant-Microbe Interact. 23, 558–565. https://doi.org/10.1094/MPMI-23-5-0558

Cheng, W., Munkvold, K.R., Gao, H., Mathieu, J., Schwizer, S., Wang, S., Yan, Y., Wang, J., Martin, G.B., Chai, J., 2011. Structural analysis of *Pseudomonas syringae* AvrPtoB bound to host BAK1 reveals two similar kinase-interacting domains in a type iii effector. Cell Host Microbe 10, 616–626. https://doi.org/10.1016/j.chom.2011.10.013

Chisholm, S.T., Coaker, G., Day, B., Staskawicz, B.J., 2006. Host-microbe interactions: Shaping the evolution of the plant immune response. Cell 124, 803–814. https://doi.org/10.1016/j.cell.2006.02.008

Choi, J., Tanaka, K., Cao, Y., Qi, Y., Qiu, J., Liang, Y., Lee, S.Y., Stacey, G., 2014. Identification of a plant receptor for extracellular ATP. Science (80-.). 343, 290–294. https://doi.org/10.1126/science.343.6168.290

Cohn, J.R., Martin, G.B., 2005. *Pseudomonas syringae* pv. *tomato* type III effectors AvrPto and AvrPtoB promote ethylene-dependent cell death in tomato. Plant J. 44, 139–154. https://doi.org/10.1111/j.1365-313X.2005.02516.x

Cook, D.E., Mesarich, C.H., Thomma, B.P.H.J., 2015. Understanding plant immunity as a surveillance system to detect invasion. Annu. Rev. Phytopathol. 53, 541–563. https://doi.org/10.1146/annurev-phyto-080614-120114

Cui, H., Tsuda, K., Parker, J.E., 2015. Effector-triggered immunity: From pathogen perception to robust defense. Annu. Rev. Plant Biol. 66, 487–511. https://doi.org/10.1146/annurev-arplant-050213-040012

Dangl, J.L., Horvath, D.M., Staskawich, B.J., 2013. Pivoting the plant immune system. Science (80-.). 341, 745–751.

Dangl, J.L., Jones, J.D.G., 2001. Defence responses to infection. Nature 411.

Daniel, X., Lacomme, C., Morel, J.B., Roby, D., 1999. A novel myb oncogene homologue in *Arabidopsis thaliana* related to hypersensitive cell death. Plant J. 20, 57–66. https://doi.org/10.1046/j.1365-313x.1999.00578.x

De Lorenzo, G., Ferrari, S., Giovannoni, M., Mattei, B., Cervone, F., 2019. Cell wall traits that influence plant development, immunity, and bioconversion. Plant J. 97, 134–147. https://doi.org/10.1111/tpj.14196

de Torres-Zabala, M., Truman, W., Bennett, M.H., Lafforgue, G., Mansfield, J.W., Rodriguez Egea, P., Bögre, L., Grant, M., 2007. *Pseudomonas syringae* pv. *tomato* hijacks the *Arabidopsis* abscisic acid signalling pathway to cause disease. EMBO J. 26, 1434–1443. https://doi.org/https://doi.org/10.1038/sj.emboj.7601575

Denancé, N., Sánchez-Vallet, A., Goffner, D., Molina, A., 2013. Disease resistance or growth: the role of plant hormones in balancing immune responses and fitness costs. Front. Plant Sci. 4, 155. https://doi.org/10.3389/fpls.2013.00155

Deplancke, B., Mukhopadhyay, A., Ao, W., Elewa, A.M., Grove, C.A., Martinez, N.J., Sequerra, R., Doucette-Stamm, L., Reece-Hoyes, J.S., Hope, I.A., Tissenbaum, H.A., Mango, S.E., Walhout, A.J.M., 2006. A gene-centered *C. elegans* protein-dna interaction network. Cell 125, 1193–1205. https://doi.org/10.1016/j.cell.2006.04.038

Deslandes, L., Olivier, J., Theulieres, F., Hirsch, J., Feng, D.X., Bittner-Eddy, P., Beynon, J., Marco, Y., 2002. Resistance to *Ralstonia solanacearum* in *Arabidopsis thaliana* is conferred by the recessive *RRS1-R* gene, a member of a novel family of resistance genes. Proc. Natl. Acad. Sci. U. S. A. 99, 2404–2409. https://doi.org/10.1073/pnas.032485099

Dodds, P.N., Rathjen, J.P., 2010. Plant immunity: Towards an integrated view of plant-pathogen interactions. Nat. Rev. Genet. 11, 539–548. https://doi.org/10.1038/nrg2812

Dubois, M., Skirycz, A., Claeys, H., Maleux, K., Dhondt, S., De Bodt, S., Vanden Bossche, R., De Milde, L., Yoshizumi, T., Matsui, M., Inzé, D., 2013. ETHYLENE RESPONSE FACTOR6 acts as a central regulator of leaf growth under water-limiting conditions in *Arabidopsis.* Plant Physiol. 162, 319–332. https://doi.org/10.1104/pp.113.216341

Duplan, V., Rivas, S., 2014. E3 ubiquitin-ligases and their target proteins during the regulation of plant innate immunity. Front. Plant Sci. 5, 1–6. https://doi.org/10.3389/fpls.2014.00042

Edwards, J.M., Roberts, T.H., Atwell, B.J., 2012. Quantifying ATP turnover in anoxic coleoptiles of rice (*Oryza sativa*) demonstrates preferential allocation of energy to protein synthesis. J. Exp. Bot. 63, 4389–4402. https://doi.org/10.1093/jxb/ers114

Eitas, T.K., Dangl, J.L., 2010. NB-LRR proteins: Pairs, pieces, perception, partners, and pathways. Curr. Opin. Plant Biol. 13, 472–477. https://doi.org/10.1016/j.pbi.2010.04.007

Elphinstone, J.G., Allen, C., Prior, P., and Hayward, A.C. (2005). The current bacterial wilt situation: a global overview.: 9–28.

Engler, C., Youles, M., Gruetzner, R., Ehnert, T.M., Werner, S., Jones, J.D.G., Patron, N.J., Marillonnet, S., 2014. A Golden Gate modular cloning toolbox for plants. ACS Synth. Biol. 3, 839–843. https://doi.org/10.1021/sb4001504

Engler, C., Youles, M., Gruetzner, R., Ehnert, T.M., Werner, S., Jones, J.D.G., Patron, N.J., Marillonnet, S., 2012. MoClo Tool Kit - Supplementary Data 2 - Moduls + AB resistance 7–9.

Esker, P.D., Savary, S., McRoberts, N., 2012. Crop loss analysis and global food supply: Focusing now on required harvests. CAB Rev. Perspect. Agric. Vet. Sci. Nutr. Nat. Resour. 7. https://doi.org/10.1079/PAVSNNR20127052

Essuman, K., Summers, D.W., Sasaki, Y., Mao, X., DiAntonio, A., Milbrandt, J., 2017. The SARM1 Toll/Interleukin-1 receptor domain possesses intrinsic NAD+ cleavage activity that promotes pathological axonal degeneration. Neuron 93, 1334-1343.e5. https://doi.org/10.1016/j.neuron.2017.02.022

Essuman, K., Summers, D.W., Sasaki, Y., Mao, X., Yim, A.K.Y., DiAntonio, A., Milbrandt, J., 2018. TIR domain proteins are an ancient family of NAD+-consuming enzymes. Curr. Biol. 28, 421-430.e4. https://doi.org/10.1016/j.cub.2017.12.024

Fagard, M., Vaucheret, H., 2000. (Trans)gene silencing in plants: How Many Mechanisms? Annu. Rev. Plant Physiol. Plant Mol. Biol. 51, 167–194. https://doi.org/10.1146/annurev.arplant.51.1.167

Falak, N., Imran, Q.M., Hussain, A., Yun, B.W., 2021. Transcription factors as the “Blitzkrieg” of plant defense: A pragmatic view of nitric oxide’s role in gene regulation. Int. J. Mol. Sci. 22, 1–23. https://doi.org/10.3390/ijms22020522

FAO, 2020. COVID-19 and the risk to food supply chains: how to respond. Food Agric. Organ. United Nations 1–7. https://doi.org/10.4060/ca8388en

Farmer, E., Farmer, E., Mousavi, S., Lenglet, A., 2013. Leaf numbering for experiments on long distance signalling in *Arabidopsis*. Protoc. Exch. 1–10. https://doi.org/10.1038/protex.2013.071

Fei, Q., Xia, R., Meyers, B.C., 2013. Phased, secondary, small interfering RNAs in posttranscriptional regulatory networks. Plant Cell 25, 2400–2415. https://doi.org/10.1105/tpc.113.114652

Feng, J.-X., Liu, D., Pan, Y., Gong, W., Ma, L.-G., Luo, J.-C., Deng, X.W., Zhu, Y.-X., 2005. An annotation update via cDNA sequence analysis and comprehensive profiling of developmental, hormonal or environmental responsiveness of the *Arabidopsis* AP2/EREBP transcription factor gene family. Plant Mol. Biol. 59, 853–868. https://doi.org/10.1007/s11103-005-1511-0

Fones, H. and Gurr, S. (2015). The impact of Septoria tritici Blotch disease on wheat: An EU perspective. Fungal Genet. Biol. 79: 3–7.

Fry, W.E., Birch, P.R.J., Judelson, H.S., Grünwald, N.J., Danies, G., Everts, K.L., Gevens, A.J., Gugino, B.K., Johnson, D.A., Johnson, S.B., McGrath, M.T., Myers, K.L., Ristaino, J.B., Roberts, P.D., Secor, G., Smart, C.D., 2015. Five reasons to consider *Phytophthora infestans* a reemerging pathogen. Phytopathology 105, 966–981. https://doi.org/10.1094/PHYTO-01-15-0005-FI

FSIN, Global Network Against Food Crises, 2021. Global report on food crises 2021. Food Secur. Inf. Netw. 1–202.

Galan, J.E., Collmer, A., 1999. Type III secretion machines : bacterial devices for protein delivery into host cells 284, 1322–1329.

Gardan, L., Shafik, H., Belouin, S., Broch, R., Grimont, F., and Grimont, P.A. (1999). DNA relatedness among the pathovars of *Pseudomonas syringae* and description of *Pseudomonas tremae* sp. *nov*. and *Pseudomonas cannabina* sp. *nov*. (ex Sutic and Dowson 1959). Int. J. Syst. Bacteriol. 49, 469-478.

Gardiner, D.M., McDonald, M.C., Covarelli, L., Solomon, P.S., Rusu, A.G., Marshall, M., Kazan, K., Chakraborty, S., McDonald, B.A., Manners, J.M., 2012. Comparative pathogenomics reveals horizontally acquired novel virulence genes in fungi infecting cereal hosts. PLoS Pathog. 8. https://doi.org/10.1371/journal.ppat.1002952

Garner, C.M., Kim, S.H., Spears, B.J., Gassmann, W., 2016. Express yourself: Transcriptional regulation of plant innate immunity. Semin. Cell Dev. Biol. 56, 150–162. https://doi.org/10.1016/j.semcdb.2016.05.002

Geng, X., Mackey, D., 2011. Dose-response to and systemic movement of dexamethasone in the GVG-inducible transgene system in *Arabidopsis*, in: McDowell, J.M. (Ed.), Plant Immunity: Methods and Protocols. Humana Press, Totowa, NJ, pp. 59–68. https://doi.org/10.1007/978-1-61737-998-7_6

Gibbs, D.J., Conde, J.V., Berckhan, S., Prasad, G., Mendiondo, G.M., Holdsworth, M.J., 2015. Group VII ethylene response factors coordinate oxygen and nitric oxide signal transduction and stress responses in plants. Plant Physiol. 169, 23–31. https://doi.org/10.1104/pp.15.00338

Gizjen M. (2008). Diane Cuppels and the history of *Pseudomonas syringae* pv. *tomato* DC3000. IS-MPMI Report. 1:4–5. http://www.ismpminet.org/newsletter/pdf/0801.pdf

Godfray, H.C.J., 2015. The debate over sustainable intensification. Food Secur. 7, 199–208. https://doi.org/10.1007/s12571-015-0424-2

Godfray, H. C. J., Beddington, J. R., Crute, I. R., Haddad, L., Lawrence, D., Muir, J. F., Pretty, J., Robinson, S., Thomas, S. M., Toulmin, C. (2010). Food security: the challenge of feeding 9 billion people. *Science,* 327, 5967, pp. 812-818.

Goodspeed, D., Chehab, E.W., Min-Venditti, A., Braam, J., Covington, M.F., 2012. *Arabidopsis* synchronizes jasmonate-mediated defense with insect

circadian behavior. Proc. Natl. Acad. Sci. 109, 4674–4677. https://doi.org/10.1073/pnas.1116368109

Goss, E.M., Cardenas, M.E., Myers, K., Forbes, G.A., Fry, W.E., Restrepo, S., Grünwald, N.J., 2011. The plant pathogen *Phytophthora andina* emerged via hybridization of an unknown phytophthora species and the irish potato famine pathogen, *P. infestans*. PLoS One 6. https://doi.org/10.1371/journal.pone.0024543

Gottig, N., Garavaglia, B.S., Garofalo, C.G., Zimaro, T., 2010. Mechanisms of infection used by *Xanthomonas axonopodis* pv . *citri i*n citrus canker disease.

Grafton, R.Q., Daugbjerg, C., Qureshi, M.E., 2015. Towards food security by 2050. Food Secur. 7, 179–183. https://doi.org/10.1007/s12571-015-0445-x

Grant, M., Brown, I., Adams, S., Knight, M., Ainslie, A., Mansfield, J., 2000. The *RPM1* plant disease resistance gene facilitates a rapid and sustained increase in cytosolic calcium that is necessary for the oxidative burst and hypersensitive cell death. Plant J. 23, 441–450. https://doi.org/10.1046/j.1365-313X.2000.00804.x

Gu, Y.-Q., Wildermuth, M.C., Chakravarthy, S., Loh, Y.-T., Yang, C., He, X., Han, Y., Martin, G.B., 2002. Tomato transcription factors pti4, pti5, and pti6 activate defense responses when expressed in *Arabidopsis* . Plant Cell 14, 817–831. https://doi.org/10.1105/tpc.000794

Gust, A.A., Pruitt, R., Nürnberger, T., 2017. Sensing danger: key to activating plant immunity. Trends Plant Sci. 22, 779–791. https://doi.org/10.1016/j.tplants.2017.07.005

Hann, D.R., Domínguez-Ferreras, A., Motyka, V., Dobrev, P.I., Schornack, S., Jehle, A., Felix, G., Chinchilla, D., Rathjen, J.P., Boller, T., 2014. The *Pseudomonas* type III effector HopQ1 activates cytokinin signaling and interferes with plant innate immunity. New Phytol. 201, 585–598. https://doi.org/10.1111/nph.12544

Hertel, T.W., 2015. The challenges of sustainably feeding a growing planet. Food Secur. 7, 185–198. https://doi.org/10.1007/s12571-015-0440-2

Hirano, S.S., Upper, C.D., 2000. Bacteria in the leaf ecosystem with emphasis on *Pseudomonas syringae* - a pathogen, ice nucleus, and epiphyte. Microbiol. Mol. Biol. Rev. 64, 624–653. https://doi.org/10.1128/mmbr.64.3.624-653.2000

Horsefield, S., Burdett, H., Zhang, X., Manik, M.K., Shi, Y., Chen, J., Qi, T., Gilley, J., Lai, J.S., Rank, M.X., Casey, L.W., Gu, W., Ericsson, D.J., Foley, G., Hughes, R.O., Bosanac, T., Von Itzstein, M., Rathjen, J.P., Nanson, J.D., Boden, M., Dry, I.B., Williams, S.J., Staskawicz, B.J., Coleman, M.P., Ve, T., Dodds, P.N., Kobe, B., 2019. NAD+ cleavage activity by animal and plant TIR domains in cell death pathways. Science (80-.). 365, 793–799. https://doi.org/10.1126/science.aax1911

Huang, C.Y., Wang, H., Hu, P., Hamby, R., Jin, H., 2019. Small RNAs – big players in plant-microbe interactions. Cell Host Microbe 26, 173–182. https://doi.org/10.1016/j.chom.2019.07.021

Huang, S., Monaghan, J., Zhong, X., Lin, L., Sun, T., Dong, O.X., Li, X., 2014. HSP90s are required for NLR immune receptor accumulation in *Arabidopsis.* Plant J. 79, 427–439. https://doi.org/10.1111/tpj.12573

Hubert, D.A., Tornero, P., Belkhadir, Y., Krishna, P., Takahashi, A., Shirasu, K., Dangl, J.L., 2003. Cytosolic HSP90 associates with and modulates the *Arabidopsis* RPM1 disease resistance protein. EMBO J. 22, 5679–5689. https://doi.org/10.1093/emboj/cdg547

Ime Edet, S., Samuel, N.E., Etim, A.E., Titus, E., 2014. Impact of overpopulation on the biological diversity conservation in boki local government area of Cross River State, Nigeria. Am. J. Environ. Eng. 2014, 94–98. https://doi.org/10.5923/j.ajee.20140405.02

Inoue, H., Hayashi, N., Matsushita, A., Xinqiong, L., Nakayama, A., Sugano, S., Jiang, C.-J., Takatsuji, H., 2013. Blast resistance of CC-NB-LRR protein Pb1 is mediated by WRKY45 through protein–protein interaction. Proc. Natl. Acad. Sci. 110, 9577 LP – 9582. https://doi.org/10.1073/pnas.1222155110

Jauvion, V., Rivard, M., Bouteiller, N., Elmayan, T., Vaucheret, H., 2012. RDR2 partially antagonizes the production of RDR6-Dependent siRNA in sense transgene-mediated PTGS. PLoS One 7, e29785.

Jenkins, K.A., Mansell, A., 2010. TIR-containing adaptors in Toll-like receptor signalling. Cytokine 49, 237–244. https://doi.org/10.1016/j.cyto.2009.01.009

Jones, J.D.G., Dangl, J.L., 2006. The plant immune system. Nature 444, 323–329. https://doi.org/10.1038/nature05286

Jones, J.D.G., Vance, R.E., Dangl, J.L., 2016. Intracellular innate immune surveillance devices in plants and animals. Science (80-.). 354. https://doi.org/10.1126/science.aaf6395

Joshi-Saha, A., Valon, C., Leung, J., 2011. Abscisic acid signal off the STARTing block. Mol. Plant 4, 562–580. https://doi.org/10.1093/mp/ssr055

Jubic, L.M., Saile, S., Furzer, O.J., El Kasmi, F., Dangl, J.L., 2019. Help wanted: helper NLRs and plant immune responses. Curr. Opin. Plant Biol. 50, 82–94. https://doi.org/10.1016/j.pbi.2019.03.013

Jung, S., Lee, H.-J., Lee, Y., Kang, K., Kim, Y.S., Grimm, B., Back, K., 2008. Toxic tetrapyrrole accumulation in protoporphyrinogen IX oxidase-overexpressing transgenic rice plants. Plant Mol. Biol. 67, 535–546. https://doi.org/10.1007/s11103-008-9338-0

Juroszek, P., Von Tiedemann, A., 2015. Linking plant disease models to climate change scenarios to project future risks of crop diseases: A review. J. Plant Dis. Prot. 122, 3–15. https://doi.org/10.1007/BF03356525

Kadota, Y., Sklenar, J., Derbyshire, P., Stransfeld, L., Asai, S., Ntoukakis, V., Jones, J.D., Shirasu, K., Menke, F., Jones, A., Zipfel, C., 2014. Direct Regulation of the NADPH Oxidase RBOHD by the PRR-Associated Kinase BIK1 during Plant Immunity. Mol. Cell 54, 43–55. https://doi.org/10.1016/j.molcel.2014.02.021

Kang, H.-G., Fang, Y., Singh, K.B., 1999. A glucocorticoid-inducible transcription system causes severe growth defects in *Arabidopsis* and induces defense-related genes. Plant J. 20, 127–133. https://doi.org/https://doi.org/10.1046/j.1365-313X.1999.00575.x

Kapranov, P., Cheng, J., Dike, S., Nix, D.A., Duttagupta, R., Willingham, A.T., Stadler, P.F., Hertel, J., Hackermüller, J., Hofacker, I.L., Bell, I., Cheung, E., Drenkow, J., Dumais, E., Patel, S., Helt, G., Ganesh, M., Ghosh, S.,

Piccolboni, A., Sementchenko, V., Tammana, H., Gingeras, R., T., 2007. RNA maps reveal new RNA classes and a possible function for pervasive transcription. Science (80-.). 316, 1484–1488. https://doi.org/10.1126/science.1138341

Katagiri, F., Thilmony, R., He, S.Y., 2002. The *Arabidopsis thaliana-Pseudomonas syringae* Interaction. Arab. B. 1, e0039. https://doi.org/10.1199/tab.0039

Katagiri, F., Tsuda, K., 2010. Understanding the plant immune system. Mol. Plant-Microbe Interact. 23, 1531–1536. https://doi.org/10.1094/MPMI-04-10-0099

Katiyar-Agarwal, S., Jin, H., 2010. Role of small RNAs in host-microbe interactions. Annu. Rev. Phytopathol. 48, 225–246. https://doi.org/10.1146/annurev-phyto-073009-114457

Katiyar-Agarwal, S., Morgan, R., Dahlbeck, D., Borsani, O., Villegas, A., Zhu, J.-K., Staskawicz, B.J., Jin, H., 2006. A pathogen-inducible endogenous siRNA in plant immunity. Proc. Natl. Acad. Sci. 103, 18002–18007. https://doi.org/10.1073/pnas.0608258103

Kazan, K., Lyons, R., 2014. Intervention of phytohormone pathways by pathogen effectors. Plant Cell 26, 2285–2309. https://doi.org/10.1105/tpc.114.125419

Keller, H., Boyer, L., Abad, P., 2016. Disease susceptibility in the Zig-Zag model of host-microbe interactions: Only a consequence of immune suppression? Mol. Plant Pathol. 17, 475–479. https://doi.org/10.1111/mpp.12371

Kempin, S.A., Savidge, B., Yanofsky, M.F., 1995. Molecular basis of the cauliflower phenotype in *Arabidopsis*. Science (80-.). 267, 522–525. https://doi.org/10.1126/science.7824951

Kim, M.G., da Cunha, L., McFall, A.J., Belkhadir, Y., DebRoy, S., Dangl, J.L., Mackey, D., 2005. Two *Pseudomonas syringae* type iii effectors inhibit RIN4-regulated basal defense in *Arabidopsis*. Cell 121, 749–759. https://doi.org/https://doi.org/10.1016/j.cell.2005.03.025

Kim, M.G., Geng, X., Lee, S.Y., Mackey, D., 2009. The *Pseudomonas syringae* type III effector AvrRpm1 induces significant defenses by activating the *Arabidopsis* nucleotide-binding leucine-rich repeat protein RPS2. Plant J. 57, 645–653. https://doi.org/https://doi.org/10.1111/j.1365-313X.2008.03716.x

Kim, S., Park, J., Yeom, S.I., Kim, Y.M., Seo, E., Kim, K.T., Kim, M.S., Lee, J.M., Cheong, K., Shin, H.S., Kim, S.B., Han, K., Lee, J., Park, M., Lee, H.A., Lee, Hye Young, Lee, Y., Oh, S., Lee, J.H., Choi, Eunhye, Choi, Eunbi, Lee, S.E., Jeon, J., Kim, H., Choi, G., Song, H., Lee, J.K., Lee, S.C., Kwon, J.K., Lee, Hea Young, Koo, N., Hong, Y., Kim, R.W., Kang, W.H., Huh, J.H., Kang, B.C., Yang, T.J., Lee, Y.H., Bennetzen, J.L., Choi, D., 2017. New reference genome sequences of hot pepper reveal the massive evolution of plant disease-resistance genes by retroduplication. Genome Biol. 18, 1–11. https://doi.org/10.1186/s13059-017-1341-9

Kim, S.H., Qi, D., Ashfield, T., Helm, M., Innes, R.W., 2016. Using decoys to expand the recognition specificity of a plant disease resistance protein. Science (80-.). 351, 684–687. https://doi.org/10.1126/science.aad3436

King, E.O., Ward, M.K., Raney, D.E., 1954. Two simple media for the demonstration of pyocyanin and fluorescin. J. Lab. Clin. Med. 44, 301—307.

Kiselev, K. V., Aleynova, O.A., Ogneva, Z. V., Suprun, A.R., Dubrovina, A.S., 2021. 35S promoter-driven transgenes are variably expressed in different organs of *Arabidopsis thaliana* and in response to abiotic stress. Mol. Biol. Rep. 48, 2235–2241. https://doi.org/10.1007/s11033-021-06235-x

Koivuniemi, A., Aro, E.M., Andersson, B., 1995. Degradation of the D1- and D2-proteins of photosystem II in higher plants is regulated by reversible phosphorylation. Biochemistry 34, 16022–16029. https://doi.org/10.1021/bi00049a016

Koornneef, M., Meinke, D., 2010. The development of *Arabidopsis* as a model plant. Plant J. 61, 909–921. https://doi.org/10.1111/j.1365-313X.2009.04086.x

Kourtchenko, O., Andersson, M.X., Hamberg, M., Brunnström, A., Göbel, C., McPhail, K.L., Gerwick, W.H., Feussner, I., Ellerström, M., 2007. Oxo-phytodienoic acid-containing galactolipids in *Arabidopsis*: jasmonate signaling

dependence. Plant Physiol. 145, 1658–1669. https://doi.org/10.1104/pp.107.104752

Le Roux, C., Huet, G., Jauneau, A., Camborde, L., Trémousaygue, D., Kraut, A., Zhou, B., Levaillant, M., Adachi, H., Yoshioka, H., Raffaele, S., Berthomé, R., Couté, Y., Parker, J.E., Deslandes, L., 2015. A receptor pair with an integrated decoy converts pathogen disabling of transcription factors to immunity. Cell 161, 1074–1088. https://doi.org/10.1016/j.cell.2015.04.025

Lee, H.A., Yeom, S.I., 2015. Plant NB-LRR proteins: Tightly regulated sensors in a complex manner. Brief. Funct. Genomics 14, 233–242. https://doi.org/10.1093/bfgp/elv012

Lee, S., Moon, J.S., Ko, T.-S., Petros, D., Goldsbrough, P.B., Korban, S.S., 2003. Overexpression of *Arabidopsis* phytochelatin synthase paradoxically leads to hypersensitivity to cadmium stress. Plant Physiol. 131, 656–663. https://doi.org/10.1104/pp.014118

Leister, D., 2004. Tandem and segmental gene duplication and recombination in the evolution of plant disease resistance genes. Trends Genet. https://doi.org/10.1016/j.tig.2004.01.007

Lewis, L.A., Polanski, K., de Torres-Zabala, M., Jayaraman, S., Bowden, L., Moore, J., Penfold, C.A., Jenkins, D.J., Hill, C., Baxter, L., Kulasekaran, S., Truman, W., Littlejohn, G., Prusinska, J., Mead, A., Steinbrenner, J., Hickman, R., Rand, D., Wild, D.L., Ott, S., Buchanan-Wollaston, V., Smirnoff, N., Beynon, J., Denby, K., Grant, M., 2015. Transcriptional dynamics driving MAMP-triggered immunity and pathogen effector-mediated immunosuppression in *Arabidopsis* leaves following infection with *Pseudomonas syringae* pv *tomato* DC3000. Plant Cell 27, 3038–3064. https://doi.org/10.1105/tpc.15.00471

Li, H., Wang, Y., Wu, M., Li, L., Li, C., Han, Z., Yuan, J., Chen, C., Song, W., Wang, C., 2017. Genome-wide identification of AP2/ERF transcription factors in cauliflower and expression profiling of the ERF family under salt and drought stresses. Front. Plant Sci.

Li, L., Kim, P., Yu, L., Cai, G., Chen, S., Alfano, J.R., Zhou, J.-M., 2016. Activation-dependent destruction of a co-receptor by a *Pseudomonas*

syringae effector dampens plant immunity. Cell Host Microbe 20, 504–514. https://doi.org/10.1016/j.chom.2016.09.007

Li, L., Li, M., Yu, L., Zhou, Z., Liang, X., Liu, Z., Cai, G., Gao, L., Zhang, X., Wang, Y., Chen, S., Zhou, J.M., 2014. The FLS2-associated kinase BIK1 directly phosphorylates the NADPH oxidase RbohD to control plant immunity. Cell Host Microbe 15, 329–338. https://doi.org/10.1016/j.chom.2014.02.009

Li, S., Wang, C., Zhou, L., Shou, H., 2014. Oxygen deficit alleviates phosphate overaccumulation toxicity in OsPHR2 overexpression plants. J. Plant Res. 127, 433–440. https://doi.org/10.1007/s10265-014-0628-0

Li, X., Kapos, P., Zhang, Y., 2015. NLRs in plants. Curr. Opin. Immunol. 32, 114–121. https://doi.org/10.1016/j.coi.2015.01.014

Liang, W., van Wersch, S., Tong, M., Li, X., 2019. TIR-NB-LRR immune receptor SOC3 pairs with truncated TIR-NB protein CHS1 or TN2 to monitor the homeostasis of E3 ligase SAUL1. New Phytol. 221, 2054–2066. https://doi.org/10.1111/nph.15534

Licausi, F., Ohme-Takagi, M., Perata, P., 2013. APETALA2/Ethylene Responsive Factor (AP2/ERF) transcription factors: mediators of stress responses and developmental programs. New Phytol. 199, 639–649. https://doi.org/10.1111/nph.12291

Ling, T., Bellin, D., Vandelle, E., Imanifard, Z., Delledonne, M., 2017. Host-mediated s-nitrosylation disarms the bacterial effector HopAI1 to reestablish immunity. Plant Cell 29, 2871–2881. https://doi.org/10.1105/tpc.16.00557

Lipper, L., Thornton, P., Campbell, B.M., Baedeker, T., Braimoh, A., Bwalya, M., Caron, P., Cattaneo, A., Garrity, D., Henry, K., Hottle, R., Jackson, L., Jarvis, A., Kossam, F., Mann, W., McCarthy, N., Meybeck, A., Neufeldt, H., Remington, T., Sen, P.T., Sessa, R., Shula, R., Tibu, A., Torquebiau, E.F., 2014. Climate-smart agriculture for food security. Nat. Clim. Chang. 4, 1068–1072. https://doi.org/10.1038/nclimate2437

Liu, J., Jung, C., Xu, J., Wang, H., Deng, S., Bernad, L., Arenas-Huertero, C., Chua, N.-H., 2012. Genome-wide analysis uncovers regulation of long

intergenic noncoding RNAs in *Arabidopsis* . Plant Cell 24, 4333–4345. https://doi.org/10.1105/tpc.112.102855

Liu, N., Hake, K., Wang, W., Zhao, T., Romeis, T., Tang, D., 2017. Calcium-dependent protein kinase5 associates with the truncated NLR protein TIR-NBS2 to contribute to exo70B1-mediated immunity. Plant Cell 29, 746–759. https://doi.org/10.1105/tpc.16.00822

Liu, X., Grabherr, H.M., Willmann, R., Kolb, D., Brunner, F., Bertsche, U., Kühner, D., Franz-Wachtel, M., Amin, B., Felix, G., Ongena, M., Nürnberger, T., Gust, A.A., 2014. Host-induced bacterial cell wall decomposition mediates pattern-triggered immunity in *Arabidopsis*. Elife 3, 1–24. https://doi.org/10.7554/elife.01990

Lu, D., Wu, S., Gao, X., Zhang, Y., Shan, L., He, P., 2010. A receptor-like cytoplasmic kinase, BIK1, associates with a flagellin receptor complex to initiate plant innate immunity. Proc. Natl. Acad. Sci. U. S. A. 107, 496–501. https://doi.org/10.1073/pnas.0909705107

Macho, A.P., Zipfel, C., 2015. Targeting of plant pattern recognition receptor-triggered immunity by bacterial type-III secretion system effectors. Curr. Opin. Microbiol. 23, 14–22. https://doi.org/10.1016/j.mib.2014.10.009

Mackey, D., Belkhadir, Y., Alonso, J.M., Ecker, J.R., Dangl, J.L., 2003. *Arabidopsis* RIN4 is a target of the type III virulence effector AvrRpt2 and modulates RPS2-mediated resistance. Cell 112, 379–389. https://doi.org/10.1016/S0092-8674(03)00040-0

Mackey, D., Holt, B.F., Wiig, A., Dangl, J.L., 2002. RIN4 interacts with *Pseudomonas syringae* type III effector molecules and is required for RPM1-mediated resistance in *Arabidopsis*. Cell 108, 743–754. https://doi.org/10.1016/S0092-8674(02)00661-X

Majhi, B.B., Sreeramulu, S., Sessa, G., 2019. Brassinosteroid-signaling kinase5 associates with immune receptors and is required for immune responses. Plant Physiol. 180, 1166–1184. https://doi.org/10.1104/pp.18.01492

Maqbool, A., Saitoh, H., Franceschetti, M., Stevenson, C.E.M., Uemura, A., Kanzaki, H., Kamoun, S., Terauchi, R., Banfield, M.J., 2015. Structural basis of pathogen recognition by an integrated HMA domain in a plant NLR immune receptor. Elife 4, 1–24. https://doi.org/10.7554/eLife.08709

Marcec, M.J., Gilroy, S., Poovaiah, B.W., Tanaka, K., 2019. Mutual interplay of Ca 2+ and ROS signaling in plant immune response. Plant Sci. 283, 343–354. https://doi.org/10.1016/j.plantsci.2019.03.004

Mardones, F.O., Rich, K.M., Boden, L.A., Moreno-Switt, A.I., Caipo, M.L., Zimin-Veselkoff, N., Alateeqi, A.M., Baltenweck, I., 2020. The COVID-19 Pandemic and global food security. Front. Vet. Sci. 7, 1–8. https://doi.org/10.3389/fvets.2020.578508

Matzke, M.A., Mette, M.F., Matzke, A.J.M., 2000. Transgene silencing by the host genome defense: implications for the evolution of epigenetic control mechanisms in plants and vertebrates. Plant Mol. Biol. 43, 401–415. https://doi.org/10.1023/A:1006484806925

McDonald, B.A., Stukenbrock, E.H., 2016. Rapid emergence of pathogens in agro-ecosystems: Global threats to agricultural sustainability and food security. Philos. Trans. R. Soc. B Biol. Sci. 371. https://doi.org/10.1098/rstb.2016.0026

Meng, X., Xu, J., He, Y., Yang, K.Y., Mordorski, B., Liu, Y., Zhang, S., 2013. Phosphorylation of an ERF transcription factor by *Arabidopsis* MPK3/MPK6 regulates plant defense gene induction and fungal resistance. Plant Cell 25, 1126–1142. https://doi.org/10.1105/tpc.112.109074

Meng, X., Zhang, S., 2013. MAPK Cascades in plant disease resistance signaling. Annu. Rev. Phytopathol. 51, 245–266. https://doi.org/10.1146/annurev-phyto-082712-102314

Mermigka, G., Amprazi, M., Mentzelopoulou, A., Amartolou, A., Sarris, P.F., 2020. Plant and animal innate immunity complexes: fighting different enemies with similar weapons. Trends Plant Sci. 25, 80–91. https://doi.org/10.1016/j.tplants.2019.09.008

Meyers, B.C., Kozik, A., Griego, A., Kuang, H., Michelmore, R.W., 2003. Genome-wide analysis of NBS-LRR-encoding genes in *Arabidopsis*. Plant Cell 15, 809–834. https://doi.org/10.1105/tpc.009308

Meyers, B.C., Morgante, M., Michelmore, R.W., 2002. TIR-X and TIR-NBS proteins: Two new families related to disease resistance TIR-NBS-LRR proteins encoded in *Arabidopsis* and other plant genomes. Plant J. 32, 77–92. https://doi.org/10.1046/j.1365-313X.2002.01404.x

Miller, R.N.G., Alves, G.S.C., Van Sluys, M.A., 2017. Plant immunity: Unravelling the complexity of plant responses to biotic stresses. Ann. Bot. 119, 681–687. https://doi.org/10.1093/aob/mcw284

Mine, A., Seyfferth, C., Kracher, B., Berens, M.L., Becker, D., Tsuda, K., 2018. The defense phytohormone signaling network enables rapid, high-amplitude transcriptional reprogramming during effector-triggered immunity. Plant Cell 30, 1199–1219. https://doi.org/10.1105/tpc.17.00970

Mizoi, J., Shinozaki, K., Yamaguchi-Shinozaki, K., 2012. AP2/ERF family transcription factors in plant abiotic stress responses. Biochim. Biophys. Acta 1819, 86–96. https://doi.org/10.1016/j.bbagrm.2011.08.004

Moore, J.W., Loake, G.J., Spoel, S.H., 2011. Transcription dynamics in plant immunity. Plant Cell 23, 2809–2820. https://doi.org/10.1105/tpc.111.087346

Murashige, T., Skoog, F., 1962. A revised medium for rapid growth and bio assays with tobacco tissue cultures. Physiol. Plant. 15, 473–497. https://doi.org/10.1111/j.1399-3054.1962.tb08052.x

Nakano, T., Suzuki, K., Fujimura, T., Shinshi, H., 2006. Genome-wide analysis of the ERF gene family in *Arabidopsis* and rice. Plant Physiol. 140, 411–432. https://doi.org/10.1104/pp.105.073783

Nandety, R.S., Caplan, J.L., Cavanaugh, K., Perroud, B., Wroblewski, T., Michelmore, R.W., Meyers, B.C., 2013. The role of TIR-NBS and TIR-X proteins in plant basal defense responses. Plant Physiol. 162, 1459–1472. https://doi.org/10.1104/pp.113.219162

Narusaka, M., Shirasu, K., Noutoshi, Y., Kubo, Y., Shiraishi, T., Iwabuchi, M., Narusaka, Y., 2009. *RRS1* and *RPS4* provide a dual Resistance-gene system

against fungal and bacterial pathogens. Plant J. 60, 218–226. https://doi.org/10.1111/j.1365-313X.2009.03949.x

Navarro, L., Dunoyer, P., Jay, F., Arnold, B., Dharmasiri, N., Estelle, M., Voinnet, O., Jones, J.D.G., 2006. A plant miRNA contributes to antibacterial resistance by repressing auxin signaling. Science (80-.). 312, 436–439. https://doi.org/10.1126/science.1126088

Navarro, L., Jay, F., Nomura, K., He, S.Y., Voinnet, O., 2008. Suppression of the microRNA pathway by bacterial effector proteins. Science (80-.). 321, 964–967. https://doi.org/10.1126/science.1159505

Navarro, L., Zipfel, C., Rowland, O., Keller, I., Robatzek, S., Boller, T., Jones, J.D.G., 2004. The transcriptional innate immune response to flg22. Interplay and overlap with Avr gene-dependent defense responses and bacterial pathogenesis. Plant Physiol. 135, 1113–1128. https://doi.org/10.1104/pp.103.036749

Nelson, C.J., Millar, A.H., 2015. Protein turnover in plant biology. Nat. Plants 1, 15017. https://doi.org/10.1038/nplants.2015.17

Ngou, B.P.M., Ahn, H.K., Ding, P., Jones, J.D.G., 2020. Mutual potentiation of plant immunity by cell-surface and intracellular receptors. bioRxiv 1–29. https://doi.org/10.1101/2020.04.10.034173

Nimchuk, Z., Marois, E., Kjemtrup, S., Leister, R.T., Katagiri, F., Dangl, J.L., 2000. Eukaryotic fatty acylation drives plasma membrane targeting and enhances function of several type iii effector proteins from *Pseudomonas syringae*. Cell 101, 353–363. https://doi.org/https://doi.org/10.1016/S0092-8674(00)80846-6

Nishimura, M.T., Anderson, R.G., Cherkis, K.A., Law, T.F., Liu, Q.L., Machius, M., Nimchuk, Z.L., Yang, L., Chung, E.H., El Kasmi, F., Hyunh, M., Nishimura, E.O., Sondek, J.E., Dangl, J.L., 2017. TIR-only protein RBA1 recognizes a pathogen effector to regulate cell death in *Arabidopsis*. Proc. Natl. Acad. Sci. U. S. A. 114, E2053–E2062. https://doi.org/10.1073/pnas.1620973114

Niu, D., Lii, Y.E., Chellappan, P., Lei, L., Peralta, K., Jiang, C., Guo, J., Coaker, G., Jin, H., 2016. miRNA863-3p sequentially targets negative immune

regulator ARLPKs and positive regulator SERRATE upon bacterial infection. Nat. Commun. 7, 11324. https://doi.org/10.1038/ncomms11324

Obaisi, A.I., 2017. Overpopulation: a threat to sustainable agriculture and food security in developing countries? A Review. Ijafs 6, 921–927. https://doi.org/10.13140/RG.2.2.20613.04325

Oerke, E.C., 2006. Crop losses to pests. J. Agric. Sci. 144, 31–43. https://doi.org/10.1017/S0021859605005708

Olesen, J.E., Trnka, M., Kersebaum, K.C., Skjelvåg, A.O., Seguin, B., Peltonen-Sainio, P., Rossi, F., Kozyra, J., Micale, F., 2011. Impacts and adaptation of European crop production systems to climate change. Eur. J. Agron. 34, 96–112. https://doi.org/10.1016/j.eja.2010.11.003

Olivier, D., Maina, M., Andrew, O.E., Peter, M.M., and Careen, I.C. (2018). Application of molecular and biotechnological techniques in plant disease management: A review. African J. Biotechnol. 17: 938–948

Ortigosa, A., Gimenez-Ibanez, S., Leonhardt, N., Solano, R., 2019. Design of a bacterial speck resistant tomato by CRISPR/Cas9-mediated editing of SlJAZ2. Plant Biotechnol. J. 17, 665–673. https://doi.org/10.1111/pbi.13006

Ortiz, D., de Guillen, K., Cesari, S., Chalvon, V., Gracy, J., Padilla, A., Kroj, T., 2017. Recognition of the magnaporthe oryzae effector AVR-pia by the decoy domain of the rice NLR immune receptor RGA5. Plant Cell 29, 156–168. https://doi.org/10.1105/tpc.16.00435

Ouwerkerk, P.B., de Kam, R.J., Hoge, H.J., Meijer, A.H., 2001. Glucocorticoid-inducible gene expression in rice. Planta 213, 370–378. https://doi.org/10.1007/s004250100583

Panchy, N., Lehti-Shiu, M., Shiu, S.-H., 2016. Evolution of gene duplication in plants. Plant Physiol. 171, 2294–2316. https://doi.org/10.1104/pp.16.00523

Pandey, S.P., Somssich, I.E., 2009. The role of WRKY transcription factors in plant immunity. Plant Physiol. 150, 1648–1655. https://doi.org/10.1104/pp.109.138990

Pickett, F.B., Meeks-Wagner, D.R., 1995. Seeing double: appreciating genetic redundancy. Plant Cell 7, 1347–1356. https://doi.org/10.1105/tpc.7.9.1347

Prior, P. (Philippe), Allen, C. (Caitilyn), Elphinstone, J.G., 1997. International Bacterial Wilt Symposium (2nd : 1997 : Gosier, G. Bacterial wilt disease :molecular and ecological aspects.

Prosekov, A.Y., Ivanova, S.A., 2018. Food security: The challenge of the present. Geoforum 91, 73–77. https://doi.org/10.1016/j.geoforum.2018.02.030

Pruneda-Paz, J.L., Breton, G., Nagel, D.H., Kang, S.E., Bonaldi, K., Doherty, C.J., Ravelo, S., Galli, M., Ecker, J.R., Kay, S.A., 2014. A genome-scale resource for the functional characterization of *Arabidopsis* transcription factors. Cell Rep. 8, 622–632. https://doi.org/10.1016/j.celrep.2014.06.033

Rajeevkumar, S., Anunanthini, P., Sathishkumar, R., 2015. Epigenetic silencing in transgenic plants. Front. Plant Sci. 6, 1–8. https://doi.org/10.3389/fpls.2015.00693

Read, A.F., 1994. The evolution of virulence. Trends Microbiol. 2, 73–76. https://doi.org/10.1016/0966-842X(94)90537-1

Sakuma, Y., Liu, Q., Dubouzet, J.G., Abe, H., Shinozaki, K., Yamaguchi-Shinozaki, K., 2002. DNA-binding specificity of the ERF/AP2 domain of *Arabidopsis* DREBs, transcription factors involved in dehydration- and cold-inducible gene expression. Biochem. Biophys. Res. Commun. 290, 998–1009. https://doi.org/10.1006/bbrc.2001.6299

Sarris, P.F., Cevik, V., Dagdas, G., Jones, J.D.G., Krasileva, K. V., 2016. Comparative analysis of plant immune receptor architectures uncovers host proteins likely targeted by pathogens. BMC Biol. 14. https://doi.org/10.1186/s12915-016-0228-7

Sarris, P.F., Duxbury, Z., Huh, S.U., Ma, Y., Segonzac, C., Sklenar, J., Derbyshire, P., Cevik, V., Rallapalli, G., Saucet, S.B., Wirthmueller, L., Menke, F.L.H., Sohn, K.H., Jones, J.D.G., 2015. A plant immune receptor detects pathogen effectors that target WRKY transcription factors. Cell 161, 1089–1100. https://doi.org/10.1016/j.cell.2015.04.024

Saucet, S.B., Ma, Y., Sarris, P.F., Furzer, O.J., Sohn, K.H., Jones, J.D.G., 2015. Two linked pairs of *Arabidopsis* TNL resistance genes independently

confer recognition of bacterial effector AvrRps4. Nat. Commun. 6. https://doi.org/10.1038/ncomms7338

Savary, S., Ficke, A., Aubertot, J.N., Hollier, C., 2012. Crop losses due to diseases and their implications for global food production losses and food security. Food Secur. 4, 519–537. https://doi.org/10.1007/s12571-012-0200-5

Savary, S., Willocquet, L., Pethybridge, S.J., Esker, P., McRoberts, N., Nelson, A., 2019. The global burden of pathogens and pests on major food crops. Nat. Ecol. Evol. 3, 430–439. https://doi.org/10.1038/s41559-018-0793-y

Schmid, M., Davison, T.S., Henz, S.R., Pape, U.J., Demar, M., Vingron, M., Schölkopf, B., Weigel, D., Lohmann, J.U., 2005. A gene expression map of *Arabidopsis thaliana* development. Nat. Genet. 37, 501–506. https://doi.org/10.1038/ng1543

Schnurr, J.A., Guerra, D.J., 2000. The CaMV-35S promoter is sensitive to shortened photoperiod in transgenic tobacco. Plant Cell Rep. 19, 279–282. https://doi.org/10.1007/s002990050012

Schubert, D., Lechtenberg, B., Forsbach, A., Gils, M., Bahadur, S., Schmidt, R., 2004. Silencing in *Arabidopsis* T-DNA transformants: the predominant role of a gene-specific RNA sensing mechanism versus position effects. Plant Cell 16, 2561–2572. https://doi.org/10.1105/tpc.104.024547

Segarra, G., Van der Ent, S., Trillas, I., Pieterse, C.M.J., 2009. MYB72, a node of convergence in induced systemic resistance triggered by a fungal and a bacterial beneficial microbe. Plant Biol. 11, 90–96. https://doi.org/https://doi.org/10.1111/j.1438-8677.2008.00162.x

Segretin, M.E., Pais, M., Franceschetti, M., Chaparro-Garcia, A., Bos, J.I.B., Banfield, M.J., Kamoun, S., 2014. Single amino acid mutations in the potato immune receptor R3a expand response to *Phytophthora effectors*. Mol. Plant-Microbe Interact. 27, 624–637. https://doi.org/10.1094/MPMI-02-14-0040-R

Seo, E., Choi, D., 2015. Functional studies of transcription factors involved in plant defenses in the genomics era. Brief. Funct. Genomics 14, 260–267. https://doi.org/10.1093/bfgp/elv011

Shan, L., He, P., Li, J., Heese, A., Peck, S.C., Nürnberger, T., Martin, G.B., Sheen, J., 2008. Bacterial effectors target the common signaling partner BAK1 to disrupt multiple MAMP receptor-signaling complexes and impede plant immunity. Cell Host Microbe 4, 17–27. https://doi.org/10.1016/j.chom.2008.05.017

Shao, F., Golstein, C., Ade, J., Stoutemyer, M., Dixon, J.E., Innes, R.W., 2003. Cleavage of *Arabidopsis* PBS1 by a bacterial type III effector. Science (80-.). 301, 1230–1233. https://doi.org/10.1126/science.1085671

Shao, Z.Q., Xue, J.Y., Wu, P., Zhang, Y.M., Wu, Y., Hang, Y.Y., Wang, B., Chen, J.Q., 2016. Large-scale analyses of angiosperm nucleotide-binding site-leucine-rich repeat genes reveal three anciently diverged classes with distinct evolutionary patterns. Plant Physiol. 170, 2095–2109. https://doi.org/10.1104/pp.15.01487

Son, G.H., Wan, J., Kim, H.J., Nguyen, X.C., Chung, W.S., Hong, J.C., Stacey, G., 2012. Ethylene-responsive element-binding factor 5, ERF5, is involved in chitin-induced innate immunity response. Mol. Plant. Microbe. Interact. 25, 48–60. https://doi.org/10.1094/MPMI-06-11-0165

Stevens, R.B. (1960). Cultural practices in disease control. In plant pathology: an advanced treatise, volume III: The diseases population epidemics and control, J.G. Horsfall, ed. (London: Academic Press Inc.), pp. 357–429.

Stirnweis, D., Milani, S.D., Jordan, T., Keller, B., Brunne, S., 2014. Substitutions of two amino acids in the nucleotide-binding site domain of a resistance protein enhance the hypersensitive response and enlarge the PM3F resistance spectrum in wheat. Mol. Plant-Microbe Interact. 27, 265–276. https://doi.org/10.1094/MPMI-10-13-0297-FI

Stroud, H., Ding, B., Simon, S.A., Feng, S., Bellizzi, M., Pellegrini, M., Wang, G.-L., Meyers, B.C., Jacobsen, S.E., 2013. Plants regenerated from tissue culture contain stable epigenome changes in rice. Elife 2, e00354. https://doi.org/10.7554/eLife.00354

Stukenbrock, E.H., Bataillon, T., Dutheil, J.Y., Hansen, T.T., Li, R., Zala, M., McDonald, B.A., Wang, J., Schierup, M.H., 2011. The making of a new pathogen: Insights from comparative population genomics of the domesticated

wheat pathogen *Mycosphaerella graminicola* and its wild sister species. Genome Res. 21, 2157–2166. https://doi.org/10.1101/gr.118851.110

Suffert, F., Sache, I., and Lannou, C. (2011). Early stages of septoria tritici blotch epidemics of winter wheat: build-up, overseasoning, and release of primary inoculum. Plant Pathol. 60: 166–177.

Sun, H.H., Fukao, Y., Ishida, S., Yamamoto, H., Maekawa, S., Fujiwara, M., Sato, T., Yamaguchi, J., 2013. Proteomics analysis reveals a highly heterogeneous proteasome composition and the post-translational regulation of peptidase activity under pathogen signaling in plants. J. Proteome Res. 12, 5084–5095. https://doi.org/10.1021/pr400630w

Sun, Y., Zhu, Y.X., Balint-Kurti, P.J., Wang, G.F., 2020. Fine-tuning immunity: players and regulators for plant NLRs. Trends Plant Sci. 25, 695–713. https://doi.org/10.1016/j.tplants.2020.02.008

Swinnen, J., McDermott, J., 2020. COVID-19 and global food security.

TAIR (The *Arabidopsis* Information Resource), https://www.arabidopsis.org/index.jsp.

Takatsuji, H. (2014). Development of disease-resistant rice using regulatory components of induced disease resistance. Front. Plant Sci. 5: 630.

Tang, D., Wang, G., Zhou, J.M., 2017. Receptor kinases in plant-pathogen interactions: More than pattern recognition. Plant Cell 29, 618–637. https://doi.org/10.1105/tpc.16.00891

The World Bank, 2022. Food security update: https://www.worldbank.org/en/topic/agriculture/brief/food-security-update

Thomma, B.P.H.J., Nürnberger, T., Joosten, M.H.A.J., 2011. Of PAMPs and effectors: The blurred PTI-ETI dichotomy. Plant Cell 23, 4–15. https://doi.org/10.1105/tpc.110.082602

Thor, K., Jiang, S., Michard, E., George, J., Scherzer, S., Huang, S., Dindas, J., Derbyshire, P., Leitão, N., DeFalco, T.A., Köster, P., Hunter, K., Kimura, S., Gronnier, J., Stransfeld, L., Kadota, Y., Bücherl, C.A., Charpentier, M., Wrzaczek, M., MacLean, D., Oldroyd, G.E.D., Menke, F.L.H., Roelfsema, M.R.G., Hedrich, R., Feijó, J., Zipfel, C., 2020. The calcium-permeable

channel OSCA1.3 regulates plant stomatal immunity. Nature 585, 569–573. https://doi.org/10.1038/s41586-020-2702-1

Tian, W., Hou, C., Ren, Z., Wang, C., Zhao, F., Dahlbeck, D., Hu, S., Zhang, L., Niu, Q., Li, L., Staskawicz, B.J., Luan, S., 2019. A calmodulin-gated calcium channel links pathogen patterns to plant immunity. Nature 572, 131–135. https://doi.org/10.1038/s41586-019-1413-y

Tilman, D., Fargione, J., Wolff, B., D'Antonio, C., Dobson, A., Howarth, R., Schindler, D., Schlesinger, W.H., Simberloff, D., Swackhamer, D., 2001. Forecasting agriculturally driven global environmental change. Science (80-.). 292, 281–284. https://doi.org/10.1126/science.1057544

Toruño, T.Y., Stergiopoulos, I., Coaker, G., 2016. Plant-pathogen effectors: cellular probes interfering with plant defenses in spatial and temporal manners. Annu. Rev. Phytopathol. 54, 419–441. https://doi.org/10.1146/annurev-phyto-080615-100204

Tsuda, K., Mine, A., Bethke, G., Igarashi, D., Botanga, C.J., Tsuda, Y., Glazebrook, J., Sato, M., Katagiri, F., 2013. Dual regulation of gene expression mediated by extended MAPK activation and salicylic acid contributes to robust innate immunity in *Arabidopsis thaliana*. PLOS Genet. 9, e1004015.

Tsuda, K., Somssich, I.E., 2015. Transcriptional networks in plant immunity. New Phytol. 206, 932–947. https://doi.org/https://doi.org/10.1111/nph.13286

Udmale, P., Pal, I., Szabo, S., Pramanik, M., Large, A., 2020. Global food security in the context of COVID-19: A scenario-based exploratory analysis. Prog. Disaster Sci. 7, 100120. https://doi.org/https://doi.org/10.1016/j.pdisas.2020.100120

UN, 2022. Global issues: Population. https://www.un.org/en/global-issues/population

UN, 2020. The sustainable development goals report 2019 (assessed September 18, 2020). United Nations, New York 1–9.

Vailleau, F., Daniel, X., Tronchet, M., Montillet, J.-L., Triantaphylidès, C., Roby, D., 2002. A R2R3-MYB gene, *AtMYB30*, acts as a positive regulator of

the hypersensitive cell death program in plants in response to pathogen attack. Proc. Natl. Acad. Sci. 99, 10179 LP – 10184. https://doi.org/10.1073/pnas.152047199

Van de Weyer, A.L., Monteiro, F., Furzer, O.J., Nishimura, M.T., Cevik, V., Witek, K., Jones, J.D.G., Dangl, J.L., Weigel, D., Bemm, F., 2019. A species-wide inventory of NLR genes and alleles in *Arabidopsis thaliana*. Cell 178, 1260-1272.e14. https://doi.org/10.1016/j.cell.2019.07.038

Van Der Hoorn, R.A.L., Kamoun, S., 2008. From guard to decoy: A new model for perception of plant pathogen effectors. Plant Cell 20, 2009–2017. https://doi.org/10.1105/tpc.108.060194

Vance, R.E., Isberg, R.R., Portnoy, D.A., 2009. Patterns of pathogenesis: discrimination of pathogenic and nonpathogenic microbes by the innate immune system. Cell Host Microbe 6, 10–21. https://doi.org/10.1016/j.chom.2009.06.007

Vaucheret, H., Nussaume, L., Palauqui, J.C., Quillere, I., Elmayan, T., 1997. A transcriptionally active state is required for post-transcriptional silencing (cosuppression) of nitrate reductase host genes and transgenes. Plant Cell 9, 1495–1504. https://doi.org/10.1105/tpc.9.8.1495

Velásquez, A.C., Castroverde, C.D.M., He, S.Y., 2018. Plant–pathogen warfare under changing climate conditions. Curr. Biol. 28, R619–R634. https://doi.org/10.1016/j.cub.2018.03.054

Vellicce, G.R., Ricci, J.C.D., Hern.ndez, L., and Castagnaro, A.P. (2006). Enhanced Resistance to *Botrytis cinerea* Mediated by the Transgenic Expression of the Chitinase Gene *ch5B* in Strawberry. Transgenic Res. 15: 57–68

Wan, L., Essuman, K., Anderson, R.G., Sasaki, Y., Monteiro, F., Chung, E.H., Nishimura, E.O., DiAntonio, A., Milbrandt, J., Dangl, J.L., Nishimura, M.T., 2019. TIR domains of plant immune receptors are NAD+-cleaving enzymes that promote cell death. Science (80-.). 365, 799–803. https://doi.org/10.1126/science.aax1771

Wang, C., Zhou, M., Zhang, X., Yao, J., Zhang, Y., Mou, Z., 2017. A lectin receptor kinase as a potential sensor for extracellular nicotinamide adenine dinucleotide in *Arabidopsis thaliana*. Elife 6, 1–23. https://doi.org/10.7554/eLife.25474

Wang, G., Roux, B., Feng, F., Guy, E., Li, L., Li, N., Zhang, X., Lautier, M., Jardinaud, M.F., Chabannes, M., Arlat, M., Chen, S., He, C., Noël, L.D., Zhou, J.M., 2015. The decoy substrate of a pathogen effector and a pseudokinase specify pathogen-induced modified-self recognition and immunity in plants. Cell Host Microbe 18, 285–295. https://doi.org/10.1016/j.chom.2015.08.004

Wang, Jiachang, Liu, X., Zhang, A., Ren, Y., Wu, F., Wang, G., Xu, Y., Lei, C., Zhu, S., Pan, T., Wang, Yongfei, Zhang, H., Wang, F., Tan, Y.Q., Wang, Yupeng, Jin, X., Luo, S., Zhou, C., Zhang, Xiao, Liu, J., Wang, S., Meng, L., Wang, Yihua, Chen, X., Lin, Q., Zhang, Xin, Guo, X., Cheng, Z., Wang, Jiulin, Tian, Y., Liu, S., Jiang, L., Wu, C., Wang, E., Zhou, J.M., Wang, Y.F., Wang, H., Wan, J., 2019. A cyclic nucleotide-gated channel mediates cytoplasmic calcium elevation and disease resistance in rice. Cell Res. 29, 820–831. https://doi.org/10.1038/s41422-019-0219-7

Wang, Jizong, Hu, M., Wang, Jia, Qi, J., Han, Z., Wang, G., Qi, Y., Wang, H.W., Zhou, J.M., Chai, J., 2019a. Reconstitution and structure of a plant NLR resistosome conferring immunity. Science (80-.). 364. https://doi.org/10.1126/science.aav5870

Wang, Jizong, Wang, Jia, Hu, M., Wu, S., Qi, J., Wang, G., Han, Z., Qi, Y., Gao, N., Wang, H.W., Zhou, J.M., Chai, J., 2019b. Ligand-triggered allosteric ADP release primes a plant NLR complex. Science (80-.). 364. https://doi.org/10.1126/science.aav5868

Wang, T., Chang, C., Gu, C., Tang, S., Xie, Q., Shen, Q.H., 2016. An E3 ligase affects the NLR receptor stability and immunity to powdery mildew. Plant Physiol. 172, 2504–2515. https://doi.org/10.1104/pp.16.01520

Wang, H.-L. V, Chekanova, J.A., 2017. Long noncoding RNAs in plants bt-Long Non Coding RNA Biology, in: Rao, M.R.S. (Ed.),. Springer Singapore, Singapore, pp. 133–154. https://doi.org/10.1007/978-981-10-5203-3_5

Weinhold, A., Kallenbach, M., Baldwin, I.T., 2013. Progressive 35S promoter methylation increases rapidly during vegetative development in transgenic *Nicotiana attenuata* plants. BMC Plant Biol. 13, 99. https://doi.org/10.1186/1471-2229-13-99

Weintraub, H., 1993. The MyoD family and myogenesis: redundancy, networks, and thresholds. Cell 75, 1241–1244. https://doi.org/10.1016/0092-8674(93)90610-3

WHO COVID-19 Dashboard, 2022. https://covid19.who.int/

WHO, 2021. Novel coronavirus 2019. https://www.who.int/emergencies/diseases/novel-coronavirus-2019

Williams, S.J., Yin, L., Foley, G., Casey, L.W., Outram, M.A., Ericsson, D.J., Lu, J., Boden, M., Dry, I.B., Kobe, B., 2016. Structure and function of the TIR domain from the grape NLR protein RPV1. Front. Plant Sci. 7, 1–13. https://doi.org/10.3389/fpls.2016.01850

Williams, S.J., Sohn, K.H., Wan, L., Bernoux, M., Sarris, P.F., et al. (2014). Structural basis for assembly and function of a heterodimeric plant immune receptor. Science 344: 299–303.

Windram, O., Madhou, P., Mchattie, S., Hill, C., Hickman, R., Cooke, E., Jenkins, D.J., Penfold, C.A., Baxter, L., Breeze, E., Kiddle, S.J., Rhodes, J., Atwell, S., Kliebenstein, D.J., Kim, Y. sung, Stegle, O., Borgwardt, K., Zhang, C., Tabrett, A., Legaie, R., Moore, J., Finkenstadt, B., Wild, D.L., Mead, A., Rand, D., Beynon, J., Ott, S., Buchanan-Wollaston, V., Denby, K.J., 2012. *Arabidopsis* defense against *Botrytis cinerea*: Chronology and regulation deciphered by high-resolution temporal transcriptomic analysis. Plant Cell 24, 3530–3557. https://doi.org/10.1105/tpc.112.102046

Winter, D., Vinegar, B., Nahal, H., Ammar, R., Wilson, G. V, Provart, N.J., 2007. An “electronic fluorescent pictograph” browser for exploring and analyzing large-scale biological data sets. PLoS One 2, 1–12. https://doi.org/10.1371/journal.pone.0000718

Wu, C.H., Abd-El-Haliem, A., Bozkurt, T.O., Belhaj, K., Terauchi, R., Vossen, J.H., Kamoun, S., 2017. NLR network mediates immunity to diverse plant

pathogens. Proc. Natl. Acad. Sci. U. S. A. 114, 8113–8118. https://doi.org/10.1073/pnas.1702041114

Xiao, S., Calis, O., Patrick, E., Zhang, G., Charoenwattana, P., Muskett, P., Parker, J.E., Turner, J.G., 2005. The atypical resistance gene, *RPW8*, recruits components of basal defence for powdery mildew resistance in *Arabidopsis*. Plant J. 42, 95–110. https://doi.org/10.1111/j.1365-313X.2005.02356.x

Xie, Z., Nolan, T.M., Jiang, H., Yin, Y., 2019. AP2/ERF transcription factor regulatory networks in hormone and abiotic stress responses in *Arabidopsis* . Front. Plant Sci. .

Xin, X.-F., Nomura, K., Aung, K., Velásquez, A.C., Yao, J., Boutrot, F., Chang, J.H., Zipfel, C., He, S.Y., 2016. Bacteria establish an aqueous living space in plants crucial for virulence. Nature 539, 524–529. https://doi.org/10.1038/nature20166

Xin, X.F., He, S.Y., 2013. *Pseudomonas syringae* pv. *tomato* DC3000: A model pathogen for probing disease susceptibility and hormone signaling in plants. Annu. Rev. Phytopathol. 51, 473–498. https://doi.org/10.1146/annurev-phyto-082712-102321

Xu, F., Kapos, P., Cheng, Y.T., Li, M., Zhang, Y., Li, X., 2014. NLR-associating transcription factor bHLH84 and its paralogs function redundantly in plant immunity. PLoS Pathog. 10. https://doi.org/10.1371/journal.ppat.1004312

Xu, J., Meng, J., Meng, X., Zhao, Y., Liu, J., Sun, T., Liu, Y., Wang, Q., Zhang, S., 2016. Pathogen-responsive MPK3 and MPK6 reprogram the biosynthesis of indole glucosinolates and their derivatives in arabidopsis immunity. Plant Cell 28, 1144–1162. https://doi.org/10.1105/tpc.15.00871

Yang, X.-Y., Chen, W.-P., Rendahl, A.K., Hegeman, A.D., Gray, W.M., Cohen, J.D., 2010. Measuring the turnover rates of *Arabidopsis* proteins using deuterium oxide: an auxin signaling case study. Plant J. 63, 680–695. https://doi.org/10.1111/j.1365-313X.2010.04266.x

Yuliar, Nion, Y.A., and Toyota, K. (2015). Recent trends in control methods for bacterial wilt diseases caused by *Ralstonia solanacearum*. Microbes Environ. 30:1–11.

Zabala, M. de T., Littlejohn, G., Jayaraman, S., Studholme, D., Bailey, T., Lawson, T., Tillich, M., Licht, D., Bölter, B., Delfino, L., Truman, W., Mansfield, J., Smirnoff, N., Grant, M., 2015. Chloroplasts play a central role in plant defence and are targeted by pathogen effectors. Nat. Plants 1. https://doi.org/10.1038/NPLANTS.2015.74

Zeng, W., Brutus, A., Kremer, J.M., Withers, J.C., Gao, X., Da Jones, A.D., He, S.Y., 2011. A genetic screen reveals *Arabidopsis* Stomatal and/or apoplastic defenses against *Pseudomonas syringae* pv. *tomato* DC3000. PLoS Pathog. 7. https://doi.org/10.1371/journal.ppat.1002291

Zhang, J., Coaker, G., Zhou, J.M., Dong, X., 2020a. Plant immune mechanisms: from reductionistic to holistic points of view. Mol. Plant 13, 1358–1378. https://doi.org/10.1016/j.molp.2020.09.007

Zhang, J., Coaker, G., Zhou, J.M., Dong, X., 2020b. Plant immune mechanisms: from reductionistic to holistic points of view. Mol. Plant 13, 1358–1378. https://doi.org/10.1016/j.molp.2020.09.007

Zhang, J., Shao, F., Li, Y., Cui, H., Chen, L., Li, H., Zou, Y., Long, C., Lan, L., Chai, J., Chen, S., Tang, X., Zhou, J.-M., 2007. A *Pseudomonas syringae* effector inactivates MAPKs to suppress PAMP-induced immunity in plants. Cell Host Microbe 1, 175–185. https://doi.org/10.1016/j.chom.2007.03.006

Zhang, X., Bernoux, M., Bentham, A.R., Newman, T.E., Ve, T., Casey, L.W., Raaymakers, T.M., Hu, J., Croll, T.I., Schreiber, K.J., Staskawicz, B.J., Anderson, P.A., Sohn, K.H., Williams, S.J., Dodds, P.N., Kobe, B., 2017. Multiple functional self-association interfaces in plant TIR domains. Proc. Natl. Acad. Sci. U. S. A. 114, E2046–E2052. https://doi.org/10.1073/pnas.1621248114

Zhao, H., Li, Teng, Wang, K., Zhao, F., Chen, J., Xu, G., Zhao, J., Li, Ting, Chen, L., Li, L., Xia, Q., Zhou, T., Li, H.Y., Li, A.L., Finkel, T., Zhang, X.M., Pan, X., 2019. AMPK-mediated activation of MCU stimulates mitochondrial Ca2+ entry to promote mitotic progression. Nat. Cell Biol. 21, 476–486. https://doi.org/10.1038/s41556-019-0296-3

Zhao, Y., Thilmony, R., Bender, C.L., Schaller, A., He, S.Y., Howe, G.A., 2003. Virulence systems of *Pseudomonas syringae* pv. *tomato* promote bacterial

speck disease in tomato by targeting the jasmonate signaling pathway. Plant J. 36, 485–499. https://doi.org/10.1046/j.1365-313X.2003.01895.x

Zhou, J., Tang, X., Martin, G.B., 1997. The Pto kinase conferring resistance to tomato bacterial speck disease interacts with proteins that bind a cis-element of pathogenesis-related genes. EMBO J. 16, 3207–3218. https://doi.org/https://doi.org/10.1093/emboj/16.11.3207

Zhou, J.M., Chai, J., 2008. Plant pathogenic bacterial type III effectors subdue host responses. Curr. Opin. Microbiol. 11, 179–185. https://doi.org/10.1016/j.mib.2008.02.004

Zhou, J.M., Zhang, Y., 2020. Plant immunity: danger perception and signaling. Cell 181, 978–989. https://doi.org/10.1016/j.cell.2020.04.028

Zhou, Z., Wu, Y., Yang, Y., Du, M., Zhang, X., Guo, Y., Li, C., Zhou, J.-M., 2015. An *Arabidopsis* plasma membrane proton ATPase modulates JA signaling and is exploited by the *Pseudomonas syringae* effector protein AvrB for stomatal invasion. Plant Cell 27, 2032–2041. https://doi.org/10.1105/tpc.15.00466

Zhu, N., Zhang, D., Wang, W., Li, X., Yang, B., Song, J., Zhao, X., Huang, B., Shi, W., Lu, R., Niu, P., Zhan, F., Ma, X., Wang, D., Xu, W., Wu, G., Gao, G.F., Tan, W., 2020. A novel coronavirus from patients with pneumonia in china, 2019. N. Engl. J. Med. 382, 727–733. https://doi.org/10.1056/NEJMoa2001017

Zipfel, C., Oldroyd, G.E.D., 2017. Plant signalling in symbiosis and immunity. Nature 543, 328–336. https://doi.org/10.1038/nature22009